Development of Detection Techniques Based on Surface Chemistry

Xingkai Hao

Thesis submitted to the University of Ottawa
in partial Fulfillment of the requirements for the
Doctorate in Philosophy Degree in Chemical Engineering

uOttawa

Department of Chemical and Biological Engineering

Faculty of Engineering

University of Ottawa

Abstract

Rapid and high-sensitivity detections of biological analytes are critically important to ensure timely diagnosis of disease and effective monitoring of public health. Although various new biosensing platforms have been established as alternatives to conventional laboratory methods, most of these biosensing platforms suffer from insufficient sensitivities that severely limit their wide applications. To improve the detection sensitivities of these biosensors, surface modifications based on poly(amidoamine) (PAMAM) dendrimers and rolling circle amplification (RCA) have been proven to be effective methods.

In this thesis, surface modification strategies based on PAMAM dendrimers and RCA have been applied on three biosensing platforms, including enzyme-linked immunosorbent assay (ELISA), localized surface plasmon resonance (LSPR) sensor chip, and affinity membrane, to improve their detection sensitivities. For the ELISA platform, glass-bottom and poly(styrene) 96-well plates are surface modified by dendrimer-aptamer conjugates to improve detection performances of human platelet-derived growth factor-BB using ELISA. The results show that the ELISA performed using the modified 96-well plates presents a much broader linear detection range and a significantly lower limit of detection (LOD) than conventional ELISA plates. For the LSPR platform, the dendrimer and aptamer modification strategy is employed to surface modify LSPR sensor chips for sensitive detection of the SARS-CoV-2 virus, and an RCA-AuNPs complex is developed to amplify the detection signals. The results show that the modified chip can sensitively detect the SARS-CoV-2 virus with a LOD of 148 vp/mL, suggesting that the modified LSPR chip and signal amplification method can be used for early diagnosis of Covid-19. For the affinity membrane platform, nylon membranes with dendrimer and dual-RCA surface modifications are developed to detect *Escherichia coli* O157:H7 in food samples. The surface-modified membranes significantly reduce the detection time of the target bacteria to two hours instead of

several days using traditional bacterial detection methods. In addition, the new membranes achieve higher sample throughputs (around 4-5 mL/s) with a lower LOD (10 cells/ 250 mL) in processing real-world food samples compared to other similar detection platforms. The excellent properties of our surface modification approaches may provide further advantages when employed in other platforms, such as target separation and enrichment, antifouling and antibacterial, and drug delivery applications.

Resúmé

Les détections rapides et à haute sensibilité d'analytes biologiques sont d'une importance critique pour assurer un diagnostic rapide des maladies et une surveillance efficace de la santé publique. Bien que plusieurs nouvelles plateformes de biodétection aient été établies comme alternatives aux méthodes de laboratoire conventionnelles, la plupart de ces plateformes souffrent de sensibilités insuffisantes qui limitent sévèrement leurs larges applications. En vue d'améliorer les sensibilités de détection de ces biocapteurs, les modifications de surface basées sur les dendrimères poly(amidoamine) (PAMAM) et l'amplification par cercle roulant (RCA) se sont avérées être des méthodes efficaces.

Dans ce mémoire, les stratégies de modification de surface basées sur les dendrimères PAMAM et la RCA ont été appliquées sur trois plateformes de biodétection, y compris le test immuno-enzymatique (ELISA), la puce de détection à résonance plasmonique de surface localisée (LSPR) ainsi que la membrane d'affinité, afin d'améliorer leurs sensibilités de détection. Pour la plateforme ELISA, des plaques à 96 puits en verre et en poly(styrène) sont modifiées en surface par des conjugués dendrimère-aptamère afin d'améliorer les performances de détection du facteur de croissance dérivé des plaquettes humaines-BB par ELISA. Les résultats montrent que l'ELISA réalisé à l'aide des plaques 96 puits modifiées présente une plage de détection linéaire beaucoup plus large et une limite de détection (LOD) nettement inférieure à celle des plaques ELISA classiques. Pour la plateforme LSPR, la stratégie de modification des dendrimères et des aptamères est employée pour modifier la surface des puces de détection LSPR pour une détection sensible du virus SARS-CoV-2, et un complexe RCA-AuNPs est développé pour amplifier les signaux de détection. Les résultats montrent que notre puce modifiée peut détecter de manière sensible le virus du SRAS-CoV-2 avec une LOD de 148 vp/mL, ce qui suggère que la puce LSPR modifiée et la méthode d'amplification du signal peuvent être utilisées pour le diagnostic précoce du Covid-19.

Pour la plateforme de membrane d'affinité, des membranes en nylon avec des modifications de surface de dendrimère et de double RCA sont développées pour détecter *Escherichia coli* O157:H7 dans des échantillons alimentaires. Les membranes modifiées en surface réduisent considérablement le temps de détection de la bactérie cible à deux heures au lieu de plusieurs jours avec les méthodes traditionnelles de détection bactérienne. En outre, les nouvelles membranes permettent d'atteindre des débits d'échantillons plus élevés (environ 4-5 mL/s) avec une LOD plus faible (10 cellules/250 mL) lors du traitement d'échantillons alimentaires réels par rapport à d'autres plateformes de détection similaires. Les excellentes propriétés de nos approches de modification de surface peuvent offrir d'autres avantages lorsqu'elles sont employées dans d'autres plateformes, telles que la séparation et l'enrichissement des cibles, les applications antisalissures et antibactériennes, et l'administration de médicaments.

Copyright Statement

All materials in this thesis that have previously been published in journals allow their use in graduate theses. Full references for the original publication are provided where required.

Statement of contributions of collaborators

I hereby declare that I am the sole author of this thesis.

I designed the methodologies of the project and performed all the experiments and data analysis. The scientific guidance and editorial comments for the written work were provided by my supervisors, Dr. Cao and Dr. Zou.

Other sources of assistance in academic discussion and comments will be listed as co-authors in relevant journal papers.

Acknowledgments

My sincere thanks must first be extended to my supervisors, Dr. Xudong Cao and Dr. Shan Zou, for their knowledgeable guidance, continued encouragement and understanding, and financial support during my Ph.D. studies. My supervisors are mentors and friends for me, not only in labs but also in life. Many thanks to them for supporting and encouraging me whenever I encountered difficulties and challenges.

I would like to acknowledge the Natural Sciences and Engineering Research Council of Canada (NSERC), the China Scholarship Council (CSC), and the University of Ottawa for their generous financial support.

I would also like to take the opportunity to thank Dr. Jean-Philippe St-Pierre at the University of Ottawa for providing access and training on the fluorescence microscope and microplate reader, Dr. Marianne Fenech at the University of Ottawa for providing access to the plasma machine, Dr. Min Lin at the Canadian Food Inspection Agency for providing bacterial samples, and Dr. Oltion Kodra at Energy, Mining and Environment Research Centre, National Research Council Canada for his assistance with the XPS analysis. I would like to extend my gratitude to the faculty members in our department for providing academic services and technical support. Many thanks to Francine Pétrin, Chantal Dubé, Frantz Célestin, James Macdermid, Gérard Nina and Franco Ziroldo. My acknowledgments are also extended to Zhong Wang (DLS), Yingshu Leng (Raman), and Xiaotan Zhu (SEM) for their help with materials characterizations and to Jahanbakhsh Jahanzamin and Brian Dorus for their assistance in English language editing of the documents.

I would like to extend my thanks to my colleagues and friends in the department. I thank Shuiying Li, Man Lu, Luisa Metzler, and Jordan Nhan for their friendship, instruction, and suggestions during my research journey. I also feel lucky and grateful for having

other colleagues and friends during my Ph.D. studies, including Yubo Qin, Taisa Stumpf, Danni Zou, Brian Dorus, Tongda Li, Zhiwen Su, and Hesham Ismail.

Last but not least, I would like to thank my warm family, the selfless help of my parents and my beloved wife, Kaixuan Yao, and the sweet company of my kids. Without them, none of this would have been possible.

Table of Contents

List of Figures

List of Tables

Nomenclature, abbreviations and symbols

Nomenclature and abbreviations

2D	Two dimensional
3D	Three dimensional
ABTS	2,2′-azino-bis (3-ethylbenzothiazoline-6-sulfonic acid)
AFM	Atomic force microscope
AgNPs	Silver nanoparticles
APTES	3-aminopropyl-triethoxysilane
AuNPs	Gold nanoparticles
Avidin-HRP	Avidin-labeled horseradish peroxidase
BSA	Bovine serum albumin
-C=O	Carbonyl
-COOH	Carboxyl group
cRCA	Capturing RCA
CV	Coefficient of variation
Cy3	Cyanine 3
Cy5	Cyanine 5
DLS	Dynamic light scattering
DMF	N-Dimethylformamide
EDC	1-ethyl-3-(3-dimethylaminopropyl) carbodiimide hydrochloride
ELDAA	Enzyme-linked dendrimer-aptamer assay
ELISA	Enzyme-linked immunosorbent assay
FAM	Fluorescein
FITC-NH_2	5-(aminoacetamido) fluorescein (fluoresceinyl glycine amide)
G3	Generation 3 dendrimers
G3.5-COOH	Generation 3.5 carboxylated poly(amidoamine) dendrimers
G4	Generation 4 dendrimers
G4-COOH	Generation 4 carboxylated poly(amidoamine) dendrimers

G4-NH_2	Generation 4 aminated poly(amidoamine) dendrimers
G6.5-COOH	Generation 6.5 carboxylated poly(amidoamine) dendrimers
G7	Generation 7 dendrimers
G7-COOH	Generation 7 carboxylated poly(amidoamine) dendrimers
GO	Graphene oxide
IgG	Immunoglobulin G
LAMP	Loop-mediated isothermal amplification
LOD	Limit of detection
LSPR	Localized surface plasmon resonance
MERS	Middle East Respiratory Syndrome
MSF	Mesoporous silica film
MSN	Mesoporous silica nanoparticle
MWCNTs	Multi-walled carbon nanotubes
-NH_2	Amino group
NHS	N-hydroxysuccinimide
-OH	Hydroxyl
OTA	Ochratoxin A
PAH	Poly (allylamine hydrochloride)
PAMAM	Poly(amidoamine)
PBS	Phosphate-buffered saline
PCL	Poly(caprolactone)
PCR	Polymerase chain reaction
PDA	Polydopamine
PDGF-BB	Human platelet-derived growth factor BB
PDMS	Poly(dimethylsiloxane)
PE	Poly(ethylene)
PEG	Poly(ethylene glycol)
PEI	Poly(ethyleneimine)
PET	Poly(ethylene terephthalate)

PGMA	Poly(glycidyl methacrylate)
POEGMA	Poly(oligo(ethylene glycol) methyl ether methacrylate)
PP	Poly(propylene)
PPI	Poly(propyleneimine)
PS	Poly(styrene)
PSBMA	Poly (sulfobetaine methacrylate)
PSS	Poly(sodium 4-styrenesulfonate)
PTFE	Poly(tetrafluoroethylene)
PVDF	Poly(vinylidene fluoride)
QCM	Quartz crystal microbalance
QDs	Quantum dots
RCA	Rolling circle amplification
rGO	Reduced graphene oxide
RMS	Root mean square
S/N	Signal-to-noise ratio
SAMs	Silane-based self-assembled monolayers
SARS-CoV-2	Severe Acute Respiratory Syndrome Coronavirus 2
SEM	Scanning Electron Microscopy
SPCE	Screen-printed carbon electrode
SPR	Surface plasmon resonance
SRBD	Spike protein receptor-binding domain
sRCA	Signaling RCA
ssDNA	Single-stranded DNA
TEM	Transmission electron microscopy
WCA	Water contact angles
XPS	X-ray photoelectron spectroscopy

Symbols

vp/mL	Viral particles per milliliter
RU	Response units
a.u.	Arbitrary unit
bp	Base pair
°C	Degree Celsius
h	Hour
kbp	Kilo base pair
min	Minute
nt	Nucleotide
kDa	Kilo Dalton
CFU	Colony forming unit

Chapter 1 Introduction

Detection techniques are becoming increasingly important in food safety, medical care, and public health [1-3]. Although conventional laboratory detection methods present high accuracy and sensitivity in terms of the detection results, they require expensive instruments, skilled workers, and complicated sample pre-treatment processes, thus taking several days to weeks to get the results [4, 5]. Alternatively, biosensors (*i.e.,* repaid detection devices) have been developed to overcome the disadvantages of traditional detection methods [6-8]. These platforms offer significantly shorter overall detection times, compared to conventional methods, due to not requiring complicated sample pre-treatment steps. Being inexpensive, portable, and easy to use, biosensors can greatly reduce detection expenses and achieve on-site detection. However, the detection sensitivities of biosensors are usually unsatisfactory since they are easily influenced by target concentrations and sample matrices because of the simplified sample pre-treatment steps, thus limiting their applications [9-11].

The detection process in biosensors involves two critical steps: biorecognition and signal transduction [12, 13]. In the biorecognition step, analytes are recognized and separated from the sample matrices by specific interactions between the targets and the bioligands, such as aptamers, antibodies, and peptides on the detection surfaces [12-14]. The next step, signal transduction, transduces the information from the biorecognition step into interpretable output signals, such as electrical, optical, or magnetic signals [12, 13]. Therefore, improving biorecognition and signal transduction performances is essential for enhancing the detection sensitivities of biosensors [12, 13].

Surface modifications have been reported as effective ways to enhance the detection sensitivities of biosensors by improving biorecognition and signal transduction performances [15, 16]. Our research group, in recent years, has focused on surface modification using poly(amidoamine) (PAMAM) dendrimers and rolling circle

amplification (RCA) to improve the detection performances of microfluidic detection platforms [15, 16]. The PAMAM dendrimer modified microfluidic devices present improved surface density of bioligands to achieve more efficient target-capturing performances and exhibit excellent nonfouling properties to improve the detection signal transduction by reducing background noises [17, 18]. As a promising genetic amplification method, RCA can be either applied on the detection surface to improve the overall target-capturing ability or used as signal amplification ligands to amplify detection signals [15, 16]. However, the applications of these surface modification methods on other detection platforms are less reported. In this work, these surface modification approaches have been successfully applied to glass, polystyrene, gold nanoparticle, and nylon surfaces to develop new biosensors with improved detection performances.

This document is divided into seven chapters. Chapter 1 provides an introduction to this document. Chapter 2 provides an in-depth literature review of surface modification materials and approaches for improving the detection performances of biosensors. The main challenges and possible approaches based on reported works are highlighted, and necessary considerations for biosensor designs are discussed. Chapters 3-6 discuss the work performed to improve the detection performances of biosensors using the abovementioned surface modification approaches. Specifically, Chapters 3 and 4 focus on surface modification of glass-bottom and poly(styrene) 96-well plates using PAMAM dendrimers and aptamers to improve detection performances of enzyme-linked immunosorbent assay. Chapter 5 discusses surface modification and signal amplification techniques used to improve the detection sensitivity of localized surface plasmon resonance biosensor chips for SARS-CoV-2 virus detection. Chapter 6 is focused on approaches to surface modify nylon membranes with dual-RCA for high-throughput and sensitive whole-cell detection of *E.coli* O157:H7 in foods. Finally, Chapter 7 provides the conclusions, outlooks, and scholarly contribution.

References

1. Food Microbial Pathogen Detection and Analysis Using DNA Microarray Technologies. Foodborne Pathogens and Disease, 2008. **5**(4): p. 531-550.
2. Luo, S.-C., et al., Nanofabricated SERS-active substrates for single-molecule to virus detection in vitro: A review. Biosensors and Bioelectronics, 2014. **61**: p. 232-240.
3. Sadik, O.A., A.K. Wanekaya, and S. Andreescu, Advances in analytical technologies for environmental protection and public safety. J Environ Monit, 2004. **6**(6): p. 513-22.
4. Stewart, E.J., Growing Unculturable Bacteria. Journal of Bacteriology, 2012. **194**(16): p. 4151-4160.
5. Smyth, W.F., Recent applications of capillary electrophoresis-electrospray ionisation-mass spectrometry in drug analysis. ELECTROPHORESIS, 2005. **26**(7-8): p. 1334-1357.
6. Gravesen, P., J. Branebjerg, and O.S. Jensen, Microfluidics-a review. Journal of Micromechanics and Microengineering, 1993. **3**(4): p. 168-182.
7. Tanaka, R., et al., A novel enhancement assay for immunochromatographic test strips using gold nanoparticles. Analytical and Bioanalytical Chemistry, 2006. **385**(8): p. 1414-1420.
8. Kwiatek, O., et al., Quantitative one-step real-time RT-PCR for the fast detection of the four genotypes of PPRV. Journal of Virological Methods, 2010. **165**(2): p. 168-177.
9. Morbioli, G.G., et al., Technical aspects and challenges of colorimetric detection with microfluidic paper-based analytical devices (μPADs) - A review. Analytica Chimica Acta, 2017. **970**: p. 1-22.
10. Dalmasso, A., et al., A multiplex PCR assay for the identification of animal species in feedstuffs. Molecular and Cellular Probes, 2004. **18**(2): p. 81-87.
11. Engvall, E., [28] Enzyme immunoassay ELISA and EMIT, in Methods in Enzymology. 1980, Academic Press. p. 419-439.
12. Soleymani, L. and F. Li, Mechanistic Challenges and Advantages of Biosensor Miniaturization into the Nanoscale. ACS Sensors, 2017. **2**(4): p. 458-467.
13. Kim, Y., J. Gonzales, and Y. Zheng, Sensitivity-Enhancing Strategies in Optical Biosensing. Small, 2021. **17**(4): p. 2004988.
14. Roy, L., P. Buragohain, and V. Borse, Strategies for sensitivity enhancement of point-of-care devices. Biosensors and Bioelectronics: X, 2021: p. 100098.
15. Jiang, Y., et al., Developing a dual-RCA microfluidic platform for sensitive *E.coli* O157: H7 whole-cell detections. Analytica Chimica Acta, 2020. **1127**: p. 79-88.
16. Li, S., et al., *In situ* rolling circle amplification surface modifications to improve *E.coli* O157: H7 capturing performances for rapid and sensitive microfluidic detection applications. Analytica Chimica Acta, 2021. **1150**: p. 338229.
17. Hao, X., et al., Aptamer surface functionalization of microfluidic devices using dendrimers as multi-handled templates and its application in sensitive

detections of foodborne pathogenic bacteria. Analytica chimica acta, 2019. **1056**: p. 96-107.
18. Qin, Y., et al., Developing a non-fouling hybrid microfluidic device for applications in circulating tumour cell detections. Colloids and Surfaces B: Biointerfaces, 2017. **151**: p. 39-46.

Chapter 2 Literature Review:

A review of Sensitivity-enhancing Approaches in Affinity-based Biosensing: Surface Modification Materials and Strategies

Abstract

Surface modification is among the most widely used approaches for improving the performance of biosensing assays, as it can significantly enhance biorecognition and signal transduction by providing the detection surface with improved properties, such as increased surface area, a higher number of bioligand binding sites, improved electron transduction, and enhanced antifouling property. However, a summarization of surface modification materials and strategies for improving the detection sensitivity of affinity-based biosensors has been overlooked. Therefore, various surface modification materials and approaches employed on affinity-based biosensing platforms for sensitivity improvement reported in recent years have been reviewed and discussed here. After elaborating on the advantages and disadvantages of each surface modification strategy and providing relevant application examples, some design considerations for utilizing a combination of different surface modification methods are discussed. It is hoped that this review can offer biosensor designers a more comprehensive overview to compare several surface modification materials and strategies to utilize the most suitable one based on their design criteria.

2.1 Introduction

Biosensing as a technique for rapid detection and/or quantification of biological analytes has been widely used in food safety, medical care, and public health [1-4]. Common biological targets include chemicals, bacteria, viruses, peptides, proteins, and nucleic acids [5-10]. Since conventional detection methods require expensive instruments, skilled personnel, and complex sample pre-treatment processes, it takes several days to weeks to get the results [11, 12]. In contrast, the biosensing assays simplify the sample preparation steps and also require lower sample volumes and therefore have the advantages of being fast turnaround, portable, easy to use, cost-effective, and suitable for on-site detection [13-15]. As a result of these advantages, some commercialized biosensing devices, such as blood glucose meters and pregnancy testing papers, can be rountinely used without supervisons from the health care professionals. However, the detection sensitivities of most biosensing devices can be influenced by target concentration, sample preparation method, and sample matrix due to simplified pre-treatment and scale-downed sample volume [16-18]. For example, detection sensitivities of biosensors may be reduced because of unexpected protein adsorptions on detection surfaces [19, 20]. As detection sensitivity is regarded as one of the critical parameters to determine the performance of biosensing devices, different sensitivity-enhancing strategies have been suggested and summarized into three main categories [1, 21]: 1) amplifying the biosensing signal using nanoparticles or nuclear acid amplifications to improve detection limits; 2) introducing fluid mixing and analyte concentrating schemes to increase analyte–sensor contact; and 3) a combination of these two approaches. However, this classification is incomplete since it does not include surface modification methods as one of the most useful sensitivity-enhancing strategies.

Biosensing generally involves two major steps--biorecognition and signal transduction [1, 22]. The biorecognition step includes the recognition and separation of the analytes from their surrounding matrix based on the bioaffinity mechanism via specific

interactions between the targets and their corresponding detection ligands on the detection surfaces. The most commonly used detection ligands are antibodies and aptamers [1, 21, 22], as reported in about 80% of the publications. Besides antibodies and aptamers, other types of detection ligands include peptides [23], receptors [24], and molecularly imprinted polymers (artificial antibodies) [25]. The efficiency of biorecognition is an important factor for the detection sensitivity and is determined by the binding kinetics of the detection ligand and the target [22, 26]. The binding kinetics of the biorecognition reaction is described by the equation below [27]

$$[\mathrm{PL}] = \frac{[\mathrm{P}]\times[\mathrm{L}]}{\mathrm{K_d}} \qquad (1)$$

in which [P] is the bulk concentration of the detection target, [L] is the number of ligands on the detection surface, [PL] is the number of targets captured by surface ligands, and K_d is the dissociation constant. Based on this equation, the detection sensitivity can be improved in three ways: 1) by increasing the number of ligands on the detection surfaces, 2) by improving the bulk concentration of analytes, and 3) by decreasing the dissociation constant. For example, target pre-enrichment using magnetic nanoparticles or pre-amplification using genetic amplification methods, such as polymerase chain reaction (PCR) and loop-mediated isothermal amplification (LAMP), have been reported as effective ways of improving the bulk concentration of the detection target [28, 29]. Additionally, surface modification using multi-handed dendrimers or surface rolling circle amplification (RCA) are also effective ways to improve the density of surface detection ligands [19, 30]. Finally, many studies have attempted to lower the dissociation constant of biosensors by manipulating the reaction environment properties, such as pH, temperature, and ionic concentration [31-33].

The signal transduction step translates the information of the biorecognition events into readable outputs, such as electrical, optical, or magnetic signals [1, 22]. The signal transduction efficiency is another critical factor influencing the detection sensitivity, and it is usually influenced by signal intensities as well as background noises [22, 34]. Signal amplification is one of the major methods of signal enhancement. For instance,

nucleic acid amplification techniques, such as RCA, LAMP, and PCR, have been widely used to amplify signals in DNA-based detection systems [35-37]; nanoparticle-based amplification methods using gold nanoparticles (AuNPs), magnetic nanoparticles, quantum dots (QDs), and silver nanoparticles (AgNPs) have also been widely utilized to amplify the detection signals of many optical biosensors [7, 38]; amplification methods based on enzymes, such as horseradish peroxidase, catalase, and glucose oxidase have been reported as effective methods to improve the detection sensitivity by catalyzing the conversion of chromogenic substrates into colored products [39-41]. As background noises influence the signal-to-noise ratio (S/N), thereby affecting detection sensitivities, reducing background noises is another possible approach to improve detection sensitivity [34, 42]. Many surface blocking agents, such as poly(amidoamine) (PAMAM) dendrimers, bovine serum albumin (BSA), and poly(ethylene glycol) (PEG) have been reported to lower the background signals by reducing nonspecific adsorptions, thus enhancing the S/N [39, 43, 44]. Moreover, blocking agents can also provide the detection surfaces with homogeneous functional groups that can further conjugate with detection ligands for target capturing. For example, dendrimers are reported to not only block the detection surfaces and prevent nonspecific adsorption, but also provide multiple functional groups for immobilization of aptamers to detect *E.coli* O157:H7 and circulating tumor cells [45, 46]. In addition, these surface blocking materials can be also combined with signal-amplification complexes, such as QDs, AuNPs, and horseradish peroxidase to enhance the detection signals [7-9].

In previous reviews, methods for improving signal transduction by signal amplification and surface anti-fouling approaches have been well summarized [42, 47-50]. However, improving the biorecognition unit, specifically by enhancing surface-ligand density, is mostly overlooked, resulting in challenges in selecting proper methods to design biosensing surfaces. Therefore, surface modification materials and strategies for improving detection sensitivity (Figure 2.1) have been summarized in the current review. Moreover, examples of surface design procedures as well as the advantages and

disadvantages of each surface modification method are provided. The ultimate goal of the authors is that this review can provide sensor designers with an overview of different surface modification approaches so that they can compare several strategies and utilize the most suitable one based on their design criteria.

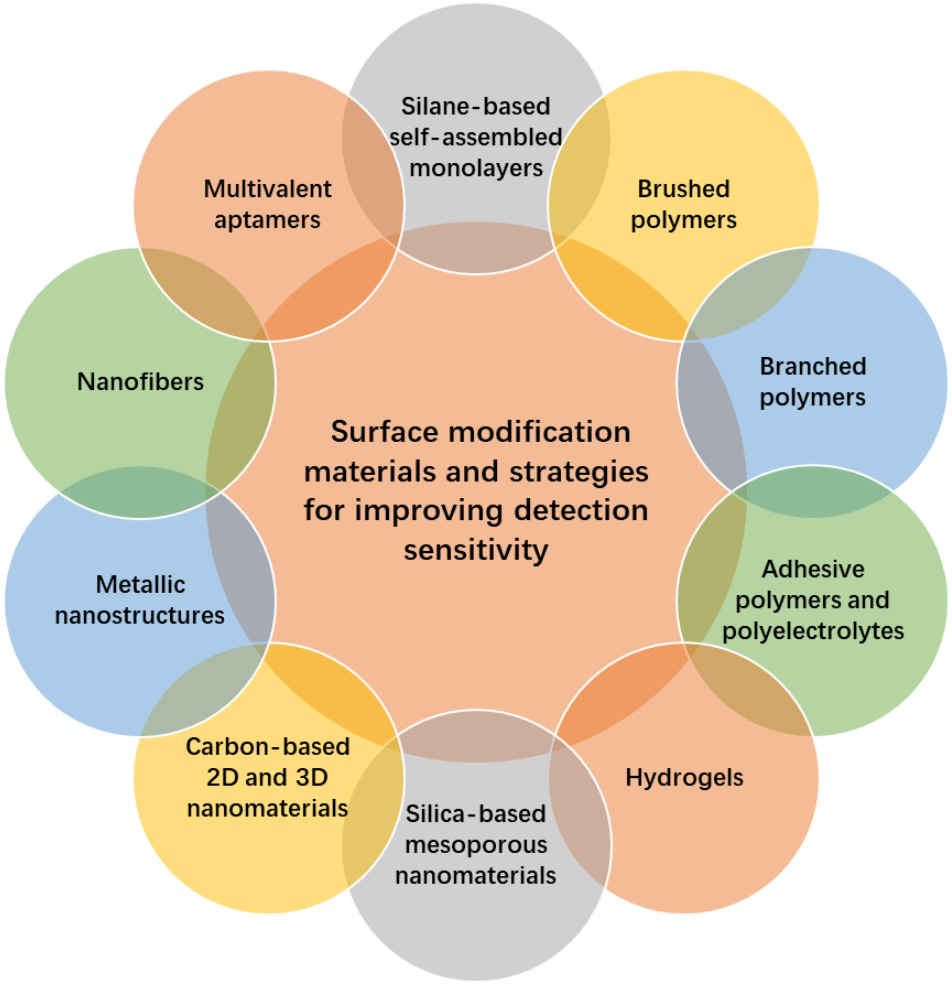

Figure 2.1. Surface modification materials and strategies for improving detection sensitivity.

2.2 Physical Adsorption and Surface Activation

For bioaffinity-based biosensing, the detection ligands need to be attached to the detection surfaces, such as glass and poly(styrene) (PS) substrates or gold nanoparticles, to achieve the biorecognition of targets. Hence, the quantity and quality of the detection ligands attached to the detection surfaces determine the detection sensitivity, which greatly relies on the methods employed to immobilize the ligands on the detection surfaces [51]. Therefore, finding a surface modification method for attaching a high

number of detection ligands with minimum bioactivity loss on the detection surfaces is critical for achieving higher detection sensitivity [18, 51, 52]. Physical adsorption is one of the most straightforward surface modification methods [18, 51-53]. In this method, the bioligands are directly introduced to the surfaces and physically adsorbed on the surfaces via van der Waals forces, hydrogen bonding, electrostatic adsorption, or hydrophobic interactions. The physical adsorption-based methods have the advantage of achieving simple and fast ligand immobilizing on the surfaces compared to other methods that may need surface pre-treatment steps as well as controlling temperature and humidity [54, 55]. However, unlike the covalent bond, the physical adsorption forces are weaker and less stable. Consequently, physically-adsorbed detection ligands suffer from random orientation and exchanging, which can negatively influence the quantity and quality of the surface ligands resulting in a lower detection sensitivity [18, 56-58]. Moreover, the physical adsorbed ligands may be weak against variations in pH, solution ionic content, and temperature resulting in low reproducibility [53, 59, 60]. To improve the quantity and quality of surface detection ligands in the case of physical adsorption, several surface activation strategies have been used so that detection ligands can covalently bind to the detection surfaces.

To form covalent bonds with detection ligands, activation methods are required to introduce chemically active functional groups, such as carboxyl, amino, and hydroxyl, on the detection surface since most detection-substrate materials, such as PS, glass, and polydimethylsiloxane (PDMS), are chemically inert [61-67]. Surface activation, the most critical step in the surface modification process, can be achieved by either wet or dry chemistries as the two common methods to create surface functional groups. In wet chemistry methods, oxidizing agents such as H_2SO_4, HCl, KOH, H_2O_2, and HNO_3 are typically involved in generating oxygen-containing moieties on the surfaces [68]. For example, PS surfaces treated with $KMnO_4$-H_2SO_4 solution at 60 $^{\circ}$C for 30 min can generate carboxyl groups [61-63], glass surfaces treated with a methanol-HCl solution for 30 min can generate hydroxyl groups, and poly(ethylene) (PE) and poly(propylene)

(PP) processed with $KMnO_4$-H_2CrO_4/H_2SO_4 solution can be enriched by oxygen-containing surface functional groups [69-73]. However, wet chemical methods are non-specific as they result in various oxygen-containing function groups on the surfaces. Moreover, chemical agents generally oxidize the side chain of the polymers; therefore, surface functionalization may not be reproducible between polymers with different molecular weights, crystallinity, or tacticity. More importantly, the abovementioned wet reactions require corrosive reagents that generate hazardous chemical waste and can even result in a nonuniform surface etching, thus making it unsuitable and impractical for conventional biochemistry laboratories [74]. In contrast, dry chemistry methods modify the substrate surfaces without using corrosive reagents, making these methods much "cleaner" and the final surface less damaged and smoother compared with wet chemistry methods [68, 74]. Commonly used dry chemistry approaches include plasma, UV light, radiation, and ozone treatments [68]. For example, plasma, as the most widely used dry chemistry method, can be equipped with different gas sources and thus generate various functional groups on the surfaces of different substrates (Table 2.1). The UV/ozone methods can etch PS and PDMS surfaces to generate hydroxyl groups on the surfaces [75, 76].

Table 2.1. Functional groups generated on the surface of substrate materials treated by plasma using different gases.

Plasma Gas	Generated functional groups	Substrate material*	References
Oxygen	Oxygen-containing functional groups	PCL, PE, PET, PDMS, glass, and PS	[70, 77-81]
Carbon dioxide	Carboxyl functional groups	PP, PS, and PE	[82-84]
Ammonia, nitrogen, and allylamine	Amine functional groups	PS, PTFE, and PDMS	[83, 85-87]
Inert gases	Radical sites	PTFE, PE, PET, and PVDF	[88-92]

*Abbreviations: poly(caprolactone) (PCL), poly(ethylene) (PE), poly(ethylene terephthalate) (PET), poly(dimethylsiloxane) (PDMS), poly(styrene) (PS), poly(tetrafluoroethylene) (PTFE), poly(vinylidene fluoride) (PVDF), and poly(propylene) (PP)

Besides forming covalent bonds with detection ligands, detection surface functional groups formed in the surface activation step can be used for covalent binding of other surface-modifying agents, such as dendrimers, brushed polymers, and nanoparticles, in order to further improve the detection performance of the surface. Since the details of these conjugations depend on the type of coating material used for surface modification, the next section discusses different surface modification approaches, providing examples of how these materials can cover the detection surface and result in improved detection sensitivity.

2.3 Surface modification materials and strategies for improving detection sensitivity

2.3.1 Surface modification with silane-based self-assembled monolayers (SAMs)

Silane-based self-assembled monolayers (SAMs) are a large group of coating materials widely used to modify surface-activated detection substrates. The electrophilic alkoxy pockets of silane molecules can rapidly react with nucleophilic centers (*e.g.,* hydroxyl groups) of the activated substrates to form silanol bonds (-O-Si-) on the surfaces [93-95]. As a result, the silane-treated surfaces can be enriched with various functional groups, such as amino, epoxy, or chloro, depending on the head groups of silane molecules (Figure 2.2A). Such silane derivatives provide multiple surface modification strategies (Table 2.2) to covalently immobilize bioligands on the detection surfaces via direct or indirect methods (*i.e.,* post-modification with other surface coatings), thus offering higher ligand immobilization density and better ligand binding stability in comparison with physical adsorption-based methods [95, 96]. For example, Dixit et al. improved the detection sensitivity of a typical enzyme-linked immunosorbent assay (ELISA) by covalently immobilizing antibodies on 3-aminopropyltriethoxysilane (APTES) modified 96-well plates (Figure 2.2B) [95]. In this protocol, they initially activated the surface of the 96-well plate with KOH and O_2 plasma, after which the activated plates were treated with APTES to enrich the surfaces with amino functional groups. Subsequently, the antibodies were covalently immobilized on the APTES-

treated surface via N-hydroxysuccinimide/1-ethyl-3-(3-dimethylaminopropyl)carbodiimide hydrochloride (NHS/EDC) reactions. Since covalent antibody immobilization results in a higher density of primary antibodies on the detection surfaces, the results showed that this APTES ELISA procedure is 16-times more sensitive than the standard ELISA working based on physical adsorption. Huang et al. also used a similar approach by covalently binding antibodies on the APTES-modified silicon surface [97]. The surface-antibody binding was improved by 32%, and the antigen-binding was elevated by 16% compared to the physical adsorption-based method.

Moreover, the SAMs can be pre-synthesized with other polymers to achieve better surface immobilization of bioligands. For example, Pirri et al. synthesized silane-based copoly(DMA−NAS−MAPS) using radical copolymerization of N, N-dimethylacrylamide, N-acryloyloxysuccinimide, and 3-(trimethoxysilyl)propyl methacrylate to modify the glass substrate for immobilizing amino-modified DNA molecules on the surfaces [98]. The copoly(DMA-NAS-MAPS)-modified glass showed 10-times higher DNA enrichment density than conventional silanization methods and also reduced the nonspecific adsorption of interfering biomolecules onto the glass surface. When the copoly(DMA-NAS-MAPS) was employed on a silicon nitride substrate to develop an aptamer-based bioassay for thrombin analysis (Figure 2.2C) [99], the copoly(DMA-NAS-MAPS)-modified assay showed 4-times improved detection sensitivity in comparison with the surface modification by a conventional silanization method using (3-Glycidyloxypropyl)trimethoxysilane.

In addition, SAMs with -Br and -Cl head groups can be treated with NaN_3 to result in -N_3 functional groups for achieving “click” reactions [100, 101]. For example, Chen et al. have reported a biosensor using aptamer-functionalized mesoporous silica nanoparticles (MSNs) for fluorescence detection of thrombin (Figure 2.2D) [102]. In their study, MSNs were functionalized by trimethyl chlorosilane and further azidated

with NaN_3, after which the azidated MSNs were loaded with fluorescein (signaling probe) and were subsequently capped with alkyne modified double-strand DNA via the “click" chemistry method to block the pores of MSNs. These aptamer-functionalized MSNs can be triggered by thrombin to release fluorescein for achieving detection purposes. This “click" chemistry-modified MSN system has the advantage of nearly zero leakage of signaling probes and also shows better stability and reproducibility. In contrast, in other MSN-based detection systems in which aptamers are electrostatically adsorbed on the surface of MSNs to block their pores [103, 104], the pore-blocking stability may be easily affected by changes in external conditions.

For the convenience of readers in selecting the appropriate SAMs for their applications, a list of frequently used SAMs, their functional groups, and their possible reactive groups is provided in Table 2.2. For further detailed information regarding bioconjugation reactions and cross-linker selections, the reader is referred to [68, 105].

Table 2.2. Frequently used silane-based self-assembled monolayers (SAMs), their functional groups, and their possible reactive groups.

Name	Surface functional groups	Possible reactive groups
3-(Aminopropyl)triethoxysilane	$-NH_2$	-COOH (NHS/EDC reaction) [105], -SH (NHS ester and maleimide linkers) [105], and $-NH_2$ (-NHS ester linkers (both ends)) [105], and epoxy groups [106]
3-(Mercaptopropyl)trimethoxysilane	-SH*	-SH (maleimide linkers (both ends)) [105], -C=O (maleimide and hydrazide linker) [105], $-NH_2$ (NHS ester and maleimide linkers) [105], $-N_3$ (iodoacetamide alkyne linker, click chemistry) [107], -C=C (thiol-ene Click reactions) [108], Acrylate/ methacrylate (thiol-ene, click reactions) [108], -C=N=O [109],and epoxy groups [110]
3-(Isocyanatopropyl)triethoxysilane	-C=N=O	$-NH_2$ [111], -OH [111], -SH [109]
3-(Bromopropyl)trimethoxysilane	-Br (changed to $-N_3$ by NaN_3)	alkynes (click reactions) [100]
3-(Chloropropyl)triethoxysilane	-Cl (changed to $-N_3$ by NaN_3)	alkynes (click reactions) [101]
3-(Azidopropyl)triethoxysilane	$-N_3$	alkynes (click reactions) [112]
3-(Trimethoxysilyl)propyl acrylate/methacrylate	acrylate/ methacrylate	-SH (thiol-ene, click reactions) [108], and acrylate/ methacrylate (polymerization) [113]
3-(Glycidyloxypropyl)trimethoxysilane	epoxy	$-NH_2$ [106], -COOH [114], -SH [110], -OH [114], and anhydrides [115]

*Note: thiols can be oxidized to disulfides, so the reaction should be processed with protective gases.

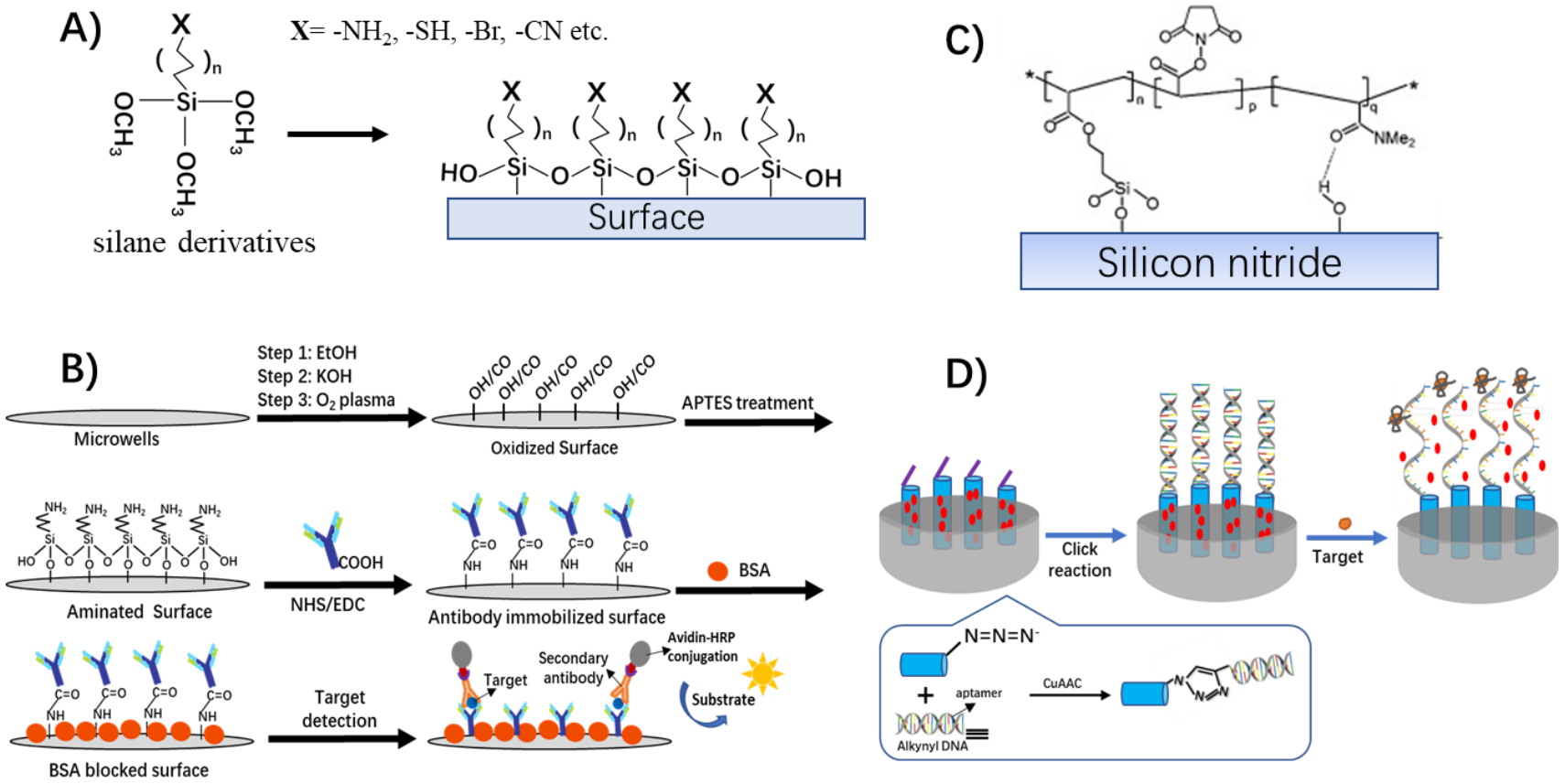

Figure 2.2. Surface modification using silane-based self-assembled monolayers (SAMs) for biosensing applications. A) Structure of silane derivatives-modified surface. B) Modification of 96-well plate surface using APTES and antibody immobilization strategy [95]. C) Surface structure of copoly(DMA-NAS-MAPS)-modified silicon nitride [99]. D) Synthesis of aptamer-functionalized MSN-based controlled release system for thrombin detection [102].

2.3.2 Surface modification with brushed polymers

Brushed or linear polymers are commonly applied on detection surfaces to provide more functional groups for improving bioligand binding capacity [116]. Since brushed polymers can be synthesized with different functional groups at both ends, they can easily conjugate on different detection surfaces via one end and leave the other functional groups for the conjugation of other desired biomolecules. Unlike silane-based SAMs, the hydrophilic brushed polymers form an extremely thin polymer film on the coated surfaces that provides excellent non-fouling properties to reduce non-specific interactions on detection surfaces [116]. These brushed polymers can also act as spacers and provide detection ligands with better conjugation orientations, increased flexibility, and improved bioactivity when tethering the bioligands to the detection surfaces [68]. Poly(ethylene glycol) (PEG) is one of the most frequently used brushed polymers to improve the performance of biosensors [68, 117, 118]. For example, when PEG was applied to link antibodies on the detection surfaces, the system showed reduced non-specific protein adsorptions, and the surface-conjugated antibodies were more stable against denaturation, thus greatly improving detection sensitivity [117]. Furthermore, using a PEG linker tethers the ssDNA on the detection surface of a DNA hybridization sensor which improves the detection sensitivity in comparison with the direct binding method due to the fact that the PEG linker significantly reduces steric hindrance for DNA hybridization [118].

Recently, newly developed brushed polymers were employed to improve the detection sensitivity of different biosensors. For example, poly(oligo(ethylene glycol) methyl ether methacrylate) (POEGMA) was employed to surface modify a gold-based biosensor to improve the detection sensitivity of a cardiac disease biomarker detection [119]. In this case, the POEGMA was grafted on the surface of the gold film via surface-initiated atom transfer radical polymerization, after which a sandwich immunoassay with signal amplification by silver nanotubes was employed on the POEGMA-modified surface for the biomarker detection (Figure 2.3A). The detection results showed that

using a POEGMA brush could intensify the detection signal 151 times and decrease the limit of detection (LOD) 14 times compared to the assay without POEGMA modification. Liu et al. prepared a silica particle-self-assembled monolayer on a glass slide and coated the particles with a poly(glycidyl methacrylate) (PGMA) brush layer to create high-performance three dimensional (3D) brush microarrays (Figure 2.3B) [120]. The coated polymer brushes contain abundant epoxy groups that can improve the number of surface detection ligands for enhancing the detection sensitivity. The resultant 3D microarrays were employed to study the interactions between monosaccharides with lectins. The final results showed that the 3D brush microarrays have higher reaction efficiencies and lower LODs (by at least 1 order of magnitude) in comparison to those of two-dimensional (2D) microarrays.

Moreover, some copolymer brushes can combine the properties of different unit polymers to achieve improved surface performances. For example, Lei et al. developed a microarray with surface modification using a multi-functional 3D polymer brush layer for protein and peptide analysis. Specifically, poly(glycidyl methacrylate-co-2-hydroxyethyl methacrylate) (poly (GMA-co-HEMA)) as multi-functional 3D polymer brushes were conjugated to an APTES-modified glass slide via surface-initiated atom transfer radical polymerization. The HEMA unit effectively prevents the nonspecific adsorption of biomolecules, and the GMA unit provides sufficient oxirane groups for the covalent immobilization of biomolecules (Figure 2.3C) [121]. When the abovementioned microarray was employed in rabbit antihuman immunoglobulin G (IgG) antibody assays, the results showed that the poly (GMA-co-HEMA) brush presented a 5 times higher ligand-binding capacity, improved surface hydrophilicity, and less nonspecific protein adsorption than the 2D IgG microarray, resulting in improved detection sensitivity. Recently, to improve the detection performance of traditional piezoelectric quartz crystal microbalance (QCM) sensors for Covid-19 detection, Forinová et al. applied poly(N-(2-hydroxypropyl) methacrylamide-co-carboxybetaine methacrylamide-co-sulfobetaine methacrylamide) (poly(HPMAA-co-

CBMAA-co-SBMAA)) brushes to surface modify the QCM chip, followed by conjugating capturing antibodies (against nucleocapsid protein) on the immobilized polymer brushes (Figure 2.3D) [122]. In this design, each unit of poly(HPMAA-co-CBMAA-co-SBMAA) brush has its specific function for detection sensitivity improvement: the HPMAA unit provides the detection surface with antifouling characteristics against nonionic adsorptions, the CBMAA unit provides multiple carboxyl groups for multivalent conjugation of antibodies, and the SBMAA unit enhances the antifouling property due to its permanent negative charge. This brush coating enables the system of sensitive Covid-19 detection in clinical samples with a LOD of 1.3×10^4 PFU/mL within only 20 minutes.

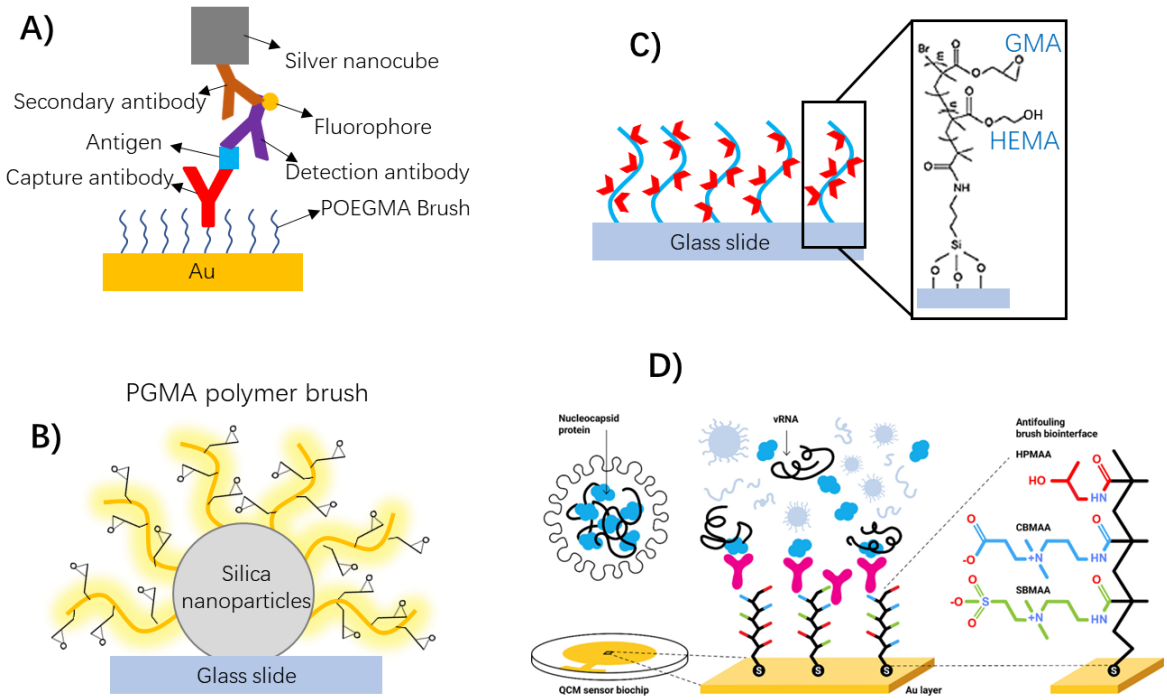

Figure 2.3. Examples of biosensors modified with brushed polymers for improvement of detection sensitivity. A) POEGMA modified gold-based biosensor for sensitive detection of cardiac biomarker B-type natriuretic peptide [119]. B) PGMA coated silica particle-based glycoprotein microarrays [120]. C) Poly (GMA-co-HEMA) modified antibody-based microarrays [121]. D) Piezoelectric quartz microbalance sensor chips with surface modification of poly(HPMAA-co-CBMAA-co-SBMAA) brush for sensitive detection of Covid-19, reprinted from Ref. [122] with copyright of American Chemical Society.

2.3.3 Surface modification with branched polymers

Dendrimers, such as poly(amidoamine) (PAMAM), poly(propyleneimine) (PPI), poly(ester amides), and phosphorus dendrimers, are a large group of branched polymers that have been extensively used to modify the surface of biosensors. Because of their highly branched structures, versatile terminal groups, and providing control of the number of functional groups by changing the generation, dendrimers offer the advantage of increasing the number of surface functional groups when they are immobilized on the detection substrates; therefore, the dendrimer-modified detection surfaces would have more binding sites for the conjugation of bioligands to improve the detection sensitivity. Moreover, dendrimers have excellent non-fouling properties against non-specific adsorptions on the detection surfaces, which lowers the background signals, thereby improving the S/N of the biosensors. Compared with their linear analogous (*i.e.,* brush coatings), dendrimer-modified detection surfaces have shown better detection sensitivity as well as non-fouling properties [123].

Recently, Hao et al. developed a dendrimer-aptamer-modified microfluidic device for *E.coli* detection (Figure 2.4A) [45]. In their design, the surfaces of APTES-modified microfluidic channels were covered with generation 7 (G7) PAMAM dendrimers; subsequently, *E.coli* aptamers were conjugated on the surface of these immobilized dendrimers. The results showed that G7 PAMAM modification results in a significantly increased number of aptamers on the surfaces of microfluidic channels as well as improved non-fouling characteristics in comparison with generation 4 (G4) PAMAM-modified surfaces, leading to a low LOD of 10^2 cells/mL. As another example, Idris et al. developed a PPI dendrimer-based electrochemical biosensor for alpha-feto protein detection [124]. In their protocol, AuNPs and generation 3 (G3) PPI dendrimers were electrodeposited on a glassy carbon electrode, followed by the conjugation of target-capturing antibodies on the surface of dendrimers. Their results showed a LOD of 0.00185 ng/mL, ten times lower than other similar immunosensors, highlighting the significance of the increased bioligand density and non-fouling properties of

dendrimer-modified surfaces. Han et al. developed a dendrimer-antibody-based ELISA by surface modification of a polyethylene-glycol (PEG)-functionalized 96 well-plate with G4 PAMAM dendrimers on which the capturing antibodies were conjugated from their Fc region [125]. Compared with conventional ELISA, the detection surfaces of this dendrimer-modified ELISA could conjugate more antibodies and also provide better orientation for antibodies, exposing their antigen-capturing sites (Fab regions) toward the targets. Authors also indicated that PAMAM dendrimers with hydroxyl terminal groups show less non-specific interactions with proteins than those with amino and carboxyl terminal groups. Their results showed the dendrimer-modified ELISA to be 8 times more sensitive compared with standard ELISA.

Moreover, dendrimers decorated with ferrocene have been proven to be an ideal material for modifying electrode surfaces as dendrimers improve the attachment of ferrocene to electrodes and play a key role as multielectron transfer mediators in electrochemical response processes [126]. For example, Kowalczyk et al. used this surface modification strategy in designing an electrochemical sensor for the sensitive detection of C-reactive protein in blood samples (Figure 2.4B) [127]. They immobilized poly(ethyleneimine) (PEI) dendrimer-ferrocene complexes on an electrode surface and chemically conjugated target-specific antibodies on the surface of the PEI dendrimers. The results showed that dendrimers provided the most favorable binding orientation of antibodies, improved the surface density of antibodies, and enhanced electron transfer. Compared with conventional designs, this ferrocene/PEI/antibody sensor showed a wider linear range, from 1 to 5104 ng/mL, and a lower LOD of 0.5 ng/mL.

Two points should be considered when using the dendrimers to improve the detection sensitivity of biosensing platforms: 1) overcrowding: after a certain point, to continue increasing the number of detection ligands on the surface of dendrimers may result in overcrowding of the ligands, which reduces the flexibility or changes the structures of the bioligands, both affecting the target capturing ability [68]; and 2) surface

deactivation: after conjugation of detection ligands on the surface of dendrimers, the unreacted functional groups need to be deactivated to avoid other biomolecules binding to dendrimers, as non-specific biomolecules binding may result in the increase of background signals and can also disrupt the functionalities of detection ligands. The deactivation step is also important for the non-fouling properties of dendrimer-modified surfaces, as different procedures result in different terminal groups that may influence the non-fouling characteristic of the surface. For example, to quench NHS/EDC-activated carboxyl dendrimer-modified surface, ethylenediamine treatment will result in converting the original carboxyl groups to amino functional groups, ethanolamine treatment will result in surfaces with hydroxyl functional groups, and increasing the pH to over 8.0 will rapidly hydrolyze the NHS esters to regenerate the original carboxyl groups [105]. The amino groups on the dendrimer surfaces have been reported to adsorb more live cells than the carboxyl groups due to the negative charge of the live cells [46], and the hydroxyl groups have been proved to be more effective in reducing nonspecific adsorption of proteins than carboxyl and amino groups on dendrimers [125].

Branched peptides, also known as Y-shape peptides, are another type of branched materials that have also been widely used to modify the detection surfaces to improve the detection sensitivity of biosensors. As peptides are zwitterionic molecules containing both $-COO^-$ and $-HN_3^+$, the charged groups easily form a layer of hydration on the surface via hydrogen bonds, making the surface hydrophilic and decreasing non-specific protein adsorptions via hydrophobic bonds [128]. When peptide coating makes the net surface charge close to neutral, the peptide coatings can also prevent electrostatic adsorptions[128]. For detection purposes, the branched peptides can be employed as templates, similar to dendrimers, to conjugate multiple copies of bioligands for target-capturing improvement [129, 130]. For example, Wang et al. developed a branched peptide-based aptasensor for the sensitive detection of breast cancer genes [129]. In this case, branched zwitterionic peptides were immobilized on the surface of a conducting polymer, followed by conjugating aptamers against target genes on the branches of the

peptides. The surface-immobilized branched zwitterionic peptides act as templates by allowing more aptamer conjugations and also render the detection surface non-fouling, enabling the sensitive detection of targets in 5% (v/v) human plasma with a LOD of 0.03 fM, about 57 times more sensitive than previous PEG-based sensors [131]. In addition, Liu et al. developed an ultra low-fouling electrochemical aptasensor for cancer cell quantification based on anti-fouling branched peptides (Figure 2.4C) [130]. They covalently immobilized branched zwitterionic peptides onto electrodeposited polyaniline films. The branched peptides improved the non-fouling properties of the detection surface, preventing the non-specific adsorption of cells and proteins. After conjugating aptamers (against MCF-7 breast cancer cells) on the branches of the immobilized peptides, the sensor exhibited excellent detection sensitivity and selectivity with a LOD as low as 20 cells/mL and a linear response range from 50 to 10^6 cells/mL. They proved that the non-fouling characteristic of the branched peptide-modified surfaces was significantly superior to that observed with linear peptides and PEGs.

Moreover, branched peptides with recognition domains (*i.e.,* peptide aptamers) can also be used as an all-in-one unit to capture the targets [128, 132], which has the advantages of simple surface chemical treatments and high chemical and conformational stability[128]. For example, Liu et al. developed antifouling biosensors for protein quantification in serum samples based on all-in-one branched peptides (Figure 2.4D) [132]. In this design, unlike the peptide-aptamer sensor, the branched peptides were designed with recognizing sequences for capturing the targets alongside the antifouling sequences ((AVWGRWHD)4(KE)2KE-) for improving the surface non-fouling properties. This all-in-one design has the advantages of an improved number of detection ligands, enhanced non-fouling properties, eliminated secondary chemical conjugation steps, and well-orientated capturing sequences. The assay showed a broader linear detection range, from 0.1 ng/mL to 10 μg/mL, and a lower LOD (45 pg/mL, S/N = 3) compared to the previous reports. Due to the excellent anti-fouling

feature of the detection surfaces in this design, the results showed good reproducibility, having a relative standard deviation of 2.49%.

As one of the most important limitations of using branched peptides, the non-fouling property of the branched peptides depends on the net charge of the modified surface. As a result, the anti-fouling sequences need to be appropriately designed to ensure that the branched peptide-modified surfaces would be nearly neutral, complicating the overall design process. Moreover, the generation of the most branched peptides is limited to two, making them have much fewer branches than most dendrimers. Therefore, the detection sensitivity of branched peptide-modified biosensors might be inferior to the ones using dendrimer-based surface modifications.

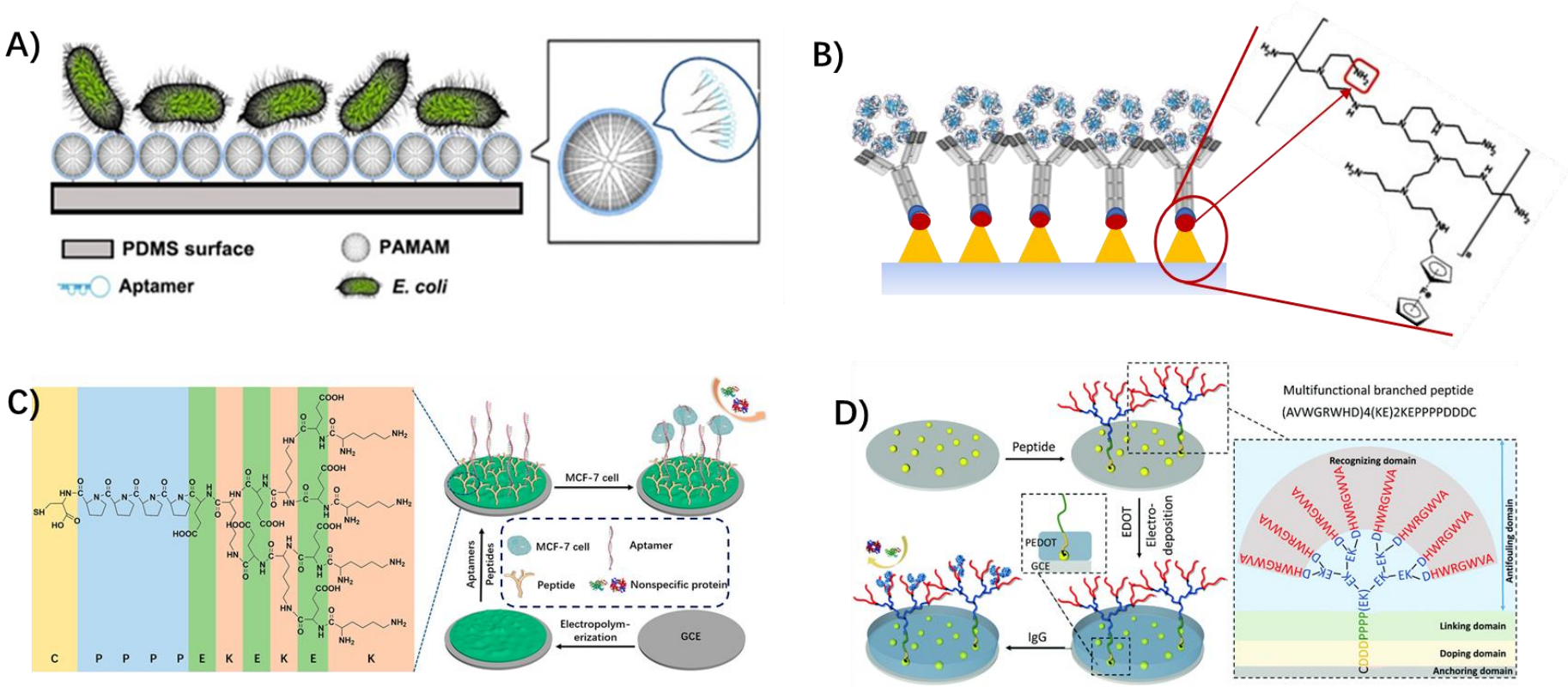

Figure 2.4. Examples of biosensor designs with surface modification using dendrimers or branched peptides for detection sensitivity improvement. A) Microfluidic channels with surface modification of G7 PAMAM dendrimers and aptamers for *E.coli* detection [45]. B) Electrode surface modification using poly(ethyleneimine) dendrimer decorated with ferrocene and antibodies for detection of C-reactive protein [127]. C) Electrodeposited polyaniline film modified with branched peptides/aptamers for detection of breast cancer cells, reprinted from Ref. [130] with permission of American Chemical Society. D) Detection surface modified with all-in-one branched peptides for detection of IgG in blood serum, reprinted from Ref. [132] with permission of American Chemical Society.

2.3.4 Surface modification with bioinspired adhesive polymers and polyelectrolytes

Polydopamine (PDA) is a bioinspired polymer widely used in the surface modification of biosensors [133-135]. The PDA presents excellent adhesive properties, which makes it easy to be deposited on all types of inorganic and organic substrates [133-135]. For example, Lee et al. synthesized PDA film via self-polymerization of dopamine and deposited the PDA films on a wide range of materials, including noble metals, oxides, polymers, semiconductors, and ceramics [136]. Moreover, the quinones on the surface of PDA films are reported to easily react with other functional groups such as amines, imidazoles, and thiols via Michael addition reactions (Figure 2.5A) [137]; therefore, the PDA can be employed as anchoring points for further surface immobilization of other biomolecules. Additionally, compared with the widely used NHS/EDC approach, the quinone-amine reaction is reported to be more resistant to hydrolysis, resulting in higher reaction efficiency [138]. A study also showed that electrodes modified with PDA film yield more IgG binding capacity than the ones modified with traditional poly(pyrrole), showing the great potential of PDA surface modification in improving the surface ligands density [139]. However, since PDA is chemically active, non-specific adsorptions can easily take place on the PDA-modified surfaces. To solve this problem, PDA is often combined with other antifouling materials before being used for modifying the sensor surfaces [140, 141]. For example, Xu et al. developed an electrochemical biosensor for the detection of a tumor biomarker by surface modification of a glass carbon electrode with copolymerized PDA and poly (sulfobetaine methacrylate) (PSBMA) (Figure 2.5C) [140]. This modified surface provides two functions: 1) PDA can conjugate many aptamers via thiol groups on the detection surface for improved target capturing, and 2) PSBMA, as a zwitterionic polymer, makes the sensing interface non-fouling. The detection results showed that the modified sensor had excellent sensitivity with a LOD of 3.3 fg/mL and was able to analyze real human serum samples with a satisfying accuracy because of the improved antifouling property. Another recent study employed a one-step surface modification of

gold electrodes using PDA and ethanolamine to develop an antibody-based bioassay (Figure 2.5D) [141]. In this study, the non-fouling properties and detection sensitivity were compared with the two-step functionalization strategies (*i.e.,* surface modification with PDA then blocked with ethanolamine). The results indicated that the one-step method showed better surface non-fouling property and detection sensitivity in comparison with the two-step modification approach. The authors also demonstrated that the presence of ethanolamine not only had minor influence on the immobilization of antibodies, but also improved the specific recognition of the targets. Due to the presence of ethanolamine as a surface blocker, the biosensor did not need any further blocking steps using BSA buffers during the whole analysis process.

Chitosan is another bioinspired polymer synthesized by the deacetylation of chitin extracted from the exoskeleton of shellfish or crustaceans [142]. Chitosan and its derivatives have been reported as popular surface coating materials for improving the detection sensitivity of biosensors [143-145]. Chitosan, as a polycationic polymer with one amino group and two hydroxyl groups on its backbone (Figure 2.5B), shows positive charges on its amine groups when pH<pKa (usually pH=6.5), allowing it to be adsorbed on negatively charged materials to form composites or multilayer structures via electrostatic forces. In contrast, at basic pHs, the amines are not in their ionized form, which promotes chemical reactions when reacting with activated carboxylic acids (*i.e.,* NHS esters) or aldehydes [142, 146]. Moreover, the solubility of chitosan in an aqueous solution can be adjusted by changing the pH (usually soluble below pH 6.5), making the thickness of the chitosan coatings on the detection surfaces controllable [142, 146]. Solution casting is the most straightforward method to deposit chitosan coatings on the detection surface; however, spin coating is usually employed if denser and smoother coatings are desired [142, 147]. In addition, layer-by-layer assembly and electrodeposition can also be used to achieve the desired surface structure [146].

The porous morphology of chitosan films makes it possible to entrap large-sized

biomolecules inside the film via co-deposition methods (*i.e.,* mixing biomolecules in the chitosan solution before deposition) for detection purposes [142, 147]. For example, an optical detection sensor was developed by depositing a chitosan solution containing tyrosinase on a microscope glass slide via spin coating [147]. The target molecules (*i.e.,* phenol) could penetrate the chitosan film to be oxidized by tyrosinase, resulting in color changes. Although chitosan films with entrapped biomolecules are simply prepared using co-deposition methods, this approach is barely employed in affinity-based biosensors as it is unstable for bioligand immobilization, resulting in leakage of the bioligands during the detection. Furthermore, co-deposition methods are unsuitable for detecting large molecules since these large molecules cannot diffuse into the porous chitosan film.

In contrast with co-deposition methods, for most affinity-based biosensors, bioligands are usually immobilized after modifying the detection surfaces with chitosan coatings [142, 146, 148, 149]. For example, the negatively charged bioligands can be rapidly adsorbed on the chitosan-modified surfaces by electrostatic interactions because of the positive charge of the chitosan chains [148, 149]. The amino and hydroxyl functional groups on the chitosan backbone can also provide various chemical strategies to covalently bind bioligands on the detection surfaces [150-152]. Moreover, to expand the applications of chitosan in different detection platforms, various chitosan derivatives have also been synthesized to provide more diverse backbone structures, such as sugar-modified, phosphorylated, quaternized, cyclodextrin linked, thiolated, sulfated, and azidated, to conjugate with various types of materials [142]. Recently, Li et al. developed a piezoelectric biosensor for chicken immunoglobulin Y detection using a QCM sensor with carboxymethyl chitosan surface modification that was subsequently immobilized with mouse anti-chicken immunoglobulin Y antibodies. (Figure 2.5E) [153]. This chitosan coating features two advantages: 1) provides the detection surface with abundant carboxymethyl groups for amine coupling of antibodies, which creates a more stable baseline signal, improving data repeatability

after surface regeneration; and 2) reduces non-specific bindings on detection surfaces due to its polyampholyte and hydrophilic nature. Because of these advantages, the results showed that the carboxymethyl chitosan-modified sensor presented a LOD down to 270 ng/mL, more sensitive than a carboxymethyl cellulose-modified sensor used for comparison.

Poly(allylamine hydrochloride) (PAH) and poly (4-styrene sulfonate) (PSS) are two important polyelectrolytes that have been extensively used in the fabrication of AuNP-based biosensors [154-157]. As a cationic polyelectrolyte, PAH can provide the detection substrates with positive charges to adsorb negatively charged AuNPs. This PAH surface modification is normally combined with PSS to form multilayer structures (*i.e.,* PAH/PSS/PAH) (Figure 2.5F, graph in the middle). Since PSS is an anionic polyelectrolyte, it can be coated on the surface of the PAH layer by electrostatic adherence and subsequently used for the immobilization of the next PAH layer. This layer-by-layer polyelectrolyte deposition method by PAH and PSS can provide a higher surface coverage of AuNPs immobilization compared with other positively charged surface coatings, such as APTES, ethylenediamine, and PEI, resulting in higher detection sensitivity [154, 156]. Depending on the size of AuNPs, the surface coverage of AuNPs is normally plateaued upon the adsorption of 10-20 layers of PAH/PSS bilayer structure [154, 158, 159]. However, when the surface coverage reaches a high level, the AuNPs tend to aggregate on the detection surface, which may reduce the signal intensity, broaden the peak band, and thus affect the sensor sensitivity [160, 161]. Recently, a copolymer of poly(styrene-b-4-vinyl pyridine) (*i.e.,* PS-b-P4VP) has been employed as an alternative to the PAH/PSS surface modification method in order to reduce the aggregation of AuNPs on the detection surfaces [155] (Figure 2.5F). The results showed that in comparison with other surface coating methods (*i.e.,* APTES, PAH/PSS, and poly(4-vinyl pyridine)), the PS-b-P4VP copolymer-modified surface was deposited by a monolayer of non-aggregated AuNPs with higher surface uniformity and coverage, leading to improved sensitivity and resolution for localized surface

plasmon resonance (LSPR) sensing. In addition to PAH/PSS, other polyelectrolytes, such as poly(diallyl dimethylammonium chloride) (+)/PSS(−) [162], PAH (+)/ poly(acrylic acid) (−) [163], and poly(diallyl dimethylammonium chloride)(+)/PSS(-) [164], can also be employed for sensor surface modifications. More detailed applications and examples can be found in a recent review [165].

It should be mentioned that the PDA and chitosan can be used as a part of the polyelectrolyte bilayer to improve the adhesiveness of the bilayer to surrounding materials, owning to the adhesive properties of PDA and chitosan. For example, the poly (acrylic acid-g-dopamine) (*i.e.,* PAA-dopamine)(-) and PAH (+) have been employed to modify different silicon-based substrates, such as quartz, silicon wafer, and glass slides [166]. The results showed that the PAA-dopamine/PAH layers presented excellent stability in highly acidic, basic, and concentrated salt solutions. This bilayer can be functionalized by combining thiol modifications and oxidization-induced cross-linking methods to further immobilize other biomolecules. In another study, a polyelectrolyte complex prepared by chitosan (+)/kappa-carrageenan (-) dopped with AuNPs encapsulating glucose oxidase was employed to modify a gold electrode for glucose sensing [167]. The chitosan in the polyelectrolyte complex improved the adhesiveness of the coating bilayer leading to an increased loading density of AuNPs and glucose oxidase, enhancing the detection performance of the glucose sensor.

However, there are two major limitations when using polyelectrolytes for layer-by-layer surface modification. First, external conditions, such as temperature, pH, and ionic content of the solvent, need to be carefully controlled as they may influence the electrical charge of the surfaces as well as the association rate of each adsorbed layer due to electrostatic adsorption. The second limitation is that this surface modification method is time-consuming. Since detection surfaces typically need 10-20 layers of polyelectrolyte bilayer to reach the maximum surface coverage of nanoparticles, the whole surface modification usually takes 4-6 hours to achieve the desired results, even

though it takes several minutes to assemble one single layer. Being time-consuming complicates the fabrication process and also accumulates errors in each assembled layer, limiting reproductivity among sensor chips.

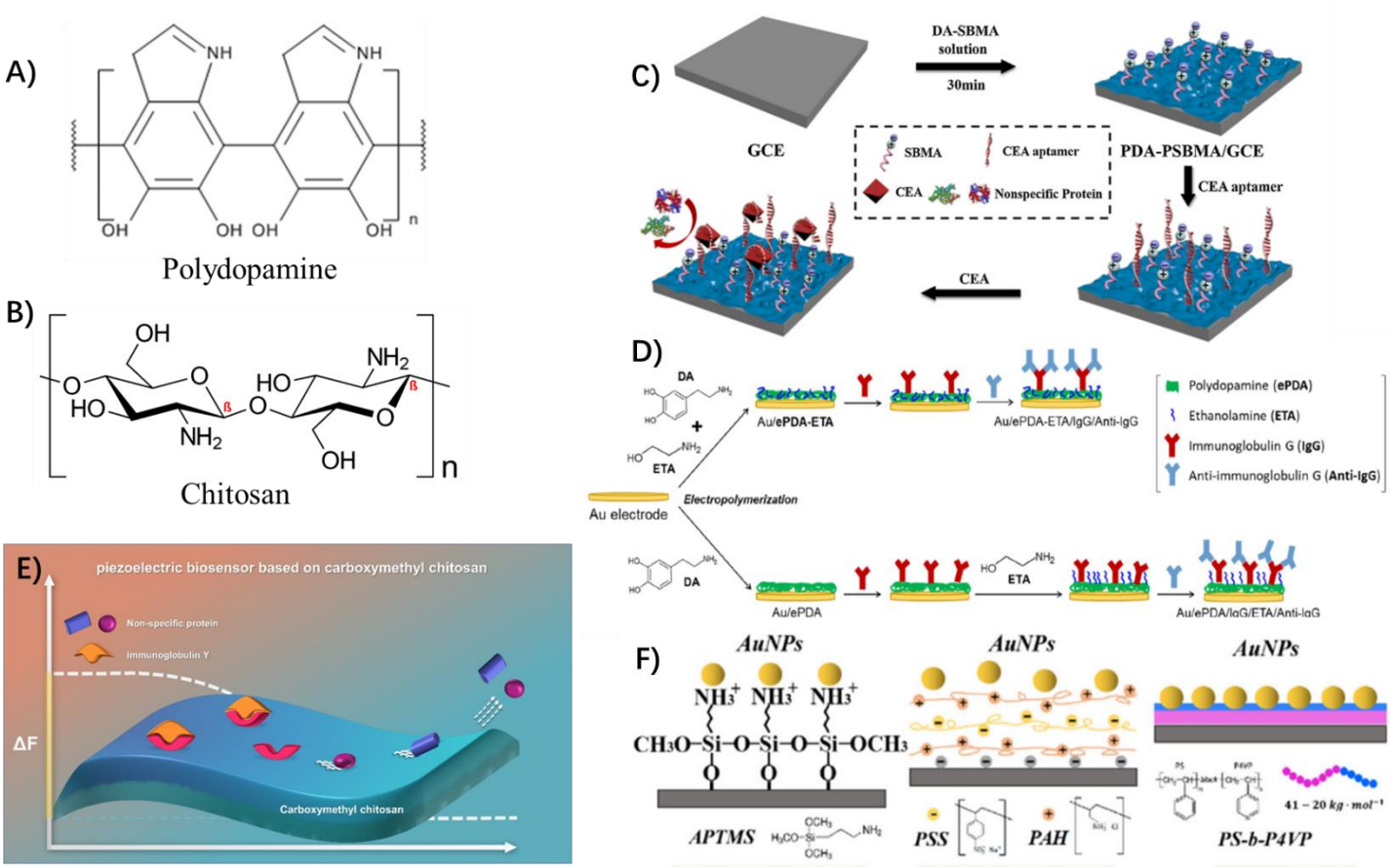

Figure 2.5. Chemical structure of polydopamine and chitosan and applications of bioinspired polymers and polyelectrolytes. A) Chemical structure of polydopamine. B) Chemical structure of chitosan. C) Surface modification of a glass carbon electrode with copolymerized PDA and PSBMA for detection of tumor biomarker; reprinted from Ref. [140] with permission of Elsevier. D) One-step surface modification of gold electrodes using PDA and ethanolamine to developed an antibody-based bioassay, reprinted from Ref. [141]. E) A piezoelectric biosensor based on carboxymethyl chitosan surface modification for chicken immunoglobulin Y detection, reprinted from Ref. [153] with permission of Elsevier. F) Surface modification of LSPR biosensor using poly(styrene-b-4-vinylpyridine) to reduce aggregations of AuNPs on the detection surfaces, reprinted from Ref. [155].

2.3.5 Surface modification with hydrogels

Hydrogel coatings have been extensively used to improve the performance of sensors [116, 168], as they offer a wide choice of functional groups, provide a large surface area, make 3D network structures, and have good biocompatibility [116, 168]. When hydrogels are used to modify the detection surfaces, the density of the detection ligands can be significantly improved compared to 2D surface modification methods [169, 170]. Hydrogels can trap various biomolecules inside their inner network structures, which can be subsequently broken based on changes in external conditions, releasing the entrapped biomolecules to achieve some "smart" designs for improving detection sensitivities [171-173].

Aptamer-based hydrogels can be fabricated by incorporating acrydite-modified aptamers into polyacrylamide gels during polymerization [169]. These hydrogels provide the detection surface with a high density of ligands due to their hydrophilicity and 3D structures. [169, 170]. Recently, Zezza et al. immobilized aptamer hydrogel on the glass surface and developed a microarray for ssDNA analysis (Figure 2.6A) [170]. They demonstrated that the aptamer hydrogel-modified surface significantly increased the binding capacity of ssDNA (2.36 pmol/cm^2) compared to the planar surface modification (0.08 pmol/cm^2) because the 3D structure of the hydrogel network provides more immobilization sites for detection aptamers. They also evidenced that the microarray showed low fluorescence background noise due to the excellent transparency of hydrogels, greatly decreasing the S/N and leading to high detection sensitivity. Aptamer-based hydrogel sensors can also achieve controlled release of signaling molecules for signal amplification designs [171, 172]. For example, Yan et al. developed a target-responsive aptamer hydrogel to detect non-glucose targets with glucometer readout (Figure 2.6B) [171]. In this design, a large amount of glucoamylase was trapped inside the aptamer hydrogel formed by hybridizing aptamers and their partially complementary DNA polymer strands. When target molecules are introduced, the aptamers detach from their complementary DNA polymer strands and bind to the

targets, resulting in the hydrogel breakdown and glucoamylase release. The released glucoamylase rapidly hydrolyzes the amylose to produce a large amount of glucose to be quantified using a glucometer.

Crosslinked dextran hydrogels have been employed in surface modification of surface plasmon resonance (SPR) sensor chips since the 1990s [174-176]. The 3D carboxymethyl dextran-modified SPR sensor surfaces (*i.e.,* gold film) feature better SPR sensitivity than 2D carboxyl surface modifications. For example, carboxymethyl dextran-coated SPR chips can detect analytes with molecular weights as low as 0.18 kDa [177]. Moreover, the carboxymethyl dextran-modified SPR sensor surfaces provide multiple carboxyl function groups as detection ligand binding sites, resulting in improved detection sensitivity. Recently, the applications of dextran hydrogels have been expanded to various groups of sensors, such as fluorescence [178, 179], electrochemical [180], and QCM sensors [181, 182]. For example, dextran-based QCM biosensors for studying antigen-antibody interactions have been fabricated by coating carboxymethyl dextran (2000 kDa) on the gold surface of the chip (Figure 2.6C) [181]. The performance of this sensor was compared with the ones modified by conventional carboxymethyl dextran (500 kDa) and 2D carboxyls. The results showed that the 3D carboxymethyl dextran (2000 kDa) surface outperformed 2D carboxyl and the traditional 3D carboxymethyl dextran (500 kDa) surfaces by 4 and 2 times higher protein immobilization, respectively. The 3D carboxymethyl dextran surface was also capable of sensitive detection (8.1 Hz) of small molecules with a molecular weight of 0.67 kDa.

PEG-based hydrogel coatings are also widely used to improve detection sensitivities [183-186]. The PEG macromers can be homobifunctional or heterobifunctional with different end groups, such as methyloxyl, carboxyl, amine, thiol, azide, vinyl sulfone, acetylene, and acrylate. The homobifunctional macromers are typically used to form hydrogel networks, while heterobifunctional macromers can introduce other functional

groups to bind with different biomolecules in the network structure of hydrogels [183, 184]. Recently, a hydrogel-based electrobiosensor was developed for antigen detection using surface modifications of electrodes with heparin-functionalized PEG hydrogel entrapping antibodies (Figure 2.6D) [184]. In this design, antibodies against human IgG were mixed with heparin-functionalized PEG hydrogel before hydrogel solidification in order to entrap the antibodies inside the hydrogel structure. Subsequently, this hydrogel was immobilized on the surface of the electrodes for impedance measurements of antigens. The results showed that this simple surface modification using hydrogel could greatly improve the detection sensitivity, achieving an ultralow LOD (down to the femtomolar levels) for antigen detection. For more examples, readers are recommended to consult some excellent reviews [169, 187, 188].

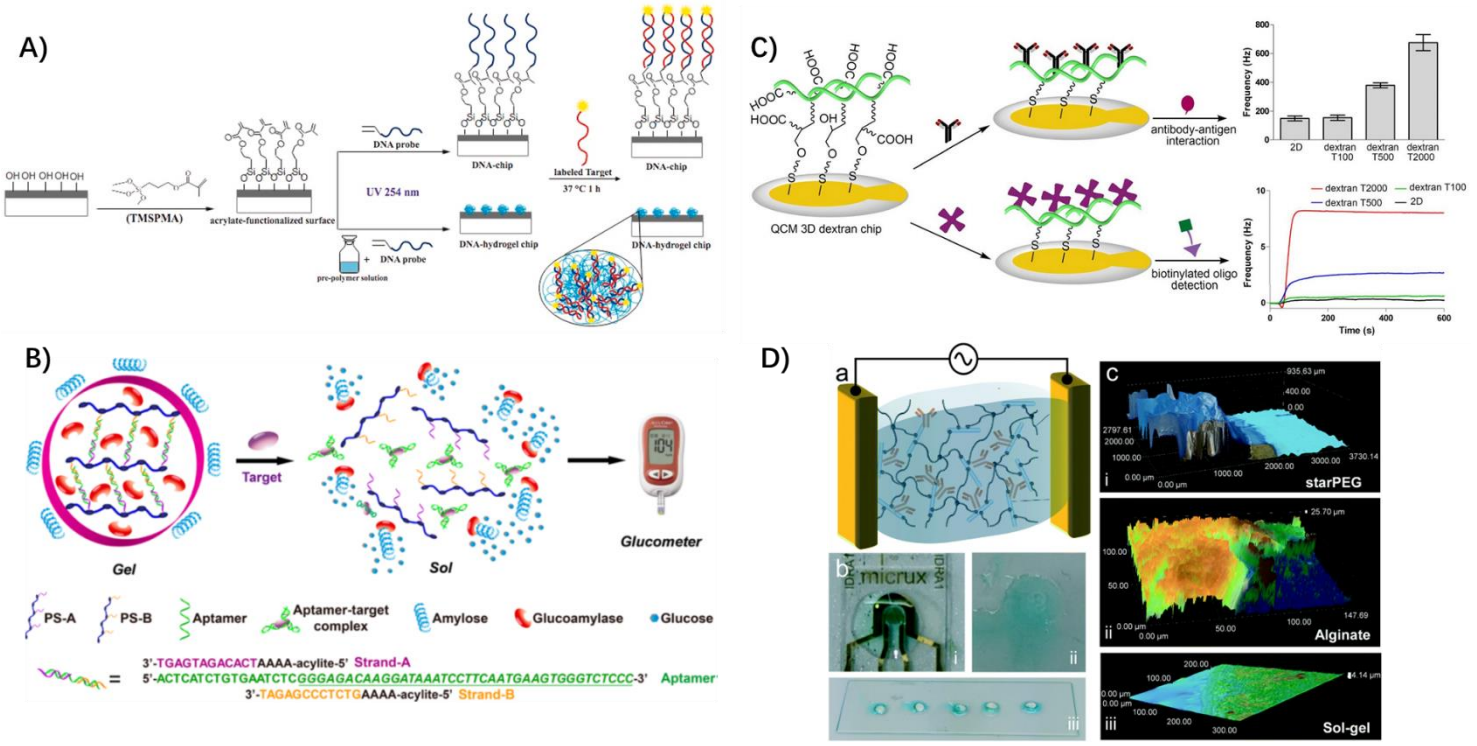

Figure 2.6. Examples of hydrogel-based biosensors. A) Immobilization process of oligonucleotides for both 2D and 3D microarrays, reprinted from Ref. [170]. B) A target-responsive aptamer hydrogel for detecting non-glucose targets with glucometer readout, reprinted from Ref. [171] with permission of American Chemical Society. C) 3D carboxymethyl dextran sensor chip surfaces for real-time detection of biomolecular interactions by a QCM biosensor, reprinted from Ref. [181]. D) A hydrogel with entrapped antibodies as surface modification of electrodes for impedance measurements, reprinted from Ref. [184].

2.3.6 Surface modification with silica-based mesoporous nanomaterials

Mesoporous materials have been employed as a class of excellent surface modification materials in biosensing devices due to their well-ordered mesostructures with distinctive properties of large surface area, narrow pore-size distribution, tunable pore sizes, mechanical stability, and easy surface functionalization [189, 190]. Because of these unique characteristics, mesoporous materials have been widely used alongside enzymes, aptamers, antibodies, and cells to greatly improve the detection sensitivities of different biosensing systems, such as electrochemical, fluorescent, and colorimetric biosensors [189, 190]. As some examples of reviews on the application of mesoporous materials in biosensing technology, Moritz et al. have classified different types of mesoporous materials as well as their principles and applications in biosciences [191]; Hasanzadeh et al. have reviewed mesoporous materials, including MCM-41, MCM-48, and SBA for applications in biosensors [189]; and Yang et al. have focused on reviewing the applications of mesoporous materials on the enzyme-based and enzyme-mimic biosensors [190].

As mesoporous materials provide larger surface areas than 2D materials, they offer superior bioligand immobilization ability, improving the detection sensitivity of biosensors [192, 193]. For example, an electrochemical aptasensor was developed using the surface modification of a gold electrode with mesoporous silica film (MSF) for sensitive detection of streptomycin (Figure 2.7A) [192]. Specifically, the MSF was coated on the surface of the gold electrode by electrodeposition, after which the coated surface was functionalized with APTES to introduce the sensor surface with amino functional groups. After this step, the amino-functionalized MSF was covalently conjugated with AgNPs that were further conjugated with aptamers to achieve the desired detection surface. In the presence of target molecules, the surface aptamers bind with targets, which hinders the diffusion of the redox probe hexacyanoferrate through the nanochannels of the mesoporous film, resulting in a signal decrease. The concentration of the target can be quantified based on the signal changes. Compared to

other similar devices, this sensor has been reported to have superior sensitivity, with a LOD of 0.33 fg/mL in milk and blood serum matrices. MSF not only provides a large surface area to bind more aptamers but also lets the targets rapidly infuse through the surface 3D matrix, providing a short characteristic diffusion time. These two factors promote the binding kinetic process, thus improving the detection sensitivity.

The large void spaces and controllable pore size allow mesoporous materials to load a high amount of signaling materials and be gated by other biomolecules, such as aptamers, antibodies, and proteins, to achieve a controlled-release biosensing design [103, 194, 195]. For example, Liu et al. developed an aptamer-gated system by surface modification of an electrode using vertically ordered MSF for sensitive detection of various targets (Figure 2.7B) [194]. In this design, the MSFs were immobilized on the surface of the electrode and then functionalized with amino groups. Subsequently, a large number of signaling molecules (*i.e.,* $Ru(bipy)_3^{2+}$) were loaded into the pores of the MSFs, and the pores were sealed by aptamers via electrostatic attraction between positively charged MSFs and negatively charged aptamers, resulting in a sensor surface ready for target detection. In the presence of targets, the aptamers bind with them and detach from the MSF surface, leading to ungated pores and subsequent release of signaling probes. The released signaling materials can cause a reduced electrochemiluminescence intensity that can be used to quantify the concentration of targets. This biosensor design was highly sensitive because a small number of targets can trigger a vast amount of signaling materials to release, resulting in significant and measurable changes in detection signals. The sensitivity of this biosensing assay was validated by employing three types of aptamers as the gating materials to detect lysozyme, adenosine, and K^+, outperforming other reported methods by having LODs of 0.06 nM, 0.75 nM, and 0.5 μM, respectively.

Although these controlled-release biosensing systems present high detection sensitivity, there also have some drawbacks. The first one is the leaking problem, meaning that the

unstable and insufficient capping may lead to the leaking of signaling material and cause false-positive results; therefore, using a proper surface immobilization method is essential. The capping method using electrostatic attraction between the mesoporous and capping materials, as mentioned in Figure 2.7B, is considered an easy-to-conduct and universal method but lacks stability, as the electrostatic attraction forces may easily be eliminated by external condition changes, such as ionic concentration, temperature, and pH, that results in the leakage of signaling material. In contrast with the electrostatic attraction-based method, covalent conjugation methods have been proven to be more stable in capping the pores [101, 196, 197]. Moreover, the aptamer-capping formats can also affect the detection performances of aptamer-capped mesoporous materials. For example, the capping aptamers with a "stopper" design (Figure 2.7C)— mesoporous materials are covalently conjugated with aptamers that can form a hairpin structure, and the hairpin structure is like a "stopper" to block off the pores — can experience secondary structure changes once binding to targets, resulting in leaving the pores open [197]. Therefore, this capping format typically has a fast target response because the pores are easy to open; however, inappropriate design may lead to failure or unstable capping, resulting in the leakage of signaling materials affecting detection sensitivity. Moreover, the capping aptamers with a "bridge" design (Figure 2.7D) — the mesoporous materials are covalently conjugated with ssDNA arms that are subsequently attached to aptamers via complementary base pairing to seal the pores — can separate from the ssDNA arms once binding to the targets, leading to open pores [196]. Although being more stable than the "stopper" design, there is a probability that ssDNA arms in the "bridge" design do not detach from the aptamers upon introduction of targets due to powerful base pairings between two sequences. This results in unreleased or slow-released signaling materials, leading to detection failure or limiting the detection speed.

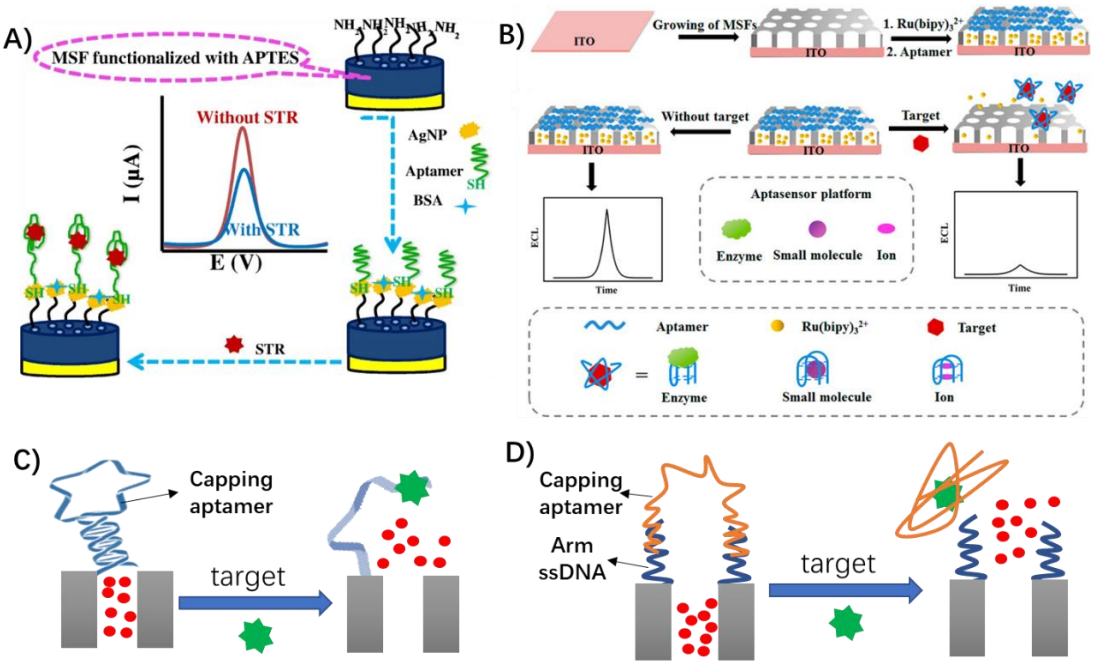

Figure 2.7. Examples of biosensors based on mesoporous materials for improving detection sensitivity and aptamer capping formats of mesoporous materials for controlled-release biosensing systems. A) A gold electrode with surface modification using mesoporous silica film for sensitive detection of streptomycin, reprinted from Ref. [192] with permission of Springer Nature. B) A controlled-release biosensing system using electrodes with surface modification using aptamer-gated mesoporous silica film loaded with signaling materials for sensitive detection of different targets, reprinted from Ref. [194] with permission of American Chemical Society. C) Capping aptamers with "stopper" design. D) Capping aptamers with "bridge" design.

2.3.7 Surface modification with carbon-based 2D and 3D nanomaterials

Graphene-based materials, including graphene, graphene oxide (GO), and reduced graphene oxide (rGO), have been reported as excellent 2D materials for improving the detection sensitivity of different biosensors as they feature large surface area (2630 m^2/g) [198], excellent thermal conductivity (above 3000 W/mK) [199], high electron transfer rate (2.5 × 105 $cm^2/V/s$) [199], and capability to immobilize different molecules [200]. For example, studies have shown that modifying the detection surfaces of electrochemical sensors with graphene-based materials can significantly improve detection sensitivity. This is because these graphene-based materials not only promote electron transfer between bioreceptors and transducers, which results in improved signal sensitivity, but also enhance the number of bioreceptors on the detection surfaces due to their large surface area, which results in an increased target

capturing ability [200-204]. Moreover, graphene-based materials have very high transparency (*i.e.,* 98% with a single-layer or double-layer graphene [199]) as well as excellent fluorescent-quenching ability [205-207], which makes them suitable for being widely used in optical biosensors to achieve "signal-on-off" designs [205-207]. Recently, Zhang et al. developed a "signal-off" fluorescent aptasensor based on fluorescence-labeled double-stranded DNA on a GO nanosheet for ochratoxin A (OTA) detection (Figure 2.8B) [208]. Specifically, the OTA aptamers were hybridized with their complementary DNA sequences labeled with fluorescein (*i.e.,* cDNA-FAM probes) to form double-stranded conjugates that coexisted with GO, showing fluorescence signals. However, once there were OTA molecules in the detection system, the OTA was captured by the aptamers, resulting in the release of cDNA-FAM probes. The free probes were adsorbed onto the GO nanosheets, resulting in a fluorescence "signal-off" because of the signal quenching through fluorescence resonance energy transfer. The concentration of the OTA can be quantified based on the change in the signal intensity after target capturing. This aptasensor exhibited superior sensitivity (LOD 11 pg/mL) in comparison with other nanomaterials and single-stranded DNA-based aptasensors.

Since the surface chemical structures of the graphene-based materials are different, sensor surfaces modified by different graphene-based materials present different surface properties; therefore, different post-surface-modification approaches are employed to conjugate other molecules. Pristine graphene is known to be relatively inert with low chemical reactivity and solubility, as the surface shows few active functional groups (Figure 2.8A). Therefore, the immobilization of biomolecules on the surface of graphene can be achieved in three ways [209, 210]: 1) by generating oxygen-containing functional groups, such as epoxy bridges, hydroxyl, and carboxyl groups, via oxidizing the graphene for further covalent binding of biomolecules, 2) by forming covalent bonds between free radicals or dienophiles and C═C bonds of pristine graphene; and 3) by forming non-covalent immobilization via π–π stacking interactions between biomolecules and pristine graphene. In contrast with pristine graphene, GO is

an oxidized product of graphene that contains carboxyl groups at the edge and hydroxyl and epoxy groups on the basal plane, while the remaining regions are unmodified (Figure 2.8A). These chemical structures provide abundant functional groups for GO to tether with other biomolecules, which gives GO unique properties. For example, carboxyl groups provide GO with pH-dependent negative charges that can promote electrostatic interaction with positively charged biomolecules, hydroxyl and epoxide groups make GO hydrophilic, and the unchanged structures enable GO to bind with biomolecules via π–π interactions [209, 210]. The rGO, as a result of GO reduction by thermal or chemical treatments [211], has similar functional groups as GO but less surface oxygen content, resulting in less negative surface charge as well as inferior water dispersibility and hydrophilicity. Because of having different properties, the effects are different when applying GO and rGO to improve biosensor performance. For example, a recent study investigated GO and rGO as AuNPs supporting materials in an LSPR biosensor [212]. The results indicated that rGO surpassed GO in improving the detection sensitivity of AuNPs-based LSPR biosensors because the rGO-supported AuNPs showed greater dispersion and enhanced stability, inhibiting agglomerations of AuNPs through closer contact between rGO and AuNPs.

Graphene-based materials can be deposited on the surfaces of biosensors via different techniques such as drop-casting, spin-coating, and electrostatic interaction-based methods on positively charged surfaces [213]. Electrophoretic deposition and electrochemical reduction of GO are also two widely used methods for coating inert surfaces with graphene-based materials with different chemical derivatives [213]. Since graphene-based materials need to be dispersed into a solution matrix before being immobilized on the surfaces, dispersivity would be an important property of graphene-based materials being applied on sensor surfaces; however, it is hard to achieve a homogenous dispersion because of π–π interactions that can result in the restacking of graphene layers, leading to ununiformed surfaces. Various methods have been developed to overcome this issue by functionalizing graphene with different molecules,

such as isocyanates, aliphatic amines, and aromatics, to achieve stable dispersions in organic solvents [210, 214]. However, these functionalizations may affect some electrical and mechanical properties of graphene-based materials [210]. In addition, grafting graphene with polymers or adding surfactants or small molecules containing aromatic rings can also improve the dispersivity of graphene-based materials in polar aprotic solvents without damaging the as-mentioned properties [214-217].

Multi-walled carbon nanotubes (MWCNTs) are the 3D format of multiply-nested single-walled carbon nanotubes (*i.e.,* a wrapped sheet of graphene) (Figure 2.8A). Compared with graphene, MWCNTs have the same chemical properties but tubular structures with variable diameters up to 100 nm and lengths ranging from a few nanometers to several micrometers [218]. Because of their unique structure, MWCNTs feature many unique properties, such as large surface areas, good electrical conductivity, tunable lengths, and high strength [218], which make MWCNTs ideal candidates to be employed on the surfaces of biosensors to improve their detection performances [219-222]. For example, Zhou et al. developed a simple electrochemical aptasensor for the sensitive detection of tetracycline [223]. After immobilizing COOH-MWCNTs on the surface of the glassy carbon electrode by drop-casting, they conjugated the amino-modified anti-tetracycline aptamers on the surface-coated MWCNTs by NHS/EDC chemistry, resulting in an aptasensor ready for target detection. In the presence of tetracycline, the aptamers conjugate to targets, leading to a reduced peak current signal that can be used to quantify the target concentration. The results showed that the sensor could detect tetracycline with high specificity and a LOD of 0.005 μM, more sensitive than other similar devices. The sensitivity improvement is because of the fact that the MWCNT coating provides the sensor better conductivity and biocompatibility, improving the Faradaic current changes upon analyte binding.

Moreover, the MWCNTs can also be used with other surface modification materials, such as AuNPs, dendrimers, and chitosan, to modify the detection surfaces [222, 224,

225]. For example, Güner et al. developed an electrochemical immunosensor for sensitive *E.coli* detection by immobilizing antibodies on a graphite electrode coated with a nanocomposite film consisting of polypyrrole, AuNPs, MWCNT, and chitosan (*i.e.,* /PPy/AuNP/MWCNT@Chi) (Figure 2.8C) [222]. The results indicated that this biosensor was more sensitive than similar reported devices, with a LOD of 30 CFU/mL in PBS buffer. They have shown that the detection sensitivity improvement came from the following advantages: 1) polypyrrole provided the film with excellent electrical conductivity and stability, 2) AuNPs improved the adsorption capacity of antibodies and generated electrochemical signal, thereby improving the detection sensitivity, 3) MWCNTs provided a higher surface area on the electrodes to accommodate more antibodies on the detection surface, and 4) chitosan provided the film-forming ability and excellent adhesion for the nanocomposite film and also rendered the coated surface with abundant functional groups so that a large number of pyrrole can be conjugated to improve the electron transfer.

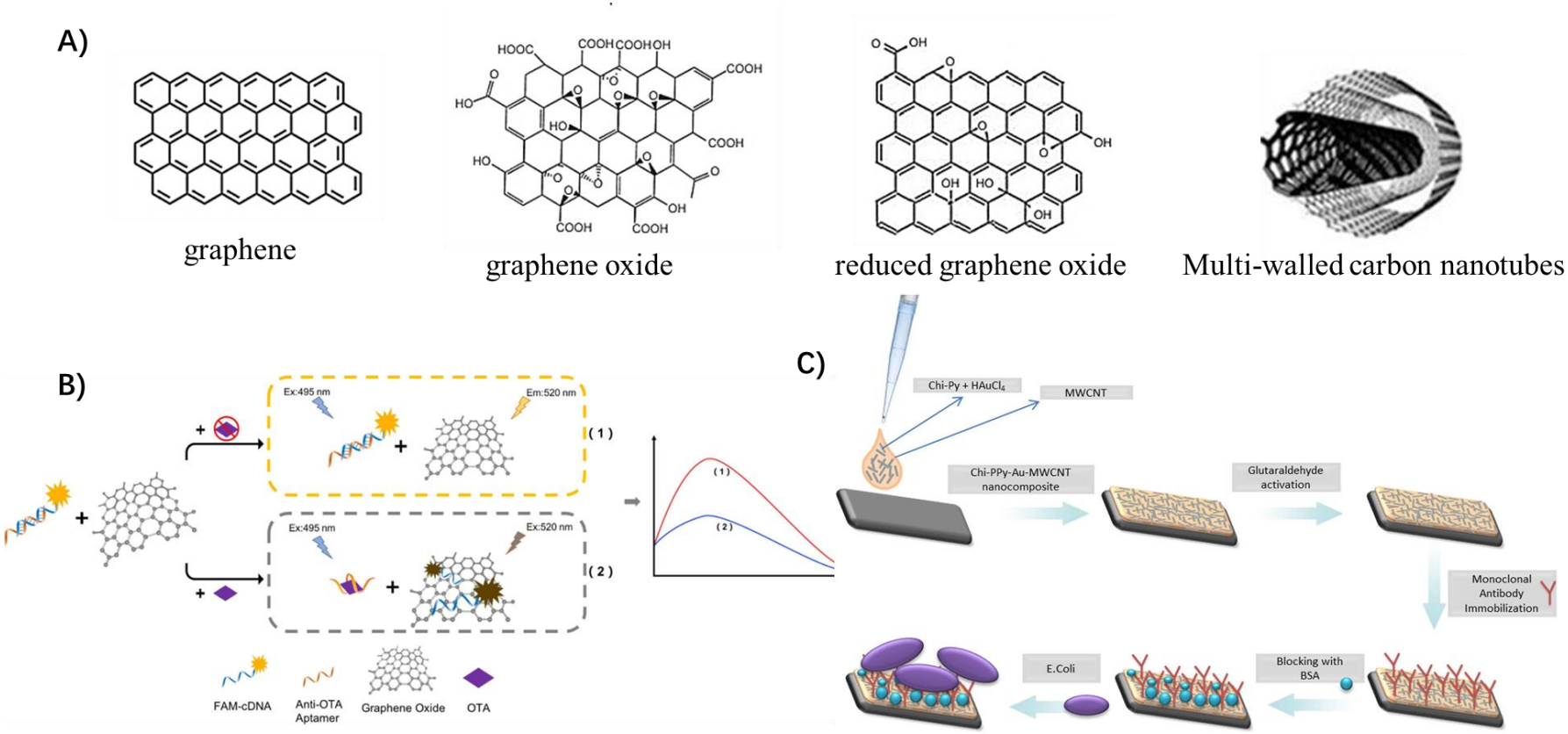

Figure 2.8. Chemical structure of carbon-based materials and their applications in biosensing technology. A) Chemical structures of graphene, graphene oxide, reduced graphene oxide, and multi-walled carbon nanotubes. B) A "signal-off" design using graphene oxide nanosheet and aptamers for ochratoxin A detection, reprinted from Ref. [208]. C) An electrochemical immunosensor for sensitive detection of *E.coli* by surface modification of a graphite electrode using /PPy/AuNP/MWCNT@Chi nanocomposite film, reprinted from Ref. [222] with permission of Elsevier

2.3.8 Surface modification with metallic nanostructures

Metallic nanostructured materials have been proven to provide excellent properties when employed in the surface modification of biosensors. Detection surfaces with modification of nanostructures may have the following advantages [226, 227]. Firstly, the nanostructured surfaces have 2× to 1000× larger surface areas than the surfaces modified by planar materials, so they can load a more significant number of bioligands without changing the overall surface dimensions. Moreover, when nanostructures are applied on the surface of the electrodes, the increased surface area can result in higher currents and enhanced S/N, leading to better detection sensitivity. Besides, the nanostructured surfaces present superior conductivity when applied to electrochemical biosensors, which benefits electron transduction, leading to higher and sharper current peaks for target detection. In addition, the nanostructures on the detection surfaces can be designed to form controlled or random morphology, which benefits the immobilized biomolecules to present better orientations and structures, improving bioactivities and stabilities. Furthermore, some nanostructures on the detection surfaces can mimic enzyme activity to catalyze the conversion of certain substrates to transduce detection signals. Finally, compared with enzyme-immobilized detection surfaces, the surfaces with metallic nanostructure modification are more stable against changes in external conditions [226, 227].

Surface modification with metallic nanostructures can be achieved by the top-down and bottom-up approaches: 1) the top-down approach is to sculpt the nanostructures on the surface of the substrates by breaking down the bulk material using etching, dealloying, laser ablation, or lithographic patterning; and 2) the bottom-up techniques use different templates, such as alumina, porous materials, and self-assembled metal nanoparticles, on the surfaces of substrates to grow into different types of nanostructures [227, 228]. Different shapes of nanostructures, such as nanoparticles, nanorods, nanowires, and nanoflowers, have been employed on the detection surfaces to improve the sensitivity of biosensors [229-233]. For example, Li et al. developed a nanowire-based

electrochemical biosensor to simultaneously detect penicillin and tetracycline (Figure 2.9A) [229]. In this design, vertically aligned Pt-Au nanowires were electrodeposited on the surface of an anodic aluminum oxide membrane, after which Au segments were immobilized with L-cysteine for capturing tetracycline, and Pt nanowire segments were coated with Au nanoparticles conjugated with penicillinase enzyme. The sensor showed high sensitivity in the simultaneous detection of penicillin and tetracycline because of the hybrid nanowire/nanoparticle structures. As another example, Hu et al. designed a sandwich antibody bioassay by surface modification of glass substrate with zinc oxide (ZnO) nanorods coated with poly(oligo(ethylene glycol) methacrylate-co-glycidyl methacrylate (*i.e.,* POEGMA-co-GMA) conjugated with primary antibodies for sensitive detection of cancer biomarkers (Figure 2.9B) [230]. In this assay, the ZnO nanorods acted as surface backbones to immobilize a high number of polymer brushes and amplify the fluorescence signals from the cy3-labeled secondary antibodies without the risk of fluorescence quenching. The POEGMA-co-GMA brushes provided non-fouling properties to the nanorods to reduce non-specific adsorptions and tether with target-capturing antibodies. The results showed that the bioassay offers an excellent LOD of 100 fg/mL for detecting cancer biomarkers in human serum. Recently, Subramani et al. modified polyimide surfaces with aptamer-conjugated nanoflowers to develop a bioassay for sensitively detecting β-lactoglobulin in milk samples (Figure 2.9C) [231]. Because of the high aptamer loading efficiency of the nanoflowers, the bioassay presented an excellent LOD (down to 1 ag/ml) for detecting β-lactoglobulin in milk samples and showed a broad linear detection range from 1 ag/ml to 100 fg/ml. The LOD and linear range were proved superior to the traditional ELISA [231]. In addition, Mahshid et al. developed a nanostructured microelectrode to improve the detection performance of electrochemical steric hindrance hybridization assay for quantitative detection of large proteins (*e.g.,* antibodies) [232]. As shown in Figure 2.9D, the electrodes were surface electrodeposited with nanoclusters of Pd that were further conjugated with capturing DNAs. These capturing DNAs can hybridize with their complementary ssDNA sequences (*i.e.,* signaling DNA) capped with methylene blue

(*i.e.,* a redox-active label) at one end and recognition elements specific to the protein of interest at the other end. In the absence of target molecules, the capturing DNAs on the surface bind to signaling DNAs, resulting in the redox labels on the signaling DNAs attaching to the surface of nanoclusters, which leads to a high electrochemical signal. However, in the presence of target proteins, they can bind with recognition elements on signaling DNAs to cause fewer copies of signaling DNAs on surface of nanoclusters due to steric hindrance, which leads to a signal decrease. In comparison with conventional macro electrodes, the nanostructured electrodes presented higher detection sensitivity and allowed using longer singling oligonucleotide strands to detect proteins. Additionally, nanostructured surfaces have larger surface areas that allows them to immobilize a higher density of long capturing DNAs, leading to a higher efficiency in hybridization with longer signaling strands.

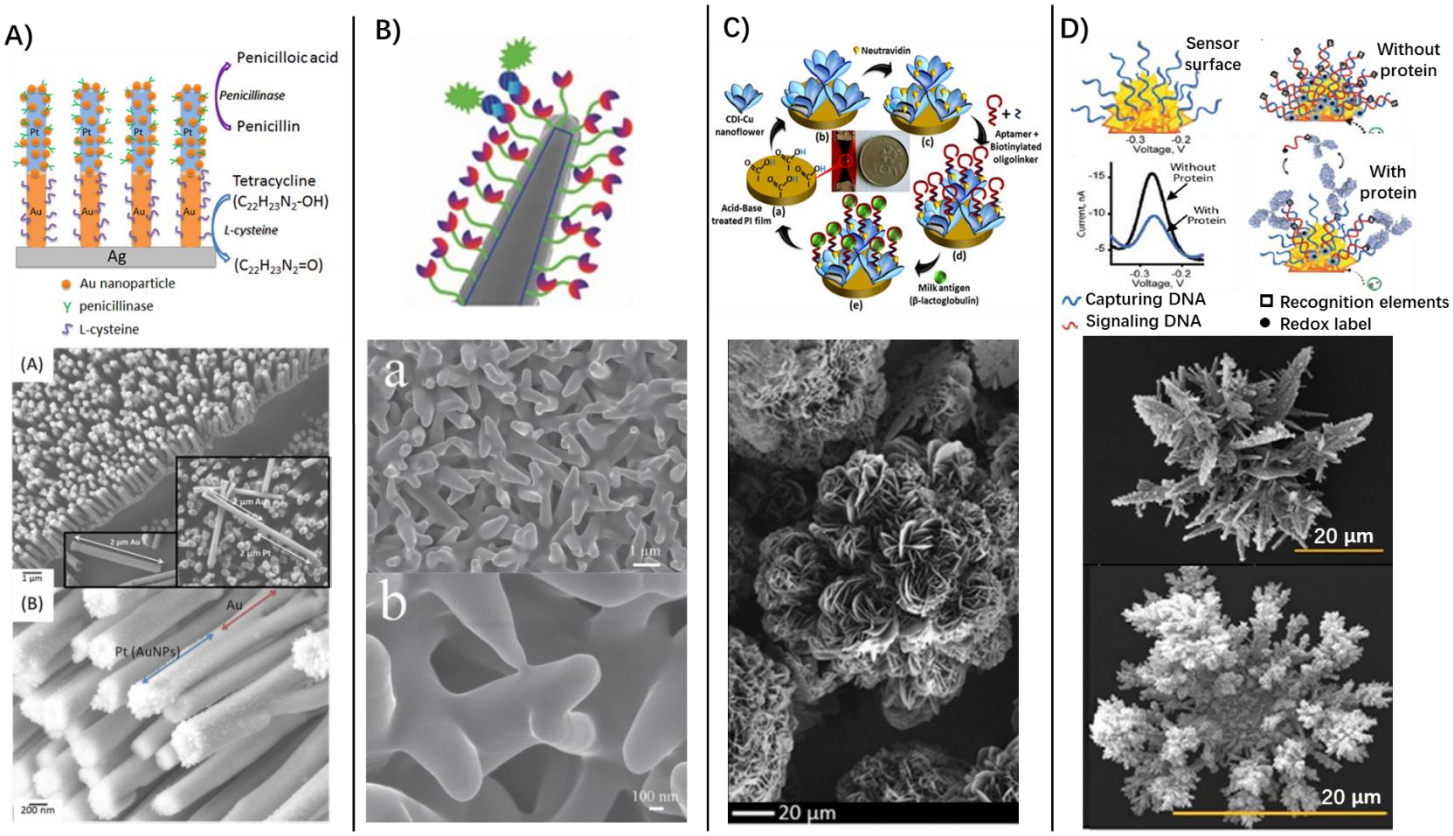

Figure 2.9. Examples of surfaces modified with different shapes of nanostructures for improving biosensors. A) A nanowire-based electrochemical biosensor for simultaneous detection of penicillin and tetracycline, reprinted from Ref. [229] with permission of Elsevier. B) An antibody-based bioassay fabricated by surface modification of glass substrate with zinc oxide nanorods coated with POEGMA-co-GMA for detection of cancer biomarkers, reprinted from Ref. [230] with permission of John Wiley and Sons. C) Modification of electrodes using aptamer-conjugated nanoflowers for the sensitive assay of β -lactoglobulin in milk, reprinted from Ref. [231]. D) Microelectrodes modified with nanoclusters for improving the detection performance of electrochemical steric hindrance hybridization assay to quantitatively detect large proteins reprinted from Ref.[232] with permission of American Chemical Society.

2.3.9 Surface modification with nanofibers

Favored as a substrate or surface modification material for improving the detection performances of different biosensors [234-239], nanofibers can be manufactured by various methods, such as self-assembly, phase separation, and electrospinning. Among these methods, electrospinning is the most widely used one since it offers an easy-to-conduct and affordable way of controlling the properties of the produced nanofibers, including diameter, structure, composition, surface to volume ratio, and intra-/inter-pore size distribution, by adjusting the electrospinning parameters, such as voltage, feed

rate, and solution properties [240, 241]. Nanofibers can be deposited on the substrate materials in different ways when employed as surface coatings. For example, the nanofibers can be directly deposited on the surface of substrate materials using electrospinning [242]. Moreover, the nanofibers can be pre-fabricated and dissolved in a solvent to be later deposited on the substrate using drop-casting or electrostatic adsorption methods [234, 239, 243]. It should be noted that for both deposition methods, adhesive polymers like chitosan and PDA can be mixed with polymer melts (*i.e.,* a polymer solution for producing nanofibers by electrospinning) or nanofiber solutions to improve surface attachment [236, 244, 245]. The detection surfaces modified with nanofibers present unique properties that can improve the detection performance. For example, the nanofiber-modified detection surfaces offer one to two orders of magnitudes larger surface area compared with surfaces modified by planar coatings, resulting in improved bioligand loadings and increased detection sensitivity [235, 246]. Moreover, the nanofibers also provide the detection surfaces with high porosity (up to 90%), which decreases the transport resistance of the analyte diffusion through the sensing layer, making the biorecognition of the target by detection ligands easier [235, 247]. In addition to these inherent advantages, polymer melts can be mixed with other polymers when preparing the nanofibers [235] and incorporate other nanomaterials, such as carbon nanotubes, QDs and AuNPs, to further improve the biosensor performances [235]. Like other materials, nanofibers also need surface activation (*i.e.,* dry or wet chemistry) to introduce surface functional groups or improve surface hydrophilicity. For example, plasma treatment is commonly used to introduce various function groups, such as carboxyl, carbonyl, hydroxyl, and amino, as well as to increase the wettability of nanofibers [248, 249]; dilute NaOH-treated poly(L-lactic acid) (p-PLLA) nanofibers can have more carboxyl groups on their surfaces [250]. The immobilization of bioligands on the nanofiber-modified surfaces can be achieved by different methods, such as adsorption, covalent binding, entrapment, molecularly imprinting, and combined techniques, depending on the properties of bioligands and nanofibers [235]. Since Mercante et al. have already well-organized the materials of

polymer melts, surface treatment methods, and the bioligand immobilization methods [235], what follows will focus on some recently published studies demonstrating how nanofibers have been used to improve the detection sensitivity of biosensors.

Recently, an aptasensor using electrospun $Ti_3C_2T_x$/polyvinylidene fluoride ($Ti_3C_2T_x$ /PVDF) nanofiber composite was developed for Ochratoxin A detection (Figure 2.10) [234]. In this case, a polymer melt was prepared by mixing $Ti_3C_2T_x$ with PVDF, and it was electrospun to produce the Ti_3C_2Tx/PVDF nanofiber composite. Subsequently, these nanofibers were dissolved in a dimethylformamide solvent, which was then drop-casted onto the surface of a screen-printed carbon electrode (SPCE). After this step, the surface-immobilized Ti_3C_2Tx/PVDF nanofibers were modified with APTES to introduce amino functional groups that were further transformed into dialdehydes. Finally, the resulting nanofibers were conjugated with amino-modified aptamers to form an aptamer/Ti_3C_2Tx/PVDF/SPCE surface ready for target detection. The results showed that adding up to 13% $Ti_3C_2T_x$ effectively increased the fiber diameter and also lowered the β-phase of PVDF nanofibers. Both improvements could effectively lower charge transfer resistance, resulting in a higher detection sensitivity (LOD=2.15 fg/mL). The results also demonstrated that the larger surface area for binding more aptamers as well as the excellent electrochemical properties of $Ti_3C_2T_x$/PVDF nanofiber composites improved sensor performance. Additionally, many other nanofiber-based biosensors have also been developed in recent years utilizing both nanofibers and other nanomaterials advantages. For example, a carbon nanofiber/AuNPs-based aptasensor was developed for the detection of the SARS-CoV-2 receptor-binding domain [236]; a titanium dioxide nanoparticle loaded graphitized carbon nanofiber (*i.e.,* TiO_2/GNF) composite was employed on a glassy carbon electrode for the sensitive detection of organophosphorus pesticide residues [239]; an aptasensor was developed using carbon nanofibers loaded with NiCo-metal-organic frameworks (*i.e.,* NiCo-MOF@C) to decorate the surface of a glassy carbon electrode for rapid detection of Helicobacter pylori [237]; and, a polycaprolactone/polypyrrole/MWCNT nanofiber-modified

electrode was used to develop an antibody-based biosensor for sensitive detection of TNF-α biomarker [238].

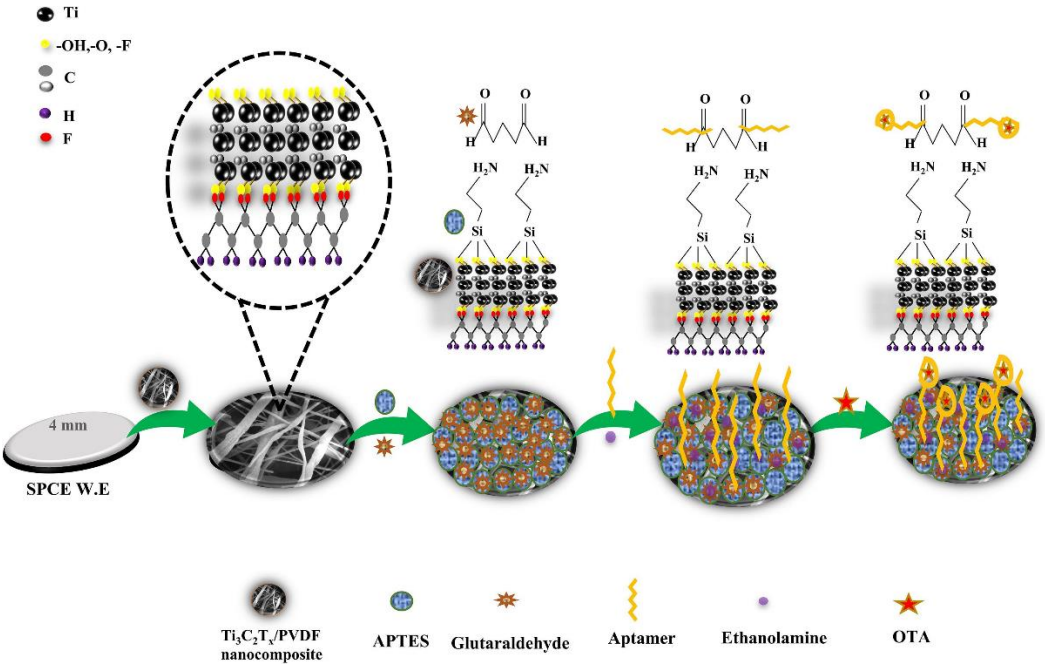

Figure 2.10. An aptasensor using the surface modification of SPCE electrodes with electrospun $Ti_3C_2T_x$/polyvinylidene fluoride nanofiber composite for sensitive detection of Ochratoxin A, reprinted from Ref. [234] with permission of Elsevier.

2.3.10 Surface modification with multivalent aptamers

Multivalent aptamers are also frequently used for surface modification of biosensors because they provide more binding ligands, leading to a higher chance and a higher avidity of interactions of the capturing event on detection surfaces [251]. Since aptamers are DNA/RNA sequences, the detection surface can be modified using nucleic acid amplification methods, such as hybridization chain reaction, strand-displacement amplification, and rolling circle amplification, to produce multivalent aptamer structures [30, 252-254]. For example, Jiang et al. developed a fluorescent microfluidic sensing platform for detecting *E.coli* O157:H7 by running RCA reactions on a PAMAM dendrimer surface-modified microfluidic channel (Figure 2.11A) [30]. In this design, microfluidic channels were surface-immobilized with PAMAM dendrimers templates that were further conjugated with primers for initiating an RCA reaction. Subsequently, an RCA reaction was carried out on the surface of the microfluidic channel, generating

long ssDNA chains containing tandem repeating units of *E.coli* aptamers on the surface. This design improves the capturing performance of the surface by three folds: 1) surface dendrimer templates provide multiple binding sites for conjugation of multi-branched RCA products, 2) surface dendrimers render the surface non-fouling, reducing the detection noises, and 3) RCA reaction results in having a high number of *E.coli* aptamers. Moreover, a signaling RCA was carried on top of the captured *E.coli* cells to further improve the detection signals. Because of these advantages, the detection result showed that the multivalent aptamer-modified microfluidic channel improved *E.coli* capturing efficiency almost 5-times compared to the monomer aptamer modified. Moreover, this RCA surface modification allowed the detection to work under a higher throughput while maintaining sufficient capturing efficiencies.

Aptamers can also be pre-conjugated with other nanomaterials, such as nanoparticles, linear or branched polymer scaffolds, and DNA scaffolds, to form multivalent structures to be immobilized on the detection surfaces [255-257]. For example, Liu et al. developed a multivalent aptamer nanoclimber functionalized microfluidic device for the sensitive detection of leukemia cells (Figure 2.11B) [255]. In this design, the multivalent aptamer nanoclimbers were synthesized by conjugating multiple aptamers on a flexible backbone of linear polymer scaffolds. Subsequently, the resulting nanoclimbers were immobilized on the surface of PDMS-based microfluidic channels for specifically capturing leukemia cells. This multivalent aptamer nanoclimber design improved the target-capturing efficiency due to the following advantages: 1) the long and flexible polymer backbone better adapts the surface topography of leukemia cells; 2) the enhanced aptamer density on the surface of microfluidic channels improves the capturing probability of leukemia cells; and 3) the multivalent aptamer can bind with multiple receptors on the surface of leukemia cells, which dramatically enhances the binding interactions. The detection results showed that these multivalent aptamer nanoclimbers improved the binding avidity of leukemia cells 57.5 times compared with the monoaptamer approach, leading to high capturing efficiency of 92.2%. For more

detailed information about designs, strategies, and applications of multivalent aptamer approaches, readers are referred to a recently published review [251].

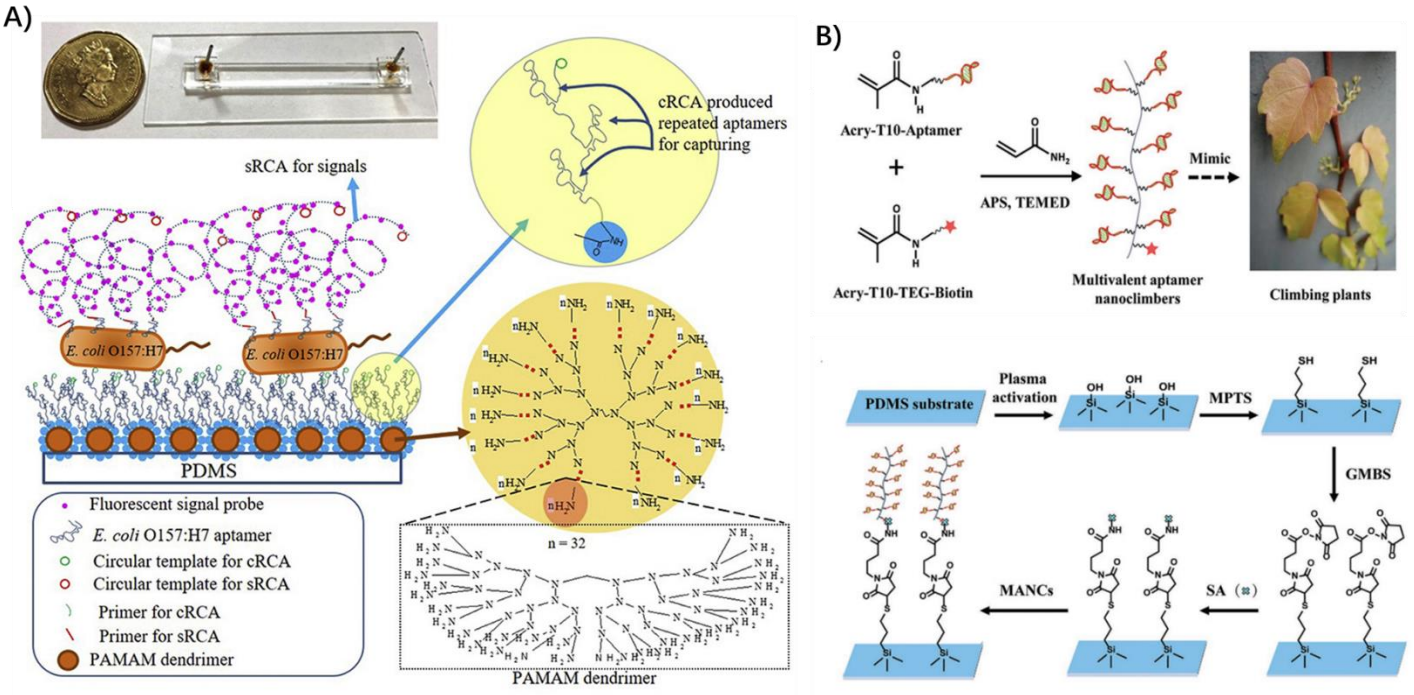

Figure 2.11. Examples of multivalent aptamer designs used for surface modification of biosensors. A) A multivalent-aptamer sensing platform for detecting *E. coli* O157:H7 using RCA reactions on PAMAM dendrimers -modified microfluidic channel surface, reprinted from Ref. [30] with permission of Elsevier. B) A multivalent aptamer nanoclimber functionalized microfluidic device for sensitive detection of leukemia cells, reprinted from Ref. [255], with permission of John Wiley and Sons.

2.4 Further Considerations

Currently, a combination of multiple sensitivity-enhancing approaches is being applied to biosensor designs to improve their performance since no single approach can ultimately improve detection sensitivity. For example, the design shown in Figure 2.11A) combines surface modification using dendrimers to increase the number of bioligands binding sites and also render the surface non-fouling, 2) employs surface RCA reaction to increase the density of bioligands on the detection surface, and 3) uses signaling RCA layer to improve the detection signals. However, if the microchannels could be designed as microfluidic mixers (instead of straight channels) to increase ligand-target interaction by introducing turbulence, the detection sensitivity could be

even further improved [1, 258]. According to the abovementioned example, biosensor designers can utilize a combination of sensitivity-enhancing strategies by 1) applying multiple surface-modification approaches to render the surface non-fouling and improve the loading density of detection ligands on the detection surfaces, 2) performing signal amplification steps after capturing the target, 3) employing mixing designs to enhance analyte-bioligand interactions via turbulent flow, and 4) designing upstream reaction cells for pre-enrichment or pre-amplification of targets in the sample.

Besides, the following factors that can significantly affect the sensitivity need to be carefully considered to achieve the optimum detection performance: 1) the surface bioligands loading density should be optimized using the results from target detections instead of holding the idea of "the more, the better" because bioligands overcrowding the detection surface may change their spatial structures, affecting their detection performance; 2) external conditions, such as pH, temperature and ionic concentration, should be carefully studied, as these factors may significantly influence the bioligand immobilization reaction and the target capturing event; 3) appropriate chemical reactions for conjugating the bioligands to the detection surface should be carefully chosen to ensure the bioligands are properly positioned to expose their capturing sites toward the targets; 4) surface deactivation steps are also essential, as a proper surface deactivation can minimize non-specific bindings from the sample matrix; the deactivated surface should preferably possess neutral surface charges to avoid electrostatic interactions between the detection surface and the targets; and 5) an appropriate blocking step is also necessary for detection surfaces to prevent non-specific surface interactions, in which the surface blocking agent should not react with the surface detection ligands and the sample matrix.

2.5 Conclusion

Surface modification approaches show great potential in improving the detection sensitivities of affinity-based biosensors. Herein, the goal was to offer a comprehensive

review discussing the surface modification materials and strategies for improving the detection sensitivity of affinity-based biosensing platforms. Firstly, two critical steps (*i.e.,* biorecognition and signal transduction) in biosensing were introduced, and the problems of direct immobilization of bioligands on detection surfaces (*i.e.,* the physical adsorption approach) were discussed, highlighting the importance of further surface modifications for enhancing the detection sensitivity. Most importantly, the surface modification materials and approaches were summarized, and the design considerations were discussed using some examples of their applications. It was also elaborated that these surface modification strategies could provide more stable surface binding sites for bioligands, improve the bioligand binding density, achieve controlled-release designs, and offer other excellent properties for improving detection sensitivities, such as enhanced nonfouling properties and improved electron transduction. It is hoped that this overview could improve biosensor designs by optimizing sensor surfacemodification strategies when optimizing biosensing perofrmamnces.

References

1. Kim, Y., J. Gonzales, and Y. Zheng, Sensitivity-Enhancing Strategies in Optical Biosensing. Small, 2021. **17**(4): p. 2004988.
2. Millare, B., et al., Dependence of the quality of adhesion between poly (dimethylsiloxane) and glass surfaces on the conditions of treatment with oxygen plasma. Langmuir, 2008. **24**(22): p. 13218-13224.
3. Luo, S.-C., et al., Nanofabricated SERS-active substrates for single-molecule to virus detection in vitro: A review. Biosensors and Bioelectronics, 2014. **61**: p. 232-240.
4. Sadik, O.A., A.K. Wanekaya, and S. Andreescu, Advances in analytical technologies for environmental protection and public safety. J Environ Monit, 2004. **6**(6): p. 513-22.
5. Modica-Napolitano, J.S. and K. Singh, Mitochondria as targets for detection and treatment of cancer. Expert Reviews in Molecular Medicine, 2004. **4**(9): p. 1-19.
6. Boulter-Bitzer, J.I., H. Lee, and J.T. Trevors, Molecular targets for detection and immunotherapy in Cryptosporidium parvum. Biotechnology Advances, 2007. **25**(1): p. 13-44.
7. Li, Z., et al., Rapid and sensitive detection of protein biomarker using a portable fluorescence biosensor based on quantum dots and a lateral flow test strip.

Analytical chemistry, 2010. **82**(16): p. 7008-7014.
8. Wang, Y., et al., Impedimetric immunosensor based on gold nanoparticles modified graphene paper for label-free detection of Escherichia coli O157:H7. Biosensors and Bioelectronics, 2013. **49**: p. 492-498.
9. Jiang, Y., S. Zou, and X. Cao, A simple dendrimer-aptamer based microfluidic platform for *E.coli* O157:H7 detection and signal intensification by rolling circle amplification. Sensors and Actuators B: Chemical, 2017. **251**: p. 976-984.
10. Chen, R.-K., et al., Quantification of cow milk adulteration in goat milk using high-performance liquid chromatography with electrospray ionization mass spectrometry. Rapid Communications in Mass Spectrometry, 2004. **18**(10): p. 1167-1171.
11. Stewart, E.J., Growing Unculturable Bacteria. Journal of Bacteriology, 2012. **194**(16): p. 4151-4160.
12. Smyth, W.F., Recent applications of capillary electrophoresis-electrospray ionisation-mass spectrometry in drug analysis. ELECTROPHORESIS, 2005. **26**(7-8): p. 1334-1357.
13. Gravesen, P., J. Branebjerg, and O.S. Jensen, Microfluidics-a review. Journal of Micromechanics and Microengineering, 1993. **3**(4): p. 168-182.
14. Tanaka, R., et al., A novel enhancement assay for immunochromatographic test strips using gold nanoparticles. Analytical and Bioanalytical Chemistry, 2006. **385**(8): p. 1414-1420.
15. Kwiatek, O., et al., Quantitative one-step real-time RT-PCR for the fast detection of the four genotypes of PPRV. Journal of Virological Methods, 2010. **165**(2): p. 168-177.
16. Morbioli, G.G., et al., Technical aspects and challenges of colorimetric detection with microfluidic paper-based analytical devices (μPADs) - A review. Analytica Chimica Acta, 2017. **970**: p. 1-22.
17. Dalmasso, A., et al., A multiplex PCR assay for the identification of animal species in feedstuffs. Molecular and Cellular Probes, 2004. **18**(2): p. 81-87.
18. Engvall, E., [28] Enzyme immunoassay ELISA and EMIT, in Methods in Enzymology. 1980, Academic Press. p. 419-439.
19. Li, S., et al., *In situ* rolling circle amplification surface modifications to improve *E.coli* O157: H7 capturing performances for rapid and sensitive microfluidic detection applications. Analytica Chimica Acta, 2021. **1150**: p. 338229.
20. Masson, J.-F., et al., Reduction of nonspecific protein binding on surface plasmon resonance biosensors. Analytical and bioanalytical chemistry, 2006. **386**(7-8): p. 1951-1959.
21. Roy, L., P. Buragohain, and V. Borse, Strategies for sensitivity enhancement of point-of-care devices. Biosensors and Bioelectronics: X, 2021: p. 100098.
22. Soleymani, L. and F. Li, Mechanistic Challenges and Advantages of Biosensor Miniaturization into the Nanoscale. ACS Sensors, 2017. **2**(4): p. 458-467.
23. Liu, Q., J. Wang, and B.J. Boyd, Peptide-based biosensors. Talanta, 2015. **136**: p. 114-127.
24. Bohbot, J.D. and S. Vernick, The emergence of insect odorant receptor-based

biosensors. Biosensors, 2020. **10**(3): p. 26.
25. Haupt, K. and K. Mosbach, Molecularly imprinted polymers and their use in biomimetic sensors. Chemical reviews, 2000. **100**(7): p. 2495-2504.
26. Myszka, D.G., Improving biosensor analysis. Journal of molecular recognition, 1999. **12**(5): p. 279-284.
27. Hans, B. and B. Hans, Enzyme Kinetics Principles and Methods. 2008: Wiley Vch Valag.
28. Brandão, D., S. Liébana, and M.I. Pividori, Multiplexed detection of foodborne pathogens based on magnetic particles. New biotechnology, 2015. **32**(5): p. 511-520.
29. Lo, C.-Y., et al., Rapid enrichment of phosphopeptides from tryptic digests of proteins using iron oxide nanocomposites of magnetic particles coated with zirconia as the concentrating probes. Journal of proteome research, 2007. **6**(2): p. 887-893.
30. Jiang, Y., et al., Developing a dual-RCA microfluidic platform for sensitive *E.coli* O157: H7 whole-cell detections. Analytica Chimica Acta, 2020. **1127**: p. 79-88.
31. Carothers, J.M., et al., Selecting RNA aptamers for synthetic biology: investigating magnesium dependence and predicting binding affinity. Nucleic acids research, 2010. **38**(8): p. 2736-2747.
32. Chang, A.L., M. McKeague, and C.D. Smolke, Facile characterization of aptamer kinetic and equilibrium binding properties using surface plasmon resonance, in Methods in enzymology. 2014, Elsevier. p. 451-466.
33. Hianik, T., et al., Influence of ionic strength, pH and aptamer configuration for binding affinity to thrombin. Bioelectrochemistry, 2007. **70**(1): p. 127-133.
34. Hassibi, A., H. Vikalo, and A. Hajimiri, On noise processes and limits of performance in biosensors. Journal of applied physics, 2007. **102**(1): p. 014909.
35. DOES, W.P., Polymerase chain reaction. Journal of Investigative Dermatology, 2013. **133**.
36. Tomita, N., et al., Loop-mediated isothermal amplification (LAMP) of gene sequences and simple visual detection of products. Nature protocols, 2008. **3**(5): p. 877-882.
37. Nallur, G., et al., Signal amplification by rolling circle amplification on DNA microarrays. Nucleic acids research, 2001. **29**(23): p. e118-e118.
38. Xu, H., et al., Aptamer-functionalized gold nanoparticles as probes in a dry-reagent strip biosensor for protein analysis. Analytical Chemistry, 2009. **81**(2): p. 669-675.
39. Engvall, E. and P. Perlmann, Enzyme-linked immunosorbent assay (ELISA). Protides of the biological fluids, 1971: p. 553-556.
40. Marzocchi, E., et al., Chemiluminescent detection systems of horseradish peroxidase employing nucleophilic acylation catalysts. Analytical biochemistry, 2008. **377**(2): p. 189-194.
41. Comer, J., Semiquantitative specific test paper for glucose in urine. Analytical Chemistry, 1956. **28**(11): p. 1748-1750.

42. Lichtenberg, J.Y., Y. Ling, and S. Kim, Non-specific adsorption reduction methods in biosensing. Sensors, 2019. **19**(11): p. 2488.
43. Park, K.D., et al., Bacterial adhesion on PEG modified polyurethane surfaces. Biomaterials, 1998. **19**(7): p. 851-859.
44. Qin, Y., et al., Developing an ultra non-fouling SU-8 and PDMS hybrid microfluidic device by poly (amidoamine) engraftment. Colloids and Surfaces B: Biointerfaces, 2015. **127**: p. 247-255.
45. Hao, X., et al., Aptamer surface functionalization of microfluidic devices using dendrimers as multi-handled templates and its application in sensitive detections of foodborne pathogenic bacteria. Analytica chimica acta, 2019. **1056**: p. 96-107.
46. Qin, Y., et al., Developing a non-fouling hybrid microfluidic device for applications in circulating tumour cell detections. Colloids and Surfaces B: Biointerfaces, 2017. **151**: p. 39-46.
47. Li, F., et al., Aptamers facilitating amplified detection of biomolecules. Analytical chemistry, 2015. **87**(1): p. 274-292.
48. Thapa, K., W. Liu, and R. Wang, Nucleic acid-based electrochemical biosensor: Recent advances in probe immobilization and signal amplification strategies. Wiley Interdisciplinary Reviews: Nanomedicine and Nanobiotechnology, 2022. **14**(1): p. e1765.
49. Kurup, C.P., N.F. Mohd-Naim, and M.U. Ahmed, Recent trends in nanomaterial-based signal amplification in electrochemical aptasensors. Critical Reviews in Biotechnology, 2022. **42**(5): p. 794-812.
50. Mahmoudpour, M., et al., Rational design of smart nano-platforms based on antifouling-nanomaterials toward multifunctional bioanalysis. Advances in Colloid and Interface Science, 2022: p. 102637.
51. Sonawane, M.D. and S.B. Nimse, Surface modification chemistries of materials used in diagnostic platforms with biomolecules. Journal of Chemistry, 2016. **2016**.
52. Lequin, R.M., Enzyme Immunoassay (EIA)/Enzyme-Linked Immunosorbent Assay (ELISA). Clinical Chemistry, 2005. **51**(12): p. 2415.
53. Lemeshko, S., et al., Oligonucleotides form a duplex with non-helical properties on a positively charged surface. Nucleic Acids Research, 2001. **29**(14): p. 3051-3058.
54. Lee, S., et al., Improved porous silicon microarray based prostate specific antigen immunoassay by optimized surface density of the capture antibody. Analytica chimica acta, 2013. **796**: p. 108-114.
55. Järås, K., et al., ENSAM: Europium nanoparticles for signal enhancement of antibody microarrays on nanoporous silicon. Journal of proteome research, 2008. **7**(3): p. 1308-1314.
56. Zhang, J., et al., Simultaneous detection of deoxynivalenol and zearalenone by dual-label time-resolved fluorescence immunoassay. Journal of the Science of Food and Agriculture, 2011. **91**(2): p. 193-197.
57. Rao, M.K.K., K. Kapila, and R.M. Gupta, ENZYME LINKED

IMMUNOSORBENT ASSAYS REVISITED. Medical Journal Armed Forces India, 1997. **53**(1): p. 45-51.
58. Shiyun, Z., et al., Predicting detection limits of enzyme-linked immunosorbent assay (ELISA) and bioanalytical techniques in general. Analyst, 2013. **139**(2): p. 439-445.
59. Prusak-sochaczewski, E. and J.H.T. Luong, An improved ELISA method for the detection of Salmonella typhimurium. Journal of Applied Bacteriology, 1989. **66**(2): p. 127-135.
60. Steiner, J.M., S.R. Teague, and D.A. Williams, Development and analytic validation of an enzyme-linked immunosorbent assay for the measurement of canine pancreatic lipase immunoreactivity in serum. Can J Vet Res, 2003. **67**(3): p. 175-82.
61. Zammatteo, N., et al., Amination of polystyrene microwells: application to the covalent grafting of DNA probes for hybridization assays. Analytical biochemistry, 1996. **236**(1): p. 85-94.
62. Wei, C., et al., An immunoassay for dibutyl phthalate based on direct hapten linkage to the polystyrene surface of microtiter plates. PloS one, 2011. **6**(12): p. e29196.
63. Petryayeva, E., W.R. Algar, and U.J. Krull, Adapting fluorescence resonance energy transfer with quantum dot donors for solid-phase hybridization assays in microtiter plate format. Langmuir, 2013. **29**(3): p. 977-987.
64. Bosnjakovic, A., et al., A dendrimer-based immunosensor for improved capture and detection of tumor necrosis factor-α cytokine. Analytica chimica acta, 2012. **720**: p. 118-125.
65. Kaur, J. and C.R. Suri, Direct hapten coated ELISA for immunosensing of low molecular weight analytes. Nat Protoc Exch. doi, 2007. **10**.
66. Dharanivasan, G., et al., Gold nanoparticles assisted characterization of amine functionalized polystyrene multiwell plate and glass slide surfaces. Applied Nanoscience, 2015. **5**(1): p. 39-50.
67. Kaur, J., et al., Direct hapten coated immunoassay format for the detection of atrazine and 2,4-dichlorophenoxyacetic acid herbicides. Analytica Chimica Acta, 2008. **607**(1): p. 92-99.
68. Goddard, J.M. and J. Hotchkiss, Polymer surface modification for the attachment of bioactive compounds. Progress in Polymer Science, 2007. **32**(7): p. 698-725.
69. Eriksson, J.C., et al., Characterization of KMnO4/H2SO4-oxidized polyethylene surfaces by means of ESCA and 45Ca2+ adsorption. Journal of Colloid & Interface Science, 1984. **100**(2): p. 381-392.
70. Kong, J.-S., D.-J. Lee, and H.-D. Kim, Surface modification of low-density polyethylene (LDPE) film and improvement of adhesion between evaporated copper metal film and LDPE. Journal of Applied Polymer Science, 2001. **82**(7): p. 1677-1690.
71. Rasmussen, J.R., E.R. Stedronsky, and G.M. Whitesides, Introduction, modification, and characterization of functional groups on the surface of low-

density polyethylene film. Journal of the American Chemical Society, 1977. **99**(14): p. 4736-4745.
72. Ba G, D.S., V.P. Kumar, and S. Maiti, Chemical modification of LDPE film. Journal of Applied Polymer Science, 2015. **71**(7): p. 1041-1048.
73. Tao, G., et al., Surface Functionalized Polypropylene: Synthesis, Characterization, and Adhesion Properties. Macromolecules, 2001. **34**(22): p. 7672-7679.
74. Desai, S.M. and R.P. Singh, Surface Modification of Polyethylene. Advances in Polymer Science, 2004.
75. Darain, F., et al., On-chip detection of myoglobin based on fluorescence. Biosensors and Bioelectronics, 2009. **24**(6): p. 1744-1750.
76. Berdichevsky, Y., et al., UV/ozone modification of poly (dimethylsiloxane) microfluidic channels. Sensors and Actuators B: Chemical, 2004. **97**(2-3): p. 402-408.
77. Vesel, A., Modification of polystyrene with a highly reactive cold oxygen plasma. Surface and Coatings Technology, 2010. **205**(2): p. 490-497.
78. Guruvenket, S., et al., Plasma surface modification of polystyrene and polyethylene. Applied Surface Science, 2004. **236**(1): p. 278-284.
79. Clark, D.T. and A. Dilks, Esca applied to polymers. XXIII. RF glow discharge modification of polymers in pure oxygen and helium–oxygen mixtures. Journal of Polymer Science: Polymer Chemistry Edition, 1979. **17**(4): p. 957-976.
80. Oyane, A., et al., Simple surface modification of poly(ϵ-caprolactone) to induce its apatite-forming ability. Journal of Biomedical Materials Research Part A, 2005. **75A**(1): p. 138-145.
81. A, Y.J.K., et al., Surface characterization and in vitro blood compatibility of poly(ethylene terephthalate) immobilized with insulin and/or heparin using plasma glow discharge. Biomaterials, 2000. **21**(2): p. 121-130.
82. Aouinti, M., P. Bertrand, and F. Poncin-Epaillard, Characterization of Polypropylene Surface Treated in a CO2 Plasma. Plasmas and Polymers, 2003. **8**(4): p. 225-236.
83. Wang, M.-J., Y.-I. Chang, and F. Poncin-Epaillard, Acid and basic functionalities of nitrogen and carbon dioxide plasma-treated polystyrene. Surface and Interface Analysis, 2005. **37**(3): p. 348-355.
84. Terlingen, J.G.A., et al., Introduction of functional groups on polyethylene surfaces by a carbon dioxide plasma treatment. Journal of Applied Polymer Science, 1995. **57**(8): p. 969-982.
85. Yang, et al., Investigation on the mechanism of nitrogen plasma modified PDMS bonding with SU-8. Applied Surface Science: A Journal Devoted to the Properties of Interfaces in Relation to the Synthesis and Behaviour of Materials, 2016.
86. Gurzawska, K., et al., Effect of nanocoating with rhamnogalacturonan-I on surface properties and osteoblasts response. Journal of Biomedical Materials Research Part A, 2012. **100A**(3): p. 654-664.
87. Hu, Y., et al., Porous polymer scaffolds surface-modified with arginine-glycine-

aspartic acid enhance bone cell attachment and differentiation in vitro. Journal of Biomedical Materials Research Part A, 2003. **64A**(3): p. 583-590.
88. Kang, E.T., et al., Surface Modification and Functionalization of Polytetrafluoroethylene Films. Macromolecules, 1996. **29**(21): p. 6872-6879.
89. Ademovic, Z., et al., Minimization of protein adsorption on poly(vinylidene fluoride). Biomolecular Engineering, 2002. **19**(2): p. 177-182.
90. Cheng, Z. and S.-H. Teoh, Surface modification of ultra thin poly (ε-caprolactone) films using acrylic acid and collagen. Biomaterials, 2004. **25**(11): p. 1991-2001.
91. Peng, W., et al., Surface functionalization of low density polyethylene films with grafted poly(ethylene glycol) derivatives. Journal of Materials Chemistry, 2001. **11**(12): p. 2951-2957.
92. Cen, L., et al., Surface modification of polymeric films and membranes to achieve antibacterial properties. Surface and Interface Analysis, 2004. **36**(8): p. 716-719.
93. Park, S.-J. and W.-Y. Jung, Effect of KOH activation on the formation of oxygen structure in activated carbons synthesized from polymeric precursor. Journal of colloid and interface science, 2002. **250**(1): p. 93-98.
94. Park, S.-J., et al., Effect of chemical treatment of Kevlar fibers on mechanical interfacial properties of composites. Journal of colloid and interface science, 2002. **252**(1): p. 249-255.
95. Dixit, C.K., et al., Multisubstrate-compatible ELISA procedures for rapid and high-sensitivity immunoassays. nature protocols, 2011. **6**(4): p. 439-445.
96. Wang, L., U.S. Schubert, and S. Hoeppener, Surface chemical reactions on self-assembled silane based monolayers. Chemical Society Reviews, 2021. **50**(11): p. 6507-6540.
97. Huang, C., et al., Site-directed immobilization antibody for alpha-fetoprotein detection by optical biosensor. Integrated Ferroelectrics, 2016. **171**(1): p. 70-78.
98. Pirri, G., et al., Characterization of a polymeric adsorbed coating for DNA microarray glass slides. Analytical chemistry, 2004. **76**(5): p. 1352-1358.
99. Guarisco, M., et al., A new aptamer immobilization strategy for protein recognition. Sensors and Actuators B: Chemical, 2017. **252**: p. 222-231.
100. Prakash, S., et al., "Click" modification of silica surfaces and glass microfluidic channels. Analytical chemistry, 2007. **79**(4): p. 1661-1667.
101. He, X., et al., ATP-Responsive Controlled Release System Using Aptamer-Functionalized Mesoporous Silica Nanoparticles. Langmuir, 2012. **28**(35): p. 12909-12915.
102. Chen, Z., et al., Stimulus-response click chemistry based aptamer-functionalized mesoporous silica nanoparticles for fluorescence detection of thrombin. Talanta, 2018. **178**: p. 563-568.
103. Chen, Z., et al., Stimulus-response mesoporous silica nanoparticle-based chemiluminescence biosensor for cocaine determination. Biosensors and Bioelectronics, 2016. **75**: p. 8-14.
104. Tan, H., et al., A novel fluorescence aptasensor based on mesoporous silica

nanoparticles for selective and sensitive detection of aflatoxin B1. Analytica Chimica Acta, 2019. **1068**: p. 87-95.
105. Hermanson, G.T., Bioconjugate techniques. 2013: Academic press.
106. González, M.G., J.C. Cabanelas, and J. Baselga, Applications of FTIR on epoxy resins-identification, monitoring the curing process, phase separation and water uptake. Infrared Spectroscopy-Materials Science, Engineering and Technology, 2012. **2**: p. 261-284.
107. Fantoni, N.Z., A.H. El-Sagheer, and T. Brown, A Hitchhiker's Guide to Click-Chemistry with Nucleic Acids. Chemical Reviews, 2021. **121**(12): p. 7122-7154.
108. Hoyle, C.E. and C.N. Bowman, Thiol–ene click chemistry. Angewandte Chemie International Edition, 2010. **49**(9): p. 1540-1573.
109. Tan, J., et al., Water-borne thiol–isocyanate click chemistry in microfluidics: rapid and energy-efficient preparation of uniform particles. Polymer Chemistry, 2015. **6**(24): p. 4366-4373.
110. De, S. and A. Khan, Efficient synthesis of multifunctional polymers via thiol–epoxy "click" chemistry. Chemical Communications, 2012. **48**(25): p. 3130-3132.
111. Kreye, O., H. Mutlu, and M.A. Meier, Sustainable routes to polyurethane precursors. Green Chemistry, 2013. **15**(6): p. 1431-1455.
112. Pla, L., et al., A gated material as immunosensor for in-tissue detection of IDH1-R132H mutation in gliomas. Sensors and Actuators B: Chemical, 2021. **345**: p. 130406.
113. Žuržul, N. and B.T. Stokke, DNA Aptamer Functionalized Hydrogels for Interferometric Fiber-Optic Based Continuous Monitoring of Potassium Ions. Biosensors, 2021. **11**(8): p. 266.
114. Minisini, B., et al., Influence of the chemical composition and formulation of fluorinated epoxy resin on its surface characteristics. European Polymer Journal, 2019. **112**: p. 452-460.
115. Paul, S., et al., Ring-opening copolymerization (ROCOP): synthesis and properties of polyesters and polycarbonates. Chemical communications, 2015. **51**(30): p. 6459-6479.
116. Liu, G., et al., The Bioanalytical and Biomedical Applications of Polymer Modified Substrates. Polymers, 2022. **14**(4): p. 826.
117. Sebra, R.P., et al., Surface Grafted Antibodies: Controlled Architecture Permits Enhanced Antigen Detection. Langmuir, 2005. **21**(24): p. 10907-10911.
118. del Campo, A. and I.J. Bruce, Substrate Patterning and Activation Strategies for DNA Chip Fabrication, in Immobilisation of DNA on Chips I, C. Wittmann, Editor. 2005, Springer Berlin Heidelberg: Berlin, Heidelberg. p. 77-111.
119. Cruz, D.F., et al., Ultrabright fluorescence readout of an inkjet-printed immunoassay using plasmonic nanogap cavities. Nano letters, 2020. **20**(6): p. 4330-4336.
120. Liu, X., et al., Development of sphere-polymer brush hierarchical nanostructure substrates for fabricating microarrays with high performance. ACS applied materials & interfaces, 2017. **9**(43): p. 38101-38108.

121. Lei, Z., et al., Poly (glycidyl methacrylate-co-2-hydroxyethyl methacrylate) brushes as peptide/protein microarray substrate for improving protein binding and functionality. ACS applied materials & interfaces, 2016. **8**(16): p. 10174-10182.
122. Forinová, M., et al., Functionalized Terpolymer-Brush-Based Biointerface with Improved Antifouling Properties for Ultra-Sensitive Direct Detection of Virus in Crude Clinical Samples. ACS Applied Materials & Interfaces, 2021. **13**(50): p. 60612-60624.
123. Barbara, K. and B. Maria, Review Dendrimers: properties and applications. Acta biochimica polonica, 2001. **48**(1): p. 199-208.
124. Idris, A.O., N. Mabuba, and O.A. Arotiba, A Dendrimer Supported Electrochemical Immunosensor for the Detection of Alpha-feto protein – a Cancer Biomarker. Electroanalysis, 2018. **30**(1): p. 31-37.
125. Han, H.J., et al., Multifunctional dendrimer-templated antibody presentation on biosensor surfaces for improved biomarker detection. Advanced functional materials, 2010. **20**(3): p. 409-421.
126. Li, H., et al., Nonenzymatic Electrochemical Biosensor Based on Novel Hydrophilic Ferrocene-terminated Hyperbranched Polymer and its Application in Glucose Detection. Electroanalysis, 2016. **28**(5): p. 1003-1011.
127. Kowalczyk, A., et al., Occlusion phenomenon of redox probe by protein as a way of voltammetric detection of non-electroactive C-reactive protein. Biosensors and Bioelectronics, 2018. **117**: p. 232-239.
128. Karimzadeh, A., et al., Peptide based biosensors. TrAC Trends in Analytical Chemistry, 2018. **107**: p. 1-20.
129. Wang, G., et al., Zwitterionic peptide anchored to conducting polymer PEDOT for the development of antifouling and ultrasensitive electrochemical DNA sensor. Biosensors and Bioelectronics, 2017. **92**: p. 396-401.
130. Liu, N., et al., Electrochemical aptasensor for ultralow fouling cancer cell quantification in complex biological media based on designed branched peptides. Analytical chemistry, 2019. **91**(13): p. 8334-8340.
131. Wang, W., et al., Low fouling label-free DNA sensor based on polyethylene glycols decorated with gold nanoparticles for the detection of breast cancer biomarkers. Biosensors and Bioelectronics, 2015. **71**: p. 51-56.
132. Liu, N., et al., Antifouling biosensors for reliable protein quantification in serum based on designed all-in-one branched peptides. Chemical Communications, 2021. **57**(6): p. 777-780.
133. Salazar, P., M. Martín, and J. González-Mora, Polydopamine-modified surfaces in biosensor applications. Polymer science: research advances, practical applications and educational aspects. Formatex Research Center SL (Spain), 2016: p. 385-396.
134. Zandieh, M., B.M. Hagar, and J. Liu, Interfacing DNA and polydopamine nanoparticles and its applications. Particle & Particle Systems Characterization, 2020. **37**(11): p. 2000208.
135. Alfieri, M.L., et al., Polydopamine at biological interfaces. Advances in Colloid

and Interface Science, 2022: p. 102689.
136. Lee, H., et al., Mussel-inspired surface chemistry for multifunctional coatings. Science (New York, N.Y.), 2007. **318**(5849): p. 426-430.
137. Barclay, T.G., et al., Versatile Surface Modification Using Polydopamine and Related Polycatecholamines: Chemistry, Structure, and Applications. Advanced Materials Interfaces, 2017. **4**(19): p. 1601192.
138. Lee, H., J. Rho, and P.B. Messersmith, Facile conjugation of biomolecules onto surfaces via mussel adhesive protein inspired coatings. Advanced materials, 2009. **21**(4): p. 431-434.
139. He, H., Q. Xie, and S. Yao, An electrochemical quartz crystal impedance study on anti-human immunoglobulin G immobilization in the polymer grown during dopamine oxidation at an Au electrode. Journal of colloid and interface science, 2005. **289**(2): p. 446-454.
140. Xu, Z., et al., Electrochemical biosensors for the detection of carcinoembryonic antigen with low fouling and high sensitivity based on copolymerized polydopamine and zwitterionic polymer. Sensors and Actuators B: Chemical, 2020. **319**: p. 128253.
141. Almeida, L.C., et al., Electrosynthesis of polydopamine-ethanolamine films for the development of immunosensing interfaces. Scientific reports, 2021. **11**(1): p. 1-12.
142. Suginta, W., P. Khunkaewla, and A. Schulte, Electrochemical biosensor applications of polysaccharides chitin and chitosan. Chemical reviews, 2013. **113**(7): p. 5458-5479.
143. Wu, S., et al., Highly sensitive and selective ion-imprinted polymers based on one-step electrodeposition of chitosan-graphene nanocomposites for the determination of Cr (VI). Carbohydrate polymers, 2018. **195**: p. 199-206.
144. Srivastava, M., et al., A chitosan-based polyaniline–Au nanocomposite biosensor for determination of cholesterol. Analytical Methods, 2014. **6**(3): p. 817-824.
145. Zouaoui, F., et al., Electrochemical sensors based on molecularly imprinted chitosan: A review. TrAC Trends in Analytical Chemistry, 2020. **130**: p. 115982.
146. Prabhu, A., et al., Reviewing the use of chitosan and polydopamine for electrochemical sensing. Current Opinion in Electrochemistry, 2022. **32**: p. 100885.
147. Abdullah, J., et al., Immobilization of tyrosinase in chitosan film for an optical detection of phenol. Sensors and Actuators B: Chemical, 2006. **114**(2): p. 604-609.
148. Xu, X.H., et al., Preparation of chitosan/glucose oxidase nanolayered films for electrode modification by the technique of layer-by-layer self-assembly. Journal of Materials Science Letters, 2003. **22**(9): p. 695-697.
149. Pedano, M.L., et al., Layer-by-Layer Deposition of Chitosan Derivatives and DNA on Gold Surfaces for the Development of Biorecognition Layers. Analytical letters, 2004. **37**(11): p. 2235-2250.
150. El Knidri, H., et al., Extraction, chemical modification and characterization of

chitin and chitosan. International journal of biological macromolecules, 2018. **120**: p. 1181-1189.
151. Chung, T.W., et al., Preparation of alginate/galactosylated chitosan scaffold for hepatocyte attachment. Biomaterials, 2002. **23**(14): p. 2827-2834.
152. Mansur, H.S., et al., Water-soluble nanoconjugates of quantum dot-chitosan-antibody for in vitro detection of cancer cells based on "enzyme-free" fluoroimmunoassay. Materials Science and Engineering: C, 2015. **52**: p. 61-71.
153. Li, H., et al., Carboxymethyl chitosan assembled piezoelectric biosensor for rapid and label-free quantification of immunoglobulin Y. Carbohydrate Polymers, 2022. **290**: p. 119482.
154. Schmitt, J., et al., Preparation and optical properties of colloidal gold monolayers. Langmuir, 1999. **15**(9): p. 3256-3266.
155. Lu, M., et al., Gold nanoparticle-enhanced detection of DNA hybridization by a block copolymer-templating fiber-optic localized surface plasmon resonance biosensor. Nanomaterials, 2021. **11**(3): p. 616.
156. Omura, N., I. Uechi, and S. Yamada, Comparison of plasmonic sensing between polymer-and silica-coated gold nanorods. Analytical Sciences, 2009. **25**(2): p. 255-259.
157. Oo, M.K.K., et al., Rapid, sensitive DNT vapor detection with UV-assisted photo-chemically synthesized gold nanoparticle SERS substrates. Analyst, 2011. **136**(13): p. 2811-2817.
158. Yang, S., et al., The optical property of core-shell nanosensors and detection of atrazine based on localized surface plasmon resonance (LSPR) sensing. Sensors, 2014. **14**(7): p. 13273-13284.
159. Al-Rubaye, A., et al. LSPR/TIRE bio-sensing platform for detection of low molecular weight toxins. in 2017 IEEE SENSORS. 2017. IEEE.
160. Tu, M.H., T. Sun, and K.T.V. Grattan, LSPR optical fibre sensors based on hollow gold nanostructures. Sensors and Actuators B: Chemical, 2014. **191**: p. 37-44.
161. Daniel, M.-C. and D. Astruc, Gold Nanoparticles: Assembly, Supramolecular Chemistry, Quantum-Size-Related Properties, and Applications toward Biology, Catalysis, and Nanotechnology. Chemical Reviews, 2004. **104**(1): p. 293-346.
162. Kumlangdudsana, P., et al., Fabrication of microelectrodes using flow layer-by-layer self assembly of gold nanoparticles. Superlattices and Microstructures, 2012. **52**(5): p. 1043-1051.
163. Kim, S., et al., Electrochemical sensors based on porous nanocomposite films with weak polyelectrolyte-stabilized gold nanoparticles. Journal of Materials Chemistry, 2011. **21**(22): p. 8008-8013.
164. Rodrigues, G.H.S., et al., Layer-by-Layer Films of Graphene Nanoplatelets and Gold Nanoparticles for Methyl Parathion Sensing. ACS Applied Nano Materials, 2019. **2**(2): p. 1082-1091.
165. Škugor Rončević, I., et al., Polyelectrolytes Assembly: A Powerful Tool for Electrochemical Sensing Application. Sensors (Basel, Switzerland), 2020. **20**(11): p. 3211.

166. Wu, J., et al., Mussel-Inspired Chemistry for Robust and Surface-Modifiable Multilayer Films. Langmuir, 2011. **27**(22): p. 13684-13691.
167. Rassas, I., et al., Highly Sensitive Voltammetric Glucose Biosensor Based on Glucose Oxidase Encapsulated in a Chitosan/Kappa-Carrageenan/Gold Nanoparticle Bionanocomposite. Sensors, 2019. **19**(1): p. 154.
168. Tavakoli, J. and Y. Tang, Hydrogel Based Sensors for Biomedical Applications: An Updated Review. Polymers, 2017. **9**(8): p. 364.
169. Khajouei, S., H. Ravan, and A. Ebrahimi, DNA hydrogel-empowered biosensing. Advances in colloid and interface science, 2020. **275**: p. 102060.
170. Zezza, P., et al., DNA -based hydrogels for high-performance optical biosensing application. Talanta, 2022. **244**: p. 123427.
171. Yan, L., et al., Target-Responsive "Sweet" Hydrogel with Glucometer Readout for Portable and Quantitative Detection of Non-Glucose Targets. Journal of the American Chemical Society, 2013. **135**(10): p. 3748-3751.
172. He, Y., et al., Switchable Target-Responsive 3D DNA Hydrogels As a Signal Amplification Strategy Combining with SERS Technique for Ultrasensitive Detection of miRNA 155. Analytical Chemistry, 2017. **89**(16): p. 8538-8544.
173. Noh, K.G. and S.Y. Park, Biosensor Array of Interpenetrating Polymer Network with Photonic Film Templated from Reactive Cholesteric Liquid Crystal and Enzyme-Immobilized Hydrogel Polymer. Advanced Functional Materials, 2018. **28**(22): p. 1707562.
174. Johnsson, B., S. Löfås, and G. Lindquist, Immobilization of proteins to a carboxymethyldextran-modified gold surface for biospecific interaction analysis in surface plasmon resonance sensors. Analytical Biochemistry, 1991. **198**(2): p. 268-277.
175. Löfås, S., et al., Methods for site controlled coupling to carboxymethyldextran surfaces in surface plasmon resonance sensors. Biosensors and Bioelectronics, 1995. **10**(9): p. 813-822.
176. Mohseni, S., et al., Development of a label-free SPR sensor for detection of matrixmetalloproteinase-9 by antibody immobilization on carboxymethyldextran chip. Biosensors and Bioelectronics, 2016. **81**: p. 510-516.
177. Löfås, S. and B. Johnsson, A novel hydrogel matrix on gold surfaces in surface plasmon resonance sensors for fast and efficient covalent immobilization of ligands. Journal of the Chemical Society, Chemical Communications, 1990(21): p. 1526-1528.
178. Díaz-Betancor, Z., M.-J. Bañuls, and Á. Maquieira, Photoclick chemistry to create dextran-based nucleic acid microarrays. Analytical and bioanalytical chemistry, 2019. **411**(25): p. 6745-6754.
179. Zhou, S., et al., Facile fabrication of dextran-based fluorescent nanogels as potential glucose sensors. Chemical Communications, 2013. **49**(82): p. 9473-9475.
180. Boujakhrout, A., et al., Decorating graphene oxide/nanogold with dextran-based polymer brushes for the construction of ultrasensitive electrochemical enzyme

biosensors. Journal of Materials Chemistry B, 2015. **3**(17): p. 3518-3524.
181. Song, S., et al., Optimization of 3D surfaces of dextran with different molecule weights for real-time detection of biomolecular interactions by a QCM biosensor. Polymers, 2017. **9**(9): p. 409.
182. Delvart, A., et al., Dextran-based polyelectrolyte multilayers: Effect of charge density on film build-up and morphology. Colloids and Surfaces B: Biointerfaces, 2022. **210**: p. 112258.
183. Alev-Tuzuner, B., et al., PEG-based hydrogel-coated test strip for on-site urea determination. International Journal of Polymeric Materials and Polymeric Biomaterials, 2019. **68**(10): p. 597-606.
184. Thiele, T., et al., StarPEG–heparin biosensors for rapid and portable diagnostics in complex biofluids. Sensors & Diagnostics, 2022.
185. Kim, J., et al., Hydrogel-based hybridization chain reaction (HCR) for detection of urinary exosomal miRNAs as a diagnostic tool of prostate cancer. Biosensors and Bioelectronics, 2021. **192**: p. 113504.
186. Lee, J., et al., Universal process-inert encoding architecture for polymer microparticles. Nature Materials, 2014. **13**(5): p. 524-529.
187. Jung, I.Y., et al., Hydrogel Based Biosensors for In Vitro Diagnostics of Biochemicals, Proteins, and Genes. Advanced Healthcare Materials, 2017. **6**(12): p. 1601475.
188. George, S.M., S. Tandon, and B. Kandasubramanian, Advancements in Hydrogel-Functionalized Immunosensing Platforms. ACS Omega, 2020. **5**(5): p. 2060-2068.
189. Hasanzadeh, M., et al., Mesoporous silica-based materials for use in biosensors. TrAC Trends in Analytical Chemistry, 2012. **33**: p. 117-129.
190. Yang, X., et al., Mesoporous materials–based electrochemical biosensors from enzymatic to nonenzymatic. Small, 2021. **17**(9): p. 1904022.
191. Moritz, M. and M. Geszke-Moritz, Mesoporous materials as multifunctional tools in biosciences: principles and applications. Materials Science and Engineering: C, 2015. **49**: p. 114-151.
192. Roushani, M. and K. Ghanbari, An electrochemical aptasensor for streptomycin based on covalent attachment of the aptamer onto a mesoporous silica thin film-coated gold electrode. Microchimica Acta, 2019. **186**(2): p. 115.
193. Tang, L., et al., A reusable electrochemical biosensor for highly sensitive detection of mercury ions with an anionic intercalator supported on ordered mesoporous carbon/self-doped polyaniline nanofibers platform. Biochemical Engineering Journal, 2017. **117**: p. 7-14.
194. Liu, J., et al., Vertically ordered mesoporous silica film-assisted label-free and universal electrochemiluminescence aptasensor platform. Analytical chemistry, 2016. **88**(23): p. 11707-11713.
195. He, D., et al., Regenerable multifunctional mesoporous silica nanocomposites for simultaneous detection and removal of mercury (II). Langmuir, 2013. **29**(19): p. 5896-5904.
196. Ribes, À., et al., Two new fluorogenic aptasensors based on capped mesoporous

silica nanoparticles to detect ochratoxin A. ChemistryOpen, 2017. **6**(5): p. 653-659.
197. Özalp, V.C., et al., Small molecule detection by lateral flow strips via aptamer-gated silica nanoprobes. Analyst, 2016. **141**(8): p. 2595-2599.
198. Suvarnaphaet, P. and S. Pechprasarn, Graphene-based materials for biosensors: a review. Sensors, 2017. **17**(10): p. 2161.
199. Balaji, A. and J. Zhang, Electrochemical and optical biosensors for early-stage cancer diagnosis by using graphene and graphene oxide. Cancer nanotechnology, 2017. **8**(1): p. 1-12.
200. Peña-Bahamonde, J., et al., Recent advances in graphene-based biosensor technology with applications in life sciences. Journal of nanobiotechnology, 2018. **16**(1): p. 1-17.
201. Huang, X., et al., An efficient signal-on aptamer-based biosensor for adenosine triphosphate detection using graphene oxide both as an electrochemical and electrochemiluminescence signal indicator. Analyst, 2015. **140**(17): p. 6015-6024.
202. Santiago, E., et al., Graphene Oxide Functionalized Biosensor for Detection of Stress-Related Biomarkers. Sensors, 2022. **22**(2): p. 558.
203. Mishyn, V., et al., Catch and release strategy of matrix metalloprotease aptamers via thiol-disulfide exchange reaction on a graphene based electrochemical sensor. Sensors & Diagnostics, 2022.
204. Abdelbasset, W.K., et al., Comparison and evaluation of the performance of graphene-based biosensors. Carbon Letters, 2022: p. 1-25.
205. Wu, X., et al., Study of fluorescence quenching ability of graphene oxide with a layer of rigid and tunable silica spacer. Langmuir, 2018. **34**(2): p. 603-611.
206. Kasry, A., et al., Highly efficient fluorescence quenching with graphene. The Journal of Physical Chemistry C, 2012. **116**(4): p. 2858-2862.
207. Zhang, H., et al., Fluorescent biosensors enabled by graphene and graphene oxide. Biosensors and Bioelectronics, 2017. **89**: p. 96-106.
208. Zhang, Q., et al., Development of a graphene oxide nanosheet and double-stranded DNA structure based fluorescent "signal off" aptasensor for ochratoxin A detection in malt. Food Chemistry: X, 2022. **14**: p. 100308.
209. Georgakilas, V., et al., Functionalization of Graphene: Covalent and Non-Covalent Approaches, Derivatives and Applications. Chemical Reviews, 2012. **112**(11): p. 6156-6214.
210. Guo, Z., et al., Surface Functionalization of Graphene-Based Materials: Biological Behavior, Toxicology, and Safe-By-Design Aspects. Advanced Biology, 2021. **5**(9): p. 2100637.
211. Erickson, K., et al., Determination of the local chemical structure of graphene oxide and reduced graphene oxide. Advanced materials, 2010. **22**(40): p. 4467-4472.
212. Carvalho, A.P., et al., Effect of Graphene *vs.* Reduced Graphene Oxide in Gold Nanoparticles for Optical Biosensors—A Comparative Study. Biosensors, 2022. **12**(3): p. 163.

213. Szunerits, S. and R. Boukherroub, Graphene-based biosensors. Interface focus, 2018. **8**(3): p. 20160132.
214. Cho, J., et al., Improving dispersion and barrier properties of polyketone/graphene nanoplatelet composites via noncovalent functionalization using aminopyrene. ACS applied materials & interfaces, 2017. **9**(33): p. 27984-27994.
215. Georgakilas, V., et al., Noncovalent functionalization of graphene and graphene oxide for energy materials, biosensing, catalytic, and biomedical applications. Chemical reviews, 2016. **116**(9): p. 5464-5519.
216. Mann, J.A. and W.R. Dichtel, Noncovalent functionalization of graphene by molecular and polymeric adsorbates. The Journal of Physical Chemistry Letters, 2013. **4**(16): p. 2649-2657.
217. Marcia, M., A. Hirsch, and F. Hauke, Perylene-based non-covalent functionalization of 2D materials. FlatChem, 2017. **1**: p. 89-103.
218. Kukovecz, Á., G. Kozma, and Z. Kónya, Multi-walled carbon nanotubes, in Springer handbook of nanomaterials. 2013, Springer. p. 147-188.
219. Han, J., et al., A novel sandwich-type immunosensor for detection of carcino-embryonic antigen using silver hybrid multiwalled carbon nanotubes/manganese dioxide. Journal of Electroanalytical Chemistry, 2017. **786**: p. 112-119.
220. Xia, J., et al., Sensitive glucose biosensor based on cyclodextrin modified carbon nanotubes for detecting glucose in honey. Journal of Food Composition and Analysis, 2022. **105**: p. 104221.
221. Bravo, I., et al., Laccase bioconjugate and multi-walled carbon nanotubes-based biosensor for bisphenol A analysis. Bioelectrochemistry, 2022. **144**: p. 108033.
222. Güner, A., et al., An electrochemical immunosensor for sensitive detection of Escherichia coli O157:H7 by using chitosan, MWCNT, polypyrrole with gold nanoparticles hybrid sensing platform. Food Chemistry, 2017. **229**: p. 358-365.
223. Zhou, L., et al., Electrochemical aptasensor for the detection of tetracycline with multi-walled carbon nanotubes amplification. Sensors and Actuators B: Chemical, 2012. **162**(1): p. 201-208.
224. Baghayeri, M., et al., Voltammetric aptasensor for bisphenol A based on the use of a MWCNT/Fe3O4@gold nanocomposite. Microchimica Acta, 2018. **185**(7): p. 320.
225. Li, S., et al., An electrochemiluminescence aptasensor switch for aldicarb recognition via ruthenium complex-modified dendrimers on multiwalled carbon nanotubes. Microchimica Acta, 2017. **184**(6): p. 1669-1675.
226. Huang, F., et al., Biosensors coupled with signal amplification technology for the detection of pathogenic bacteria: A review. Biosensors, 2021. **11**(6): p. 190.
227. Podešva, P., I. Gablech, and P. Neužil, Nanostructured gold microelectrode array for ultrasensitive detection of heavy metal contamination. Analytical chemistry, 2018. **90**(2): p. 1161-1167.
228. Kumar, S., P. Bhushan, and S. Bhattacharya, Fabrication of nanostructures with bottom-up approach and their utility in diagnostics, therapeutics, and others, in

Environmental, chemical and medical sensors. 2018, Springer. p. 167-198.
229. Li, Z., et al., Multisegment nanowire/nanoparticle hybrid arrays as electrochemical biosensors for simultaneous detection of antibiotics. Biosensors and Bioelectronics, 2019. **126**: p. 632-639.
230. Hu, W., et al., Hybrid ZnO Nanorod-Polymer Brush Hierarchically Nanostructured Substrate for Sensitive Antibody Microarrays. Advanced Materials, 2015. **27**(1): p. 181-185.
231. Subramani, I.G., et al., 1, 1'-Carbonyldiimidazole-copper nanoflower enhanced collapsible laser scribed graphene engraved microgap capacitive aptasensor for the detection of milk allergen. Scientific reports, 2021. **11**(1): p. 1-12.
232. Mahshid, S.S., A. Vallée-Bélisle, and S.O. Kelley, Biomolecular steric hindrance effects are enhanced on nanostructured microelectrodes. Analytical chemistry, 2017. **89**(18): p. 9751-9757.
233. Neupane, D. and K.J. Stine, Electrochemical Sandwich Assays for Biomarkers Incorporating Aptamers, Antibodies and Nanomaterials for Detection of Specific Protein Biomarkers. Applied Sciences, 2021. **11**(15): p. 7087.
234. Al-Dhahebi, A.M., et al., Ultrasensitive aptasensor using electrospun MXene/polyvinylidene fluoride nanofiber composite for Ochratoxin A detection. Food Chemistry, 2022. **390**: p. 133105.
235. Mercante, L.A., et al., Nanofibers interfaces for biosensing: Design and applications. Sensors and Actuators Reports, 2021. **3**: p. 100048.
236. Amouzadeh Tabrizi, M. and P. Acedo, An Electrochemical Impedance Spectroscopy-Based Aptasensor for the Determination of SARS-CoV-2-RBD Using a Carbon Nanofiber-Gold Nanocomposite Modified Screen-Printed Electrode. Biosensors (Basel), 2022. **12**(3).
237. Sarabaegi, M., et al., A novel ultrasensitive biosensor based on NiCo-MOF nanostructure and confined to flexible carbon nanofibers with high-surface skeleton to rapidly detect Helicobacter pylori. Materials Science in Semiconductor Processing, 2022. **139**: p. 106351.
238. Nadri, S., S. Habib Kazemi, and L. Nazari, A novel electrochemical biosensor based on the electrospun nanofibrous nanocomposites of PCL-PPy-MWCNT towards determination of TNF-α biomarker. Journal of Solid State Electrochemistry, 2022. **26**(6): p. 1389-1397.
239. Tao, S., et al., A sensitive and stable acetylcholinesterase biosensor with TiO2 nanoparticles anchored on graphitic carbon nanofibers for determination of organophosphate pesticides. Analytical Methods, 2022.
240. Xue, J., et al., Electrospinning and Electrospun Nanofibers: Methods, Materials, and Applications. Chemical Reviews, 2019. **119**(8): p. 5298-5415.
241. Wang, Y., T. Yokota, and T. Someya, Electrospun nanofiber-based soft electronics. NPG Asia Materials, 2021. **13**(1): p. 22.
242. Chauhan, D. and P.R. Solanki, Hydrophilic and Insoluble Electrospun Cellulose Acetate Fiber-Based Biosensing Platform for 25-Hydroxy Vitamin-D3 Detection. ACS Applied Polymer Materials, 2019. **1**(7): p. 1613-1623.
243. Yang, X., et al., Electrospun template directed molecularly imprinted nanofibers

incorporated with BiOI nanoflake arrays as photoactive electrode for photoelectrochemical detection of triphenyl phosphate. Biosensors and Bioelectronics, 2017. **92**: p. 61-67.
244. Wang, X., et al., Functional electrospun nanofibers-based electrochemiluminescence immunosensor for detection of the TSP53 using RuAg/SiO2NPs as signal enhancers. Analytical Biochemistry, 2018. **548**: p. 15-22.
245. Li, D., et al., Novel phenolic biosensor based on a magnetic polydopamine-laccase-nickel nanoparticle loaded carbon nanofiber composite. ACS applied materials & interfaces, 2014. **6**(7): p. 5144-5151.
246. Mercante, L.A., et al., Electrospinning-based (bio)sensors for food and agricultural applications: A review. TrAC Trends in Analytical Chemistry, 2017. **91**: p. 91-103.
247. Liu, Y., et al., A review on recent advances in application of electrospun nanofiber materials as biosensors. Current Opinion in Biomedical Engineering, 2020. **13**: p. 174-189.
248. Mondal, K., et al., Highly sensitive biofunctionalized mesoporous electrospun TiO2 nanofiber based interface for biosensing. ACS applied materials & interfaces, 2014. **6**(4): p. 2516-2527.
249. Mahmoudifard, M., M. Soleimani, and M. Vossoughi, Ammonia plasma-treated electrospun polyacrylonitryle nanofibrous membrane: the robust substrate for protein immobilization through glutaraldhyde coupling chemistry for biosensor application. Scientific Reports, 2017. **7**(1): p. 1-14.
250. Ma, F., et al., Highly porous poly (l-lactic) acid nanofibers as a dual-signal paper-based bioassay platform for in vitro diagnostics. Applied Surface Science, 2021. **542**: p. 148732.
251. Wang, Z., et al., Multivalent Aptamer Approach: Designs, Strategies, and Applications. Micromachines, 2022. **13**(3): p. 436.
252. Jia, L., et al., Highly sensitive electrochemical biosensor based on nonlinear hybridization chain reaction for DNA detection. Biosensors and Bioelectronics, 2016. **80**: p. 392-397.
253. Xu, J., et al., High sensitivity detection of tumor cells in biological samples using a multivalent aptamer strand displacement strategy. Analyst, 2022. **147**(4): p. 634-644.
254. Luo, L., et al., Sensitive and specific detection of tumour cells based on a multivalent DNA nanocreeper and a multiplexed fluorescence supersandwich. Chemical Communications, 2020. **56**(25): p. 3693-3696.
255. Liu, Y., et al., Highly sensitive minimal residual disease detection by biomimetic multivalent aptamer nanoclimber functionalized microfluidic chip. Small, 2020. **16**(20): p. 2000949.
256. Chen, Y., et al., Regenerative nanooctopus based on multivalent-aptamer-functionalized magnetic microparticles for effective cell capture in whole blood. Analytical chemistry, 2019. **91**(6): p. 4017-4022.
257. Yang, J., et al., *In situ*-generated multivalent aptamer network for efficient

capture and sensitive electrochemical detection of circulating tumor cells in whole blood. Analytical chemistry, 2020. **92**(11): p. 7893-7899.
258. Suh, Y.K. and S. Kang, A review on mixing in microfluidics. Micromachines, 2010. **1**(3): p. 82-111.

Chapter 3

Surface Modification of Glass-bottom 96-microwell Plates to Enhance ELISA Performances

Abstract

A sandwich enzyme-linked dendrimer-aptamer assay (ELDAA) has been developed using glass-bottom 96-microwell plates in order to improve the detection performances of a traditional enzyme-linked immunosorbent assay (ELISA). To this end, poly(amidoamine) (PAMAM) dendrimers were chemically immobilized onto glass-bottom surfaces of the microwells, and aptamers against a model analyte, *i.e.,* human platelet-derived growth factor BB (PDGF-BB), were subsequently conjugated onto the microwell surfaces via the immobilized PAMAM dendrimer templates. These layer-by-layer surface modifications were characterized using fluorescence microscopy, water contact angle, X-ray photoelectron spectroscopy, and atomic force microscopy to confirm the success of each surface modification steps. Moreover, the effects of different PAMAM dendrimer templates on the overall performances of the ELDAA were also studied. Our results showed that the new ELDAA had a much broader linear detection range that was approximately 2 times of that of a commercial ELISA and a significantly lowered limit of detection that was about 4.5 more sensitive in comparison with the standard ELISA. It can be concluded that the new ELDAA offers more versatile detection performances than the traditional ELISA technique and can be readily adapted into existing ELISA workflow, therefore offering a promising and robust alternative to the ELISA technique.

3.1 Introduction

Enzyme-linked immunosorbent assay (ELISA) is the most commonly used technique for the sensitive and quantitative evaluation of biological analytes [1-3]. There are many different types of ELISA including direct, indirect, sandwich, and competitive formats

[4-6]. With a sandwich ELISA test, capturing primary antibodies or antigens in an indirect or competitive ELISA are physically adsorbed onto surfaces of microwells upon which a commonly used sandwich detection format is subsequently carried out. As a result, the quantity of surface-immobilized primary antibodies or antigens is the most critical parameter affecting the performances of ELISA tests [1, 3]. Unfortunately, adsorptions of primary antibodies or antigens to the well-plate surfaces – while commonly used – are relatively weak interactions that are modulated by hydrophobic interactions and Van der Waals forces. This results in a limited amount of physically adsorbed primary antibodies or antigens on the well-plate surfaces [7, 8]. Sandwich ELISAs can be improved by increasing the number of primary antibodies immobilized onto the well-plate surfaces, and many different surface modification approaches have been attempted. For example, poly(styrene) (PS) 96-well plates have been treated by radiation to introduce negatively charged carboxyl groups to the treated surfaces in order to increase ionic interactions with positively charged primary antibodies [9]. Although the quantity of the attached antibodies has been improved, the stability of the attached antibodies on the surfaces is still a challenge. For example, immobilized antibodies by ionic interactions have been reported to be washed off the surfaces during washing steps that utilize detergents or vigorous agitation [10, 11] or displaced by other non-specific proteins in the samples [8, 12-14]. As a result, these losses of capturing antibodies from the capturing surfaces are known to significantly deteriorate ELISA detection performances, such as limit of detection (LOD) and detection range [1, 7, 15]. Alternatively, efforts have been made to covalently immobilize antibodies onto the surfaces of the microwells in an attempt to overcome these problems [13, 16, 17]; however they leave much to be desired. For example, covalently immobilized antibodies have been shown to tether to the surface in random orientations [18, 19], and reagents used in the chemical binding processes are known to negatively affect the antigen-binding sites of the immobilized antibodies [13, 20, 21]. These issues have significantly decreased both the quantity and quality of functional primary antibodies available for effective target binding on microwell surfaces [13, 18-21].

Poly(amidoamine) (PAMAM) dendrimers are spherically shaped polymers that feature numerous functional groups, such as -OH, -COOH, and $–NH_2$ on their surfaces. As a result of their unique structures, PAMAM dendrimers are increasingly being used as a template to be chemically immobilized onto various detection surfaces in order to provide multiple binding sites for subsequent conjugation with desired capturing elements, either aptamers or antibodies [22, 23]. In comparison with their linear analogues, PAMAM dendrimers present much larger surface areas, thereby allowing increased surface area and enhanced probabilities to capture targeted analytes [24]. In addition, since the amount of immobilized binding sites is a critical factor in determining the overall performance of ELISA [1, 15, 25, 26], it is essential to design a strategy to increase the amount of the immobilized binding sites on the capturing surface.

In this study, we report a simple approach to surface modify glass-bottom 96-well plates first with PAMAM dendrimers and subsequently with aptamers to develop an enzyme-linked dendrimer-aptamer assay (ELDAA) in order to improve the detection performances of a traditional ELISA. Specifically, the glass-bottom 96-well plates are chemically immobilized with PAMAM dendrimers as templates with multifunctional handles to allow subsequent attachment of numerous copies of aptamers that are designed to specifically capture target biomolecules. In comparison with the traditional ELISA techniques, the current ELDAA design offers the following unique features: 1) the chemical surface immobilization of aptamers allows for both more stable and better control of aptamer attachments to the microwell surfaces [13, 27]; 2) the PAMAM dendrimer surface modification renders the modified microwell surfaces nonfouling, which prevents non-specific interactions of non-targets with the modified surfaces, decreasing background noises and thus increasing detection sensitivities [23, 28]; and 3) aptamers are much smaller in size when compared with antibodies; as a result, multiple copies of aptamers can be conjugated to the microwell surfaces via multi-

handled dendrimer templates to readily enhance the number of binding sites on the microwell surfaces, thereby improving testing performances [29, 30]. Our results showed that the new ELDAA design exhibited overall enhanced testing performances when used to quantify platelet-derived growth factor-BB (PDGF-BB), a model biomolecule for quantification. In particular, the linear detection range was increased by 2 folds, and the limit of detection was decreased by 4.5 folds in comparison with the performances of a commercial PDGF-BB ELISA kit.

3.2 Experimental

3.2.1 General Approach of Sandwich ELDAA

In this study, we report a new method to develop a sandwich ELDAA by modifying glass-bottom 96-well plates for more effective and sensitive quantification of human PDGF-BB, a model molecule that can be readily replaced by other biomolecules of interest. As shown in Figure 3.1, the glass-bottom 96-well plate is initially treated with oxygen plasma to introduce -OH functional groups on the glass surface [31], which is followed by surface amination with 3-aminopropyl-triethoxysilane (APTES). Subsequently, the aminated surface is covalently reacted with PAMAM dendrimers that provide multiple binding sites for further attachment of multiple copies of aptamers that are designed to specifically bind PDGF-BB. For signal read-outs, the captured PDGF-BB molecules will interact with biotinylated secondary antibodies that subsequently conjugate with avidin labelled horseradish peroxidase (avidin-HRP), which will react with a substrate, *i.e.,* 2,2′-azino-bis (3-ethylbenzothiazoline-6-sulfonic acid) (ABTS), to generate optical signals that can be detected using a plate reader.

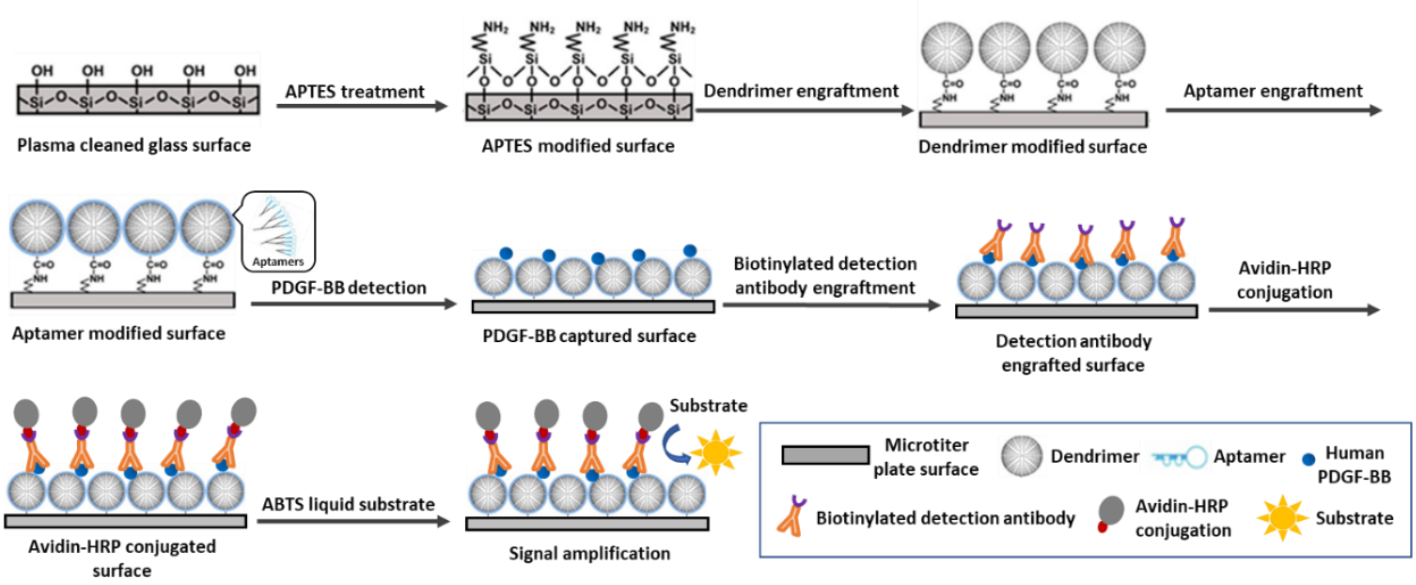

Figure 3.1. Schematic illustration showing the general approach to prepare an ELDAA using a glass-bottom 96-well plate for quantification of human PDGF-BB.

3.2.2 Materials

N-hydroxysuccinimide (NHS), 3-aminopropyl-triethoxysilane (99%) (APTES), 1-ethyl-3-(3-dimethylaminopropyl) carbodiimide hydrochloride (EDC), 5-(aminoacetamido) fluorescein (fluoresceinyl glycine amide) (FITC-NH_2), and rhodamine-NHS were purchased from Thermo Fisher Scientific (Ottawa, ON). Anhydrous alcohol, Tween-20, phosphate-buffered saline (PBS) (0.01 M, pH 7.4), 2,2′-azino-bis(3-ethylbenzothiazoline-6-sulfonic acid) (ABTS) liquid substrate solution and bovine serum albumin (BSA) were purchased from Sigma-Aldrich (Oakville, ON). N, N-Dimethylformamide (DMF) was obtained from VWR (Mississauga, ON). Poly(amidoamine) (PAMAM) dendrimer generation 4 with carboxyl functional groups (G4-COOH) and generation 7 with carboxyl functional groups (G7-COOH) were purchased from Dendritech (Midland, MI). Human EGF, human FGF, sonic hedgehog, BMP-4 and Human PDGF-BB Standard ABTS ELISA Development Kit were purchased from PeproTech (Rocky Hill, NJ). Glass-bottom 96-well plates were purchased from Cellvis (Mountain View, CA). High binding poly(styrene) 96-well plates were purchased from Corning (Corning, NY). Aptamers were custom synthesized by Integrated DNA Technologies (Coralville, IA). Aptamer sequences used

in this study are listed below:

Capturing aptamer (*i.e.,* aptamer against human PDGF-BB) [32, 33]:

5'/NH_2, 12C Spacer/TAC TCA GGG CAC TGC AAG CAA TTG TGG TCC CAA TGG GCT GAG TA /3'

Fluorescently labelled Cy3-aptamer:

5'/NH_2, 12C Spacer/TAC TCA GGG CAC TGC AAG CAA TTG TGG TCC CAA TGG GCT GAG TA /Cy3/3'

Scrambled sequence used as a control:

5'/NH_2,12C Spacer /TCC TCA AAG CAC CGC ATG CAA CAG TAG TTC AGA TAC ATT GCG TA/3'

3.2.3 Surface Modifications and Characterizations

3.2.3.1 Glass-bottom Microwell Surface Amination

To introduce amino functional groups to the glass bottom surfaces of the 96-microwell plates, a well-established method was used with minor modifications [28]. Specifically, plate bottom glass surfaces were treated using an oxygen plasma cleaner (Model SP100, Anatech Ltd, Battle Creek, MI) at 100 mTorr and 118 W for 10 s to introduce -OH functional groups onto the plate glass surfaces [28], and 100 μL 5 vol % APTES in anhydrous ethyl alcohol was immediately reacted with the plasma-treated surfaces for 10 s. Subsequently, the APTES solution was removed, and the treated surfaces were washed, in sequence, with anhydrous ethyl alcohol, 70 vol % ethyl alcohol, and water (note this gradient washing scheme was developed to avoid APTES precipitation on the glass surfaces). Finally, the resulting APTES treated plate was dried using a nitrogen gas stream.

To confirm the success of the surface amination, a well-established fluorescent labelling technique was used [34, 35]. In brief, the aminated surfaces were fluorescently labelled with rhodamine-NHS. As rhodamine-NHS readily reacts with primary amines, the labelling technique can semi-quantitatively evaluate the relative amount of amino

functional groups on the treated surfaces [34, 35]. In a typical experiment, 100 μL rhodamine-NHS solution (20 μg/mL) in PBS (pH 7.4) was added into each wells of 96-well plates already treated with APTES at room temperature for 30 min. After the labelling reaction, the microwells were extensively washed, and fluorescence images of the labelled surfaces were documented by an inverted fluorescence microscope (Olympus IX81, Richmond Hill, ON) equipped with a high-resolution charge-coupled device (CCD) camera (QImaging, Surrey, BC). Finally, the collected images were analyzed by Image-Pro Plus 6.0 software (Media Cybernetics Inc., Rockville, MD) to evaluate the fluorescence intensities of the surfaces of interests.

3.2.3.2 PAMAM-COOH Engraftment

To immobilize PAMAM-COOH onto the aminated microwell surfaces obtained from the previous step, each aminated microwells were reacted with 100 μL reaction mixtures containing 1 μM PAMAM-COOH, 5 mM NHS, and 2 mM EDC in 0.1 M MES solution (pH 6.0) at room temperature. The reaction was allowed to be carried out for 2 h, after which the microwells were extensively washed with PBS (pH 7.4) and stored in PBS (pH 8.0) for future use [36].

3.2.3.3 Aptamer Engraftment

To conjugate aptamers onto the PAMAM-COOH modified microwell surfaces, each microwells were treated with 100 μL reaction mixtures containing 5 mM NHS and 2 mM EDC in 0.1 M MES solution (pH 6.0) at room temperature for 30 min to activate the carboxyl functional groups [28]. This step was followed by reacting with 200 μL 5 μM aptamer solution in PBS (pH 7.4) for 2 h, and finally washed with PBS (pH 7.4) to remove the unreacted aptamers. To confirm the success of this conjugation step and to evaluate the relative amount of the immobilized aptamers, fluorescently labelled Cy3-aptamers were also used, and the surface fluorescence intensities of the resulting microwell surfaces were evaluated as detailed in Section 3.2.3.1.

3.2.3.4 Water Contact Angle Measurements

To further confirm the success of each step of the surface modification, water contact angle (WCA) measurements were carried out using a goniometer (AST Products Inc., Billerica, MA) [37]. For each sample surface, three measurements (2 readings per measurement, total of 6 readings) were taken at random (and different) locations on a sample surface of interest, and the averaged values were reported.

3.2.3.5 X-ray Photoelectron Spectroscopy (XPS)

Surface modifications were also characterized using XPS. Specifically, XPS spectra were obtained using a Kratos Axis Ultra DLD spectrometer (Kratos Analytical Ltd, Manchester, UK) with monochromatized Al Kα X-rays. The take-off angles for all measurements were fixed at 45 °, and 284.6 eV was used as a reference position for the C-H(C) peak. High resolution spectra of C 1s and N 1s peaks were analyzed by CasaXPS Version 2.3.19 PR1.0. (Casa Software Ltd., Teignmouth, UK).

3.2.3.6 Atomic Force Microscopy (AFM)

To study the morphological changes due to surface modifications, a Veeco Di Multimode V AFM (Santa Barbara, CA) was used. Surfaces of interest were probed in contact mode and the results were analyzed by NanoScope software (Santa Barbara, CA). The root mean square (RMS) roughness of each surface was calculated using NanoScope software (Santa Barbara, CA).

3.2.4 ELDAA Performance Evaluation

To evaluate the performance of ELDAA, a standard human PDGF-BB sandwich ELISA protocol was carried out using the dendrimer-aptamer modified microwells with some modifications, *i.e.,* the eliminations of both the primary antibody incubation and all subsequent blocking steps. Briefly, to each wells of the dendrimer-aptamer modified 96-microwell plates, 100 µL of either samples of interests or PDGF-BB standards were transferred and incubated at room temperature for 2 h. After extensive washes with

washing solution (0.05 % Tween-20 in PBS (pH 7.4)), the microwells were incubated with 100 μL 0.25 μg/mL biotinylated secondary antibody at room temperature for 2 h and thoroughly washed. Subsequently, the resulting microwells were incubated with 100 μL avidin-HRP conjugate for 30 min, carefully washed, and finally reacted with 100 μL ABTS substrate solution at room temperature for 15 min before the absorbance was measured using a BioTek microplate spectrophotometer (Winooski, VT) at 405 nm with a reference wavelength at 650 nm. In parallel, Corning® 96-well flat-bottom high binding microplates (Corning, NY) were used to analyze the same sets of samples by following the vendor's protocol (PeproTech lnc., Rocky Hill, NJ).

3.2.5 Statistical Analysis

The statistical analysis was performed using Microsoft Excel software (version 2303). To ensure the reliability and robustness of the results, all experiments were carried out in triplicate (otherwise indicated in figure captions), both within the same day and across different days, and the mean values with their corresponding standard deviations were calculated and reported. The Student's t-test, two-tailed, was employed to assess the statistical significance of the differences between the groups, with a p-value of less than 0.05 considered statistically significant.

3.3 Results and Discussion

3.3.1 Surface Characterization

In order to modify the glass-bottom surfaces of the microwells, the glass surfaces were initially treated with oxygen plasma and subsequently modified with APTES to achieve surface amination. To confirm the success of the surface amination, an amine-reactive fluorescence label (*i.e.,* rhodamine-NHS) was employed to semi-quantitatively characterize the amino functional groups on the resulting surfaces [34]. As shown in Figure 3.2A, it is evident that the glass surfaces treated with both plasma and APTES (*i.e.,* plasma+APTES+rhoadamine-NHS) were successfully aminated as the surfaces showed significantly higher fluorescence intensity (*i.e.,* 975.3 ± 40.6 a.u.) in

comparison with the control surfaces (*i.e.,* no fluorescent labels (plasma+APTES no rhodamine-NHS (32.8 ± 8.1 a.u.)) and the fluorescent labels that were only physically adsorbed (*i.e.,* plasma+ rhodamine-NHS (47.3 ± 17.2 a.u.)). In carrying out the surface amination, the optimal concentration and reaction time of APTES treatment were investigated. As shown in Figure A1 (in Appendix A), the optimal APTES concentration and reaction time were 5 vol % and 10 s, respectively. These APTES reaction conditions were used in the rest of this study unless indicated otherwise.

Likewise, to confirm the success of PAMAM-COOH generation 7 (*i.e.,* G7-COOH) conjugation to the microwell surfaces, FITC-NH_2 was used as a fluorescent label to react with the carboxyl functional groups on the dendrimer modified surfaces (Appendix A for labelling method). As shown in Figure 3.2B, there was a significant increase in fluorescence intensity after the G7-COOH modified microwells were labelled with fluorescent FITC-NH_2 (*i.e.,* G7 modified + FITC-NH_2 chemically reacted), indicating that the microwells were successfully functionalized by carboxyl functional groups; this conclusion was further supported by the fact that there was no significant difference in fluorescence intensities between G7-COOH modified microwells without fluorescent labels (*i.e.,* G7 modified + no FITC-NH_2 label) and those with only physically adsorbed labels (*i.e.,* G7 modified + FITC-NH_2 physically adsorbed). Furthermore, as shown in Figure A2 (Appendix A), 1 μM was selected as the optimum G7-COOH concentration for surface conjugations.

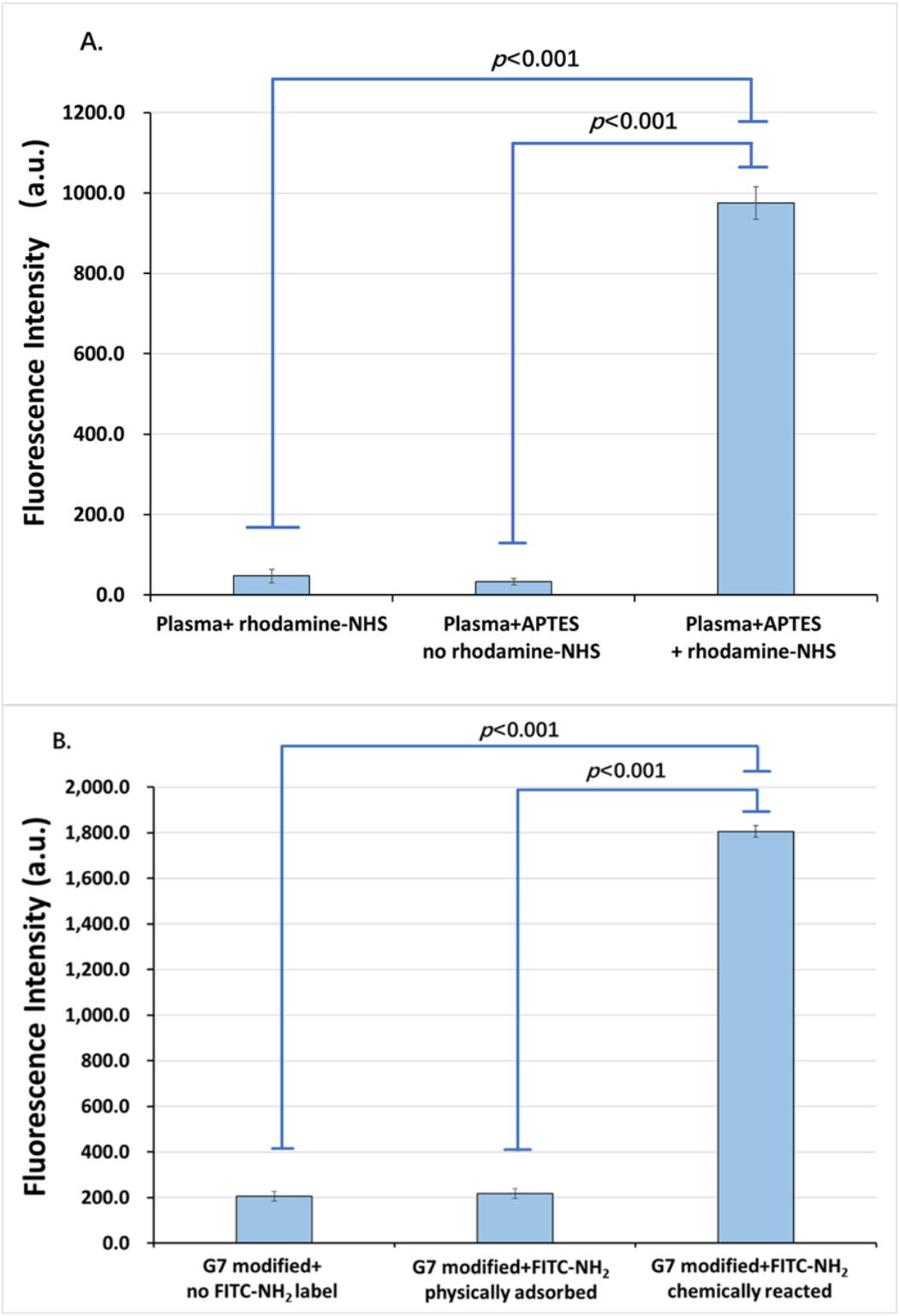

Figure 3.2. Fluorescence intensities of functionalized microwells. A). Fluorescence intensities of amine-functionalized microwells labelled by rhodamine-NHS to confirm the success of APTES modification (error bars indicate standard deviation, n=12). B). Fluorescence intensities of G7-COOH modified microwells labelled by FITC-NH_2 to confirm the success of G7-COOH modification (error bars indicate standard deviation, n=12).

To confirm the success of aptamer attachment to the dendrimer modified microwells via G4-COOH or G7-COOH templates, fluorescently labelled aptamers with free amino groups (*i.e.,* Cy3-aptamers-NH_2) were used to attach to the surfaces of dendrimer modified microwells. As shown in Figure 3.3A, in comparison with the dendrimer modified surfaces, Cy3-aptamer modified microwells via dendrimer templates showed significantly ($p<0.001$) increased fluorescence intensity, strongly suggesting that the chemical conjugation of the aptamers to the dendrimers – for both the cases of G4-COOH and G7-COOH – was successful. This conclusion is further supported by the observation that there was no statistical difference ($p>0.05$) in fluorescence intensities between dendrimer-modified microwells and dendrimer-modified microwells with Cy3-aptamers physically adsorbed. A closer analysis of the data shows that in comparison with the G4-aptamer-Cy3 modified microwells, the G7-aptamer-Cy3 modified microwells emitted higher fluorescence intensity, demonstrating that there were more copies of fluorescently labelled aptamers conjugated to the G7-modified microwell surfaces. This observation strongly suggests that G7-modified microwells have more capacity for aptamer surface engraftment, likely as a result of G7 having more functional groups for aptamer conjugation than G4 [28]. In addition, it is worthwhile to note that the dendrimer-aptamer surface modification approach is arguably more effective than the dendrimer-antibody approach to increase capturing surface binding sites because antibodies and dendrimers have comparable molecular sizes, whereas aptamers are much smaller in sizes [30, 38]. Furthermore, as shown in Figure A3 (Appendix A), 5 μM was determined to be the optimum aptamer concentration to conjugate aptamers to both G4 and G7 modified surfaces in order to achieve the maximum amount of aptamers on the resulting surfaces.

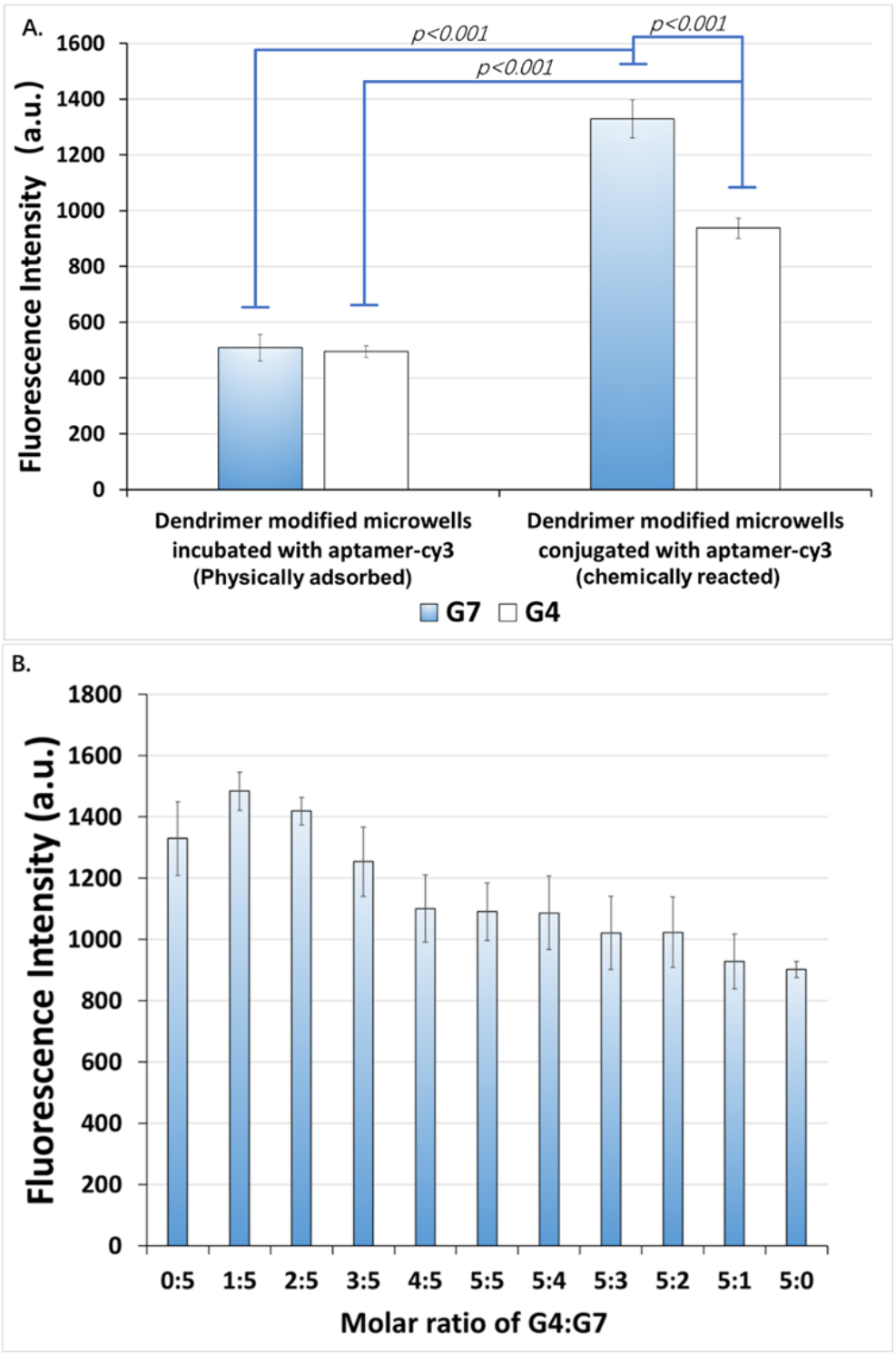

Figure 3.3. Fluorescence intensities of dendrimer modified microwells after conjugation with Cy3-aptamers. A) Fluorescence intensities of G4 and G7 modified surfaces conjugated with Cy3-aptamers (error bars indicate standard deviation, n=8). B) Effects of surface modifications using mixtures of G4 and G7 at different ratios as demonstrated by the relative amount of Cy3-labelled aptamers on the surfaces (error bars indicate standard deviation, n=12).

In a separate set of experiments, fluorescently labelled Cy3-aptamers were also used to study the effects of using mixtures of G4 and G7 at different ratios on surface modifications. Specifically, the surfaces of microwells were modified with reaction mixtures containing both G4 and G7 prepared with different molar ratios (*e.g.,* G4:G7=1:5 means that the reaction mixture containing 1 μM G4 and 5 μM G7 solutions). As shown in Figure 3.3B, it is clear that G7 dendrimer templates (see Sample 0:5) had a higher capacity to subsequently immobilize aptamers than G4 templates (Sample 5:0). This result is expected since G7 templates have more functional groups for aptamer conjugation than G4 [28]. It is also noted that for the very same reason, there is a general decreasing trend in the number of aptamers conjugated (shown in fluorescence intensity) to the dendrimer templates as the molar ratio of G4 in the mixture increased. However, a closer analysis of the data suggests that the number of aptamers conjugated to the surface via the mixture of G4 and G7 templates peaked when the G4:G7 molar ratio was at 1:5. This observation is unexpected and does not agree with the general trend. While the reason for this observation is not entirely clear, it is likely that the smaller G4 molecules may have filled voids between G7 molecules (G4 = 4.5 nm and G7 = 8.1 nm in diameters) on the surfaces [39], resulting in more densely packed surfaces and therefore more available functional groups on the surfaces for subsequent aptamer conjugations. This explanation is further supported by the fact that G4 molecules are known to be more deformable to fit into small spaces [40-42]. However, the benefit of using the more deformable G4 in the mixture quickly diminishes with the higher molar ratio of G4 in the mixture since G4 templates have significantly fewer functional groups than G7 templates for further conjugation with the aptamers. Therefore, microwells modified by either G4, G7 or a mixture of G4&G7 at a ratio of 1:5 (referred to as G4&G7 hereinafter) were prepared and their performances were compared.

To confirm the success of surface modification, the resulting surfaces of each modification step were analyzed by WCA and XPS. As shown in Figure 3.4A, the WCA

of the bare glass surface was 26.5°±1.7°. As expected, the WCA was significantly decreased to 7.6°±1.8° after the plasma treatment, most likely due to the introduction of more hydrophilic hydroxyl groups on the glass surface. Furthermore, after APTES treatment, the WCA dramatically increased to 57.1°±1.2°, a value consistent with a previously reported value of 59.0° [43], likely due to the introduction of hydrophobic alkyl chain in APTES to the surface. Furthermore, after modifications with either G4, G7, or G4&G7, the WCAs of the resulting surfaces decreased to 16.6°±1.4°, 4.7°±0.7°, and 4.2°±0.6°, respectively, suggesting that hydrophilic dendrimers have been successfully introduced to the surfaces. It is interesting to note that G7 and G4&G7 modified surfaces had lower WCAs in comparison with the G4 modified surfaces, which is most likely caused by less surface coverage of the G4 molecules according to Cassie Equation [44, 45]. The surface coverage of the G4 modified surfaces was estimated to be 90% and both the G7 and the G4&G7 modified were over 99%, based on results from previously published studies [46-48].

To further confirm the success of the surface modifications, XPS was employed. As shown in Figure 3.4B, high-resolution scans of C 1s and N 1s were used to analyze different surfaces of interest, *i.e.,* bare glass surfaces, surfaces with APTES modification (*i.e.,* APTES modification), and G7 modification. As expected, for the glass surface C 1s scan (I), there were two main deconvoluted peaks at 284.6 eV and 287.0 eV that can be attributed to C-Si/C-C(H) and C-O, respectively [28, 49]. In contrast, after the APTES modification (II), two new peaks emerged at 286.5 eV (C-N) and 288.1 eV (HNC=O), while one peak at 287.0 eV (C-O) disappeared, suggesting the success of APTES modification on the glass surface [50]. In addition, after the surface was further modified with G7 (III), the C 1s spectrum showed a significant difference. Specifically, the peaks were decomposed into four main deconvoluted peaks. The most prominent peak at 286.5 eV can be attributed to C-N [50, 51]. It should be noted that while the C-Si/C-C(H) peak at 284.6 eV was still present in the spectrum, the peak intensity was significantly reduced in comparison with that shown in either (I) or (II),

suggesting additional materials were successfully introduced on top of the glass surface. Furthermore, two new constituent peaks at 285.8 eV for (C=O)-N [52] and at 290.2 eV for (C=O)-OH [50, 52] were evident. These two peaks are consistent with the chemical structures of the dendrimers, strongly suggesting that dendrimer surface immobilizations were successfully carried out. Similarly, XPS spectra also showed significant changes in N 1s peaks after each step of surface modifications. As expected, there was no evident N 1s peak in the case of bare glass samples (IV); however, both APTES and dendrimer modified surfaces showed clear and similar N 1s peak patterns. The N 1s peak was further decomposed into two components at 399.5 eV for HNC=O and 402.4 eV for $-NH_2$, respectively [50], indicating amide and amino structures in both APTES and dendrimer molecules. In summary, the XPS results show strong evidence to confirm the success of surface modifications, and they are in good agreement with previously published results [28, 50].

It should be noted that while only the XPS results for G7 were shown in Figure 3.4B, G4 and G4&G7 modified surfaces showed identical peak patterns only with different surface atomic ratios. Detailed results are tabulated in Table A1 in Appendix A.

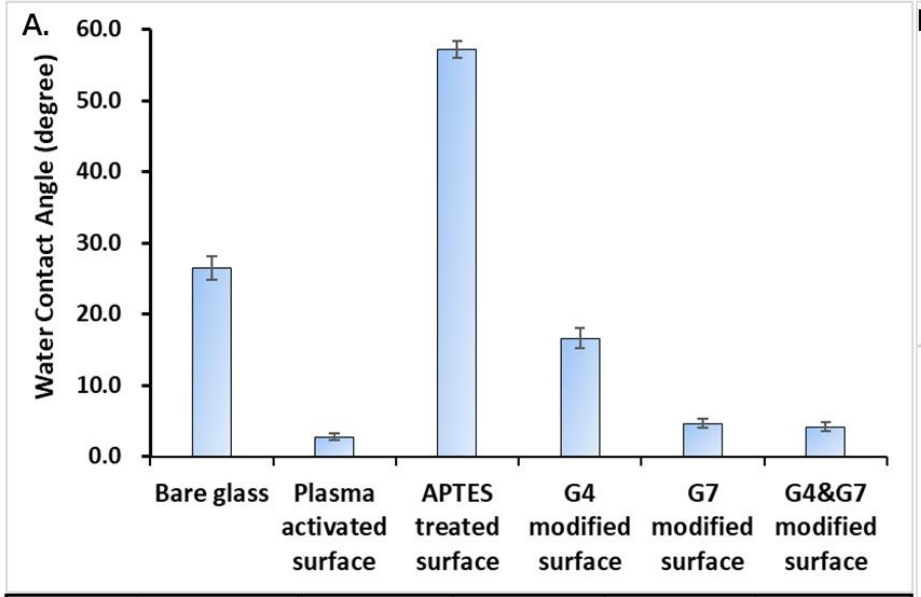

C.	Bare Glass	APTES Modification	G4 Modification	G7 Modification	G4&G7 Modification
3D Image					
Vertical View					
Roughness (nm)	0.16±0.01	0.34±0.06	0.56±0.04	0.96±0.05	1.38±0.13

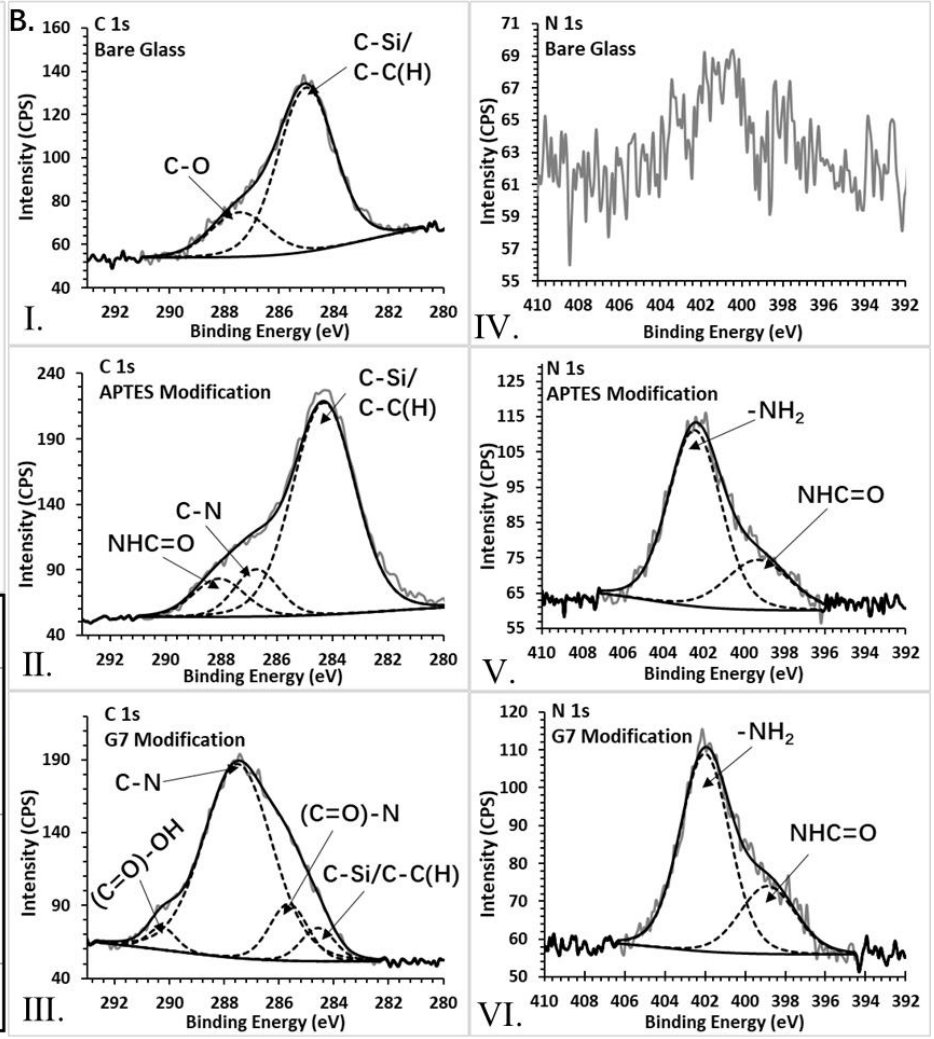

Figure 3.4. Characterizations of surface modifications. A) Water contact angle measurements of modified surfaces (error bars indicate standard deviation, n=6); B) High-resolution XPS spectra of surfaces of interest: (I) C 1s bare glass surface; (II) C 1s APTES modified glass surface; (III) C 1s G7 modified glass surface; (IV) N 1s bare glass surface; (V) N 1s APTES modified glass surface; (VI) N 1s G7 modified glass surface. C) AFM images of each modified surface (error bars indicate standard deviation, n=8).

Figure 3.4C shows topographic features of different surfaces of interest obtained by AFM. It is clear that the original glass surface had a smooth and almost atomically flat surface, and the RMS roughness was calculated to be 0.16 nm ± 0.01 nm. In comparison, when the surface was initially treated with APTES, the RMS roughness increased to 0.34 nm ± 0.06 nm, likely caused by the heterogeneous spatial distribution of the silane molecules [53]. Furthermore, surface roughness was further increased after the surfaces were modified with G4, G7, and G4&G7, as the RMS roughness was measured at 0.56 nm ± 0.04 nm, 0.96 nm ± 0.05 nm, and 1.38 nm ± 0.13 nm, respectively. The significant surface roughness changes are consistent with previously published observations[52-54], and further confirm successful dendrimer surface immobilizations on the glass surfaces. Moreover, surface height distributions of the dendrimer-modified surfaces were calculated, and the results are shown in Figure A4 in the Appendix A. The average surface height of G4&G7 modified surfaces was 7.4 ± 1.8 nm, greater than those of both the G4 and the G7 modified surfaces at 2.8 ± 0.7 nm and 5.1 ± 0.9 nm, respectively. The phenomenon is likely due to the deformation of dendrimer molecules when G4 molecules fill voids between G7 molecules, causing G4 molecules to deform into upright elliptic shapes [46, 55-57].

3.3.2 Test Specificity

To investigate test specificity, both target (*i.e.,* human PDGF-BB) and non-targets, including human EGF, human FGF, sonic hedgehog, and BMP-4, were tested at 2 ng/mL using G4-, G7-, G4&G7-aptamer modified microwells as well as high binding poly(styrene) 96-well plates. As evident in Figure 3.5A, detection signals for targets (*i.e.,* human PDGF-BB) were significantly higher than those of non-targets, suggesting

excellent detection specificities of G7- and G4&G7-aptamer modified microwells; this conclusion was further supported by the observation that detection signals were significantly reduced when analyzed by G4-, G7- and G4&G7- scrambled aptamer modified microwells. It is interesting to note that the signals of targets were 3- 4 times higher than those of non-target molecules using the G7- and G4&G7-aptamer modified microwells (without blocking steps); in contrast, the signals of targets were only 2 times those of non-targets using the poly(styrene) 96-well plates (*i.e.,* commercial ELISA, with blocking steps). This observation strongly argues for the advantages of the excellent nonfouling properties of the dendrimer-modified surfaces (either G7 or G4&G7), which have significantly lowered background noises from non-specific adsorptions to the detection surfaces even without blocking steps. However, it is also noted that G4-aptamer modified microwells showed a pronounced deteriorating detection specificity because of relatively high detection signals of non-targets. To further investigate the reason for the poor detection specificity observed in the G4-aptamer modified microwells, nonfouling properties of the surfaces of interests were further investigated as excellent surface nonfouling properties can significantly improve detection specificities [1, 3]. The nonfouling property is particularly important since no blocking steps were employed when using the surface-modified microwells in this study. Specifically, microwells with surfaces of interests, including original glass (non-modified) and dendrimer modified microwells (*i.e.,* G4, G7, and G4&G7 modified microwells) were tested using target analytes (*i.e.,* human PDGF-BB) at 2 ng/mL, and non-specific absorption signals of each microwells were compared (note that capturing aptamers were not conjugated to the dendrimer in this experiment). As shown in Figure 3.5B, dendrimer-modified microwells, including G4, G7, and G4&G7

modified, showed significantly lower background noises in comparison with the non-modified microwells. This is expected since dendrimer-modified surfaces to demonstrate nonfouling properties [23]. It has been established that surface nonfouling properties are due to the hydrophilicity and sterical hindrance of surface-immobilized dendrimers [58-60]. Specifically, the dendrimer-modified surface is hydrophilic and it exhibits a strong binding ability to interface with water molecules (*i.e.,* hydration) to form a physical and energetic barrier to prevent protein adsorption on the surface; moreover, the compression of the dendrimer coating also results in steric repulsion against approaching biomolecules, such as proteins, to prevent non-specific adsorptions. Significantly, a closer look at the data shows that G4 modified microwells showed about as twice the background noise level as either G7 and or G4&G7 modified microwells. This observation likely suggests that although dendrimer surface modifications can markedly enhance the nonfouling properties of the resulting microwell surfaces, modifications with either G7 or G4&G7 are more effective. This is because the G7 or G4&G7 modified surface showed improved surface coverage (as discussed in Figures 3.4 and A4) and coating thickness (G7 *vs.* G4), as both surface coverage and coating thickness have also been shown to be important factors to resist surface fouling [61-63]. It should also be noted that for complex samples with a multitude of proteins present, such as blood and saliva [59, 61], more stringent surface optimization should be performed to ensure complete surface coverage as well as sufficient coating thickness to achieve improved surface nonfouling property [60-63].

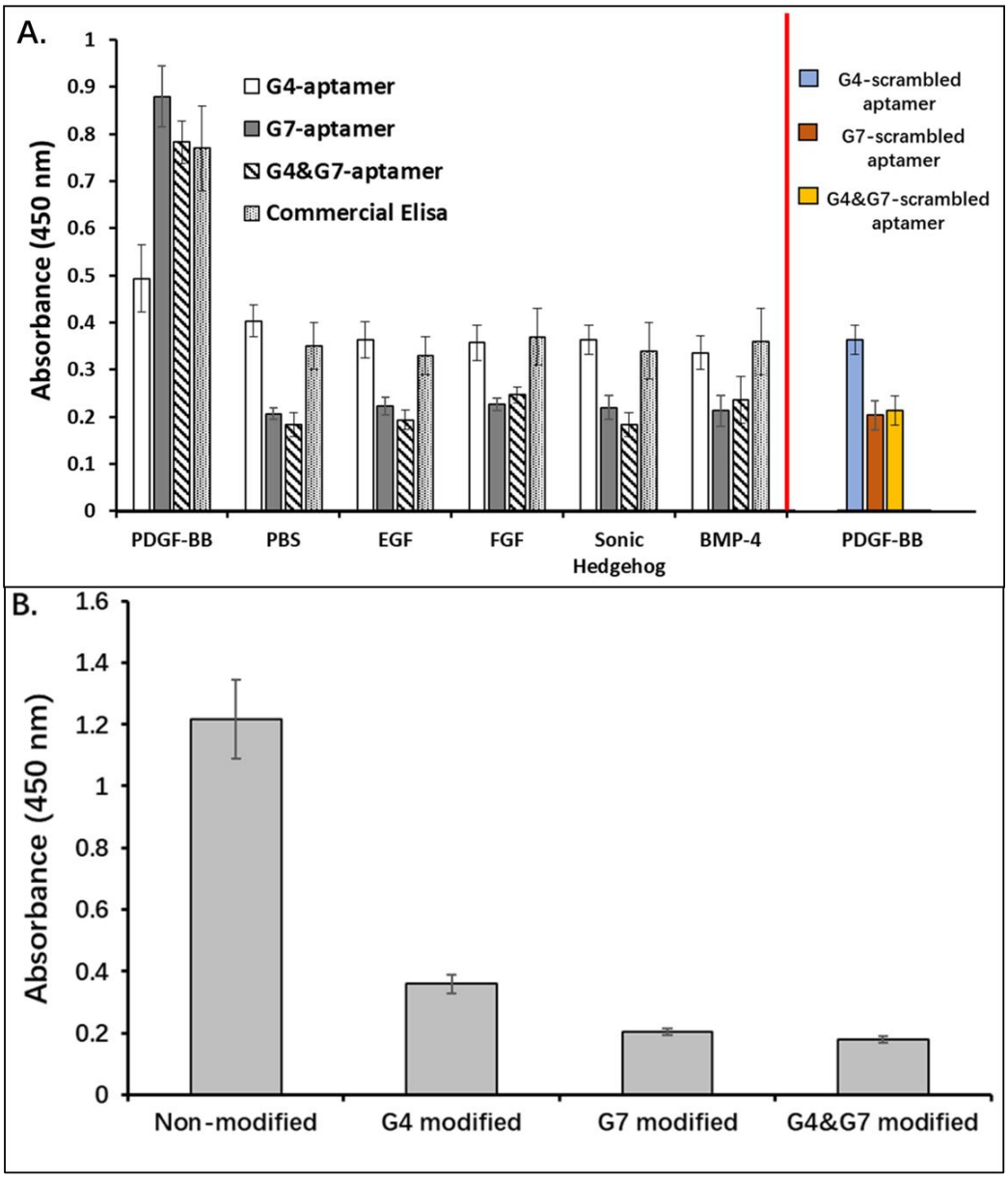

Figure 3.5. Detection specificity and nonfouling properties of the surface-modified microwells. A) Detection specificity of modified microwells of interest. Targets: human PDGF-BB and non-target analytes: human EGF, human FGF, sonic hedgehog, and BMP-4 were tested at 2 ng/mL. Error bars are standard deviations, n=3. B) Nonfouling performances of modified microwells. Human PDGF-BB (2 ng/mL) samples were tested on the surfaces without aptamer-modified coatings (error bars indicate standard deviation, n=3).

3.3.3 Evaluation of Sandwich ELDAA Performance

To evaluate the sandwich ELDAA performances, ELDAA tests of commercial human PDGF-BB standard solutions using G4-, G7-, and G4&G7-aptamer modified

microwells were conducted. In parallel, conventional ELISA tests were carried out using high binding poly(styrene) 96-well plates according to a standard protocol by the vendor for comparison. As shown in Figure 3.6, ELDAA tests conducted in G7- and G4&G7-aptamer modified microwells showed comparable signal intensities at any given PDGF-BB concentrations. More importantly, the G7- and the G4&G7-aptamer modified microwells demonstrated linear detection ranges at 0.01-3.50 ng/mL and 0.01-4.00 ng/mL, respectively; it should be noted that these linear ranges are almost 2 times that of a standard ELISA as carried out in the poly(styrene) plates (0.03-1.75 ng/mL) (see insets, Figure 3.6). The significantly increased detection range performances exhibited in both G7- and G4&G7- modified microwells are likely because of more surface immobilized aptamers as target recognition sites than surface adsorbed antibodies in the poly(styrene) plates. However, the extent of the performance improvement in linear detection range for both the G7- and the G4&G7-aptamer modified microwells is less than what one would theoretically expect given the amount of aptamers introduced to the capturing microwell surfaces via the dendrimer templates. This discrepancy might be due to steric hindrance inbetween the analyte molecules captured by the aptamer modified microwell surfaces. More specifically, since the PDGF-BB molecules are big molecules, and when they are captured by the aptamer modified microwell surfaces, it is likely that the captured PDGF-BB molecules would "shadow" nearby aptamers to prevent these aptamers from interacting with other target PDGF-BB molecules even if these aptamers are still available for binding. In comparison, ELDAA tests conducted in G4-aptamer modified microwells showed significantly lower signals, likely suggesting less immobilized aptamers on the microwell surface, as demonstrated in Figure 3.3.

In addition, the response curve slopes (Figure 3.6, insets) of the ELDAA tests conducted using both the G7- and the G4&G7-aptamer modified microwells were greater than that of standard ELISA tests carried out in high binding poly(styrene) 96-well plates, suggesting higher detection sensitivities, as detection sensitivities are determined by the slope of the response curve [64, 65]. Moreover, LODs, defined as the lowest target concentration that can provide signals at least three standard deviations greater than those from the background, were calculated [66, 67]. The LODs of G7- and G4&G7-aptamer assays were 11.4 and 12.9 pg/mL, respectively, around 4.5 times less than the LOD of commercial ELISA (53.6 pg/mL) in this study. The improved detection performances on the detection ranges, sensitivities, and LODs of G7- and G4&G7-aptamer assays are likely due to the combined effects of more surface immobilized aptamers and nonfouling properties, both as a result of dendrimer surface modification.

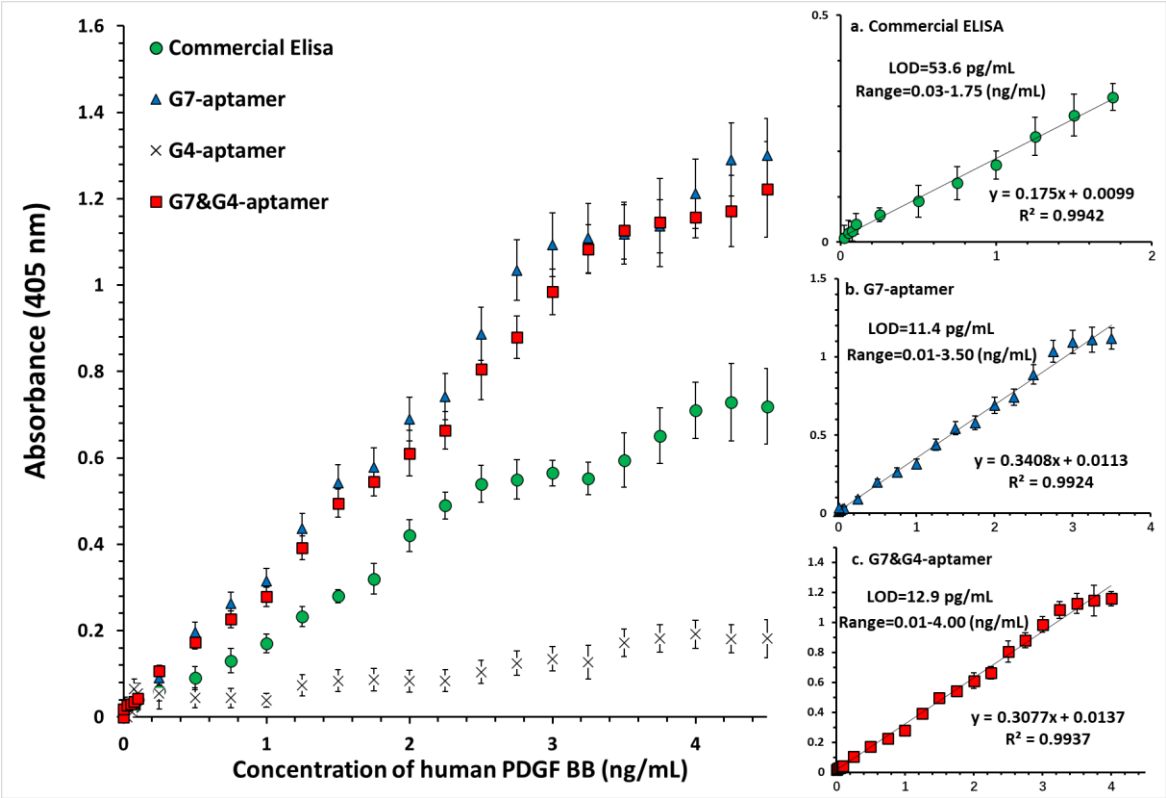

Figure 3.6. Detection performances of different assays over a wide range of target analyte concentrations. Figure insets: a) linear detection range of commercial ELISA; b) linear detection range of G7-aptamer modified microwells; c) linear detection range of G7 &G4-aptamer modified microwells. Error bars are standard deviations, n=3.

To further evaluate assay performances of G7- and G4&G7-aptamer modified microwells in samples, recovery and precision tests were performed [68]. As shown in Table 3.1, the linear detection range of commercial ELISA was 0.03-1.25 ng/mL in cell culture media; in comparison, G7-aptamer and G4&G7-aptamer modified microwells showed broader linear detection ranges at 0.01-3.25 ng/mL and 0.01-3.75 ng/mL, respectively (all linear ranges were determined when R^2>0.990). Moreover, the recoveries of the tests at the three target concentrations in cell culture media using both the G7- and G4&G7-aptamer modified microwells ranged from 95.4% to 105.3%, and precisions expressed as coefficient of variation (% CV) were all less than 10%, indicating excellent reproducibility and precision of the assays in cell culture media

[69].

Table 3.1. Evaluation of ELDAA reproducibility and precision performances using modified microwells.

	Concentration (ng/mL)	**G7-aptamer modified microwell**	**G4&G7-aptamer modified microwell**	**Commercial ELISA**
Sample Matrix	Cell Culture Media			
R^2 (n=3)		0.996	0.997	0.994
Linear Range （ng/mL）		0.01-3.25	0.01-3.75	0.03-1.25
Recovery (n=4)	0.05	105.3%±6.3%	98.2%±7.4%	98.5%±4.8%
	0.50	97.5%±7.2%	101.4%±5.0%	99.0%±2.5%
	3.00	104.9%±8.5%	95.4%±9.1%	Out of Range
Precision (%CV) (n=4)	0.05	6.0%	7.5%	4.9%
	0.50	7.4%	4.9%	2.5%
	3.00	8.1%	9.5%	Out of Range

3.4 Conclusion

We developed a sandwich dendrimer-aptamer-based assay to improve the detection performances of traditional ELISA. We demonstrated that dendrimers could be chemically immobilized on the surfaces of glass-bottom 96-well plates to provide nonfouling properties and offer multiple binding sites for further conjugation of multi-copy aptamers. Moreover, we showed that G7 and G4&G7 modified microwells could

provide better results in terms of nonfouling, aptamer-binding capacity, and surface coverage in comparison with the G4-modified microwells. Furthermore, G7- and G4&G7 modified microwells demonstrated better assay performances by exhibiting broader linear ranges, higher detection sensitivities, and lower LODs in comparison with the commercial ELISA. Our modification method improves detection performances with minor changes to traditional ELISA and therefore can be readily adapted for use for most commercial ELISA kits. By simply changing the surface-immobilized capturing aptamers, the current ELISA kit can be readily developed into ELISA kits to assay other analytes, such as nucleic acids, antibodies, and other protein antigens. In the future, the method will be improved by conjugating dendrimers onto surfaces of more commonly used polystyrene microwells, which will reduce the price of devices and increase applicability.

References

1. Engvall, E., [28] Enzyme immunoassay ELISA and EMIT, in Methods in Enzymology. 1980, Academic Press. p. 419-439.
2. Asensio, L., et al., Determination of food authenticity by enzyme-linked immunosorbent assay (ELISA). Food Control, 2008. **19**(1): p. 1-8.
3. Lequin, R.M., Enzyme Immunoassay (EIA)/Enzyme-Linked Immunosorbent Assay (ELISA). Clinical Chemistry, 2005. **51**(12): p. 2415.
4. Alhajj, M. and A. Farhana, Enzyme linked immunosorbent assay, in StatPearls [Internet]. 2022, StatPearls Publishing.
5. Systems in ELISA, in The ELISA Guidebook, J.R. Crowther, Editor. 2009, Humana Press: Totowa, NJ. p. 9-42.
6. Konstantinou, G.N., Enzyme-Linked Immunosorbent Assay (ELISA), in Food Allergens: Methods and Protocols, J. Lin and M. Alcocer, Editors. 2017, Springer New York: New York, NY. p. 79-94.
7. Hobbs, R.N., Solid-phase immunoassay of serum antibodies to peptides covalent antigen binding to adsorbed phenylalanine-lysine copolymers. Journal

of Immunological Methods, 1989. **117**(2): p. 257-266.
8. Welch, N.G., et al., Orientation and characterization of immobilized antibodies for improved immunoassays. Biointerphases, 2017. **12**(2): p. 02D301.
9. Gibbs, J. and M. Kennebunk, Immobilization Principles–Selecting the Surface. ELISA technical bulletin, 2001. **1**: p. 1-8.
10. Prusak-sochaczewski, E. and J.H.T. Luong, An improved ELISA method for the detection of Salmonella typhimurium. Journal of Applied Bacteriology, 1989. **66**(2): p. 127-135.
11. Steiner, J.M., S.R. Teague, and D.A. Williams, Development and analytic validation of an enzyme-linked immunosorbent assay for the measurement of canine pancreatic lipase immunoreactivity in serum. Can J Vet Res, 2003. **67**(3): p. 175-82.
12. Ball, V., et al., Kinetics of exchange processes in the adsorption of proteins on solid surfaces. Proceedings of the National Academy of Sciences, 1994. **91**(15): p. 7330-7334.
13. Dixit, C.K., et al., Multisubstrate-compatible ELISA procedures for rapid and high-sensitivity immunoassays. nature protocols, 2011. **6**(4): p. 439-445.
14. Huetz, P., et al., Exchange Kinetics for a Heterogeneous Protein System on a Solid Surface. Langmuir, 1995. **11**(8): p. 3145-3152.
15. Shiyun, Z., et al., Predicting detection limits of enzyme-linked immunosorbent assay (ELISA) and bioanalytical techniques in general. Analyst, 2013. **139**(2): p. 439-445.
16. Larsson, P.H., et al., Covalent binding of proteins to grafted plastic surfaces suitable for immunoassays: I. Binding capacity and characteristics of grafted polymers. Journal of immunological methods, 1987. **98**(1): p. 129-135.
17. Dixit, C.K., et al., Development of a high sensitivity rapid sandwich ELISA procedure and its comparison with the conventional approach. Analytical chemistry, 2010. **82**(16): p. 7049-7052.
18. Han, H.J., et al., Multifunctional dendrimer-templated antibody presentation on biosensor surfaces for improved biomarker detection. Advanced functional materials, 2010. **20**(3): p. 409-421.
19. Jung, Y., et al., Controlled antibody immobilization onto immunoanalytical platforms by synthetic peptide. Analytical Biochemistry, 2008. **374**(1): p. 99-105.
20. Jung, Y., J.Y. Jeong, and B.H. Chung, Recent advances in immobilization methods of antibodies on solid supports. Analyst, 2008. **133**(6): p. 697-701.

21. Peluso, P., et al., Optimizing antibody immobilization strategies for the construction of protein microarrays. Analytical biochemistry, 2003. **312**(2): p. 113-124.
22. Jiang, Y., S. Zou, and X. Cao, A simple dendrimer-aptamer based microfluidic platform for *E.coli* O157: H7 detection and signal intensification by rolling circle amplification. Sensors and Actuators B: Chemical, 2017. **251**: p. 976-984.
23. Qin, Y., et al., Developing a non-fouling hybrid microfluidic device for applications in circulating tumour cell detections. Colloids and Surfaces B: Biointerfaces, 2017. **151**: p. 39-46.
24. Barbara, K. and B. Maria, Review Dendrimers: properties and applications. Acta biochimica polonica, 2001. **48**(1): p. 199-208.
25. Zhang, J., et al., Simultaneous detection of deoxynivalenol and zearalenone by dual-label time-resolved fluorescence immunoassay. Journal of the Science of Food and Agriculture, 2011. **91**(2): p. 193-197.
26. Rao, M.K.K., K. Kapila, and R.M. Gupta, ENZYME LINKED IMMUNOSORBENT ASSAYS REVISITED. Medical Journal Armed Forces India, 1997. **53**(1): p. 45-51.
27. Bosnjakovic, A., et al., A dendrimer-based immunosensor for improved capture and detection of tumor necrosis factor-α cytokine. Analytica chimica acta, 2012. **720**: p. 118-125.
28. Hao, X., et al., Aptamer surface functionalization of microfluidic devices using dendrimers as multi-handled templates and its application in sensitive detections of foodborne pathogenic bacteria. Analytica chimica acta, 2019. **1056**: p. 96-107.
29. Jayasena, S.D., Aptamers: an emerging class of molecules that rival antibodies in diagnostics. Clinical chemistry, 1999. **45**(9): p. 1628-1650.
30. Ozalp, V.C., F. Eyidogan, and H.A. Oktem, Aptamer-gated nanoparticles for smart drug delivery. Pharmaceuticals, 2011. **4**(8): p. 1137-1157.
31. Millare, B., et al., Dependence of the quality of adhesion between poly (dimethylsiloxane) and glass surfaces on the conditions of treatment with oxygen plasma. Langmuir, 2008. **24**(22): p. 13218-13224.
32. Green, L.S., et al., Inhibitory DNA ligands to platelet-derived growth factor B-chain. Biochemistry, 1996. **35**(45): p. 14413-14424.
33. Guo, L. and Q. Zhao, Thrombin-linked aptamer assay for detection of platelet derived growth factor BB on magnetic beads in a sandwich format. Talanta, 2016. **158**: p. 159-164.

34. Yeh, P.Y., et al., Nonfouling hydrophilic poly (ethylene glycol) engraftment strategy for PDMS/SU-8 heterogeneous microfluidic devices. Langmuir, 2012. **28**(46): p. 16227-16236.
35. Holländer, A., Labelling techniques for the chemical analysis of polymer surfaces. Surface and Interface Analysis: An International Journal devoted to the development and application of techniques for the analysis of surfaces, interfaces and thin films, 2004. **36**(8): p. 1023-1026.
36. Hermanson, G.T., Bioconjugate techniques. 2013: Academic press.
37. Qin, Y., et al., Developing an ultra non-fouling SU-8 and PDMS hybrid microfluidic device by poly (amidoamine) engraftment. Colloids and Surfaces B: Biointerfaces, 2015. **127**: p. 247-255.
38. Eichman, J.D., et al., The use of PAMAM dendrimers in the efficient transfer of genetic material into cells. Pharmaceutical science & technology today, 2000. **3**(7): p. 232-245.
39. Nanjwade, B.K., et al., Dendrimers: emerging polymers for drug-delivery systems. Eur J Pharm Sci, 2009. **38**(3): p. 185-96.
40. Hierlemann, A., et al., Structural distortion of dendrimers on gold surfaces: a tapping-mode AFM investigation. Journal of the American Chemical Society, 1998. **120**(21): p. 5323-5324.
41. Li, J., et al., Visualization and characterization of poly (amidoamine) dendrimers by atomic force microscopy. Langmuir, 2000. **16**(13): p. 5613-5616.
42. Müller, T., et al., AFM studies of high-generation PAMAM dendrimers at the liquid/solid interface. Langmuir, 2002. **18**(20): p. 7452-7455.
43. Qin, M., et al., Two methods for glass surface modification and their application in protein immobilization. Colloids and Surfaces B: Biointerfaces, 2007. **60**(2): p. 243-249.
44. Cassie, A. and S. Baxter, Wettability of porous surfaces. Transactions of the Faraday society, 1944. **40**: p. 546-551.
45. Cassie, A., Contact angles. Discussions of the Faraday society, 1948. **3**: p. 11-16.
46. Tokuhisa, H., et al., Preparation and characterization of dendrimer monolayers and dendrimer− alkanethiol mixed monolayers adsorbed to gold. Journal of the American Chemical Society, 1998. **120**(18): p. 4492-4501.
47. Cha, B.J., Y.S. Kang, and J. Won, Preparation and characterization of dendrimer layers on poly (dimethylsiloxane) films. Macromolecules, 2001. **34**(19): p. 6631-6636.

48. Lopez, A.I., et al., Biofunctionalization of silicone polymers using poly (amidoamine) dendrimers and a mannose derivative for prolonged interference against pathogen colonization. Biomaterials, 2011. **32**(19): p. 4336-4346.
49. Larson, B., et al., Cold-plasma modification of oxide surfaces for covalent biomolecule attachment. Biosensors and Bioelectronics, 2005. **21**(5): p. 796-801.
50. Min, H., et al., Ambient-ageing processes in amine self-assembled monolayers on microarray slides as studied by ToF-SIMS with principal component analysis, XPS, and NEXAFS spectroscopy. Anal Bioanal Chem, 2012. **403**(2): p. 613-23.
51. Xu, Z.X., et al., Amide-linkage formed between ammonia plasma treated poly (D, L-lactide acid) scaffolds and bio-peptides: Enhancement of cell adhesion and osteogenic differentiation in vitro. Biopolymers, 2011. **95**(10): p. 682-694.
52. Demirci, S., et al., Functionalization of poly-SNS-anchored carboxylic acid with Lys and PAMAM: surface modifications for biomolecule immobilization/stabilization and bio-sensing applications. Analyst, 2012. **137**(18): p. 4254-61.
53. Satija, J., B. Karunakaran, and S. Mukherji, A dendrimer matrix for performance enhancement of evanescent wave absorption-based fiber-optic biosensors. RSC advances, 2014. **4**(31): p. 15841-15848.
54. Qin, Y., Developing a poly (dimethylsiloxane)(PDMS)/SU-8 (negative photoresist) hybrid microfluidic system for sensitive detection of circulating tumour cells. 2018, Université d'Ottawa/University of Ottawa.
55. McCain, K.S., P. Schluesche, and J.M. Harris, Modifying the adsorption behavior of polyamidoamine dendrimers at silica surfaces investigated by total internal reflection fluorescence correlation spectroscopy. Analytical chemistry, 2004. **76**(4): p. 930-938.
56. Mecke, A., et al., Deformability of poly (amidoamine) dendrimers. The European Physical Journal E, 2004. **14**(1): p. 7-16.
57. Tully, D.C. and J.M. Fréchet, Dendrimers at surfaces and interfaces: chemistry and applications. Chemical Communications, 2001(14): p. 1229-1239.
58. Katzur, V., et al., Surface-immobilized PAMAM-dendrimers modified with cationic or anionic terminal functions: Physicochemical surface properties and conformational changes after application of liquid interface stress. Journal of colloid and interface science, 2012. **366**(1): p. 179-190.
59. Eichler, M., et al., The impact of dendrimer-grafted modifications to model silicon surfaces on protein adsorption and bacterial adhesion. Biomaterials,

2011. **32**(35): p. 9168-9179.

60. Chen, S., et al., Surface hydration: Principles and applications toward low-fouling/nonfouling biomaterials. Polymer, 2010. **51**(23): p. 5283-5293.
61. Gillich, T., et al., Self-assembly of focal point oligo-catechol ethylene glycol dendrons on titanium oxide surfaces: adsorption kinetics, surface characterization, and nonfouling properties. Journal of the American Chemical Society, 2011. **133**(28): p. 10940-10950.
62. Yang, W., et al., Film thickness dependence of protein adsorption from blood serum and plasma onto poly (sulfobetaine)-grafted surfaces. Langmuir, 2008. **24**(17): p. 9211-9214.
63. Zhao, C., et al., Functional polymer thin films designed for antifouling materials and biosensors. Chemical Papers, 2012. **66**(5): p. 323-339.
64. Ingle Jr, J., Sensitivity and limit of detection in quantitative spectrometric methods. Journal of Chemical Education, 1974. **51**(2): p. 100.
65. Norrod, K.L., et al., Quantitative comparison of five SERS substrates: sensitivity and limit of detection. Applied spectroscopy, 1997. **51**(7): p. 994-1001.
66. Shrivastava, A. and V.B. Gupta, Methods for the determination of limit of detection and limit of quantitation of the analytical methods. Chronicles of Young Scientists, 2011. **2**(1): p. 21.
67. Chen, C.-S. and R.A. Durst, Simultaneous detection of Escherichia coli O157: H7, Salmonella spp. and Listeria monocytogenes with an array-based immunosorbent assay using universal protein G-liposomal nanovesicles. Talanta, 2006. **69**(1): p. 232-238.
68. Andreasson, U., et al., A practical guide to immunoassay method validation. Frontiers in neurology, 2015. **6**: p. 179.
69. Trullols, E., I. Ruisanchez, and F.X. Rius, Validation of qualitative analytical methods. TrAC Trends in Analytical Chemistry, 2004. **23**(2): p. 137-145.

Chapter 4

Surface Modification of Poly(styrene) 96-well Plates Using Aptamers via a Dendrimer-templated Strategy to Enhance ELISA Performances

Abstract

Poly(styrene) (PS) 96-well plates were surface modified to improve the detection performances of an otherwise traditional enzyme-linked immunosorbent assay (ELISA). Poly(amidoamine) generation 7 (G7) dendrimers were covalently immobilized on the surface of PS plates and subsequently conjugated with aptamers specific for a model analyte, *i.e.,* human platelet-derived growth factor BB (PDGF-BB). This surface functionalization was followed by Fourier-transform infrared spectroscopy, water contact angle, atomic force microscopy, and X-ray photoelectron spectroscopy (XPS) to confirm the success of the modifications. Moreover, the assay performances of the G7-aptamer modified PS plates were compared to those of traditional ELISA performed on regular PS 96-well plates. The G7-aptamer assay demonstrated a 2.3-time broader linear detection range and a 13-time improved detection limit than the traditional ELISA. More importantly, the new G7-aptamer modified PS plates also showed excellent analytical specificities, detection recoveries, and precisions when the targets were assayed in a cell culture media. This combined dendrimer templates and aptamers surface modification approach significantly reduces background noises and increases detection signals, and can be readily incorporated into existing ELISA workflows and many other PS microplate based high throughput and automated bioassays.

4.1 Introduction

Polystyrene (PS) microwell plates are commonly used in bioassays because of their excellent optical properties and cost-effectiveness [1]. In a typical bioassay, biomolecules (*i.e.,* antibodies, protein antigens, and enzymes) are usually physically adsorbed onto the surfaces of the PS microwell plates to construct different bioassay formats, including direct, indirect, sandwich, and competitive assays [2]. As a result, the quantity and quality of the surface-adsorbed biomolecules are important factors that determine the performances of these bioassays [3, 4]. The physical adsorption approach has long been recognized as a limiting factor affecting the detection performances since the 1990s [5, 6] and remains to be a critical issue to-date [7-9], as the physical adsorption approach has been documented to cause both denaturations of the adsorbed biomolecules (such as antibodies) and desorptions of the already adsorbed biomolecules from the capturing surface. These issues have negatively impacted the overall bioassay performances, such as narrow detection ranges, non-effective limit of detections, and irreproducible results [1, 7, 10]. To improve bioassay performances, researchers have attempted to use covalent immobilization approaches to provide more stable and better-controlled interactions between the PS microwell plate surfaces and the biomolecules of interest [1, 8, 10]; however, the covalent immobilization approaches have been shown to result in poor orientations of the immobilized antibodies [11, 12] and damaged antigen-binding sites [10, 13], leaving much to be desired [14, 15]. Because of the inert chemical properties of PS, the PS surfaces of the microwells must be first activated in order to covalently attach biomolecules of interest. To activate the PS surfaces, two general approaches have been commonly used -- wet chemical methods that typically use strong oxidizing acids [16, 17] and dry chemical

methods that employ plasma to treat the PS surfaces [1, 18]. However, the steps involved in the wet chemical methods are challenging to implement as the reaction conditions must be carefully controlled [19, 20] and are often inaccessible to a regular biochemistry laboratory. Alternatively, dry chemical methods use different gas plasma (*e.g.,* Ar, O_2, and N_2) treatments to introduce functional groups onto the PS surfaces for subsequent covalent immobilization of biomolecules [1, 18]. However, the plasma treatments have been shown to result in poorly defined functional groups on the resulting surfaces. For example, oxygen plasma has been documented to introduce a wide variety of functional groups [1, 18], resulting in poor reproducibilities and controls over subsequent biomolecule immobilizations [21]. To overcome this issue, post-surface modifications using silane-based self-assembled monolayers, such as (3-aminopropyl) triethoxysilane (APTES), have been employed after the plasma treatment achieve more consistent results [10, 22].

Blocking is another important step in bioassays as it is designed to minimize non-specific adsorptions to the capturing surfaces [23]. Although blocking agents, such as bovine serum albumin (BSA), non-fat dry milk, fish gelatin, and whole serum are commonly used, they have also been shown to have some limitations, including masking the surface-immobilized biomolecules, cross-reacting with assay components, and disrupting surface adsorbed biomolecules [24]. Poly(amidoamine) (PAMAM) dendrimers are spherically shaped polymers with high hydrophilicity. When the dendrimers are immobilized onto capturing surfaces, they can significantly prevent non-specific surface adsorptions due to their hydrophilicity and steric hindrance by the flexible branches [25-27]. Moreover, functional groups such as -OH, -COOH, or $–NH_2$

could be functionalized on PAMAM surface as binding templates for subsequent conjugations with biomolecules of interest, including antibodies and aptamers [28, 29]. Because of these unique properties, dendrimers have been widely used on different detection substrates, such as glass, poly(dimethylsiloxane) (PDMS), and gold to improve the detection sensitivities of various biosensing devices [28, 30, 31]. However, studies reporting simple methods to immobilize PAMAM dendrimers onto the surfaces of pristine PS 96-well plates to improve the performances of bioassays are very limited in the literature.

In this study, we report a surface modification method to immobilize PAMAM dendrimers on surfaces of pristine PS 96-microwell plates to improve the detection performances of a commercial ELISA. Specifically, surfaces of PS-based 96-microwell plates were initially treated with KOH and oxygen plasma to introduce functional groups without damaging the surface morphology. Subsequently, the activated surfaces were treated with (3-aminopropyl) triethoxysilane (APTES) to uniformly functionalize the surfaces with primary amines. The resulting surfaces were immobilized with carboxylated PAMAM dendrimers as templates and subsequently conjugated with aptamers to specifically capture biomolecules of interest. The use of PAMAM dendrimer in the microwell modification offers the following advantages: 1) the PAMAM dendrimer layer renders the modified microwell surfaces nonfouling property to effectively prevent non-specific interactions between the microwell surfaces and non-targets to minimize background noise [28, 29], and 2) the PAMAM dendrimers behave as multi-handled templates when immobilized on the PS surfaces to allow conjugations of multiple copies of aptamers for enhanced target capturing, thereby improving assay performances [28, 31]. Our results show that in comparison with the

regular ELISA PS 96-well plates, the new dendrimer-aptamer modified PS 96-microwell plates demonstrated much improved detection performances, including a broader linear detection range and a lower detection limit.

4.2 Experimental

4.2.1 Materials

Details of materials used in this study can be found in Appendix B. The aptamer sequences used in this study are listed below:

Capturing aptamer (i.e. aptamers against human PDGF-BB): [32]

5'/NH_2, 12C Spacer/TAC TCA GGG CAC TGC AAG CAA TTG TGG TCC CAA TGG GCT GAG TA /3'

Aptamers-biotin (i.e. biotin-labeled aptamers for surface evaluation):

5'/NH_2, 12C Spacer/TAC TCA GGG CAC TGC AAG CAA TTG TGG TCC CAA TGG GCT GAG TA /biotin/3'

Scrambled sequence as a control:

5'/NH_2,12C Spacer / TCC TCA AAG CAC CGC ATG CAA CAG TAG TTC AGA TAC ATT GCG TA/3'

4.2.2 General Approach

As shown in Figure 4.1, the PS 96-well plate is treated with, in sequence, anhydrous alcohol, KOH, and oxygen plasma, to introduce carbonyl (-C=O) and hydroxyl (-OH) functional groups onto the surfaces [10]. This step is followed by surface amination with APTES treatment. Subsequently, the aminated surface is chemically conjugated with carboxylated PAMAM dendrimers to provide multiple binding sites for further

engraftment of aptamers that specifically bind with human platelet-derived growth factor-BB (PDGF-BB), a model target molecule selected in this study. For signal read-outs, the traditional ELISA signal amplification method is carried out, *i.e.,* the captured PDGF-BB molecules are conjugated with biotinylated secondary antibodies that subsequently react with avidin-labeled horseradish peroxidase (*i.e.,* avidin-HRP), which will react with 2,2′-azino-bis (3-ethylbenzothiazoline-6-sulfonic acid) (ABTS) to generate optical signals.

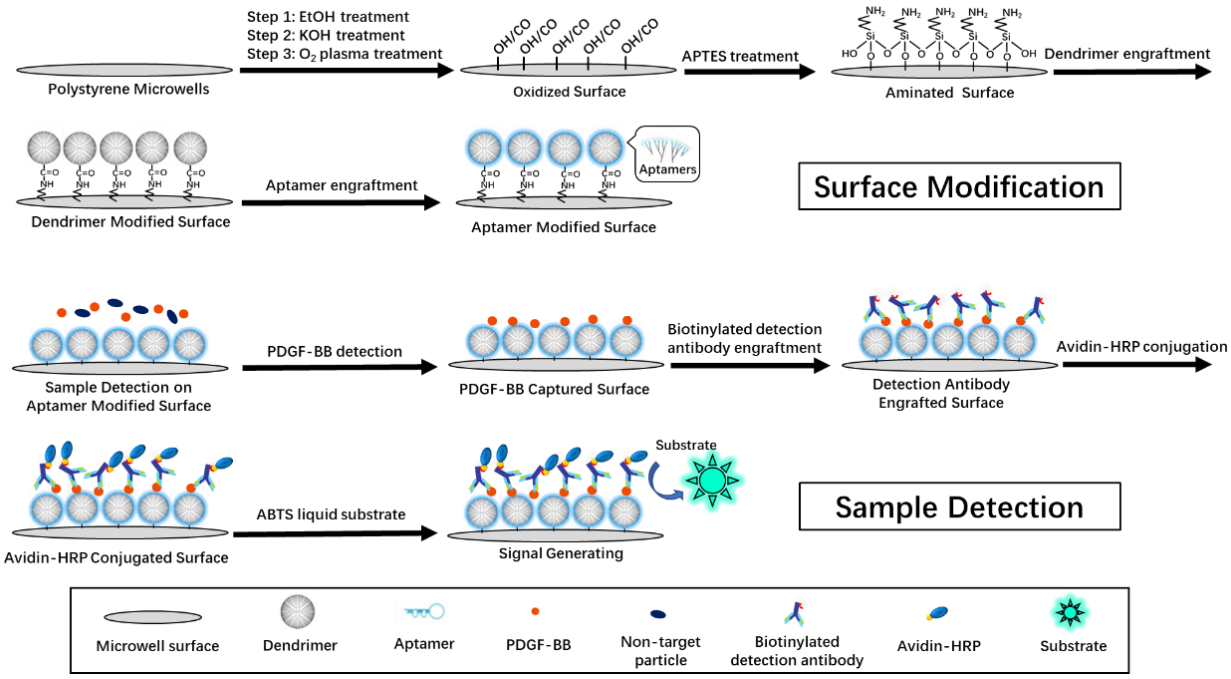

Figure 4.1. Schematic illustration showing the general approach to modify PS 96-well plates used for human PDGF-BB ELISA.

4.2.3 Surface Modifications and Characterization

4.2.3.1 Surface Amination

To introduce amino functional groups to the surfaces of PS 96-well plates, a well-established method was used with minor modifications [10]. Briefly, each well of the

PS 96-well plate was treated with 100 μL absolute ethanol for 5 min and was carefully washed, after which the treated microwells were incubated with 100 μL 1% (w/w) KOH for 10 min, washed again, and dried by a nitrogen gas stream. Subsequently, the KOH-activated microwells were treated using oxygen plasma (Plasma Etch lnc, Carson City, NV) at 100 mTorr and 100 W for 10 s to introduce nucleophilic centers (*i.e.,* -OH and -CO) onto the treated surfaces [10], after which 100 μL 1% (vol/vol) APTES was immediately added to each well of the 96-well plate to react with the plasma-treated surfaces for 1 h at room temperature. Finally, the APTES-treated microwells were washed extensively and dried by a nitrogen gas stream. To confirm the success of the surface amination, an Agilent Cary 630 FTIR-ATR (Santa Clara, CA) was used.

Furthermore, to evaluate the extent of surface amination, a well-established biotin labeling technique was employed [33]. In brief, the aminated surfaces were labeled with NHS-biotin, after which the labeled surfaces were conjugated with avidin-HRP and finally reacted with ABTS substrate to generate signals. As NHS-biotin readily reacts with primary amines, this method can be used to approximate the relative amount of amino functional groups on the surfaces of interest. In a typical experiment, 100 μL NHS-biotin (40 μg/mL) in PBS (pH 7.4) was added to each well of the aminated PS 96-well plates at room temperature for 30 min, followed by careful washes with water. Subsequently, the biotin-labeled microwells were reacted with 100 μL avidin-HRP (1:2000 dilution) in PBS (pH=7.4) for another 30 min at room temperature and then carefully washed again with water. Finally, The HRP conjugated surfaces were reacted with 100 μL ABTS substrate for 15 min for color development. Absorbance was measured using a BioTek microplate spectrophotometer (Winooski, VT) at 405 nm with

a reference wavelength at 650 nm.

4.2.3.2 Surface Immobilization of PAMAM-COOH

To immobilize dendrimer PAMAM-COOH generation 7 (*i.e.,* G7-COOH) onto the aminated surfaces of PS microwells obtained from the previous step, each aminated microwells were incubated with 100 µL reaction mixtures (*i.e.,* 1 µM G7-COOH, 5 mM NHS, and 2 mM EDC in 0.1 M MES solution (pH 6.0)) at room temperature for 2 h. Subsequently, the microwells were thoroughly washed with PBS (pH 7.4) and finally incubated in PBS (pH 8.5) for future use [34].

To confirm the success of G7-COOH engraftment, a biotin labeling method, similar to the method described in Section 4.2.3.1, was employed with minor modifications. In brief, hydrazide-biotin was used to label the carboxyl functional groups of G7 molecules immobilized on the surfaces of microwells [34], after which avidin-HRP was conjugated to the surfaces in order to generate signals when reacted with ABTS substrate. In a typical experiment, a 100 µL hydrazide-biotin reaction solution (*i.e.,* 1.24 mg EDC and 0.32 mg hydrazide-biotin in 1 mL MES (pH=5.0)) was added to each well of G7-COOH modified 96-well plates at room temperature for 2 h, after which the resulting microwells were carefully washed with PBS (pH 7.4) and stored in PBS (pH=8.5) at room temperature overnight [34]. To generate signals, the HRP functionalized microwells were reacted with ABTS substrate, as discussed in Section 4.2.3.1.

To further characterize the G7-COOH modified surfaces, water contact angles (WCA)

of surfaces of interest were measured using a goniometer (AST Products Inc., Billerica, MA). In addition, a Veeco Di Multimode V atomic force microscope (AFM) (Santa Barbara, CA) was used to compare the morphology changes before and after the surface modification. Surfaces of interest were characterized in contact mode, and the obtained data were further analyzed by NanoScope software (Veeco, Santa Barbara, CA).

4.2.3.3 Aptamer Engraftment

To engraft aptamers onto the G7-COOH modified microwells, the G7-COOH modified microwells were initially treated with a 100 µL reaction mixture including 5 mM NHS and 2 mM EDC in 0.1 M MES solution (pH 6.0) at room temperature for 15 min to activate the carboxyl functional groups [28], after which the resulting microwells were reacted with 100 µL 10 µM amine capped aptamers (*i.e.,* NH_2-aptamers) in PBS (pH 7.4) at room temperature. This reaction was allowed to be carried out for 2 h, after which the treated microwells were washed with 0.5 M Tris-HCL (pH 8.5) to stop the reaction [34]. Finally, the resulting microwells were washed with PBS (pH 7.4) and stored for future use.

To confirm the success of aptamer engraftment, biotin-labeled aptamers (*i.e.,* NH_2-aptamer-biotin) were used to react with the immobilized G7-COOH on the microwells. Subsequently, the resulting microwells were reacted with avidin-HRP and ABTS substrate to generate signals, using the same protocol as discussed in Section 4.2.3.1.

To further study each step of the surface modification, surfaces of interest were characterized using XPS. Detailed information about the XPS analysis can be found in

Appendix B.

4.2.4 Assay Performance Evaluation

To evaluate the detection performance of assays using the modified microwells, a standard human PDGF-BB sandwich ELISA protocol was carried out using the G7-aptamer modified microwells (referred to as G7-aptamer assay hereinafter) with two key modifications, *i.e.,* eliminations of both the primary antibody incubation and all blocking steps. Briefly, 100 μL of either samples of interest or PDGF-BB standards were incubated in the wells of the G7-aptamer modified 96-well plates at room temperature for 2 h and washed with a washing solution (*i.e.,* 0.05 % Tween-20 in PBS (pH 7.4)). This was followed by incubation with 100 μL 0.25 μg/mL biotinylated secondary antibody at room temperature for another 2 h. Subsequently, the resulting microwells were thoroughly washed, incubated with 100 μL avidin-HRP conjugate for 30 min, carefully washed again, and reacted with 100 μL of ABTS substrate solution at room temperature for 30 min for color development. Finally, the absorbance was measured using a BioTek microplate spectrophotometer at 405 nm with a reference wavelength at 650 nm.

4.2.5 Statistical Analysis

The statistical analysis was performed using Microsoft Excel software (version 2303). To ensure the reliability and robustness of the results, all experiments were carried out in triplicate (otherwise indicated in figure captions), both within the same day and across different days, and the mean values with their corresponding standard deviations were calculated and reported. The Student's t-test, two-tailed, was employed to assess

the statistical significance of the differences between the groups, with a p-value of less than 0.05 considered statistically significant.

4.3 Results and Discussion

4.3.1 Surface Characterization and Optimization

To confirm the success of surface amination, FTIR-ATR was used to characterize surfaces of interest, *i.e.,* PS surfaces, PS surfaces soaked in APTES (physically adsorbed), and PS surfaces modified by APTES (chemically reacted). As shown in Figure 4.2, there were no significant differences in FTIR-ATR spectra between the PS surfaces and the surfaces soaked in APTES (physically adsorbed). However, the PS surfaces modified by APTES (chemically reacted) showed additional characteristic peaks that were attributed to -NH stretching at 3400 cm^{-1} [28, 35], -CH_3 asymmetric stretching vibrations at 2973 cm^{-1} [36], Si–O–C rocking at 1167 cm^{-1} [37], Si-O-Si at 1158 cm^{-1} [35, 38], and Si-O-C at 1108 cm^{-1} [35, 38]. These characteristic peaks are strong evidence suggesting the success of PS surface amination.

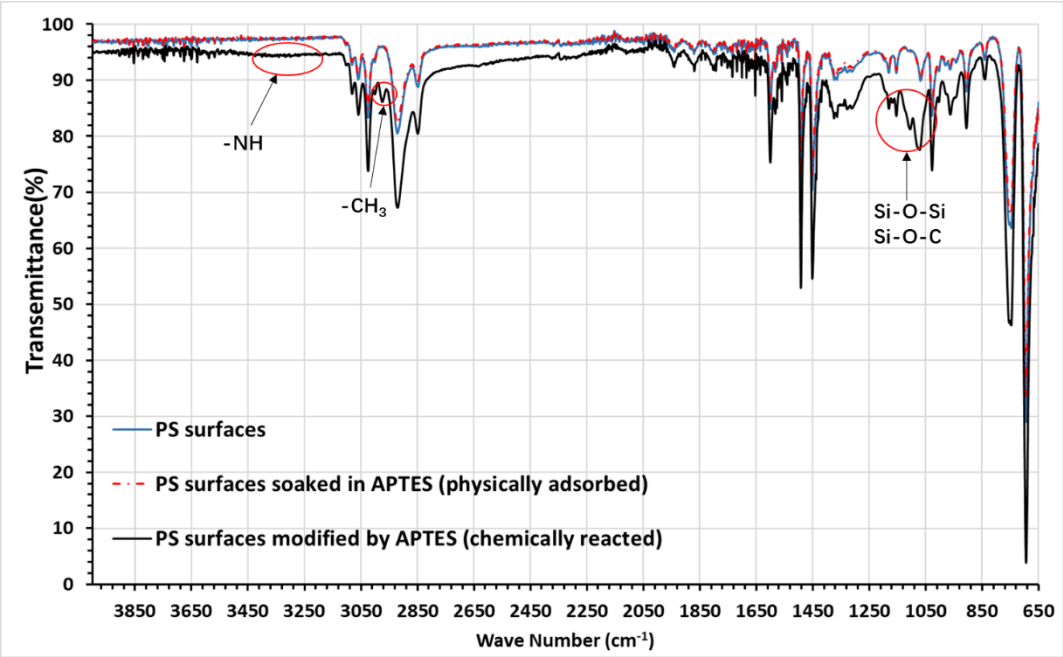

Figure 4.2. FTIR-ATR characterization of PS surface amine functionalization.

To further evaluate PS surface amination reaction conditions and investigate parameters that affected the extent of surface aminations, microwells of interest were treated using NHS-biotin to label the surface primary amines (see Section 4.2.3.1). It can be seen from Figure 4.3A that surface amination initially showed an increasing trend with increasing concentrations of APTES and peaked at 1.0 % APTES. Further increases in the APTES concentrations resulted in decreased surface amination, as it is evident that microwells treated with 1.0 % APTES (1.23±0.03) showed a significantly higher signal ($p<0.01$) than those treated with higher APTES concentrations investigated. This observation is most likely because of APTES sol-gel polymerization, a well-known observation at high ATPES concentrations [28], which would result in decreased amino functional groups on the surfaces of the microwells. Moreover, surface amination time was also evaluated. As shown in Figure 4.3B, microwells for 60 min to aminate the surfaces showed the highest signal at 1.23±0.02, significantly higher ($p<0.05$) than the

signals of microwells treated with other amination times (*i.e.,* 0.69±0.02 at 20min, 0.97±0.02 at 30 min, 1.17±0.03 at 90 min, and 0.86±0.07 at 120 min), suggesting that 60 min is the optimal amination time. It should be noted that additional amination time beyond 60 min did not result in more surface amination; this is likely due to APTES sol-gel polymerization side reactions that have been reported in the literature [10]. Therefore, treatment with 1.0 vol % APTES for 60 min was selected as the optimal amination condition and used for the rest of this study unless indicated otherwise.

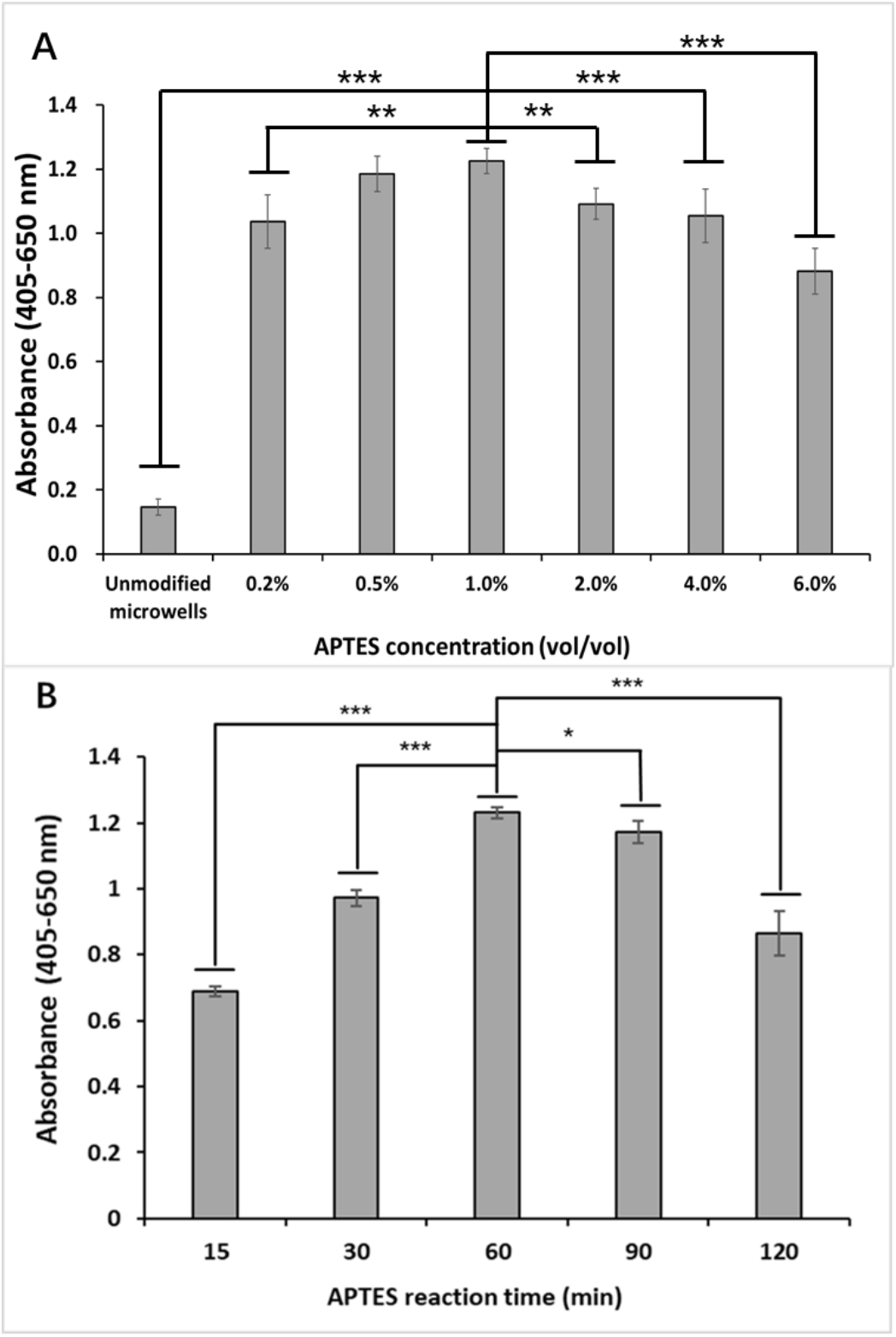

Figure 4.3. Evaluation of reaction conditions for surface amination. A) Effect of APTES concentration on surface amination; error bars indicate standard deviation, n=8. B) Effect of reaction time on surface amination; error bars indicate standard deviation, n=8. Student's t-test, p values (*<0.05, **<0.01, ***<0.001).

Similarly, to confirm the success of G7-COOH immobilization on the microwell surfaces, carboxyl functional groups of the immobilized G7 molecules were labeled with biotin that subsequently reacted with avidin-HRP in order to generate signals when reacted with ABTS substrate (see Section 4.2.3.2). As shown in Figure 4.4A, there was a significant increase in absorbance when the G7-COOH modified microwells were labeled with biotin (*i.e.,* G7 modified + hydrazide-biotin chemically reacted), indicating successful immobilization of G7-COOH onto the surfaces of microwells; this conclusion was further supported by the fact that there was no apparent absorbance difference between G7-COOH modified microwells without biotin labels (*i.e.,* G7 modified + no hydrazide-biotin) and those with only physically adsorbed labels (*i.e.,* G7 modified + hydrazide-biotin physically adsorbed). Furthermore, as shown in Figure B1 (Appendix B), 100 nM was selected as the optimum G7-COOH concentration for surface immobilization.

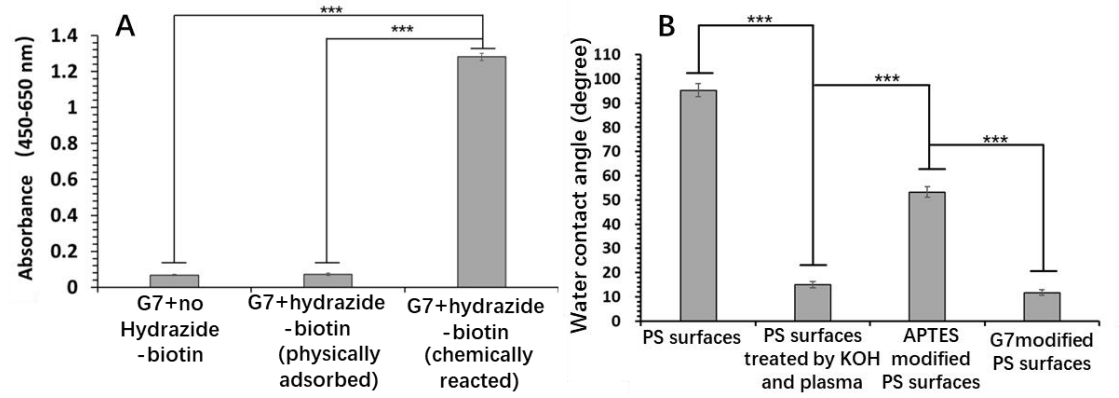

C	PS surfaces	PS surfaces treated by KOH and plasma	APTES modified PS surfaces	G7 modified PS surfaces
3D Image	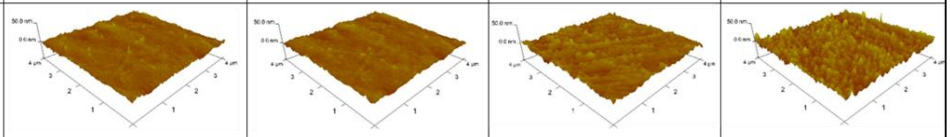			
Roughness (nm)	4.6±0.4	4.8±0.5	5.5±0.6	6.7±0.8

Figure 4.4. Evaluation of G7-COOH surface modification on PS surfaces. A) Absorbance of G7-COOH modified microwells labeled with hydrazide-biotin to confirm the success of G7-COOH modification on PS surfaces; error bars indicate standard deviation, n=5. B) Water contact angles of surfaces of interest; error bars indicate standard deviation, n=6. C) Surface morphology changes of surfaces of interest as characterized by AFM; error bars indicate standard deviation, n=6. All p values (*<0.05, **<0.01, ***<0.001), Student's t-test, 2 tails.

To further evaluate the G7-COOH dendrimer modified PS surfaces, WCA and AFM were employed to characterize the surfaces of interest, *i.e.,* PS surfaces, PS surfaces treated by KOH and plasma, APTES modified, and G7-COOH modified. As shown in Figure 4.4B, the PS surfaces showed the highest WCA of 95.2±2.7°, a value consistent with previously reported values of around 90.0° for PS surfaces [39]. As expected, the WCA of the surfaces treated by KOH and plasma was significantly decreased ($p<0.001$) to 15.0±1.3°, which is consistent with previously reported values of around 15° [1, 40]. This decrease in WCA can be attributed to the successful formation of oxygen-based hydrophilic groups, such as C–O, C=O, and O–C=O on the surfaces [1, 40]. The WCA

of the APTES-modified surfaces was increased to 53.3±2.3° , a value that is consistent with a previously reported value of 55.5° [17]. This increase in the WCA is most likely due to the introduction of hydrophobic alkyl chains because of the immobilized APTES molecules [1], suggesting successful surface aminations. Furthermore, after G7-COOH modification, the WAC was significantly reduced to 11.8±1.2°, indicating the success of G7-COOH immobilization on the surfaces [28].

Furthermore, the topographical features of different surfaces of interest were investigated using AFM in contact mode. As shown in Figure 4.4C, it is clear that the original PS surfaces and PS surfaces treated by KOH and plasma did not show any significant differences in roughness (root mean square (RMS) roughness at 4.6±0.4 nm *vs.* 4.8±0.5 nm, respectively) ($p>0.05$), indicating that the KOH and plasma treatments did not change the surface morphology. In contrast, after the surfaces were aminated with APTES, the RMS roughness increased to 5.5±0.6 nm, likely caused by the heterogeneous spatial distribution of the silane molecules [1]. Furthermore, globular-aggregate structures were observed on the G7-COOH modified PS surfaces, and the RMS roughness was further increased to 6.7±0.8 nm. The significant surface roughness changes are consistent with previously published observations [11, 28], providing further evidence that the G7-COOH molecules were successfully immobilized onto the PS surfaces.

Finally, to confirm that the aptamers were successfully immobilized on the G7-COOH modified PS microwells, biotin-labeled aptamers capped with free amino groups (*i.e.,* NH_2-aptamer-biotin) were used to immobilize the G7-COOH modified PS microwells

(see Section 4.2.3.3). As shown in Figure 4.5, in comparison to the G7-COOH modified microwells, aptamer-biotin modified microwells via G7-COOH templates (*i.e.,* G7 modified microwells + aptamer biotin (chemically reacted)) showed significantly higher ($p<0.001$) absorbance, strongly suggesting that aptamers were successfully engrafted to the PS surfaces via the G7-COOH templates; this conclusion is further supported by the evidence that there was no significant absorbance difference ($p>0.05$) between G7-COOH modified microwells and G7-COOH modified microwells with aptamer-biotin physically adsorbed (*i.e.,* G7 modified microwells + aptamer biotin (physically adsorbed)). Furthermore, as shown in Figure B2 (Appendix B), the optimum aptamer concentration was determined to be 10 μM, as maximum aptamer binding can be achieved at this aptamer concentration. To evaluate the conjugation efficiency of the aptamer to the G7-COOH, amine-capped aptamers with fluorescent tags (*i.e.,* NH_2-aptamer-cy3) were used to conjugate with G7-COOH molecules in solution to calculate the amount of aptamers conjugated to each G7-COOH molecule by measuring the fluorescence intensity of the purified products. The result showed that one G7-COOH molecule conjugated 353±41 aptamer molecules in solution, and therefore the conjugation efficiency was estimated to be 69% (*i.e.,* 353 aptamers/ 512 branches).

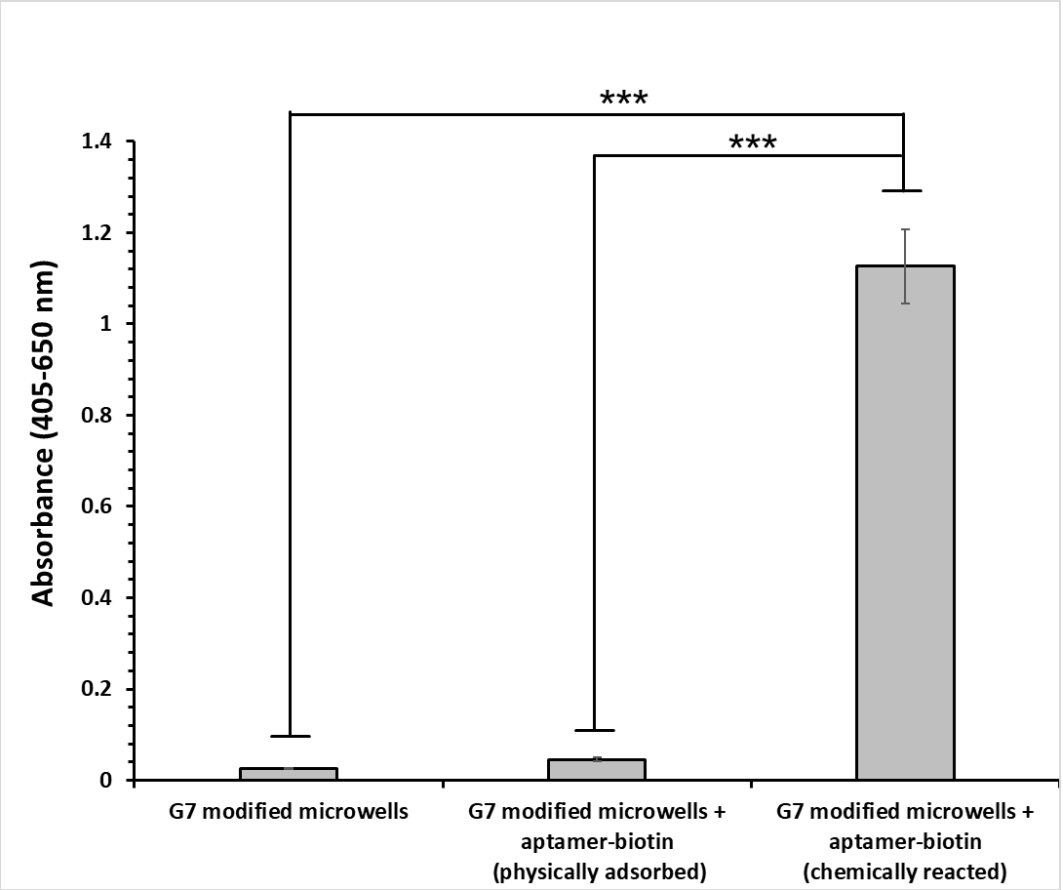

Figure 4.5. The absorbance of G7 modified microwells before and after aptamer-biotin conjugation to confirm the success of aptamer engraftment; error bars indicate standard division, n=5; *** $p<0.001$, Student's t-test, 2 tails.

Surfaces of interest (*i.e.,* PS surfaces, KOH and plasma treated surfaces, APTES treated surfaces, G7-COOH modified surfaces, and G7-aptamer modified surfaces) were further analyzed by XPS. The XPS results further confirmed the success of each step of the surface modifications (see B3 in Appendix B).

4.3.2 Assay Performance Evaluation

To evaluate the assay performances using the new G7-aptamer modified PS microwell plates, a commercially available human PDGF-BB ELISA kit was carried out using the new G7-aptamer modified PS microwell plates with some necessary modifications (see

Section 4.2.4). In parallel, a G7-scrambled aptamer assay (*i.e.,* assay carried out using G7-scrambled aptamer modified PS microwell plates), a traditional ELISA (ELISA carried out using traditional PS microplates), and a covalent antibody ELISA (ELISA carried out using PS microplates covalently immobilized with primary antibodies) were carried out for comparison. It is evident in Figure 4.6A that the assay carried out in G7-aptamer modified PS microwells showed higher signals at any given concentration in comparison with those carried out in other microplates (*i.e.,* traditional ELSA and covalent antibody ELISA). It is also worthwhile to note that detection signals collected from the assay using G7-scrambled aptamer modified microwells remained at consistently low levels (absorbance < 0.2) at all concentrations studied, suggesting that the detections are target-specific and that modifications via the dendrimer templates also serve to markedly reduce non-specific bindings as demonstrated in the literature [28, 29]; this is remarkable considering that no blocking steps were used. A closer analysis of the data reveals that the G7-aptamer assay demonstrated a linear detection range from 0.01 to 3.50 ng/mL, which is 2.3 and 1.8 times that of the traditional ELISA (0.02 to 1.50 ng/mL, similar to the vendor's data) and the covalent antibody ELISA (0.02 to 2.50 ng/mL) (see insets, Figure 4.6A), respectively. The improved linear detection range facilitates the sample preparation processes where several sample enrichments or dilution steps are required for the analyte concentration to be within the linear range [41, 42]. The increased linear detection range exhibited in the G7-aptamer assay can be explained by the significantly increased binding sites available on the PS microplate wells capturing surfaces enabled by the dendrimer templates: as aptamers are much smaller molecules in size than antibodies (1 nm *vs.* 10 nm) [43, 44], it is perceivable that numerous more copies of aptamers can be readily conjugated to the

capturing surface via the G7 dendrimer templates (size ~8 nm) than their antibodies counterparts without significant steric hindrance; this strategy would create a capturing surface with more capturing capacities for much more effective detection [45]. It is also interesting to note that covalent antibody ELISA showed a broader linear detection range than the traditional ELISA, supporting the notion that covalently conjugating primary antibodies could efficiently prevent these molecules from being washed away from the capturing surface [10], thus creating a more efficient capturing surface for the ELISA assay.

It is important to note that the G7-aptamer assay demonstrated a higher detection sensitivity than both the traditional and covalent antibody assays (Figure 4.6A, insets), as the detection sensitivity is determined by the slope of the response curve [46]. Moreover, the limit of detection (LOD) of the bioassay, as defined by the lowest target concentration that can provide signals at least three standard deviations greater than those from the background [46], were also evaluated. The result shows that the LOD of the G7-aptamer assay was 5.22 pg/mL, around 13 times lower than that of traditional ELISA (68.93 pg/mL) and 10 times lower than that of the covalent antibody ELISA approaches (54.47 pg/mL). To enhance sensitivities in an assay, one would have to either enhance the detection signals, reduce the background noise, or do both [23, 29]. As has been discussed already, the G7-aptamer assay approach has shown significantly higher detection signals at any given analyte concentrations investigated, likely due to more capturing binding sites available – via dendrimer templates – for target molecule capturing and thus more effective molecular bindings. To study how the different assay approaches (*i.e.,* G7-aptamer assay, covalent antibody ELISA, and traditional ELISA)

affect the background noise, the background noises of the three different approaches were further investigated. As evident in Figure 4.6B, the G7-aptamer assay (without blocking steps) showed significantly lower background noises than both the covalent antibody ELISA and the traditional ELISA approaches, in spite of the fact that both of the latter approaches employed blocking steps that were specifically designed to reduce background noises. This observation suggests that surface modification using G7 dendrimer can effectively minimize non-specific adsorptions better than passive surface adsorptions (*i.e.,* blocking). Furthermore, detection performances of the G7-aptamer modified assays showed no significant difference in detection signals regardless of the blocking steps (results shown in Figure B4, Appendix B), further indicating excellent nonfouling properties of G7 surface modification. Our results clearly demonstrate the two main advantages of using G7 dendrimers to modify microwells: 1) as a nonfouling layer to minimize non-specific binding, even in the absence of blocking steps, to reduce background noises; and 2) as a multi-handled template to allow subsequent conjugation of numerous copies of aptamers for more effective target binding to enhance detection signals as well as higher binding capacities to result in broader detection ranges.

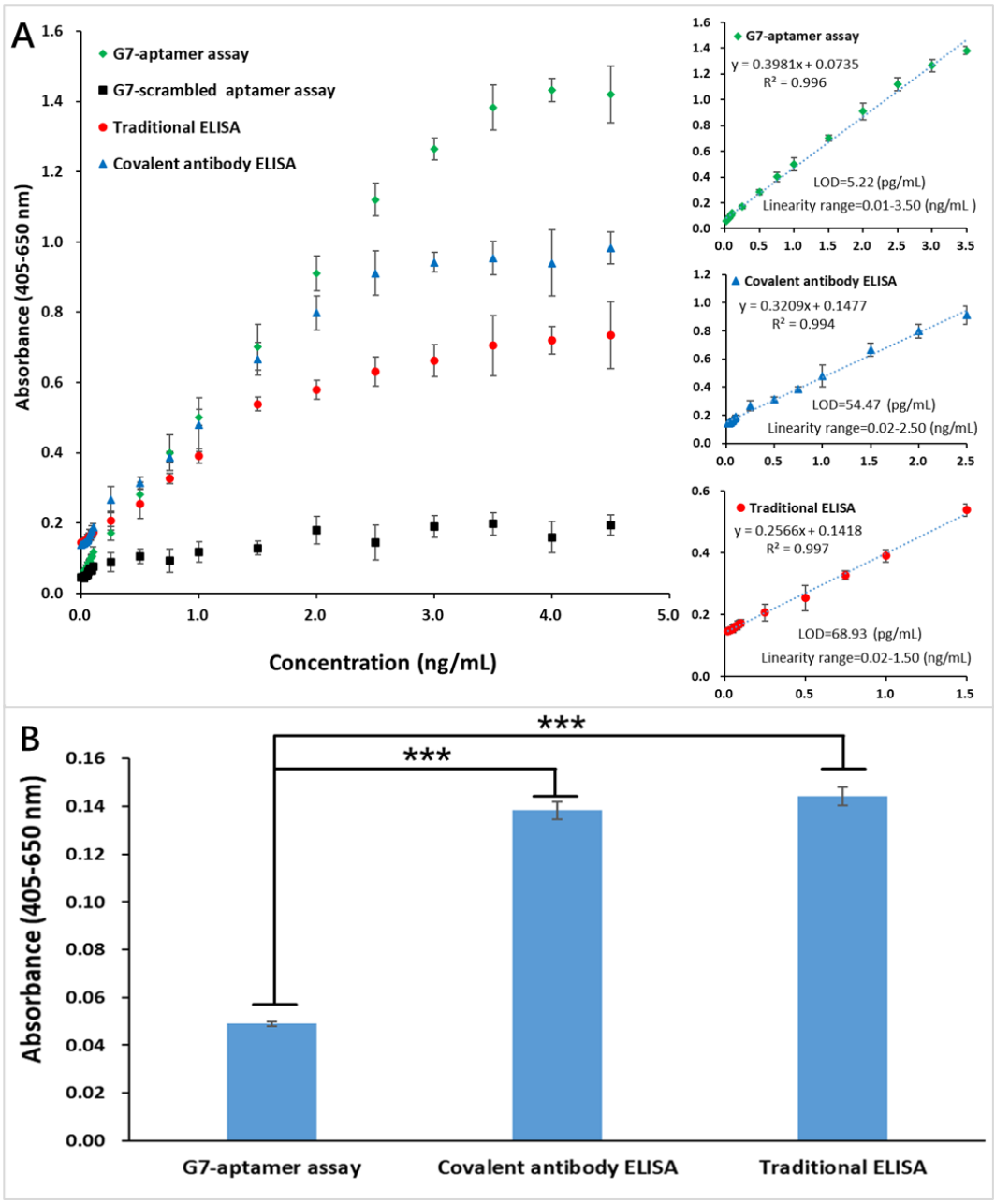

Figure 4.6. Detection performance evaluation. A) Detection performances of different detection assays. Figure insets indicate the equation of linear regressions, linear detection ranges, and LODs for G7-aptamer assay, covalent antibody ELISA, and traditional ELISA; error bars indicate standard divisions, n=3. B) Analysis of background signals of three detection assays; error bars indicate standard divisions, n=3; p values (***<0.001) were calculated by a Student's t-test, 2 tails.

To further evaluate the performances of the G7-aptamer assay for samples in a complex matrix, recovery and precision tests were performed. Specifically, a serially diluted

human PDGF-BB standard in cell culture media was used to create standard curves to calibrate the samples. Samples were prepared using human PDGF-BB standards dissolved in cell culture media with final concentrations at 3 ng/mL, 1 ng/mL, and 0.1 ng/mL, respectively, and were assayed using the new G7-aptamer modified 96-well plates. In parallel, the same sets of samples were assayed using both the traditional ELISA and the covalent antibody ELISA approaches. As shown in Table 4.1, in comparison with the linear ranges of traditional ELISA (0.02-1.25 ng/mL) and covalent antibody ELISA (0.02-2.25 ng/mL), the G7-aptamer assay exhibited a broader linear range of 0.01-3.50 ng/mL (all linear ranges were determined when R^2>0.990), indicating that G7-aptamer assay is remarkably robust as a complex matrix such as cell culture media did not impact its linear detection range; this is likely because of the improved nonfouling properties due to G7 immobilization on the PS surface. Moreover, the G7-aptamer assay exhibited excellent assay recovery and precision when detecting samples in cell culture media since the recoveries ranged from 96.5% to 106.4%, and the precisions expressed as coefficient of variation (% CV) were less than 10%.

Table 4.1. Recovery and precision of different assays as evaluated in cell culture media

	Concentration (ng/mL)	**G7-aptamer assay**	**Covalent antibody ELISA**	**Traditional ELISA**
Sample Type	Cell Culture Media			
R^2 (n=3)		0.995	0.997	0.998
Calibration Range (ng/mL)		0.01-3.50	0.02-2.25	0.02-1.25
Recovery (n=3)	0.1	98.7%±6.4%	101.6%±5.8%	101.8%±4.0%
	1	106.4%±4.4%	97.7%±2.9%	98.7%±4.5%
	3	96.5%±2.9%	out of range	out of range
Precision (%CV**) (n=3)**	0.1	6.5%	5.7%	3.90%
	1	4.1%	3.0%	4.50%
	3	3.0%	/	/

Moreover, to investigate the specificity of the G7-aptamer assay, targets (*i.e.,* human PDGF-BB) and non-targets, including human EGF, human FGF, sonic hedgehog, and BMP-4, were tested at 1 ng/mL. As shown in Figure 4.7, signals for the targets (*i.e.,* human PDGF-BB) were significantly higher ($p<0.05$) than those of the non-targets, suggesting an excellent detection specificity. These excellent detection performances, including recovery, precision, and specificity, suggest that this newly developed ELISA can be readily replaced by other aptamers to specifically recognize and capture other analytes of interest [47, 48].

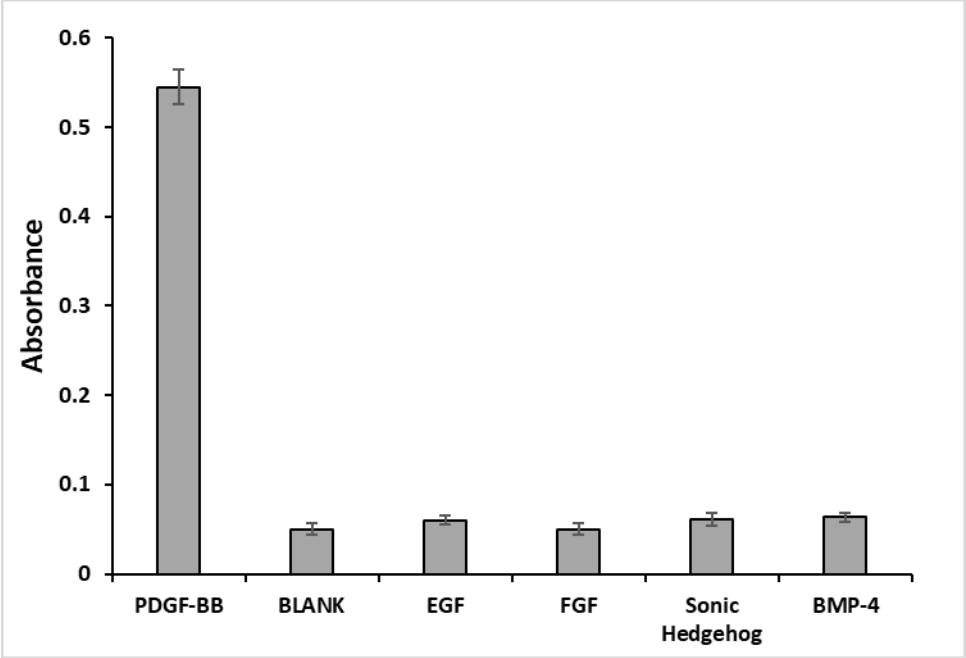

Figure 4.7. Assay specificity of the G7-aptamer modified microwells. All samples were tested at 1 ng/ml. Error bars are standard deviations, n=3.

4.4 Conclusion

In this study, a simple method to chemically immobilize aptamers onto PS 96-microwell surfaces via G7 dendrimer templates was developed to improve ELISA performances. The current surface modification approach has two major advantages in its design to use dendrimers as multi-handled templates: 1) the surface modification of dendrimers on PS surfaces renders the resulting surface nonfouling to minimize non-specific binding, thus eliminating the need to block in the bioassay to reduce background noises, and 2) the multiple functional groups introduced to the surface by the dendrimers allow subsequent conjugation of numerous copies of aptamers for more effective target binding for enhanced assay performances. As a result, we demonstrate that the modified PS 96 well-plates exhibited a much better ELISA performance – in terms of linear detection range, sensitivity, and without laborious and time-consuming blocking steps

– by following an otherwise regular ELISA workflow, suggesting promising application potentials of the current surface modification approach in many microplate-based applications, such as ELISA and other high throughput bioassays.

Reference

1. North, S.H., et al., Plasma-based surface modification of polystyrene microtiter plates for covalent immobilization of biomolecules. ACS applied materials & interfaces, 2010. **2**(10): p. 2884-2891.
2. Alhajj, M. and A. Farhana, Enzyme linked immunosorbent assay. StatPearls [Internet], 2021.
3. Engvall, E., [28] Enzyme immunoassay ELISA and EMIT, in Methods in Enzymology. 1980, Academic Press. p. 419-439.
4. Lequin, R.M., Enzyme Immunoassay (EIA)/Enzyme-Linked Immunosorbent Assay (ELISA). Clinical Chemistry, 2005. **51**(12): p. 2415.
5. Rebeski, D.E., et al., Identification of unacceptable background caused by non-specific protein adsorption to the plastic surface of 96-well immunoassay plates using a standardized enzyme-linked immunosorbent assay procedure. Journal of immunological methods, 1999. **226**(1-2): p. 85-92.
6. Butler, J.E., Solid supports in enzyme-linked immunosorbent assay and other solid-phase immunoassays. Methods, 2000. **22**(1): p. 4-23.
7. Liu, G., et al., The Bioanalytical and Biomedical Applications of Polymer Modified Substrates. Polymers, 2022. **14**(4): p. 826.
8. Tan, H.Y., et al., Quantitation of Trastuzumab and an Antibody to SARS-CoV-2 in Minutes Using Affinity Membranes in 96-Well Plates. Analytical Chemistry, 2022. **94**(2): p. 884-891.
9. Geissler, M., et al., Use of Polymer Micropillar Arrays as Templates for Solid-Phase Immunoassays. ACS Applied Polymer Materials, 2022.
10. Dixit, C.K., et al., Multisubstrate-compatible ELISA procedures for rapid and high-sensitivity immunoassays. nature protocols, 2011. **6**(4): p. 439-445.
11. Han, H.J., et al., Multifunctional dendrimer-templated antibody presentation on biosensor surfaces for improved biomarker detection. Advanced functional materials, 2010. **20**(3): p. 409-421.
12. Jung, Y., et al., Controlled antibody immobilization onto immunoanalytical platforms by synthetic peptide. Analytical Biochemistry, 2008. **374**(1): p. 99-

105.
13. Jung, Y., J.Y. Jeong, and B.H. Chung, Recent advances in immobilization methods of antibodies on solid supports. Analyst, 2008. **133**(6): p. 697-701.
14. Gao, S., J.M. Guisán, and J. Rocha-Martin, Oriented immobilization of antibodies onto sensing platforms-A critical review. Analytica chimica acta, 2022. **1189**: p. 338907.
15. Larsen, M.D., et al., Enzyme-Linked Immunosorbent Assay for Activation of the Classical Complement Pathway by-Infected Erythrocyte Surface Antigen-Specific Antibodies, in Malaria Immunology. 2022, Springer. p. 673-678.
16. Petryayeva, E., W.R. Algar, and U.J. Krull, Adapting fluorescence resonance energy transfer with quantum dot donors for solid-phase hybridization assays in microtiter plate format. Langmuir, 2013. **29**(3): p. 977-987.
17. Dharanivasan, G., et al., Gold nanoparticles assisted characterization of amine functionalized polystyrene multiwell plate and glass slide surfaces. Applied Nanoscience, 2015. **5**(1): p. 39-50.
18. Vesel, A., Modification of polystyrene with a highly reactive cold oxygen plasma. Surface and Coatings Technology, 2010. **205**(2): p. 490-497.
19. Ramsey, W., et al., Surface treatments and cell attachment. In vitro, 1984. **20**(10): p. 802-808.
20. Bentley, K.L. and R.J. Klebe, Fibronectin binding properties of bacteriologic petri plates and tissue culture dishes. Journal of biomedical materials research, 1985. **19**(7): p. 757-769.
21. Goddard, J.M. and J. Hotchkiss, Polymer surface modification for the attachment of bioactive compounds. Progress in polymer science, 2007. **32**(7): p. 698-725.
22. Vashist, S.K. and J.H. Luong, Antibody immobilization and surface functionalization chemistries for immunodiagnostics, in Handbook of Immunoassay Technologies. 2018, Elsevier. p. 19-46.
23. Mahmoudpour, M., et al., Rational design of smart nano-platforms based on antifouling-nanomaterials toward multifunctional bioanalysis. Advances in Colloid and Interface Science, 2022: p. 102637.
24. Gibbs, J., et al., Effective blocking procedures in ELISA assays. 2001, Corning Incorporated Kennebunk, ME.
25. Li, G., et al., The effect of silver-PAMAM dendrimer nanocomposites on the performance of PVDF membranes. Desalination, 2014. **338**: p. 115-120.
26. Qin, Y., et al., Developing an ultra non-fouling SU-8 and PDMS hybrid

microfluidic device by poly (amidoamine) engraftment. Colloids and Surfaces B: Biointerfaces, 2015. **127**: p. 247-255.

27. Katzur, V., et al., Surface-immobilized PAMAM-dendrimers modified with cationic or anionic terminal functions: Physicochemical surface properties and conformational changes after application of liquid interface stress. Journal of colloid and interface science, 2012. **366**(1): p. 179-190.
28. Hao, X., et al., Aptamer surface functionalization of microfluidic devices using dendrimers as multi-handled templates and its application in sensitive detections of foodborne pathogenic bacteria. Analytica Chimica Acta, 2019. **1056**: p. 96-107.
29. Qin, Y., et al., Developing a non-fouling hybrid microfluidic device for applications in circulating tumour cell detections. Colloids and Surfaces B: Biointerfaces, 2017. **151**: p. 39-46.
30. Şenel, M., C. Nergiz, and E. Çevik, Novel reagentless glucose biosensor based on ferrocene cored asymmetric PAMAM dendrimers. Sensors and Actuators B: Chemical, 2013. **176**: p. 299-306.
31. Jiang, Y., S. Zou, and X. Cao, A simple dendrimer-aptamer based microfluidic platform for *E.coli* O157: H7 detection and signal intensification by rolling circle amplification. Sensors and Actuators B: Chemical, 2017. **251**: p. 976-984.
32. Guo, L. and Q. Zhao, Thrombin-linked aptamer assay for detection of platelet derived growth factor BB on magnetic beads in a sandwich format. Talanta, 2016. **158**: p. 159-164.
33. Elsner, H.I. and S. Mouritsen, Use of psoralens for covalent immobilization of biomolecules in solid phase assays. Bioconjugate chemistry, 1994. **5**(5): p. 463-467.
34. Hermanson, G.T., Chapter 5 - Homobifunctional Crosslinkers, in Bioconjugate Techniques (Third Edition), G.T. Hermanson, Editor. 2013, Academic Press: Boston. p. 275-298.
35. Vashist, S.K., et al., One-step antibody immobilization-based rapid and highly-sensitive sandwich ELISA procedure for potential in vitro diagnostics. Scientific Reports, 2014. **4**: p. 4407.
36. Sanaeepur, H., A. Kargari, and B. Nasernejad, Aminosilane-functionalization of a nanoporous Y-type zeolite for application in a cellulose acetate based mixed matrix membrane for CO 2 separation. RSC Advances, 2014. **4**(109): p. 63966-63976.
37. Sardon, H., et al., Synthesis of room temperature self-curable waterborne hybrid

polyurethanes functionalized with (3-aminopropyl) triethoxysilane (APTES). Polymer, 2010. **51**(22): p. 5051-5057.

38. Gunda, N.S.K., et al., Optimization and characterization of biomolecule immobilization on silicon substrates using (3-aminopropyl)triethoxysilane (APTES) and glutaraldehyde linker. Applied Surface Science, 2014. **305**: p. 522-530.
39. Mirzadeh, H. and S. Bagheri, Comparison of the effect of excimer laser irradiation and RF plasma treatment on polystyrene surface. Radiation Physics and Chemistry, 2007. **76**(8): p. 1435-1440.
40. Larrieu, J., et al., Ageing of atactic and isotactic polystyrene thin films treated by oxygen DC pulsed plasma. Surface and Coatings Technology, 2005. **200**(7): p. 2310-2316.
41. Zhang, J., et al., Simultaneous detection of deoxynivalenol and zearalenone by dual-label time-resolved fluorescence immunoassay. Journal of the Science of Food and Agriculture, 2011. **91**(2): p. 193-197.
42. Shiyun, Z., et al., Predicting detection limits of enzyme-linked immunosorbent assay (ELISA) and bioanalytical techniques in general. Analyst, 2013. **139**(2): p. 439-445.
43. Watson, J.D. and F.H. Crick, Molecular structure of nucleic acids: a structure for deoxyribose nucleic acid. Nature, 1953. **171**(4356): p. 737-738.
44. Reth, M., Matching cellular dimensions with molecular sizes. Nature immunology, 2013. **14**(8): p. 765-767.
45. Wang, Z., et al., Multivalent Aptamer Approach: Designs, Strategies, and Applications. Micromachines, 2022. **13**(3): p. 436.
46. Shrivastava, A. and V.B. Gupta, Methods for the determination of limit of detection and limit of quantitation of the analytical methods. Chron. Young Sci, 2011. **2**(1): p. 21-25.
47. David, M.S. and D. Kanayeva, Enzyme Linked Oligonucleotide Assay for the Sensitive Detection of SARS-CoV-2 Variants. Frontiers in Cellular and Infection Microbiology, 2022: p. 1470.
48. Jiang, R., et al., A low-background aptasensor based on enzyme-linked multifunctional carbon nanosheets for the detection of Salmonella. Sensors and Actuators B: Chemical, 2022. **370**: p. 132412.

Chapter 5

Localized Surface Plasmon Resonance Biosensor Chip Surface Modification and Signal Amplifications Toward Rapid and Sensitive Detection of COVID-19 Infections

Abstract

We developed a multi-pronged approach to enhance the detection sensitivity of localized surface plasmon resonance (LSPR) sensor chips to detect SARS-CoV-2. To this end, poly(amidoamine) dendrimers were immobilized onto the surface of LSPR sensor chips to serve as templates to further conjugate aptamers specific for SARS-CoV-2 binding. The immobilized dendrimers were shown to reduce surface nonspecific adsorptions and increase capturing ligand density on the sensor chips, thereby improving detection sensitivity. To characterize the detection sensitivity of the surface-modified sensor chips, SARS-CoV-2 spike protein receptor-binding domain was detected using LSPR sensor chips with different surface modifications. The results showed that the dendrimer-aptamer modified LSPR sensor chip exhibited a limit of detection (LOD) of 21.9 pM, a sensitivity that was 9 times and 152 times more sensitive than the traditional aptamer- or antibody-based LSPR sensor chips, respectively. In addition, detection sensitivity was further improved by combining rolling circle amplification product and gold nanoparticles (RCA-AuNPs) in the detection to further amplify the detection signals by increasing both the target mass and plasmonic coupling effects. Using pseudo SARS-CoV-2 viral particles as detection targets, we demonstrated that the combined signal intensification approach was able to enhance the detection signals by additional 10 times and achieved a remarkable LOD of 148 vp/mL, making it one of the most sensitive SARS-CoV-2 detection assays reported to date.

These results highlight the potential of the novel LSPR-based detection platform for sensitive and rapid detection of COVID-19 infections or other viral infections and other point-of-care applications.

5.1 Introduction

The current COVID-19 pandemic has caused millions of deaths and affected economies around the world; it also has highlighted the need for improved technological preparedness for the next pandemic. During the COVID-19 pandemic, many rapid biosensors [1-8] have been developed to detect COVID-19 infections in biological samples; however, these rapid detection biosensors suffer from various significant drawbacks, such as low detection sensitivities [9, 10] and complicated sample pre-treatments [8, 11], severely limiting their application as reliable alternatives to PCR for COVID-19 detections.

Localized surface plasmon resonance (LSPR) is an optical phenomenon generated by collective electron charge oscillations in metallic nanoparticles excited by a light source [12, 13]. These charge oscillations create a highly localized evanescent field extending from the surface of the nanoparticles and this evanescent field is highly sensitive to minute local variations, such as surface mass changes due to molecular bindings [12, 14]. Therefore, LSPR-based biosensors have been widely used in many real-time and label-free detection applications [15, 16]. In fact, several LSPR biosensors have already been developed to detect COVID-19 related biological targets, including nucleic acids, antibodies, proteins, and whole viral particles [7, 16-21]. While these LSPR-based methods have demonstrated good detection performances, both in terms of detection

specificity and limit of detection (LOD), there is still a need to further improve the sensitivity of these LSPR biosensors in order to approach that achieved by PCR-based methods [22]. This is mainly due to the lack of effective signal amplification and intensification in LSPR-based biosensors. In an elegant study, gold nanoparticle-labeled antibodies were used to label captured targets in LSPR sensor chips to amplify the detection signals by taking advantage of the combined effects of increased target mass and plasmonic coupling effects on the sensor chip surface; the study showed a signal amplification of up to 15 times when compared with control [23]. In another study, a surface-bound hybridization chain reaction was employed to improve the sequence length of the target miRNA molecules captured on LSPR sensor chips and achieved a signal amplification by a factor of 2 [24]. However, these LSPR sensors with signal amplification designs are still insufficient for real-world applications.

To further improve the detection sensitivity of LSPR biosensors, two critically important considerations – non-fouling properties of the sensor chip surfaces and high surface-ligand densities on the sensor chip surfaces – must be simultaneously targeted and integrated into the sensor chip designs [25, 26]. For example, it is crucial for the sensor chip surfaces to minimize nonspecific adsorptions, thereby decreasing the background noises and ultimately enhancing the signal-to-noise ratio and thus detection sensitivity [27, 28]. Furthermore, sensor chip surfaces with more detection ligands would lead to a higher probability and stronger binding avidity for target capturing [29], thus resulting in higher detection sensitivity.

Poly(amidoamine) (PAMAM) dendrimers are hyper-branched polymers that possess multiple surface functional groups, such as -OH, -COOH, and $–NH_2$. Because of this unique structure, PAMAM dendrimers have been used as multi-handled templates via which capturing ligands, such as aptamers, can be conjugated onto a capturing surface to allow for enhanced target capturing probability and binding avidity for improved detection performances [29-31]. In addition, surface immobilization of the detection surfaces with PAMAM dendrimers can render the resulting surfaces non-fouling, thus minimizing background noises [26-28].

Rolling circle amplification (RCA) reactions can generate long single-stranded DNA molecules with hundreds or thousands of tandem repeating units – based on a circular template -- that can be designed to either capture specific targets, amplify signals, or do both [30, 32, 33]. For example, RCA-gold nanoparticle complexes (RCA-AuNPs) have been applied to conjugate with surface-captured targets on a surface plasmon resonance (SPR) sensor chips to improve detection signals by significantly increasing target mass [33].

In this study, we report our most recent efforts to enhance the detection sensitivity of regular LSPR sensor chips – prepared using a widely employed gold nanoislands/poly (allylamine hydrochloride) (PAH)/poly(sodium 4-styrenesulfonate) (PSS) method [34-37] – by implementing a multi-pronged design that aims to both reduce background noises and enhance detection signals. To reduce the background noises, both glass surfaces and gold nanoislands of the sensor chip surfaces are modified with PAMAM dendrimers to render them non-fouling to prevent non-target molecules and particles

from interacting with the sensor chip surfaces. To enhance the detection signals, the following strategies are explored: a) multiple copies of capturing aptamers specific for the targets are immobilized onto the sensor chip detection surfaces via the multi-handled PAMAM dendrimers, resulting in higher capturing probability and binding avidity for target recognition and capturing (*i.e.,* first-layer amplification); and b) RCA-AuNPs complexes that incorporate both a large number of AuNPs and tandem repeating aptamers specific for the targets are employed to bind to the surface captured targets (*i.e.,* SARS-CoV-2 pseudo viral particles) in a sandwich detection format to improve detection signals (*i.e.,* second-layer amplification) via both (1) increasing the target mass (from both RCA products and AuNPs) and (2) improving plasmonic coupling effect due to attached AuNPs [23, 33, 38, 39]. The PAMAM dendrimer-aptamer modified sensor chips are employed to detect both SARS-CoV-2 spike protein receptor-binding domain (SRBD) and SARS-CoV-2 pseudo viral particles. Our results show that the modified sensor chip is 152 times more sensitive than the antibody-immobilized sensor chip (traditional method) in detecting SRBD samples (*i.e.*, due to first-layer amplification). Moreover, the use of RCA-AuNPs signal amplification results in a 10-time additional improvement in the detection signal when detecting SARS-CoV-2 pseudo viral particles (*i.e.*, due to second-layer amplification). The LOD is 148 viral particles per milliliter (vp/mL), one of the highest sensitivities reported in whole viral particle detections amongst all detection platforms [21, 40-44], making it sufficiently sensitive for the diagnosis of early COVID-19 infections [21].

5.2 Experimental

5.2.1 Overall Design

As shown in Figure 5.1, the LSPR sensor chip surfaces are modified sequentially with generation 3.5 carboxylated PAMAM dendrimers (*i.e.*, G3.5-COOH) and generation 4 aminated PAMAM dendrimers (*i.e.,* G4-NH_2) to render the resulting surfaces non-fouling. Subsequently, the immobilized G4 dendrimers act as multi-handled templates to allow for subsequent conjugation of numerous copies of aptamers against SRBD of SARS-CoV-2 [45]. The resulting sensor chips are used to detect COVID-19 targets (*i.e.*, either SARS-CoV-2 SRBD or SARS-CoV-2 pseudo viral particles presenting spike proteins on the viral particle surfaces). For the case of SARS-CoV-2 pseudo viral particle detection, RCA-AuNPs are employed to bind with the surface-captured viral particles to further intensify detection signals by increasing the target mass and plasmonic coupling effect.

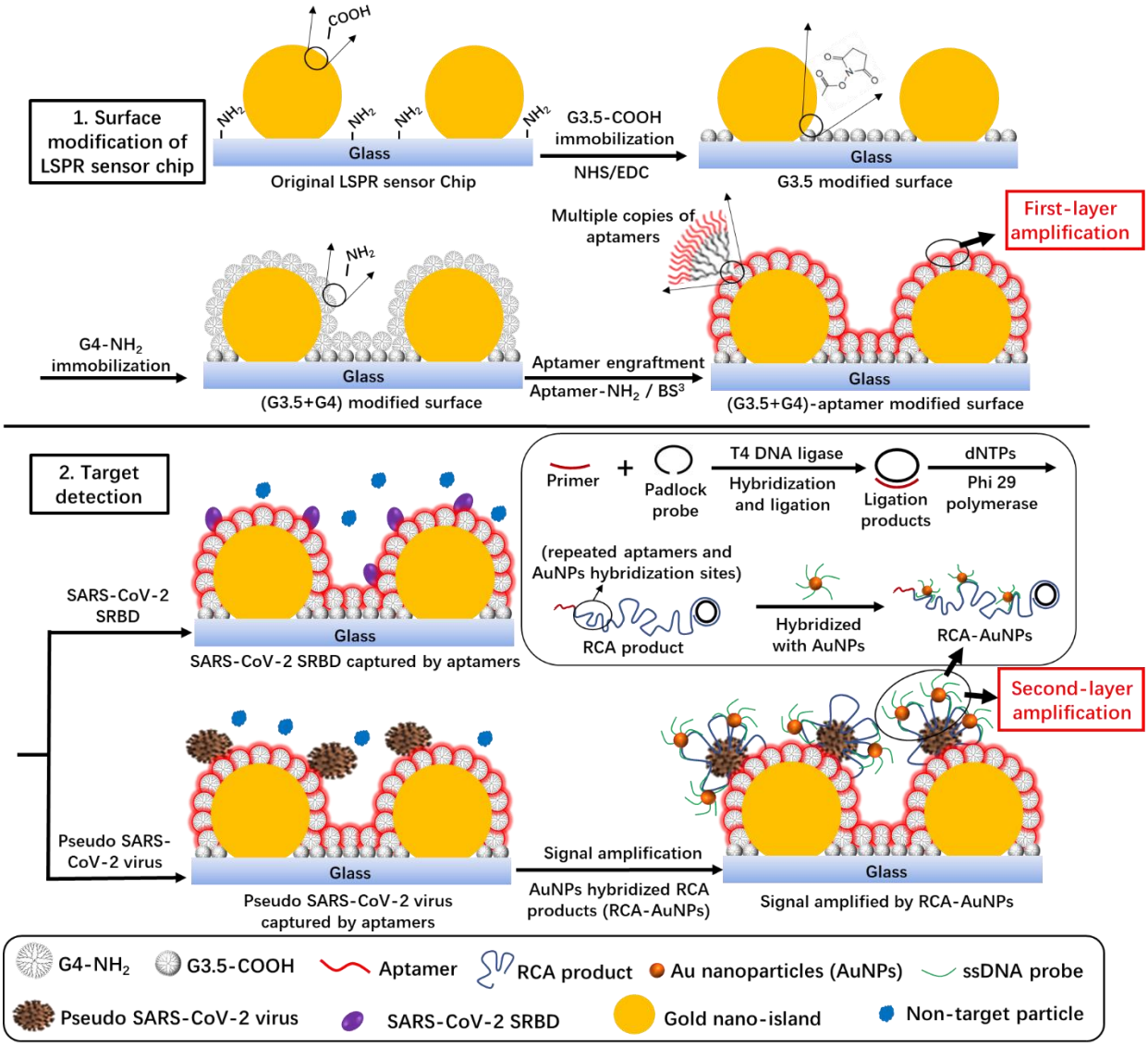

Figure 5.1 Schematic illustration showing the general approach to prepare (G3.5+G4)-aptamer modified LSPR sensor chips for sensitive detection of the SARS-CoV-2 SRBD and SARS-CoV-2 pseudo viral particles. Note that the second-layer amplification is only possible with SARS-CoV-2 pseudo viral particles as the detection targets upon which the detection sandwich format can be built.

5.2.2 Materials

Detailed information on chemicals, pseudo-SARS-CoV-2 viral particles, and DNA sequences for this study are provided in C1.1 (Appendix C); gold nanoislands/PAH/PSS LSPR sensor chips with carboxyl functionalization on gold nanoislands were prepared

as detailed in C1.2 (Appendix C); AuNP probes (*i.e.,* ssDNA-AuNPs) were prepared using well-developed approaches by conjugating AuNPs with ssDNA probes (sequence #: S_4, Table C1, Appendix C) [46, 47]; RCA products were synthesized as described in C1.3 (Appendix C).

5.2.3 Surface Modifications using PAMAM Dendrimers and Aptamers

Surface modification of the LSPR sensor chips followed the general steps outlined in Figure 5.1. Since the exposed glass areas of the original LSPR sensor chip presented -NH_2 functional groups while the gold nanoislands presented -COOH groups (C2.1, Appendix C), the sensor chip surface was first reacted with G3.5-COOH using N-hydroxysuccinimide/N-ethyl-N′-(3-(dimethylamino)propyl) carbodiimide (NHS/EDC) chemistry to immobilize G3.5-COOH on the glass areas and to convert the carboxyl surface functional groups on both the glass areas and the gold nanoislands into NHS esters [48]. Specifically, LSPR sensor chips were loaded into a Nicoya OpenSPR instrument (Kitchener, ON) to form a microfluidic channel based LSPR biosensor, after which a G3.5-COOH immobilization solution, including 50 μM G3.5-COOH, 0.1 M NHS, and 0.1 M EDC in PBS (pH=7.4), was injected into the channel to react with the LSPR sensor chip surfaces at a flow rate of 10 μL/ min for 10 min. Subsequently, the resulting sensor chip was carefully rinsed with PBS (pH 7.4) at a flow rate of 10 μL/ min until the signal baseline was stabilized.

Subsequently, G4-NH_2 was immediately immobilized onto the surfaces of the LSPR sensor chip via the NHS-esters obtained during the previous step. Briefly, a 100 μM G4-NH_2 in PBS (pH 7.4) was injected into the channel to react with the G3.5 modified

LSPR sensor chip at a flow rate of 10 µL/ min for 10 min, after which the G4 immobilized chip was rinsed with PBS (pH 7.4) at a flow rate of 10 µL/ min until the signal baseline was stabilized. In this modification step, the G4-NH_2 molecules were immobilized onto both the gold nanoislands and the immobilized G3.5 molecules. It is important that G4-NH_2 immobilization should be conducted immediately after the G3.5-COOH modification, as NHS-esters are known to be readily hydrolyzed [49]. The immobilized G4-NH_2 molecules would be used as multi-handled templates to provide multiple binding sites (*i.e.*, -NH_2 groups) in the next step to further conjugate aptamers.

Finally, to conjugate amino-capped aptamers (*i.e.,* NH_2-aptamer, specific for SRBD, sequence #: S_1, Table C1, Appendix C) onto the sensor chip surfaces via the immobilized G4-NH_2 templates, a widely used bis(sulfosuccinimidyl)suberate (BS^3) crosslinker was employed [50]. As the BS^3 crosslinker contains homobifunctional sulfo-NHS-esters that can efficiently conjugate molecules containing primary amino groups [50], the aptamer-NH_2 can be readily conjugated with the surface-immobilized G4-NH_2 molecules acting as templates. In a typical reaction, an aptamer conjugation solution containing 200 µM aptamers and 20 mM BS^3 in PBS (pH 7.4) was injected into the (G3.5+G4) modified LSPR sensor chip at a flow rate of 5 µL/ min for 20 min to conjugate aptamers onto the G3.5+G4 templated surface. Subsequently, an ethanolamine-HCL solution (1 M, pH 8.5) was injected into the modified LSPR sensor chip at a flow rate of 20 µL/ min for 5 min to deactivate the reaction, after which the sensor chip was carefully rinsed with PBS (pH 7.4) at a flow rate of 30 µL/ min until the signal baseline was stabilized.

5.2.4 Evaluation of Detection Performances using SRBD Samples

To evaluate the detection performances of the (G3.5+G4)-aptamer modified LSPR sensor chips, SRBD of the SARS-CoV-2 virus was employed. Briefly, SRBD samples of different concentrations were separately injected into the (G3.5+G4)-aptamer modified LSPR sensor chip at a flow rate of 30 μL/ min for 3.3 min, after which the sensor chip was regenerated using a regeneration buffer (*i.e.*, glycine-HCL (10 mM, pH 2.0) at a flow rate of 150 μL/ min for 0.67 min so that the sensor chip could be regenerated [51].

5.2.5 Detection of SARS-CoV-2 Pseudo Viral Particles with RCA-AuNPs Signal Amplifications

To evaluate the real-world sample detection performances of the newly developed sensor chips, pseudo SARS-CoV-2 viral particles were used as detection targets; in addition, the detection signals were subsequently intensified using an *in situ* amplification step based on RCA-AuNPs complexes. Specifically, different concentrations of pseudo viral particle suspensions were separately injected into the (G3.5+G4)-aptamer modified LSPR sensor chip at a flow rate of 30 μL/ min for 3.3 min, after which the sensor chip was carefully rinsed using running PBS (pH 7.4) at a flow rate of 30 μL/ min until the signal baseline was stabilized. Subsequently, the RCA-AuNPs complexes were injected into the sensor chip at a flow rate of 30 μL/ min for 3.3 min in order to amplify the detection signals *in situ*. To regenerate the sensor chip, the LSPR sensor chip channel was washed using a regeneration buffer at a flow rate of 150 μL/ min for 0.67 min to release the captured viral particles [51]. *Caution: all*

experiments involving SARS-CoV-2 pseudo viral particles were carried out in a certified Risk Group II (RG II, Public Health Agency of Canada) laboratory.

5.2.6 Statistical Analysis

The statistical analysis was performed using Microsoft Excel software (version 2303). To ensure the reliability and robustness of the results, all experiments were carried out in triplicate (otherwise indicated in figure captions), both within the same day and across different days, and the mean values with their corresponding standard deviations were calculated and reported. The Student's t-test, two-tailed, was employed to assess the statistical significance of the differences between the groups, with a p-value of less than 0.05 considered statistically significant.

5.3. Results and Discussion

5.3.1 Characterizations

Characterization results are detailed in Appendix C, including characterizations of carboxyl functionalized LSPR sensor chips C2.1, (G3.5+G4)-aptamer surface modifications C2.2, AuNPs and ssDNA-AuNPs conjugates C2.3, and RCA products C2.4.

5.3.2 Detection Performances of (G3.5+G4)-aptamer Sensor Chips

The surface non-fouling property is a critical consideration to enhance LSPR sensor sensitivity [52]; therefore, the surface non-fouling property of the modified sensor chips was first investigated by evaluating the detection background noises using 1 mg/mL bovine serum albumin (BSA) as a nonspecific molecule and without any blocking.

Specifically, four different sensor chips with different surface modification configurations (see Legend of Figure 5.2), including the original sensor chips (*i.e.*, gold-aptamer, black curve), sensor chips with G3.5 modification on glass areas in-between the gold nanoislands (*i.e.*, G3.5-aptamer, red curve), sensor chips with G4 modification on the gold nanoislands (*i.e.*, G4-aptamer, blue curve), and sensor chips with both G3.5 and G4 modifications (*i.e.*, (G3.5+G4)-aptamer, green curve) were tested. As shown in Figure 5.2A, gold-aptamer modified (*i.e.*, no dendrimers) sensor chips showed the highest background noises, indicating the strongest nonspecific surface adsorptions; in contrast, the (G3.5+G4)-aptamer modified sensor chips exhibited the lowest background noises, suggesting excellent non-fouling properties of the modified surfaces. As expected, both the G3.5- and G4-aptamer modified sensor chips demonstrated significantly improved non-fouling properties compared to the gold-aptamer modified surfaces (*i.e.*, no dendrimer immobilization on the sensor chip surface), as the background noises of these sensor chips were substantially lower than those of the gold-aptamer modified. This observation suggests that nonspecific adsorption occurs on both gold nanoislands and areas between the nanoislands and that the immobilized G3.5 and G4 molecules can effectively prevent nonspecific adsorptions in both areas. This significant improvement in non-fouling properties of the sensor chip surfaces -- as a result of functionalizing the sensor chip surface with a layer of dendrimers using combined (G3.5+G4) surface modifications -- results in significantly reduced background noises, thus potentially improving the detection performance of the LSPR sensor chips by enhancing the signal-to-noise ratio of the sensor chips [53, 54]. It is worth mentioning that the excellent non-fouling properties of the dendrimer-modified sensor chip eliminate the need for both blocking reagents

and reference channels specifically designed to reduce and compensate for surface nonspecific bindings in the LSPR assays, respectively [16, 55, 56].

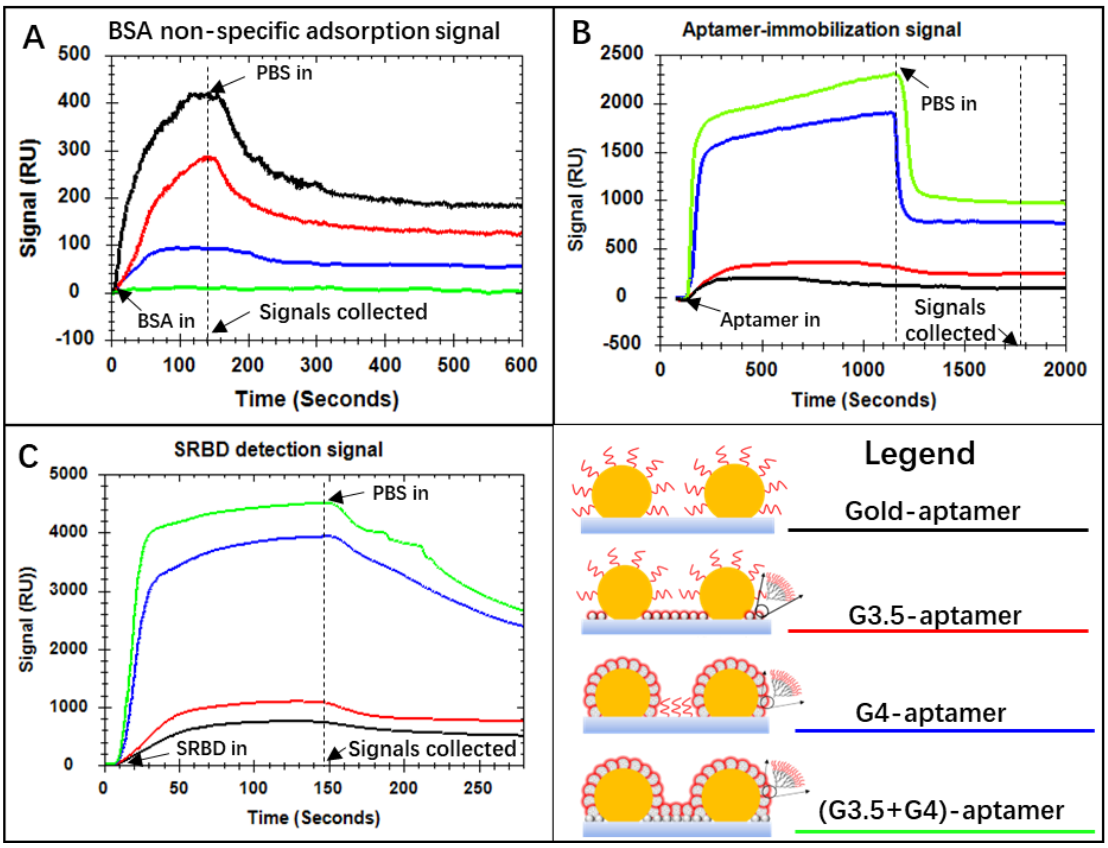

Figure 5.2. LSPR sensorgraphs of different tests to evaluate performances of different sensor chip surface modifications. A) Detection background noises of different sensor chips as evaluated in a nonspecific adsorption experiment using BSA (1 mg/mL). B) Comparison of the amount of aptamers immobilized on the surface of gold nanoisland of different sensor chips. C) Detection signals of SRBD (377.36 nM) on different modified surfaces; note: all except the (G3.5+G4)-aptamer in Figure 5.2C were blocked by BSA before SRBD testing. Legends show surfaces with different modification strategies, including gold-aptamer (the black curve), G3.5-aptamer (the red curve), G4-aptamer (the blue curve), and (G3.5+G4)-aptamer (the green curve) for all tests.

As the number of surface-immobilized detection ligands (*i.e.*, aptamers) is one of the most critical considerations affecting the detection sensitivity of biosensors [57-59], we studied the relative amount of aptamers immobilized on the surface of gold nanoislands

of different modified sensor chips (*i.e.,* gold-aptamer, G3.5-aptamer, G4-aptamer, and (G3.5+G4)-aptamer surfaces) by directly evaluating the LSPR sensorgraph signal changes before and after aptamer immobilizations. As shown in Figure 5.2B, the gold-aptamer surface showed the lowest signal, suggesting the lowest amount of immobilized aptamers, likely due to a limited number of aptamer-binding sites on the gold-nanoislands. In contrast, the (G3.5+G4)-aptamer sensor chip surface exhibited the highest aptamer-immobilization signal, approximately 10 times higher than that of the gold-aptamer surface. This significant increase of immobilized aptamers amount was most likely caused by the presence of multi-handled G4 dendrimer templates (*i.e.,* 64 binding sites per G4 molecule) via which the aptamers were immobilized on the surface of gold nanoislands. Therefore, it can be concluded that the (G3.5+G4) surface-modification configuration allows for the largest amount of aptamers to be tethered on the surface of gold nanoislands in this study.

Furthermore, to study the performances of the four modified sensor chips (*i.e.,* gold-aptamer, G3.5-aptamer, G4-aptamer, and (G3.5+G4)-aptamer surfaces), SRBD detection was carried out using these sensor chips. For this study, the gold-aptamer, G3.5-aptamer, and G4-aptamer sensors were blocked with BSA prior to SRBD detection, while this blocking step was not performed for (G3.5+G4)-aptamer sensor chips. As shown in Figure 5.2C, the detection signals from all 4 sensor chips showed patterns and trends similar to that of the gold nanoisland surface-immobilized aptamer signals seen in Figure 5.2B. Specifically, the (G3.5+G4)-aptamer sensor chip showed the highest detection signal of 4490 RU, while detection signals from other sensor chips were 735 RU (gold-aptamer surface), 1080 RU (G3.5-aptamer surface), and 3900 RU

(G4-aptamer surface), respectively. These results strongly indicate that the (G3.5+G4) surface modification on the sensor chip is the most effective design in conjugating more aptamers to the capturing surface, which further improves detection signals in comparison with other sensor chip modification approaches investigated in this study.

To further investigate the detection performances of the (G3.5+G4)-aptamer sensor chips, the sensor chips were used to detect different concentrations of SRBD samples; in parallel, the same samples were also assayed using gold-aptamer, gold-antibody (*i.e.*, antibodies against SRBD), and (G3.5+G4)-antibody modified sensor chips for comparisons. As shown in Figure 5.3, the (G3.5+G4)-aptamer modified sensor chips showed the highest detection signal at any given SRBD concentration assayed amongst all sensor chips investigated, including gold-aptamer, gold-antibody, and (G3.5+G4)-antibody. In addition, it is worthwhile to note that the (G3.5+G4)-aptamer modified sensor chips demonstrated a broader detection range (0.04 nM to 377.36 nM) than the gold-aptamer modified sensor chips (0.19 nM to 60.38 nM). This significantly increased detection range demonstrated by the (G3.5+G4)-aptamer modified sensor chips was most likely caused by the presence of a greater amount of capturing aptamers on the (G3.5+G4) modified surface than on the non-modified sensor chips, thereby providing more target capturing binding capacity by allowing both more binding sites and stronger binding avidity for target capturing [29]. Furthermore, the slope of the response curve in the linear region of the (G3.5+G4)-aptamer modified sensor chips ($k=367.56$) was significantly greater ($p<0.05$) than those of the gold-aptamer ($k=48.71$), gold-antibody ($k=3.58$) and (G3.5+G4)-antibody ($k=5.77$) modified sensor chips, suggesting a much higher detection sensitivity by the (G3.5+G4)-aptamer modified

sensor chips, as detection sensitivities are determined by the slope of the response curve [60, 61].

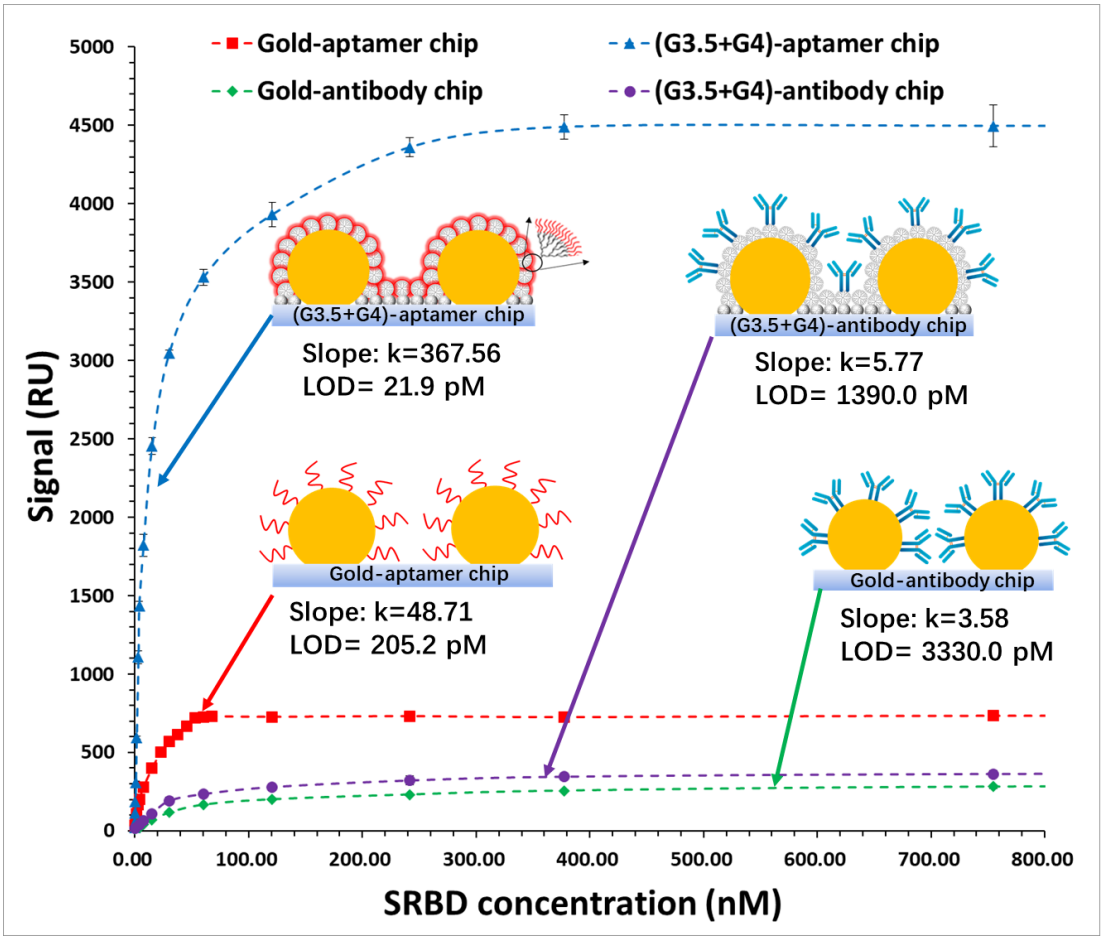

Figure 5.3. Detection performances of different modified sensor chips over a wide range of SRBD concentrations. Note: in obtaining the response curve, all detection parameters were optimized (C3, Appendix C), and the gold-aptamer and gold-antibody sensor chips were properly blocked using BSA; the LSPR sensorgraphs for creating these concentration-response curves are shown in C6 (Appendix C).

The LOD, defined as the lowest target concentration to provide a signal at least three standard deviations greater than the signal from a negative control [26], was also calculated for each type of sensor chip. The results showed that the LOD of the (G3.5+G4)-aptamer modified sensor chip was 21.9 pM, which was around 9-time more

sensitive than that of the gold-aptamer (205.2 pM) and 152-time more sensitive than that of the gold-antibody (3330.0 pM) modified sensor chip, respectively. In addition, a comparison between the (G3.5+G4)-antibody and the (G3.5+G4)-aptamer modified sensor chips reveals that the LOD of the (G3.5+G4)-antibody sensor chip was much higher (*i.e.,* 1390.0 pM *vs.* 21.9 pM). This difference is likely due to a significantly less amount of antibodies – in comparison with the amount of aptamers – conjugated onto the sensor chip surfaces via the G3.5+G4 templates, resulting in less capturing ligands on the sensor detection surfaces; indeed, aptamers are much smaller molecules than antibodies (1 nm *vs.* 10 nm) [62, 63], likely allowing more copies of aptamers to be conjugated to the sensor chip surfaces via the G3.5+G4 templates (size 4.5 nm) than their antibodies counterparts via decreased steric hindrance. To test this hypothesis, we roughly estimated the number of aptamers *vs.* antibodies on the (G3.5+G4) modified surfaces as reported elsewhere [64-66] (see details in C5, Appendix C). The result showed that the number of immobilized surface aptamers was in a range of 16-44 times greater than that of the immobilized antibodies.

5.3.3 Detection of SARS-CoV-2 Pseudo Viral Particles with RCA-AuNPs Signal Amplification (second-layer amplification)

To further study the detection performance of the (G3.5+G4)-aptamer sensor chips, SARS-CoV-2 pseudo viral particles were used as detection targets. In comparison with the SRBD, the SARS-CoV-2 viral particles present multiple spike proteins (around 26) on their surfaces [67], thus providing an opportunity for multivalent binding of single targets. This can be exploited to allow for signal amplifications to further enhance detection signals [21, 33].

Since the detection signals can be amplified using either a two-step amplification format (*i.e.,* conjugation of captured viral particles with RCA products that are subsequently hybridized with ssDNA-AuNPs) or a one-step amplification format (*i.e.*, conjugation of captured viral particles with RCA-AuNPs complex), both amplification methods were carried out and the amplified signals from the two methods were compared. As shown in Figure 5.4A, the sensorgraph of the two-step format (*i.e.,* the black curve) showed a weak signal enhancement after the first step of signal amplification employing RCA , with the signal only intensified by a factor of 1.7 (175 *vs.* 310 RU, see the black curve), an observation that is consistent with a previous study [33]. However, the detection signal was significantly enhanced by approximately 6 times (310 *vs.* 1700 RU) after introducing ssDNA-AuNPs. This is likely because a large number of ssDNA-AuNPs probes were hybridized with the RCA products, resulting in a significant enhancement of both the target mass and the plasmonic coupling effect [23, 33, 38, 39]. It should be noted that the idea of prolonging the RCA reaction time – thus the detection mass -- to better increase the mass of targets did not work well (data not shown), as longer RCA reaction times resulted in large amounts of visible white magnesium pyrophosphate precipitates that blocked the LSPR channels [68]. In comparison, the one-step amplification format (see the red curve, Figure 5.4A) exhibited no significant ($p>0.05$) difference in the final amplified signal when compared with the two-step amplification format (*i.e.,* the black curve). However, since the one-step amplification format required fewer injection steps (*i.e.,* 2 *vs.* 3 injections) and a shorter run time (500s *vs.* 800s), it was selected as the optimal signal intensification format for subsequent studies unless otherwise indicated.

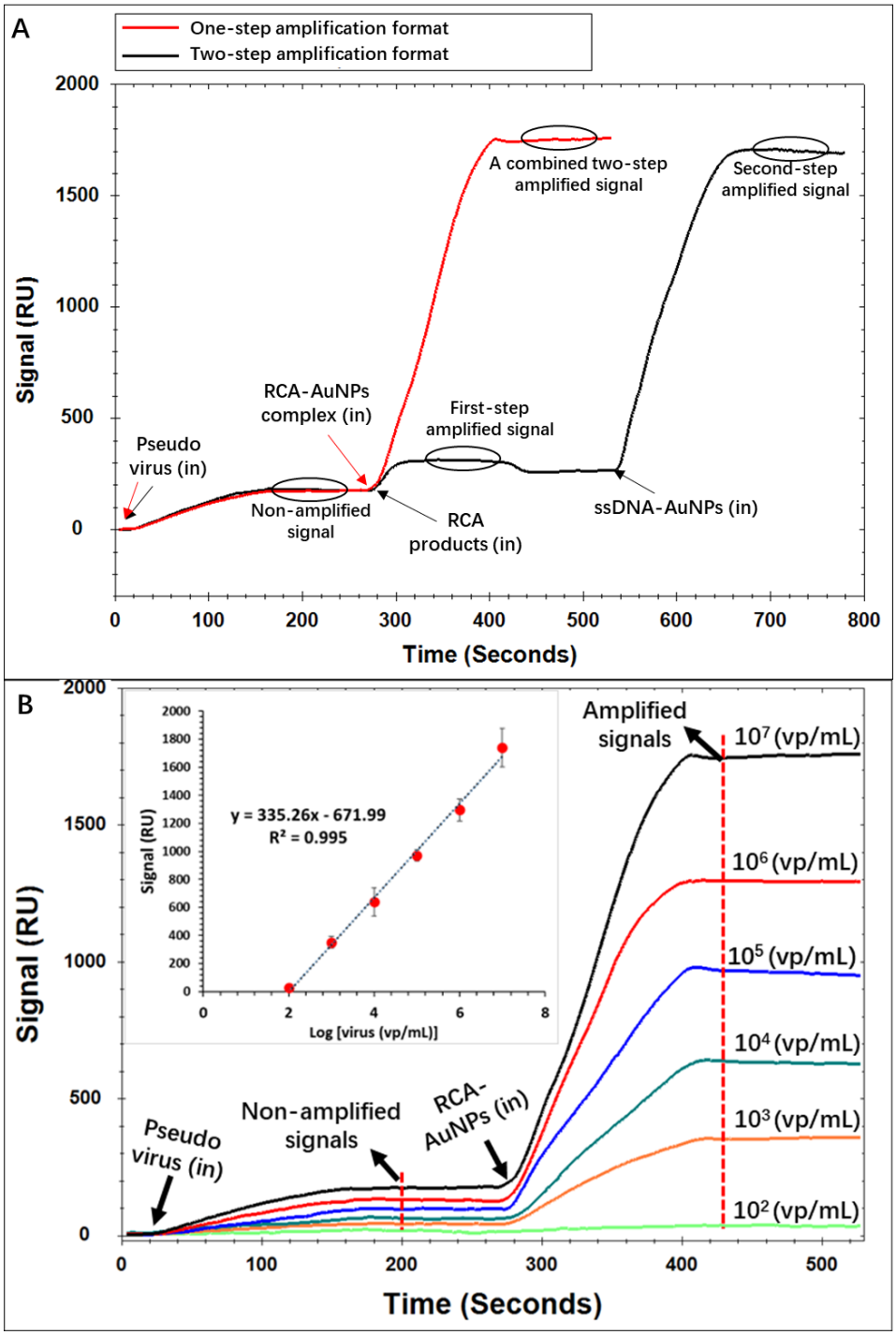

Figure 5.4. Detection of SARS-CoV-2 pseudo viral particles with RCA-AuNPs signal amplification. A) LSPR sensorgarphs of one- and two-step amplification formats for signal amplification of SARS-CoV-2 pseudo viral particles (10^7 vp/mL); and B) the LSPR sensorgraph of detection of SARS-CoV-2 pseudo viral particles with RCA-AuNPs signal amplification; inset shows the relationship between the signals and the target concentrations; error bars indicate standard deviations, n=3.

To evaluate the detection performances of pseudo SARS-CoV-2 viral particles with RCA-AuNPs signal amplification, different concentrations of pseudo SARS-CoV-2 viral particles were detected using the (G3.5+G4)-aptamer modified sensor chips, followed by a signal amplification using RCA-AuNPs. As shown in Figure 5.4B, the sensorgraph presented low detection signals at any virus concentration before signal amplification was employed; in contrast, the detection signals were increased approximately 10-fold after the RCA-AuNPs complex was applied, indicating successful (and significant) detection signal intensification. Moreover, the LSPR signal was proportional to the logarithmic value of the virus concentration with a linear equation of $y = 335.26x - 671.99$ ($R^2 = 0.995$) (inset), and the LOD was calculated to be 148 vp/mL, one of the best sensitivities reported in whole viral particle detections amongst all detection platforms [21, 40-43]. It should be noted that the typical SARS-CoV-2 viral concentration from nasopharyngeal and saliva swabbed samples is 10^4-10^{10} vp/mL [21], suggesting that the currently reported sensor chip modification and signal amplification approach can be used for early infection diagnostics to sensitively detect the SARS-CoV-2 virus. Moreover, the current approach directly detects whole viral particles; therefore, no sample pre-treatment would be required and the whole detection time can be done in less than 500 seconds, more efficient than any existing methods that require laborious sample preparations [7, 69-73]. In addition, as shown in Figure C7 (Appendix C), the modified sensor chip can be regenerated multiple times using a regeneration solution (*i.e.*, glycine-HCL (10 mM, pH 2.0)), significantly saving the overall detection time and cost.

5.3.4 Detection Specificity and Influence of Biological Mixtures.

To study the specificity of (G3.5+G4)-aptamer sensor chip for detecting the SRBD samples, the target (*i.e.,* SARS-CoV-2 SRBD) and non-targets (*i.e.,* SARS-CoV SRBD and Middle East Respiratory Syndrome (MERS)-CoV SRBD) were tested. As shown in Figure 5.5A (blue bars), signals for the target (*i.e.,* SARS-CoV-2 SRBD) were significantly higher than those of non-targets (*i.e.,* SARS-CoV SRBD and MERS-CoV SRBD), suggesting excellent detection specificity of the sensor chip for SARS-CoV-2 SRBD. To further study the specificity for pseudo viral particles detections, the SARS-CoV-2 pseudo viral particles (*i.e.,* targets) and negative pseudo viral particles with no spike protein on the surface (*i.e.,* non-targets) were detected using the (G3.5+G4)-aptamer sensor chip followed by signal amplification with RCA-AuNPs. As shown in Figure 5.5A (yellow bars), the negative pseudo viral particles (*i.e.,* non-target) showed a low signal value at 23 RU compared to SARS-CoV-2 pseudo viral particles (*i.e.,* target) with a signal value at 970 RU, indicating excellent detection specificity for SARS-CoV-2 pseudo viral particles. Moreover, the weak signal (7 RU) of the control sample (*i.e.,* Control = no viral particles) indicates minimal nonspecific interactions between the detection surface and the RCA-AuNPs. It should also be noted that in comparison with a previously reported study in which RCA-AuNPs was also used to amplify SPR sensor chip detection signals [33], the background noises detected in the current study were much lower, further demonstrating the advantages of non-fouling properties of PAMAM dendrimers on the sensor chip detection surface design that also combines signal amplifications.

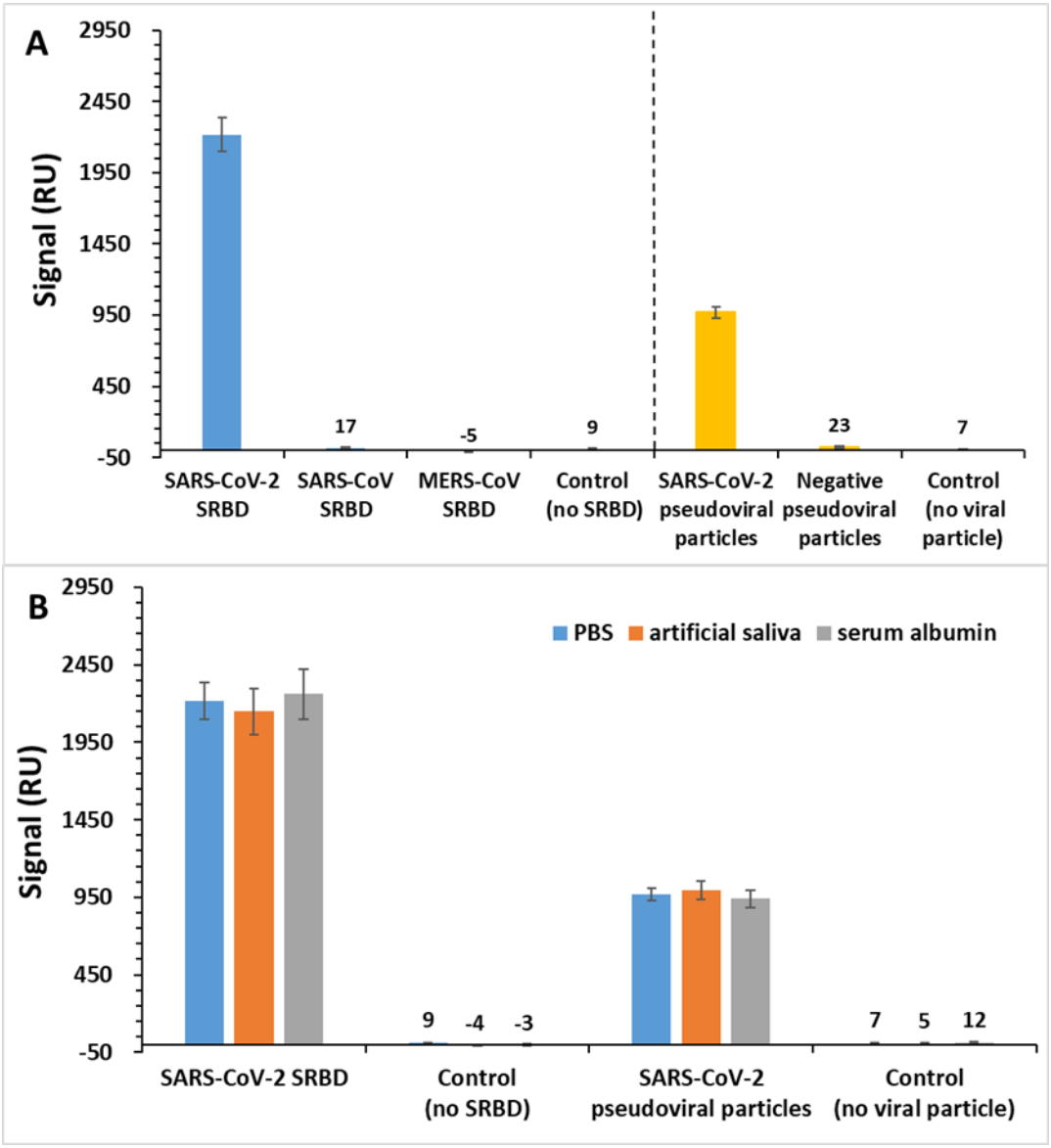

Figure 5.5. Detection specificity and influence of sample matrices. A) The detection specificity of the (G3.5+G4)-aptamer modified LSPR sensor chip; the targets are SARS-CoV-2 SRBD and SARS-CoV-2 pseudo viral particles, and nonspecific targets are SARS-CoV SRBD, MERS-CoV SRBD, and negative pseudo viral particles; all SRBD samples (blue bars) were tested at 12 nM in PBS (pH 7.4), and all pseudo viral particle samples (yellow bars) were tested at 10^5 vp/mL in PBS (pH 7.4). B) Influence of sample matrices on detection performances; the SARS-CoV-2 SRBD were tested at 12 nM, and the SARS-CoV-2 pseudo viral particles were tested at 10^5 vp/mL. Error bars are standard deviations, n=3.

To investigate device performance under conditions that mimic real world conditions, SARS-CoV-2 SRBD and SARS-CoV-2 pseudo viral particles were analyzed in PBS (pH 7.4), artificial saliva (1% v/v), and BSA (40 μg/mL) solutions [16], as biological matrices are known to influence detection performances [74, 75]. As shown in Figure 5.5B, in comparison with signals analyzed under the PBS (pH 7.4) condition, there was no significant ($p>0.05$) difference in signals when either SRBD or pseudo viral particle samples were analyzed in saliva and BSA matrices. This is likely due to the excellent non-fouling surface property of the detection surface, suggesting that the modified sensor chips were sufficiently robust to detect samples in complex biomatrices.

Table 5.1 compares the detection sensitivities achieved in the current report with those reported in recent literature. As can be seen that the LODs achieved in this study for both targets (*i.e.,* SRBD and pseudovirus) were lower than most reported results. It is interesting to note that although the LOD for SRBD detection in this study was higher than the LOD reported by Yang et al. [44] (*i.e.,* 21.9 pM *vs.* 0.83 pM), the LOD in this study for SARS-CoV-2 pseudovirus detections was lower (*i.e.,* 148 vp/mL *vs.* 391 vp/mL), likely suggesting the advantages of our RCA-AuNPs designs for multiple signal amplification. Moreover, our approach provided a universal modification strategy using the most widely used LSPR sensor chip (*i.e.,* surface with gold nanoislands), and therefore it can be readily employed in other sensor chip designs with higher plasmonic sensitivities, such as sensor surface with silver nanotriangle or nanocup structures [21, 44], in order to further improve their detection sensitivities. In addition, unlike other commercial LSPR sensor chips designed for binding kinetic studies that aim for medium surface ligand densities to quickly reach binding

equilibrium to avoid mass transfer effects [14], the current surface modification approach aims to improve the surface-ligand density for detection purposes. As a result, the current surface modification approach taken in this study could be a viable approach to expand potential applications for these commercial LSPR platforms.

Table 5.1. Sensor-based LSPR system for detection of SARS-CoV-2 spike proteins and viral particles.

Biosensor technique	Target	Immobilized ligands	Sample matrix	LOD	Ref.
Polymer receptor functionalized plasmonic optical fibers	Spike protein subunit 1	Molecularly imprinted polymer receptor	Protein in buffer	58 nM	[10]
Aptamer-PEG immobilized gold nanofilm-based optical fiber	SRBD	Aptamer against SRBD	Targets in diluted human serum	37 nM	[15]
Streptavidin-aptamer immobilized LSPR sensor chip	Spike protein subunit 1	Aptamer against SRBD	S1 protein diluted in buffer	0.26 nM	[16]
Antibody immobilized LSPR sensor chip with AuNPs signal amplification method	SARS-CoV-2 pseudovirus	Antibody against SRBD	Pseudovirus in buffer	370 vp/mL	[21]
ACE2 protein immobilized silver nanotriangle array	SRBD and Coronavirus	ACE2 protein	Buffer and Saliva	0.83 pM for SRBD, and 391 vp/mL for Coronavirus	[44]
Dendrimer-aptamer immobilized LSPR sensor chip	SRBD and SARS-CoV-2 pseudovirus	Aptamer against SRBD	Targets diluted in BSA and saliva	21.9 pM for SRBD, and 148 vp/mL for pseudovirus	This study

5.4 Conclusions

This study aims to improve the detection sensitivity of LSPR sensor chips to detect SARS-CoV-2 viral targets using a multi-pronged approach to both intensify detection signals and reduce background noises. To intensify the detection signals, three mechanisms have been employed: 1) surface immobilized PAMAM dendrimers as templates to introduce a large number of aptamers to the capturing sensor chip surfaces to enhance capturing probability and binding avidity for target recognition and capturing, 2) application of RCA to improve the target mass on the detection surface to intensify the detection signals, and 3) use of AuNPs to increase both target mass and plasmonic coupling effect to further intensify the detection signals. To reduce the background noises, surface modification with PAMAM dendrimers has been used to render the sensor chip surfaces non-fouling, thus significantly decreasing background noises. Our results demonstrated that the modified sensor chips had a LOD of 21.9 pM for SRBD detection, approximately 152 times lower than that of the traditional antibody-based sensor chips. Our results also showed that the application of the RCA-AuNPs as the second-layer signal amplification further intensified detection signals by approximately 10 times and that the overall enhanced LOD was 148 vp/mL when used to detect pseudo SARS-CoV-2 viral particles, a sensitivity sufficiently high to suggest a potential application in rapid detection of COVID-19 infections. In addition, it is perceivable that the multi-pronged approach discussed in the current study can be readily adapted for other point-of-care applications based on already well-established LSPR/SPR detection platforms.

References

1. Raziq, A., et al., Development of a portable MIP-based electrochemical sensor for detection of SARS-CoV-2 antigen. Biosensors and Bioelectronics, 2021. **178**: p. 113029.
2. Mavrikou, S., et al., Development of a portable, ultra-rapid and ultra-sensitive cell-based biosensor for the direct detection of the SARS-CoV-2 S1 spike protein antigen. Sensors, 2020. **20**(11): p. 3121.
3. Vadlamani, B.S., et al., Functionalized TiO2 nanotube-based electrochemical biosensor for rapid detection of SARS-CoV-2. Sensors, 2020. **20**(20): p. 5871.
4. Alafeef, M., et al., Rapid, ultrasensitive, and quantitative detection of SARS-CoV-2 using antisense oligonucleotides directed electrochemical biosensor chip. ACS nano, 2020. **14**(12): p. 17028-17045.
5. Lyu, A., et al., Automatic label-free immunoassay with high sensitivity for rapid detection of SARS-CoV-2 nucleocapsid protein based on chemiluminescent magnetic beads. Sensors and Actuators B: Chemical, 2021. **349**: p. 130739.
6. Huang, J.C., et al., Detection of severe acute respiratory syndrome (SARS) coronavirus nucleocapsid protein in human serum using a localized surface plasmon coupled fluorescence fiber-optic biosensor. Biosensors and Bioelectronics, 2009. **25**(2): p. 320-325.
7. Qiu, G., et al., Dual-functional plasmonic photothermal biosensors for highly accurate severe acute respiratory syndrome coronavirus 2 detection. ACS nano, 2020. **14**(5): p. 5268-5277.
8. Moitra, P., et al., Selective naked-eye detection of SARS-CoV-2 mediated by N gene targeted antisense oligonucleotide capped plasmonic nanoparticles. ACS nano, 2020. **14**(6): p. 7617-7627.
9. Baker, A.N., et al., The SARS-COV-2 spike protein binds sialic acids and enables rapid detection in a lateral flow point of care diagnostic device. ACS central science, 2020. **6**(11): p. 2046-2052.
10. Cennamo, N., et al., Proof of Concept for a Quick and Highly Sensitive On-Site Detection of SARS-CoV-2 by Plasmonic Optical Fibers and Molecularly Imprinted Polymers. Sensors, 2021. **21**(5): p. 1681.
11. Tian, B., et al., Homogeneous circle-to-circle amplification for real-time optomagnetic detection of SARS-CoV-2 RdRp coding sequence. Biosensors and Bioelectronics, 2020. **165**: p. 112356.

12. Petryayeva, E. and U.J. Krull, Localized surface plasmon resonance: Nanostructures, bioassays and biosensing—A review. Analytica chimica acta, 2011. **706**(1): p. 8-24.
13. Sepúlveda, B., et al., LSPR-based nanobiosensors. Nano today, 2009. **4**(3): p. 244-251.
14. Schasfoort, R.B., Introduction to surface plasmon resonance. 2017.
15. Cennamo, N., et al., SARS-CoV-2 spike protein detection through a plasmonic D-shaped plastic optical fiber aptasensor. Talanta, 2021. **233**: p. 122532.
16. Lewis, T., et al., Localized surface plasmon resonance aptasensor for selective detection of SARS-CoV-2 S1 protein. Analyst, 2021. **146**(23): p. 7207-7217.
17. Bong, J.-H., et al., Pig Sera-derived Anti-SARS-CoV-2 Antibodies in Surface Plasmon Resonance Biosensors. Biochip Journal, 2020. **14**(4): p. 358-368.
18. Funari, R., K.-Y. Chu, and A.Q. Shen, Detection of antibodies against SARS-CoV-2 spike protein by gold nanospikes in an opto-microfluidic chip. Biosensors and Bioelectronics, 2020. **169**: p. 112578.
19. Yeung, W.K., et al., Dispersion-enhancing surface treatment of AuNPs for a reduced probe loading and detection limit using t-SPR detection. Analyst, 2021.
20. Lew, T.T.S., et al., Epitope-Functionalized Gold Nanoparticles for Rapid and Selective Detection of SARS-CoV-2 IgG Antibodies. ACS nano, 2021.
21. Huang, L., et al., One-step rapid quantification of SARS-CoV-2 virus particles via low-cost nanoplasmonic sensors in generic microplate reader and point-of-care device. Biosensors and Bioelectronics, 2021. **171**: p. 112685.
22. Samson, R., G.R. Navale, and M.S. Dharne, Biosensors: frontiers in rapid detection of COVID-19. 3 Biotech, 2020. **10**(9): p. 385.
23. Kim, H.-M., et al., High-performance biosensor using a sandwich assay via antibody-conjugated gold nanoparticles and fiber-optic localized surface plasmon resonance. Analytica Chimica Acta, 2022. **1213**: p. 339960.
24. Miti, A., et al., A miRNA biosensor based on localized surface plasmon resonance enhanced by surface-bound hybridization chain reaction. Biosensors and Bioelectronics, 2020. **167**: p. 112465.
25. Mahmoudpour, M., et al., Rational design of smart nano-platforms based on antifouling-nanomaterials toward multifunctional bioanalysis. Advances in Colloid and Interface Science, 2022: p. 102637.
26. Hao, X., et al., Aptamer surface functionalization of microfluidic devices using dendrimers as multi-handled templates and its application in sensitive

detections of foodborne pathogenic bacteria. Analytica Chimica Acta, 2019. **1056**: p. 96-107.

27. Hao, X., et al., Surface Modification of Poly (styrene) 96-well Plates Using Aptamers via a Dendrimer-templated Strategy to Enhance ELISA Performances. Colloids and Surfaces B: Biointerfaces, 2022: p. 113003.
28. Hao, X., et al., Surface Modification of Glass-bottom 96-microwell Plates to Enhance ELISA Performances. Applied Surface Science, 2022: p. 155603.
29. Wang, Z., et al., Multivalent Aptamer Approach: Designs, Strategies, and Applications. Micromachines, 2022. **13**(3): p. 436.
30. Jiang, Y., S. Zou, and X. Cao, A simple dendrimer-aptamer based microfluidic platform for *E.coli* O157: H7 detection and signal intensification by rolling circle amplification. Sensors and Actuators B: Chemical, 2017. **251**: p. 976-984.
31. Qin, Y., et al., Developing a non-fouling hybrid microfluidic device for applications in circulating tumour cell detections. Colloids and Surfaces B: Biointerfaces, 2017. **151**: p. 39-46.
32. Jiang, Y., et al., Developing a dual-RCA microfluidic platform for sensitive *E.coli* O157: H7 whole-cell detections. Analytica Chimica Acta, 2020. **1127**: p. 79-88.
33. He, P., et al., Ultrasensitive detection of thrombin using surface plasmon resonance and quartz crystal microbalance sensors by aptamer-based rolling circle amplification and nanoparticle signal enhancement. Chemical Communications, 2014. **50**(12): p. 1481-1484.
34. Schmitt, J., et al., Preparation and optical properties of colloidal gold monolayers. Langmuir, 1999. **15**(9): p. 3256-3266.
35. Lu, M., et al., Gold nanoparticle-enhanced detection of DNA hybridization by a block copolymer-templating fiber-optic localized surface plasmon resonance biosensor. Nanomaterials, 2021. **11**(3): p. 616.
36. Omura, N., I. Uechi, and S. Yamada, Comparison of plasmonic sensing between polymer-and silica-coated gold nanorods. Analytical Sciences, 2009. **25**(2): p. 255-259.
37. Oo, M.K.K., et al., Rapid, sensitive DNT vapor detection with UV-assisted photo-chemically synthesized gold nanoparticle SERS substrates. Analyst, 2011. **136**(13): p. 2811-2817.
38. Xie, L., X. Yan, and Y. Du, An aptamer based wall-less LSPR array chip for label-free and high throughput detection of biomolecules. Biosensors and Bioelectronics, 2014. **53**: p. 58-64.

39. Guo, L. and D.-H. Kim, LSPR biomolecular assay with high sensitivity induced by aptamer–antigen–antibody sandwich complex. Biosensors and Bioelectronics, 2012. **31**(1): p. 567-570.
40. Nguyen, V.T., et al., Highly sensitive sandwich-type SPR based detection of whole H5Nx viruses using a pair of aptamers. Biosens Bioelectron, 2016. **86**: p. 293-300.
41. Ashiba, H., et al., Detection of norovirus virus-like particles using a surface plasmon resonance-assisted fluoroimmunosensor optimized for quantum dot fluorescent labels. Biosensors and Bioelectronics, 2017. **93**: p. 260-266.
42. Yakes, B.J., et al., Surface plasmon resonance biosensor for detection of feline calicivirus, a surrogate for norovirus. International Journal of Food Microbiology, 2013. **162**(2): p. 152-158.
43. Park, J.-W., et al., An ultra-sensitive detection of a whole virus using dual aptamers developed by immobilization-free screening. Biosensors and Bioelectronics, 2014. **51**: p. 324-329.
44. Yang, Y., et al., Silver nanotriangle array based LSPR sensor for rapid coronavirus detection. Sensors and Actuators B: Chemical, 2022. **359**: p. 131604.
45. Song, Y., et al., Discovery of Aptamers Targeting Receptor-Binding Domain of the SARS-CoV-2 Spike Glycoprotein. 2020.
46. Frens, G., Controlled nucleation for the regulation of the particle size in monodisperse gold suspensions. Nature physical science, 1973. **241**(105): p. 20-22.
47. Hurst, S.J., A.K.R. Lytton-Jean, and C.A. Mirkin, Maximizing DNA loading on a range of gold nanoparticle sizes. Analytical chemistry, 2006. **78**(24): p. 8313-8318.
48. Fischer, M.J., Amine coupling through EDC/NHS: a practical approach, in Surface plasmon resonance. 2010, Springer. p. 55-73.
49. Kalkhof, S. and A. Sinz, Chances and pitfalls of chemical cross-linking with amine-reactive N-hydroxysuccinimide esters. Analytical and bioanalytical chemistry, 2008. **392**(1): p. 305-312.
50. Staros, J.V., N-hydroxysulfosuccinimide active esters: bis (N-hydroxysulfosuccinimide) esters of two dicarboxylic acids are hydrophilic, membrane-impermeant, protein cross-linkers. Biochemistry, 1982. **21**(17): p. 3950-3955.

51. Zhao, Q., et al., A reusable localized surface plasmon resonance biosensor for quantitative detection of serum squamous cell carcinoma antigen in cervical cancer patients based on silver nanoparticles array. International Journal of Nanomedicine, 2014. **9**: p. 1097.
52. Antiochia, R., et al., Nanotechnology-based surface plasmon resonance affinity biosensors for in vitro diagnostics. International journal of analytical chemistry, 2016. **2016**.
53. Engvall, E., [28] Enzyme immunoassay ELISA and EMIT, in Methods in Enzymology. 1980, Academic Press. p. 419-439.
54. Lequin, R.M., Enzyme Immunoassay (EIA)/Enzyme-Linked Immunosorbent Assay (ELISA). Clinical Chemistry, 2005. **51**(12): p. 2415.
55. Rampazzi, S., et al., A localized surface plasmon resonance-based portable instrument for quick on-site biomolecular detection. IEEE Transactions on Instrumentation and Measurement, 2015. **65**(2): p. 317-327.
56. Kimura, M., et al., Distinct mutations in importin-β family nucleocytoplasmic transport receptors transportin-SR and importin-13 affect specific cargo binding. Scientific reports, 2021. **11**(1): p. 1-17.
57. Sheehan, P.E. and L.J. Whitman, Detection limits for nanoscale biosensors. Nano letters, 2005. **5**(4): p. 803-807.
58. Weber, S.G. and J.T. Long, Detection limits and selectivity in electrochemical detectors. Analytical chemistry, 1988. **60**(15): p. 903A-913A.
59. Soleymani, L. and F. Li, Mechanistic Challenges and Advantages of Biosensor Miniaturization into the Nanoscale. ACS Sensors, 2017. **2**(4): p. 458-467.
60. Ingle Jr, J., Sensitivity and limit of detection in quantitative spectrometric methods. Journal of Chemical Education, 1974. **51**(2): p. 100.
61. Norrod, K.L., et al., Quantitative comparison of five SERS substrates: sensitivity and limit of detection. Applied spectroscopy, 1997. **51**(7): p. 994-1001.
62. Watson, J.D. and F.H. Crick, Molecular structure of nucleic acids: a structure for deoxyribose nucleic acid. Nature, 1953. **171**(4356): p. 737-738.
63. Reth, M., Matching cellular dimensions with molecular sizes. Nature immunology, 2013. **14**(8): p. 765-767.
64. Unser, S., et al., Localized surface plasmon resonance biosensing: current challenges and approaches. Sensors, 2015. **15**(7): p. 15684-15716.

65. De Feijter, J., d.J. Benjamins, and F. Veer, Ellipsometry as a tool to study the adsorption behavior of synthetic and biopolymers at the air–water interface. Biopolymers: Original Research on Biomolecules, 1978. **17**(7): p. 1759-1772.
66. Hand, D.B., The refractivity of protein solutions. Journal of Biological Chemistry, 1935. **108**(3): p. 703-707.
67. Yao, H., et al., Molecular architecture of the SARS-CoV-2 virus. Cell, 2020. **183**(3): p. 730-738. e13.
68. Mori, Y., et al., Detection of loop-mediated isothermal amplification reaction by turbidity derived from magnesium pyrophosphate formation. Biochem Biophys Res Commun, 2001. **289**(1): p. 150-4.
69. Yan, C., et al., Rapid and visual detection of 2019 novel coronavirus (SARS-CoV-2) by a reverse transcription loop-mediated isothermal amplification assay. Clinical Microbiology and Infection, 2020. **26**(6): p. 773-779.
70. Lu, R., et al., Development of a novel reverse transcription loop-mediated isothermal amplification method for rapid detection of SARS-CoV-2. Virologica Sinica, 2020. **35**(3): p. 344-347.
71. Zhang, Y., et al., Rapid molecular detection of SARS-CoV-2 (COVID-19) virus RNA using colorimetric LAMP. MedRxiv, 2020.
72. Broughton, J.P., et al., CRISPR–Cas12-based detection of SARS-CoV-2. Nature biotechnology, 2020. **38**(7): p. 870-874.
73. Metsky, H.C., et al., CRISPR-based surveillance for COVID-19 using genomically-comprehensive machine learning design. BioRxiv, 2020.
74. Tombelli, S., M. Minunni, and M. Mascini, Analytical applications of aptamers. Biosensors and Bioelectronics, 2005. **20**(12): p. 2424-2434.
75. Masson, J.-F., Consideration of Sample Matrix Effects and “Biological” Noise in Optimizing the Limit of Detection of Biosensors. ACS Sensors, 2020. **5**(11): p. 3290-3292.

Chapter 6

Developing Membranes with Dual-RCA Modification for High-throughput and Sensitive Detection of *E.coli* O157:H7 Whole Cells in Foods

Abstract

We describe a membrane with dual rolling circle amplification (*i.e.*, dual-RCA) surface modification as a simple and robust platform for sensitive and high-throughput detection of *E.coli* O157:H7 whole cells in food samples. To this end, nylon membranes are surface modified by poly(amidoamine) (PAMAM) dendrimers that are further functionalized with multi-branch capturing RCA (cRCA) networks. The cRCA networks are composed of repeating aptamers that can specifically recognize and capture the *E.coli* O157:H7 whole cells; subsequently, the captured cells are conjugated with signaling RCA (sRCA) to amplify fluorescent detection signals. Our results demonstrate that the cRCA networks significantly enhanced the capturing efficiency of *E.coli* O157:H7 cells compared to unit aptamers and enabled the membranes to present excellent detection performances working under high throughputs and different food matrices. Moreover, the surface modification using dendrimers decreased the non-specific adsorption noises by approximately 96 times, and the sRCA increased the fluorescent detection signals by approximately 27 times. Our detection results showed that the membranes demonstrated excellent performances in detecting spiked *E.coli* O157:H7 in milk and orange juice samples, showing capturing efficiencies of 94%±8% and 96%±6%, and sample throughputs of 3.8 and 4.8 mL/s, respectively. The detection limit was 10 cells/250 mL for these two food samples.

6.1 Introduction

Food poisoning caused by foodborne pathogens has become a leading cause of intestinal infections and diarrheal diseases [1]. According to the World Health Organization, there are over 300 million foodborne cases caused by foodborne pathogens each year, resulting in more than six hundred thousand deaths annually worldwide [1]. As a result, rapid and sensitive detections of foodborne pathogens are urgently needed, as many foodborne bacteria can pose serious health risks even at low doses [2]. Plate culture methods are currently the "gold standard" for bacteria identification and quantification; however, they generally require multiple laborious steps and therefore take up to several days to get test results, leaving much to be desired [3, 4]. Alternative techniques such as enzyme-linked immunosorbent assay (ELISA) and polymerase chain reaction (PCR) have been explored to detect foodborne pathogens because they can provide fast sample-to-result turn-around. Unfortunately, the ELISA methods are known to be less sensitive -- with reported limit of detections (LODs) ranging between 10^3 and 10^4 cells/mL [5, 6] -- to be suitable for detections of foodborne pathogenic bacteria, particularly of those with low infectious does, such as *E.coli* O157:H7, Salmonella and Listeria [1, 2]. While much more sensitive than the ELISA methods, the PCR methods suffer from complex sample pre-treatment steps such as bacteria enrichments and DNA extractions, which significantly increase the overall detection time and thus limiting their wide application as a robustly viable foodborne bacteria detection method [7-9].

Recently microfluidic devices have emerged as a promising platform for rapid and sensitive detections of bacteria in food samples, with the lowest reported LOD around

80 cells/mL [6, 10, 11]. However, when the target bacteria concentration in the sample is low, large sample units (normally 25 mL (g) of a sample in 250 mL buffer) would be needed to accurately analyze samples with trace amounts of pathogenic organisms of concern, regardless of the detection sensitivity [12-14]. Unfortunately, it is impractical to analyze such large units of samples using microfluidic platforms due to the low sample throughputs (*i.e.*, 0.1−1 mL/h) of most microfluidic devices, as higher flow rates increase surface shear forces that can reduce target capturing efficiency [15, 16]. To improve sample throughputs, filtration-based detection techniques have been developed to both concentrate and detect target bacteria using membranes, and they have shown much higher detection throughputs (1-30 mL/min) and lower LODs (<10 cells/mL) [14, 17-19]. However, a close survey of the literature suggests that these membranes have been commonly and successfully used to detect target bacteria in clear water samples but rarely in more complex food samples. This is most likely because these membranes have been developed with smaller pore sizes (0.2-0.4 μm) than the size of bacteria (~ 1 μm) to be able to retain target bacteria on the membranes; however, this design allows the membranes to be quickly blocked by other debris in complex food samples, often resulting in detection failure.

Poly(amidoamine) (PAMAM) dendrimers are highly branched polymers that present multiple functional groups on their outer spherical surfaces. Because of these unique features, PAMAM dendrimers have been increasingly used to be immobilized to detection surfaces as templates to provide multiple binding sites to further conjugate multiple capturing ligands to improve the target-capturing probabilities [20, 21]. Moreover, the surface modification of the PAMAM dendrimers is known to render the

resulting detection surface nonfouling to significantly reduce background noises, improve the detection signal-to-noise ratio (S/N), and ultimately increase detection sensitivity [22, 23].

Rolling circle amplification (RCA) is a widely used amplification technique that can generate long single-stranded DNA/RNA chains containing hundreds or thousands of tandem repeating units based on a circular template [24, 25]. The RCA has been employed in detection systems to intensify detection signals by conjugating large amounts of signaling probes with the RCA products (*i.e.*, signaling RCA or sRCA) [26, 27]. Moreover, *in situ* RCA surface modifications have also been developed to produce tandem repeating target-specific aptamers on the detection surfaces for improving target capturing efficiencies (*i.e.*, capturing RCA or cRCA) [28, 29]. Recently, a dual-RCA microfluidic platform has been developed by employing both cRCA and sRCA for sensitive *E.coli* O157:H7 whole-cell detections [10]. The study shows that the dual-RCA detection system has significantly improved the fluorescent detection signal by approximately 250 folds, and the LOD has been improved to 80 cells/mL; the study also exhibits that the microfluidic devices with dual-RCA amplification strategies result in enhanced sample throughputs, reduced detection background noises, and improved target capturing efficiencies.

In the current study, we take advantage of the dual-RCA strategy to develop a membrane detection system to increase sample throughput for detecting *E.coli* O157:H7 cells in food samples. Specifically, unlike other detection membranes with pore sizes smaller than 0.4 μm [14, 17-19, 30-32], nylon membranes with larger pore

sizes are selected to allow the food matrix to pass through. The membranes are surface modified with dendrimers followed by *in situ* cRCA reactions to produce long single-stranded DNA (ssDNA) networks composed of tandem repeating aptamers that mesh the open pores of the membranes. The meshed networks of aptamers are designed to specifically capture the *E.coli* O157:H7 cells while allowing other food matrix debris of different sizes to pass through the open pores of the membranes. Subsequently, the captured *E.coli* O157:H7 cells are conjugated with sRCA products with multiple repeating hybridization sites to bind with fluorescently labeled ssDNA signaling probes to achieve detection signal intensification. Our design offers the following advantages: 1) the cRCA is designed to produce repeating aptamer networks to mesh the open pores of the detection membrane to enhance target capturing; 2) the sRCA is designed to amplify detection signals to achieve higher detection sensitivity; 3) the immobilization of dendrimers on the detection membrane both promotes the formation of high-density branches of cRCA products meshing the open pores of the membrane and reduces background noises, and 4) the application of membranes with a large pore size increases the sample throughputs. The results show that in comparison with other reported detection membranes and microfluidic systems for bacteria detections [6, 9-11, 14, 17-19, 30-34], the newly developed detection membranes show significantly decreased LOD (10 cells/250 mL) and much improved sample throughputs (3.8 and 4.8 mL/s) in detecting spiked *E.coli* O157:H7 in milk and orange juice samples. Overall, our data suggest that the current detection system is an excellent candidate for rapid and high-throughput detection of a trace amount of pathogenic bacteria in food samples.

6.2 Experimental

6.2.1 General Approach of Surface Modification and Target Detection

As shown in Figure 6.1, nylon membranes are initially treated with oxygen plasma to introduce -OH functional groups on the surface [35-37], followed by surface amination with 3-aminopropyl-triethoxysilane (APTES) [35]. Subsequently, the aminated surfaces are immobilized with carboxylated generation 6.5 PAMAM dendrimers (*i.e.*, G6.5-COOH) to provide multiple binding sites to conjugate multiple-branch ligation products of cRCA. After this step, the *in situ* cRCA reaction is carried out to produce extended ssDNA networks composed of repeating tandem aptamers on the detecting surfaces for specific capturing of *E.coli* O157:H7. To detect *E.coli* O157:H7 in food samples, samples are filtered using the G6.5-cRCA modified membranes. Finally, the surface-captured *E.coli* O157:H7 cells are conjugated with sRCA products that are subsequently hybridized with cy5-ssDNA signaling probes to produce fluorescent detection signals.

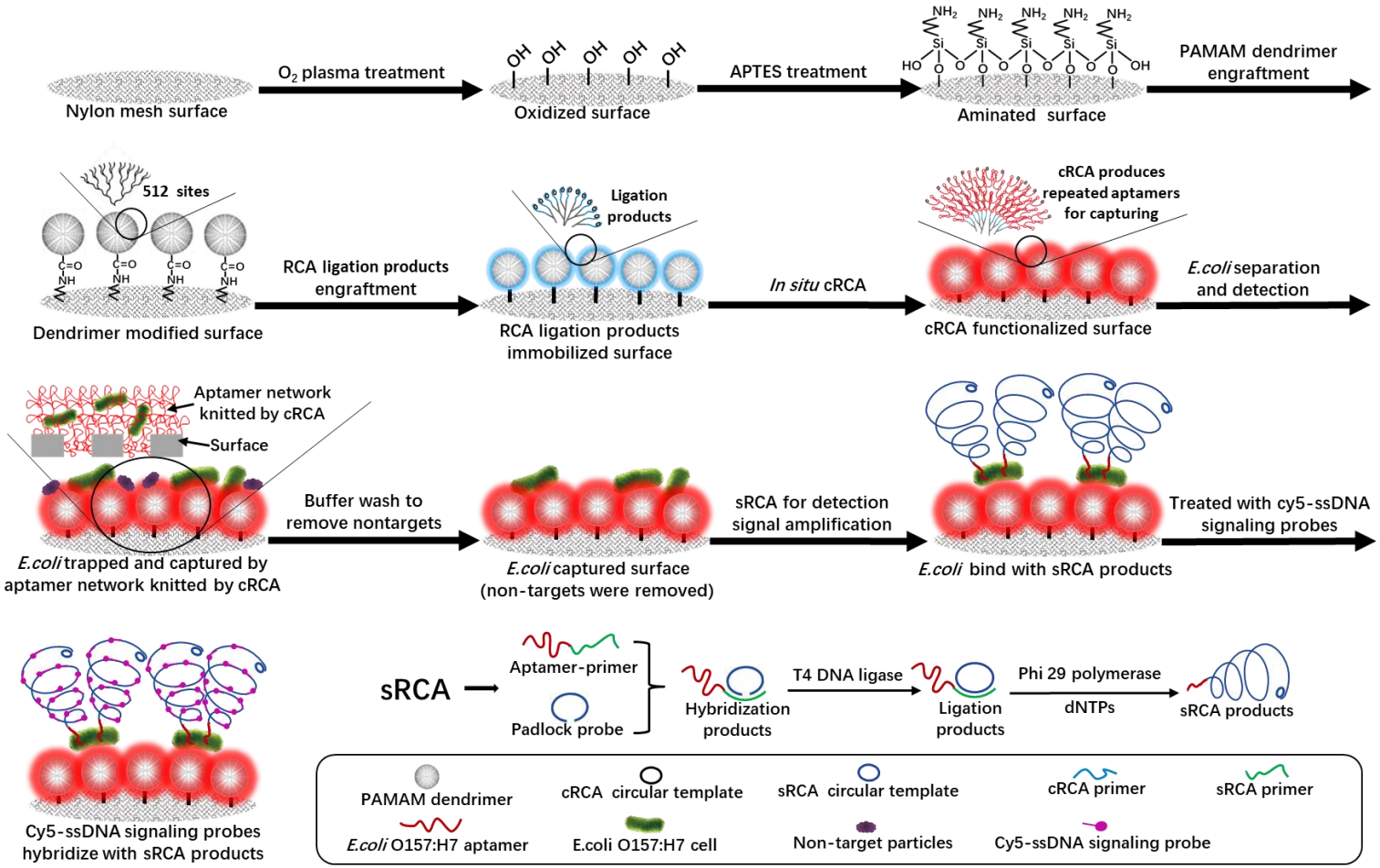

Figure 6.1. Schematic illustration of the overall approach for surface modification of nylon membrane, *E.coli* O157:H7 detection, and signal amplification.

6.2.2. Materials

Carboxylated poly(amidoamine) dendrimer generation 6.5 (G6.5-COOH), phosphate-buffered saline (PBS) tablets, n-hydroxysuccinimide (NHS), and (3-aminopropyl) triethoxysilane (APTES) were obtained from Sigma-Aldrich (Oakville, ON). 1-(3-dimethylaminopropyl)-3-ethylcarbodiimide (EDC) and 2-(N-morpholino) ethanesulfonic acid (MES) were purchased from Alfa Aesar (Ward Hill, MA). Phi29 DNA polymerase, 10×phi29 polymerase buffer (containing 330 mM Tris-acetate (pH 7.9), 100 mM magnesium acetate, 660 mM potassium acetate, 1% Tween 20, 10 mM dithiothreitol), T4 DNA ligase, 10×T4 ligation buffer (containing 400 mM Tris-HCl, 100 mM $MgCl_2$, 100 mM DTT, 5 mM ATP, pH 7.8), and deoxynucleotide triphosphate (dNTP) solution mix were purchased from Fisher Scientific (Ottawa, ON). Nylon mesh membranes (d=25 mm with meshing opening of 1 and 5 µm, respectively) were purchased from ELKO Filtering (Tamarac, FL), and nylon membrane filters (d=25 mm with a pore size of 0.45 µm) were purchased from Sigma-Aldrich (Oakville, ON). Heat-killed *E.coli* O157:H7 cells were a generous gift from the Canadian Food Inspection Agency (Ottawa, ON). Food samples, including homogenized milk (2% fat, fine-filtered) and orange juice, were purchased from a local supermarket. Aptamers were custom synthesized by Integrated DNA Technologies (Coralville, IA). The aptamer sequences used for this study are listed in Table D1 (Appendix D)

6.2.3 Nylon Membrane Surface Modification

6.2.3.1 Surface amination

To introduce amino functional groups to the surfaces of the nylon membranes, a well-established method was followed by treating the nylon membranes with oxygen plasma and 2 vol % APTES in anhydrous ethyl alcohol [35].

6.2.3.2 PAMAM dendrimer engraftment

To immobilize G6.5-COOH onto the aminated nylon membranes obtained from the previous step, the aminated membranes were reacted with a G6.5-COOH conjugation

solution containing 1 μM G6.5-COOH, 0.1 M NHS and 0.1 M EDC in 0.1 M MES solution (pH 6.0) at room temperature. The reaction was allowed to be carried out for 2 h, after which the membranes were extensively washed with and stored in PBS (pH 8.0) for future use [38].

6.2.3.3 *In situ* cRCA reaction on the G6.5-COOH modified nylon membranes

To carry out *in situ* cRCA reactions on the surfaces of membranes with G6.5-COOH modification, our previously published methods were employed with minor modifications [10]. Specifically, 5 μM cRCA ligation products were prepared using T4 DNA ligase to ligate hybridization cRCA primer (S_2, Table D1, Appendix D) and cRCA padlock probe (S_3, Table D1, Appendix D). Note: the resulting cRCA ligation products were capped with -NH_2 functional groups at 5' end of primers, allowing further conjugation with surface-immobilized G6.5-COOH molecules. Subsequently, to immobilize the cRCA ligation products on the nylon membranes via G6.5-COOH templates, the G6.5-COOH modified nylon membranes were treated using an activation solution containing 0.1 M NHS and 0.1 M EDC in 0.1M MES buffer (pH=6.0) for 15 min at room temperature, after which they were rinsed with dd water, then quickly incubated into 2 μM cRCA ligation products in PBS (pH 7.4). This reaction was allowed to carry out for 1 h, after which the resulting membranes were rinsed with dd water and dried under a nitrogen stream. After this step, to carry out *in situ* cRCA reactions, the ligation products modified membranes were incubated into a cRCA reaction mixture containing 1 × phi29 buffer, 0.4 mM dNTPs, and 0.1 U/μL phi29 polymerase, which was allowed to react at 37 ℃ for a pre-determined time (*i.e.*, 1, 2, 4 and 8 h). To stop the reaction, the resulting membranes were incubated at 65 ℃ for 10 min, after which they were rinsed with dd water and dried under a nitrogen stream.

6.2.4 sRCA Reaction

To synthesize sRCA products, 5 μM sRCA ligation products were prepared using T4 DNA ligase to ligate hybridization sRCA aptamer-primer (S_5, Table D1, Appendix D)

and sRCA padlock probe (S_6, Table D1, Appendix D) [10]. Subsequently, an sRCA reaction was carried out using a reaction mixture containing 1 μM ligation products, 1 × phi29 reaction buffer, 0.4 mM dNTPs, and 0.1 U/μL phi29 polymerase reacted at 37 °C for 1 h. To stop the reaction, the reaction mixture was heated at 65 °C for 10 min.

6.2.5 Detection of *E.coli* O157:H7 Cells

The *E.coli* O157:H7 detection was started with a capturing procedure using the G6.5-cRCA modified nylon membranes to capture the *E.coli* O157:H7, followed by a signal amplification procedure using sRCA and cy5-ssDNA signaling probes to generate fluorescent detection signals on the top of the captured *E.coli* O157:H7 cells. In a typical capturing procedure, a G6.5-cRCA modified membrane was placed in a membrane holder (Sartorius Stedim Biotech, Göttingen, Germany) connected with a vacuum system (Model: DOA-P704-AA, GAST Manufacturing, MI). Subsequently, a 250 mL sample of interest containing *E.coli* O157:H7 cells was driven through the membrane using a vacuum at -0.8 bar, after which another 250 mL PBS (pH 7.4) was used to rinse the membrane. The resulting membrane was removed from the membrane holder and placed in PBS (pH 7.4) for further signal amplification.

Subsequently, signal amplifications for the surface-captured *E.coli* O157:H7 cells were carried out. Specifically, sRCA products were employed to treat the *E.coli* O157:H7 captured membrane at room temperature for 30 min to conjugate the captured *E.coli* O157:H7 cells with sRCA products. Subsequently, the resulting membrane was rinsed with dd water to remove unreacted sRCA products, after which it was treated with 1 μM cy5-ssDNA signaling probes (*i.e.,* S_7, Table D1, Appendix D) at room temperature for 30 min to label the captured *E.coli* O157:H7 cells. Finally, the resulting membrane was carefully rinsed with dd water, and fluorescent images of *E.coli* O157:H7 cells on the whole surface area were imaged using an Axio Observer inverted fluorescence microscope (Carl Zeiss Microscopy, ON, Canada) equipped with an Axiocam 705 mono camera (Carl Zeiss Microscopy, ON, Canada). To analyze the detection results,

fluorescence intensities of the images were analyzed by ZEN 3.4 (blue edition) software (ZEISS, Oberkochen, Germany), and the numbers of captured *E.coli* O157:H7 cells were counted using ImageJ (V 1.53) software.

6.2.6 Statistical Analysis

The statistical analysis was performed using Microsoft Excel software (version 2303). To ensure the reliability and robustness of the results, all experiments were carried out in triplicate (otherwise indicated in figure captions), both within the same day and across different days, and the mean values with their corresponding standard deviations were calculated and reported. The Student's t-test, two-tailed, was employed to assess the statistical significance of the differences between the groups, with a p-value of less than 0.05 considered statistically significant.

6.3 Results and Discussions

6.3.1 Characterization and Optimization

Detailed results of characterizations and optimizations can be found in D2 (Appendix D).

6.3.2 Detection Performance Influential Factors

6.3.2.1 cRCA reaction time and membrane pore size

To study the influence of cRCA time and membrane pore size on the target capturing performance and detection flow rate, membranes with different surface modifications (*i.e.,* G6.5-unit aptamer and G6.5-cRCA with different reaction times) were employed to detect *E.coli* O157:H7 samples spiked in PBS (pH 7.4), after which sRCA signal amplification was applied. *E.coli* O157:H7 detection signals (*i.e.,* fluorescence intensities) were compared to study the capturing performance. As shown in Figure 6.2A, the membranes with a pore size of 0.45 μm showed the best performance in capturing the *E.coli* O157:H7 cells, as they presented the highest and plateaued fluorescence intensity regardless of their modification method (*i.e.,* with unit aptamer

or cRCA). This was most likely because their pore size (0.45 μm) was smaller than the size of *E.coli* O157:H7 cells (*i.e.,* 1.0-2.0 μm long with a radius of about 0.5 μm) [39], so that the majority of *E.coli* O157:H7 cells can be retained on the membranes and be captured by the surface aptamers (*i.e.,* either unit aptamers or repeating aptamers) [40]. Moreover, membranes with a pore size of 1 μm showed an increasing trend of fluorescence intensity with the increase of cRCA time, indicating an improved target-capturing performance with longer cRCA time, which was most likely because more repeating aptamer amounts were produced with longer cRCA reaction time, thereby providing higher probability and stronger binding avidity for target capturing [6, 41]. The fluorescence intensities were plateaued at 4 h cRCA, similar to the signal values observed on 0.45 μm membranes (around 980 a.u.), indicating that the 4h cRCA modified membranes (1 μm) had the same excellent capturing performance as performed on 0.45 μm membranes. In addition, in comparison with 1 μm membranes, 5 μm membranes at any given surface conditions always showed lower fluorescence intensities, most likely because their pore size is much larger than the size of *E.coli* O157:H7 cells, which leads to more number of *E.coli* O157:H7 cells passing through the membranes without being captured, indicating a lower the capturing performance. It should be noted that the fluorescence intensities of cRCA-modified membranes (either 5 μm or 1 μm) were always higher than those of unit aptamer modified membranes, indicating that cRCA-modified membranes have better target-capturing performances due to more produced surface repeating aptamers. It should also be noted that the ligation product modified membranes (*i.e.,* 0 h cRCA) showed little change in fluorescence intensities compared to detection signals of blank samples (the dotted line), as no aptamer was on the detection surface.

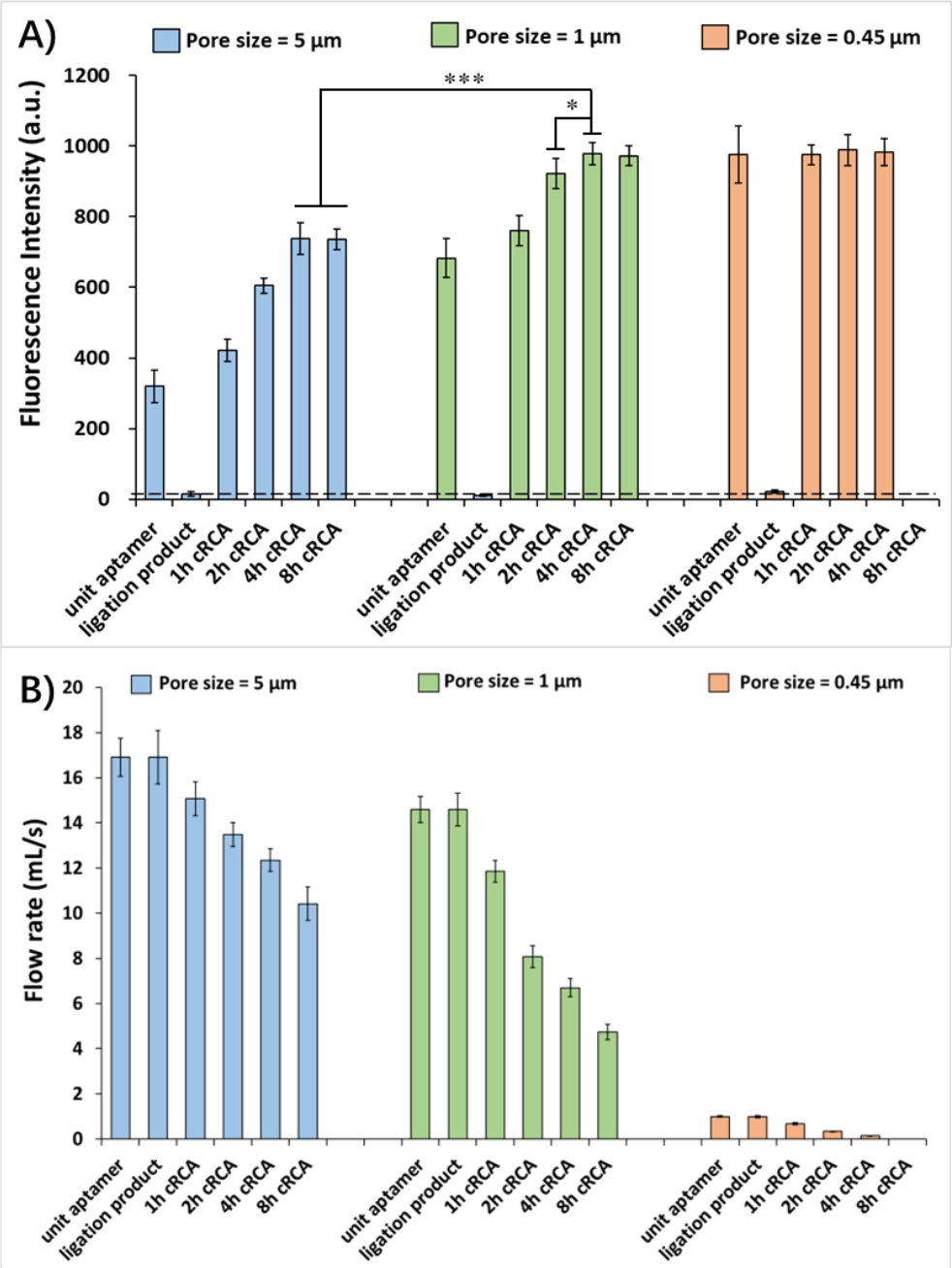

Figure 6.2. The effect of cRCA time and membrane pore size on the detection performances (*i.e.*, capturing performance and detection flow rate) of membranes with different surface modifications (*i.e.*, G6.5-unit aptamer and G6.5-cRCA with different reaction times). A) Fluorescence intensities (*i.e.*, *E.coli* O157:H7 detection signals) of different modified membranes; the dotted line indicates the detection signals of blank samples. B) Sample processing flow rates of membranes with different surface modifications. Note: *E.coli* O157:H7 (250 mL $\times 10^3$ cell/mL) spiked PBS (pH 7.4) was used for each test. Error bars indicate standard deviations, n=3; Student's t-test, p values (*<0.05, ***<0.001); the missing data of 0.45 µm membranes at 8h cRCA were due to the blockage of the membranes.

The flow rates of the samples passing through the membranes were also compared. As shown in Figure 6.2B, membranes with a pore size of 5 μm always showed a higher sample flow rate than membranes with a pore size of either 1 or 0.45 μm under any given surface conditions, suggesting a more rapid sample processing rate. Moreover, regardless of the pore size of membranes, the flow rate showed a decreasing trend with the increase of cRCA time, most likely due to the formation of multivalent aptamer networks on the membranes [29]. Specifically, with the increase of cRCA time, many long ssDNAs composed of tandem repeating aptamers were produced to form ssDNA networks that mesh the open pores of membranes, thereby decreasing the flow rate. It should be noted that samples could not pass through the 0.45 μm membranes with 8h cRCA modification, showing no flow rates, thus no detection signals in Figure 6.2A, which was most likely due to blockage of the open pores by the repeating aptamer networks. Since fluorescence intensities plateaued at 4 h cRCA for membranes with any pore size, 4 h cRCA surface modification was used for the following studies unless otherwise indicated.

To further confirm that the cRCA modification formed the repeating-aptamer networks meshing the open pores of membranes, fluorescence images of *E.coli* O157:H7 cells captured on membranes were studied, and cRCA molecular size was analyzed via dynamic light scattering (DLS) using a Zetasizer Nano-ZS (Malvern Panalytical Ltd, Malvern, UK). As shown in Figure 6.3A, it was evident that some *E.coli* O157:H7 cells were captured in the middle area of the open pores (see the white circles), indicating the formation of repeating-aptamer networks that mesh the open pores of membranes. Moreover, as shown in Figure 6.3B, in comparison with molecular sizes of G6.5 peaked at 9.9 nm and G6.5-ligation product at 13.5 nm, the G6.5-cRCA complex showed a substantially increased molecular size peaked at 1078.0 nm, indicating that the cRCA reactions could produce large-sized molecules (*i.e.*, long chains of repeating aptamers) on the detection surfaces, and therefore more likely to mesh the open pores of membranes. Note that the molecular sizes were tested using free molecules under

solution conditions, so the size of G6.5-cRCA on membranes is estimated to be roughly 30-80% of the currently tested value (*i.e.*, 323.4-862.4 nm). In addition, Zhao et al. have also confirmed that the cRCA reactions could produce 3D multivalent aptamer networks on the detection surface to improve detection performances [29].

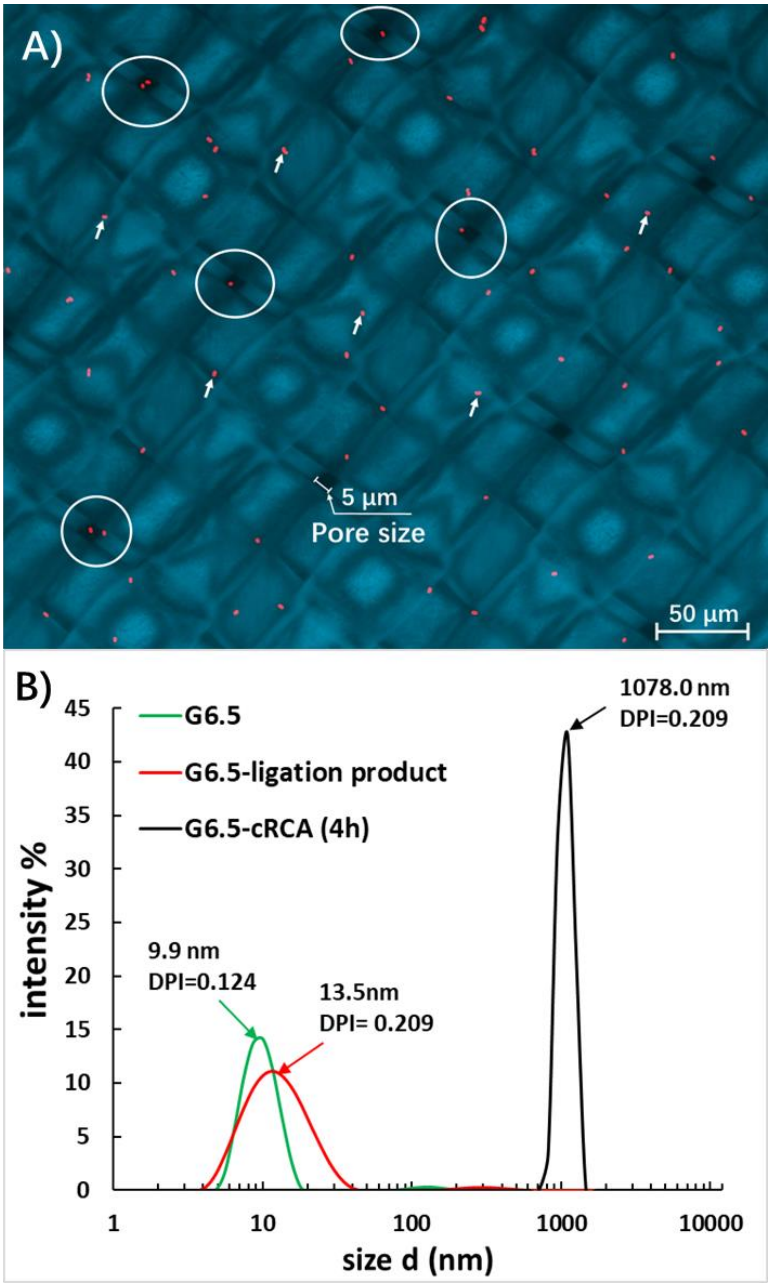

Figure 6.3. The *E.coli* O157:H7 capturing image and molecular size analysis of different molecules. A) An overlay fluorescence image of *E.coli* O157:H7 cells captured on a membrane (5 µm); the membrane was pseudo-colored in blue, and *E.coli* O157:H7 cells were pseudo-colored in red; white circles and arrows indicate that *E.coli* O157:H7 cells were captured in the middle of pores and on the surface, respectively. B) Molecular size analysis of different molecules in PBS (pH 7.4) using DLS.

6.3.2.2 G6.5 surface modification

To further study the effect of G6.5 surface modification on the capturing performance and detection flow rate, membranes with G6.5 surface modification (*i.e.*, APTES-G6.5-unit aptamer and APTES-G6.5-cRCA) and without (*i.e.*, APTES-unit aptamer and APTES-cRCA (both with BSA surface blocking)) were employed to detect *E.coli* O157:H7 samples prepared in PBS (pH 7.4), after which sRCA signal amplification was applied. *E.coli* O157:H7 detection signals (*i.e.*, fluorescence intensities) and flow rates were compared. As shown in Figure 6.4A, the APTES-G6.5-cRCA modified membranes showed significant ($p<0.05$) higher fluorescence intensities than the APTES-cRCA modified membranes (980 *vs.* 430 a.u.), indicating that the G6.5 modification could promote target capturing, probably because the surface-immobilized G6.5 molecules could conjugate more branches of ligation products on their surfaces, resulting in a higher surface density of cRCA products. This conclusion was further supported by the fact that APTES-G6.5-cRCA modified membranes showed significantly ($p<0.05$) lower flow rates than APTES-cRCA modified membranes (7 *vs.* 12 mL/s), as the higher surface density of cRCA products were more likely to mesh the open pores of membranes to decrease the flow rate. We roughly estimated the number of ligation products on each G6.5 molecule (see D6 for details, Appendix D). The result showed that one G6.5 molecule could conjugate with 436±14 ligation products in solution conditions. It should be noted that fluorescence intensities of the APTES-cRCA modified membranes were even lower than those of APTES-G6.5-unit aptamer modified membranes (430 *vs.* 680 a.u.), indicating that the influence of G6.5 surface modification on capturing performance was more profound than that of cRCA modification.

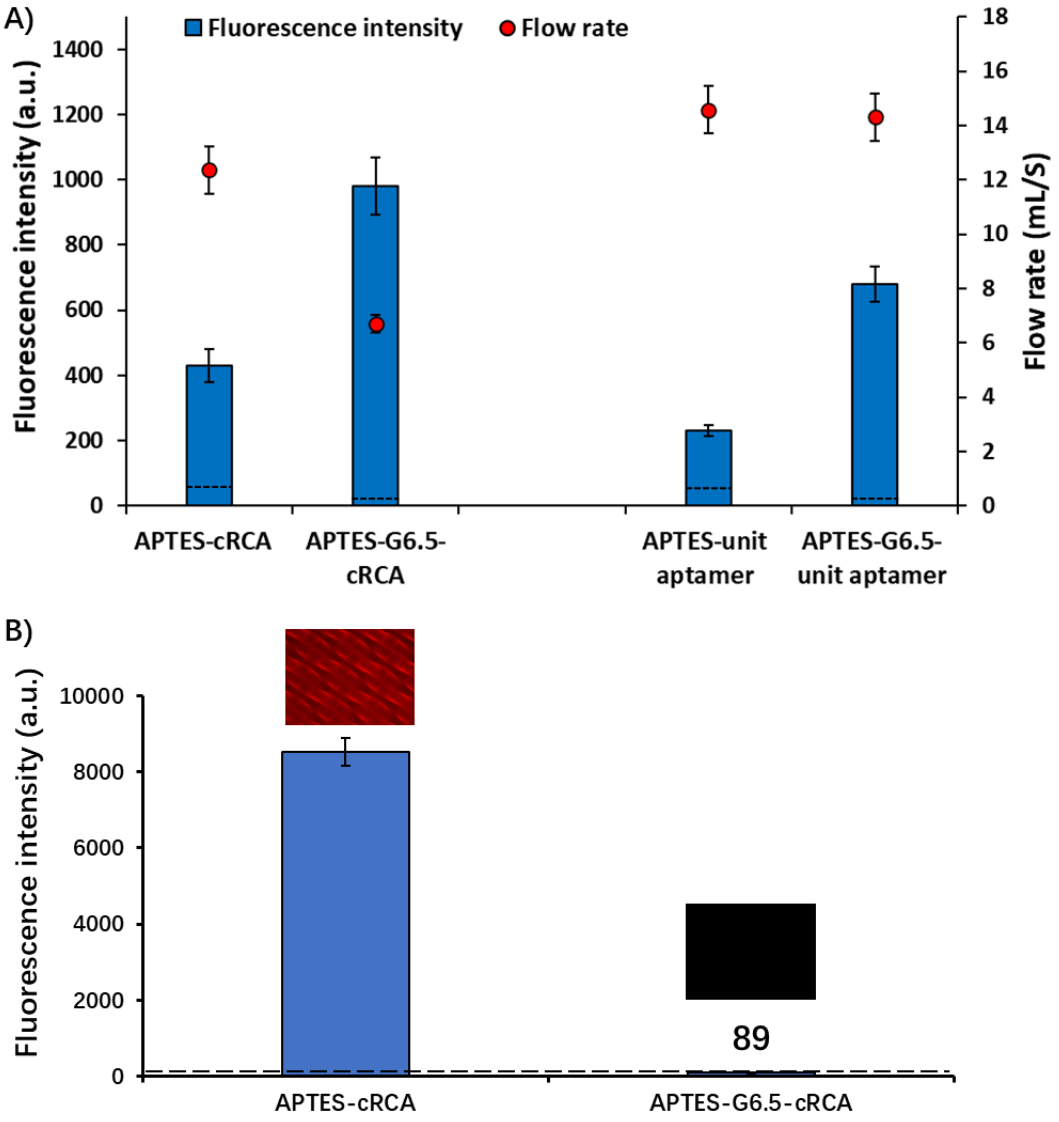

Figure 6.4. The effect of G6.5 surface modification on detection performances and background noises. A) *E.coli* O157:H7 detection signals (*i.e.*, fluorescence intensities) and the sample processing flow rates of membranes with and without G6.5 modification; the APTES-unit aptamer and APTES-cRCA surfaces were blocked with BSA to prevent surface non-specific adsorptions; the dotted lines indicate the detection signals of blank samples; and *E.coli* O157:H7 (250 mL $\times 10^3$ cell/mL) in PBS (pH 7.4) samples were used for each test. B) Background noises of different membranes incubated in signaling probes to prove that membranes with G6.5 modification can prevent non-specific adsorptions; the dotted line indicates fluorescence intensities of the surfaces treated with PBS (*i.e.*, without adsorption of signaling probes). Note: the membranes with a pore size of 1 μm were applied for all experiments; error bars indicate standard deviations, n=3.

Since fluorescence signals from non-specific adsorptions may increase the detection background noises to diminish the *E.coli* O157:H7 detection signals, the nonfouling properties of G6.5 surface modification were further studied. Specifically, membranes without G6.5 modifications (*i.e.,* APTES-cRCA (no BSA surface blocking)) and with (*i.e.,* APTES-G6.5-cRCA) were incubated in cy5-ssDNA signaling probes, orange juice, and milk, respectively, as non-specific adsorptions might come from signaling probes or food matrices, after which their background noises (*i.e.,* surface fluorescence intensities) were compared. As shown in Figure 6.4B, after treatment with signaling probes, APTES-G6.5-cRCA membranes showed a 96-time lower background noise than APTES-cRCA membranes (89 *vs.* 8500 a.u.), indicating the excellent nonfouling performance of the G6.5 surface modification against signaling probes. It should be noted that orange juice and milk incubation could not significantly ($p>0.05$) influence the background noises, as background noises of both membrane types were around 90 a.u., similar to the background noises of membranes incubated in PBS (shown in Figure D4, Appendix D).

6.3.2.3 sRCA signaling amplification

To study the influence of sRCA signaling amplification on the detection signals, *E.coli* O157:H7 cells were detected using the G6.5-cRCA modified membranes, followed signaled with different signaling methods (*i.e., E.coli* O157:H7 labeled with aptamer-cy5 or with sRCA signal amplification method). As shown in Figure 6.5A, more cells can be observed on the membranes after they were labeled with the sRCA signal amplification method than with the aptamer-cy5 (977 *vs.* 416), suggesting that the sRCA approach was more effective than the single fluorescence labeling in improving detection signals. Moreover, to further study the extent of signal amplification with sRCA, the S/Ns were compared. As shown in Figure 6.5B, the S/N of *E.coli* O157:H7 labeled with aptamer-cy5 was 1.62, and that of *E.coli* O157:H7 amplified with the sRCA was 44.33, suggesting a 27-time signal improvement. It should be mentioned that nylon and cy5 were selected as our membrane and signaling materials because the

nylon membrane presented minimum autofluorescence when the excitation wavelength exceeds 600 nm [42]; therefore, when the nylon membrane combined with the far-red fluorophores (*i.e.*, cy5, excitation wavelength: 648nm), the detection S/N could be further improved (data not shown).

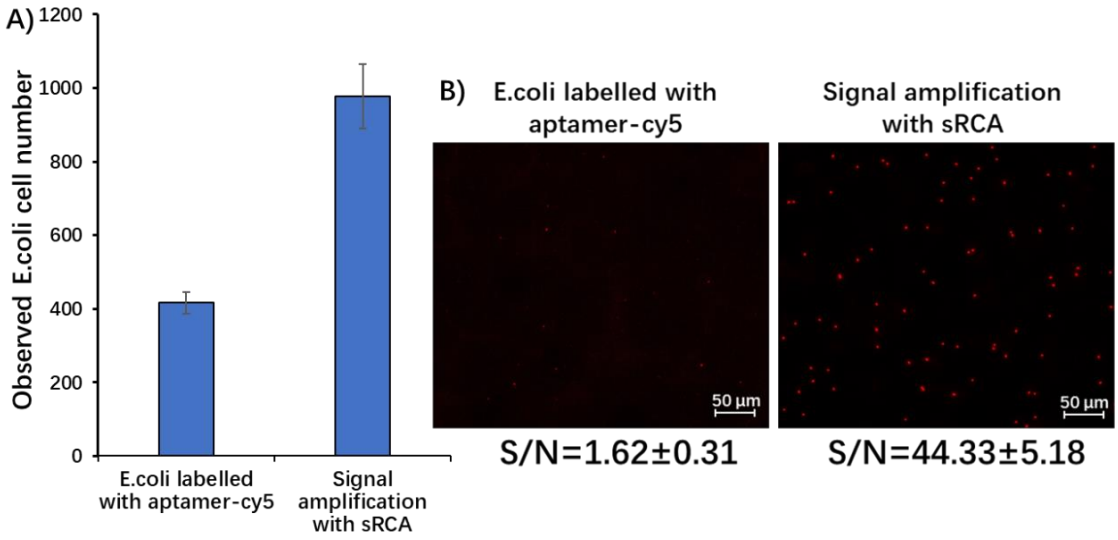

Figure 6.5. Signal amplification tests prove that sRCA can significantly increase detection signals. A) The number of *E.coli* O157:H7 cells on the G6.5-cRCA modified membranes with signal amplification (*i.e.*, sRCA approach) and without (*i.e.*, *E.coli* O157:H7 labeled with aptamer-cy5); for each test, 1000 *E.coli* O157:H7 cells in 250 mL PBS (pH 7.4) were released; error bars indicate standard deviations, n=3. B) Images of *E.coli* O157:H7 cells (10^3 cell/mL × 250 mL) in PBS detected on the G6.5-cRCA modified membranes with different signaling methods (*i.e.*, aptamer-cy5 and sRCA); the S/Ns were calculated based on the fluorescence intensities of *E.coli* O157:H7 cells *vs.* those of backgrounds (n=8). Note: the membranes with a pore size of 1 μm.

6.3.3 Detection Performances for Low-concentration Samples

To study the detection performances of the membranes for samples with low *E.coli* O157:H7 concentrations, the G6.5-cRCA and G6.5-unit aptamer modified membranes were employed to detect *E.coli* O157:H7 samples in PBS (pH 7.4) with different concentrations (*i.e.*, 100, 1000, and 10000 cells/250 mL). Since fluorescence intensities (*i.e.*, *E.coli* O157:H7 detection signals) could not be significantly changed when low concentrations of *E.coli* O157:H7 cells were employed to detect, we calculated the capturing efficiency to evaluate the capturing performance. The capturing efficiency is defined as the number of captured *E.coli* O157:H7 cells *vs.* the number of released. As

shown in Figure 6.6A, the 0.45 µm membranes with either G6.5-cRCA or G6.5-unit aptamer modifications showed high capturing efficiencies ranging from 92-100%, as the pore size is smaller than the *E.coli* O157:H7 size. The 1 µm G6.5-cRCA modified membranes showed similar capturing efficiencies ranging from 96-102 % as observed on 0.45 µm membranes. The capturing efficiencies of other membrane types were 72-76% (5 µm G6.5-cRCA membranes), 68-69% (1 µm G6.5-unit aptamer membranes), and 29-32% (5 µm G6.5-unit aptamer membranes), respectively.

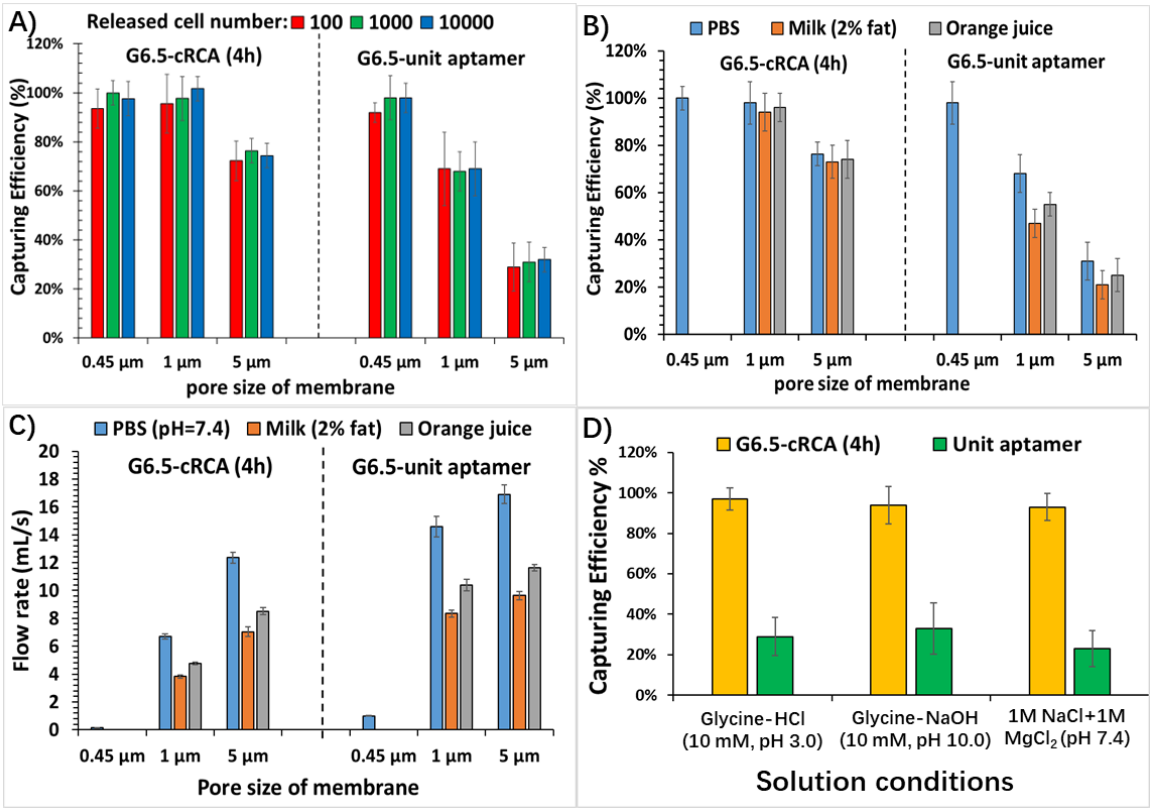

Figure 6.6. Detection performances of nylon membranes modified with G6.5-cRCA and G6.5-unit aptamers test under low *E.coli* O157:H7 concentrations. A) Capturing efficiency of the membranes tested using different numbers of *E.coli* O157:H7 cells spiked PBS (pH 7.4). B) and C) Capturing efficiency and flow rate changes of the membranes tested using *E.coli* O157:H7 cells spiked PBS (pH 7.4), milk, and orange juice samples (1000 cells/250 mL); note that the 0.45 µm membranes have no data for milk and orange juice samples, as these food matrices blocked the membrane pores; more data for capturing efficiencies can be found in Table D2 (Appendix D). D) Capturing efficiency of the membranes (1 µm) tested using *E.coli* O157:H7 cells spiked in different pH and high ionic solutions (1000 cells/250 mL). Note: error bars indicate standard deviations, n=3; the released cell numbers have been corrected using the data in Figure D5 (Appendix D).

To further evaluate the capturing efficiencies of membranes in food samples, *E.coli* O157:H7 cells spiked in milk (2% fat), orange juice, and PBS (pH 7.4) samples were analyzed using the modified membranes (*i.e.*, G6.5-cRCA and G6.5-unit aptamer modified). As shown in Figure 6.6B, the G6.5-unit aptamer modified membranes (either 1 or 5 μm) showed diminished capturing efficiencies for milk and orange juice samples *vs.* PBS samples (*i.e.*,1 μm: 47% and 55% *vs.* 68%; 5 μm: 21% and 25% *vs.* 31 %), likely because secondary structures of aptamers were influenced by the calcium and magnesium ions in milk and orange juice, resulting in a reduced binding affinity, thus diminishing the capturability [43-47]. In contrast, G6.5-cRCA modified membranes were little influenced by these food samples, as their capturing efficiencies ranged from 94-98% (1 μm) and 73-76% (5μm), indicating that the G6.5-cRCA modified membranes were more robust in confronting the food matrix effects, most likely due to the multivalent aptamers networks on the surface. Specifically, even though food matrices might influence the binding affinity of each produced repeating aptamer, the overall avidity is still strong enough to keep the *E.coli* O157:H7 cells on the surface because multivalent aptamers act on the same *E.coli* O157:H7 cell at the same time [29, 41, 48].

Moreover, as shown in Figure 6.6C, milk and orange juice samples could not pass through 0.45 μm membranes resulting in detection failure, showing no flow rate data and capturing efficiency (see Figure 6.6B), as the food matrix blocked membrane pores; however, membranes with a pore size of either 1 or 5 μm under any surface modification achieved higher flow rates (3.8-16.9 mL/s) for detecting food samples, indicating that they are more suitable for the food detections. It should be noted that other reported membranes for bacteria detection in water samples were typical with pore sizes smaller than 0.45 μm [14, 17-19, 30-32], meaning they are not suitable for food samples. Overall, the 1 μm G6.5-cRCA modified membranes seem the optimum choice for detecting *E.coli* O157:H7 in milk and orange juice samples, as they presented

excellent capturing efficiencies (94%±8% and 96%±6%) and sample throughputs (3.8 and 4.8 mL/s).

Furthermore, to further test that the G6.5-cRCA modified membranes were robust for *E.coli* O157:H7 detection under different external conditions due to multivalent aptamers networks, capturing efficiencies of G6.5-cRCA and G6.5-unit aptamer modified membranes (1 μm) were tested under different solutions (*i.e.,* solutions with pH 3.0, pH 10.0 and NaCl (1M)+$MgCl_2$ (1M)). As shown in Figure 6.6D, the capturing efficiencies of G6.5-cRCA modified membranes were around 4 times those of G6.5-unit aptamer modified (93-97% *vs.* 23-33%) under any solution condition, indicating that the multivalent aptamers networks showed excellent *E.coli* O157:H7 capturing performance even under some extreme solutions and also suggesting that the G6.5-cRCA modified membranes could also be used for detecting other food samples besides milk and orange juice.

To further evaluate the LOD of our modified membranes, membranes with G6.5-cRCA and G6.5-unit aptamer modifications were employed to detect *E.coli* O157:H7 cells spiked in PBS (pH 7.4), milk, and orange juice samples. The LOD was defined as the lowest *E.coli* O157:H7 concentration with a 95% possibility of having at least one bacterium detected [14, 49]. In our case, we tested samples with a certain concentration 20 times, and if the positive results (*i.e.,* at least one bacterium on the membranes) can be observed 19 times, we determine this concentration as the LOD. As shown in Table 6.1, compared to other membranes, the 1 μm G6.5-cRCA membranes showed the lowest LODs (*i.e.,* 10 cells/250 mL or 0.04 cell/mL) in PBS, milk, and orange juice solutions. To our best knowledge, our obtained LOD was lower than the lowest reported value (0.04 *vs.* 0.3 cell/mL) for bacteria detection using a membrane-based system [14]. It should be noted that it was difficult to precisely prepare extremely low concentrations of *E.coli* O157:H7 samples (*e.g.,* single-digit to ten-digit bacteria in a sample) for the LOD testing, so to a large extent, our LOD might be influenced by the true amount of

bacteria in samples but not by the detection performances of membranes. This argument can be supported by the fact that the 0.45 μm membranes also showed the same LOD (*i.e.*, 10 cells/250 mL) in the PBS condition, even though their pore size was smaller than the size of *E.coli* O157:H7 cells. Therefore, we infer that if ultra-low concentration samples (<10 cells/250 mL) could be accurately prepared, our LOD might be lower than the current value.

Table 6.1. Limit of detections of different membranes tested using *E.coli* O157:H7 spiked PBS, milk, and orange juice samples.*

Surface modification method	G6.5-cRCA (4h)			G6.5-unit aptamer		
Membrane pore size (μm)	0.45	1	5	0.45	1	5
LOD tested in PBS (cells/250 mL)	10	10	25	10	25	50
LOD tested in milk (cells/250 mL)	N/A	10	25	N/A	35	70
LOD tested in orange juice (cells/250 mL)	N/A	10	25	N/A	30	60

N/A: detection failure due to blockage of membrane pores.
*: Number distributions of the captured *E.coli* O157:H7 at the limit of detection points can be found in Figure D6 (Appendix D).

Moreover, the detection specificity was evaluated using the 1 μm G6.5-cRCA membranes to detect non-target samples, including *E.coli* ATCC25922, *E.coli* K12, *E.coli* ER2420, and Listeria innocua. The results showed that no cell was observed on the membranes, suggesting excellent detection specificity of our RCA-modified membranes.

To further demonstrate that our detection method is sensitive and has a high sample throughput, our LOD and flow rate were compared with other recently published membranes for bacteria detections (Table 6.2). It is clear that the detection performances obtained in this study showed a lower LOD and higher flow rate than any other reported results. Moreover, compared with other membranes that can only be used for water sample detections, our membranes were suitable for detecting whole *E.coli*

O157:H7 cells in food samples, indicating that our detection system is more rapid, sensitive, and robust. The simplicity of this design also suggests that our membranes can be rapidly adapted to detect other bacteria in food samples simply by replacing the cRCA and sRCA with other sequence designs.

Table 6.2. Comparisons of the current dual-RCA membrane approach with other recently reported membranes for bacterial detections.

Pore size	Target	Sample volume	Flow rate	LOD	Matrix	Detection method	Ref.
0.2 μm	*E.coli*	10 mL	1 mL/min	~10^4 cells/mL	water	SERS	[30]
0.4 μm	*E.coli*	10 mL	~1 mL/min	0.3 cells/mL	environmental water	LAMP	[14]
0.2 μm	Enterococcus spp	10 mL−4.2 L	~1 mL/min	20 target copies per reaction	water	LAMP	[31]
0.22 μm	*E.coli*	1 mL	1 mL/min	6.7 cells/mL	water	SERS	[19]
0.2 μm	Legionella pneumophila	200 mL	30 mL/min	4 cells/mL	drink water	ELISA like amplification	[32]
0.2 μm	Legionella pneumophila	30 mL	30 mL/min	70 cells	water	ELISA like amplification	[18]
0.2 μm	*E.coli*	100 mL	30 mL/min	1 cell/mL	water	ELISA like amplification	[17]
1.0 μm	*E.coli* O157:H7	250 mL	240-300 mL/min	10 cells/250mLor 0.04 cell/mL	milk and orange juice	Dual-RCA	This study

6.4 Conclusion

Nylon membranes with dual-RCA modification are developed for improving sample throughput to achieve rapid and sensitive detection of *E.coli* O157:H7 in food samples. Our membranes improve detection flow rates and sensitivities based on the following mechanisms: 1) to increase the sample throughput by applying membranes with large pore sizes; 2) to enhance target capturing by surface *in situ* cRCA reactions to synthesis repeating-aptamer networks; 3) to increase surface cRCA branches and decrease background noise by surface immobilization of G6.5, and 4) to amplify detection

signals using sRCA. Our results show that cRCA can significantly enhance target capturing compared to unit aptamers, the G6.5 surface modification decreased the background noises by 96 times, and sRCA amplified detection signals by 27 times. Our results also show that the G6.5-cRCA modified membranes detect *E.coli* O157:H7 spiked milk and orange juice samples with excellent capturing efficiencies (94%±8 and 96%±6%) and high sample throughputs (3.8 and 4.8 mL/s). The LODs tested under these food matrices are 10 cells/250 mL, lower than any other published results. Our results strongly suggest that our detection method is much more powerful than other approaches, such as ELISA and microfluidics, for rapid and sensitive foodborne bacteria detection. It is also expected that more cRCA and sRCA sequences can be developed to adapt to our membranes to detect more target particles in other research fields.

References

1. Organization, W.H., WHO estimates of the global burden of foodborne diseases: foodborne disease burden epidemiology reference group 2007-2015. 2015: World Health Organization.
2. Greig, J.D., et al. Infective doses and pathogen carriage. in 2010 Food Safety Education Conference. 2010.
3. Gracias, K.S. and J.L. McKillip, A review of conventional detection and enumeration methods for pathogenic bacteria in food. Canadian journal of microbiology, 2004. **50**(11): p. 883-890.
4. de Boer, E. and R.R. Beumer, Methodology for detection and typing of foodborne microorganisms. International journal of food microbiology, 1999. **50**(1-2): p. 119-130.
5. Croxen, M.A., et al., Recent advances in understanding enteric pathogenic Escherichia coli. Clinical microbiology reviews, 2013. **26**(4): p. 822-880.
6. Li, S., et al., *In situ* rolling circle amplification surface modifications to improve *E.coli* O157: H7 capturing performances for rapid and sensitive microfluidic detection applications. Analytica Chimica Acta, 2021. **1150**: p. 338229.
7. Lazcka, O., F.J. Del Campo, and F.X. Munoz, Pathogen detection: A perspective of traditional methods and biosensors. Biosensors and bioelectronics, 2007. **22**(7): p. 1205-1217.
8. Jiang, Y., S. Zou, and X. Cao, Rapid and ultra-sensitive detection of foodborne pathogens by using miniaturized microfluidic devices: a review. Analytical Methods, 2016. **8**(37): p. 6668-6681.

9. Hao, X., et al., Aptamer surface functionalization of microfluidic devices using dendrimers as multi-handled templates and its application in sensitive detections of foodborne pathogenic bacteria. Analytica chimica acta, 2019. **1056**: p. 96-107.
10. Jiang, Y., et al., Developing a dual-RCA microfluidic platform for sensitive *E.coli* O157: H7 whole-cell detections. Analytica Chimica Acta, 2020. **1127**: p. 79-88.
11. Jiang, Y., et al., Rolling circle amplification and its application in microfluidic systems for Escherichia coli O157: H7 detections. Journal of Food Safety, 2019. **39**(5): p. e12671.
12. Wang, Y. and J.K. Salazar, Culture-independent rapid detection methods for bacterial pathogens and toxins in food matrices. Comprehensive Reviews in Food Science and Food Safety, 2016. **15**(1): p. 183-205.
13. Gill, A., The importance of bacterial culture to food microbiology in the age of genomics. Frontiers in microbiology, 2017. **8**: p. 777.
14. Lin, X., et al., Asymmetric membrane for digital detection of single bacteria in milliliters of complex water samples. ACS nano, 2018. **12**(10): p. 10281-10290.
15. Tsao, S.C.-H., et al., Capture and on-chip analysis of melanoma cells using tunable surface shear forces. Scientific reports, 2016. **6**(1): p. 1-10.
16. Zagorodko, O., et al., Surface plasmon resonance (SPR) for the evaluation of shear-force-dependent bacterial adhesion. Biosensors, 2015. **5**(2): p. 276-287.
17. Ezenarro, J.J., et al., Development of an integrated method of concentration and immunodetection of bacteria. Analytical and bioanalytical chemistry, 2018. **410**(1): p. 105-113.
18. Párraga-Niño, N., et al., New system for the detection of Legionella pneumophila in water samples. Talanta, 2018. **189**: p. 324-331.
19. Gao, S., B. Pearson, and L. He, Mapping bacteria on filter membranes, an innovative SERS approach. Journal of microbiological methods, 2018. **147**: p. 69-75.
20. Jiang, Y., S. Zou, and X. Cao, A simple dendrimer-aptamer based microfluidic platform for *E.coli* O157: H7 detection and signal intensification by rolling circle amplification. Sensors and Actuators B: Chemical, 2017. **251**: p. 976-984.
21. Qin, Y., et al., Developing a non-fouling hybrid microfluidic device for applications in circulating tumour cell detections. Colloids and Surfaces B: Biointerfaces, 2017. **151**: p. 39-46.
22. Hao, X., et al., Surface modification of poly (styrene) 96-well plates using aptamers via a dendrimer-templated strategy to enhance ELISA performances. Colloids and Surfaces B: Biointerfaces, 2023. **221**: p. 113003.
23. Hao, X., et al., Surface modification of glass-bottom 96-microwell plates to enhance ELISA performances. Applied Surface Science, 2023. **610**: p. 155603.
24. Beyer, S., P. Nickels, and F.C. Simmel, Periodic DNA nanotemplates synthesized by rolling circle amplification. Nano Letters, 2005. **5**(4): p. 719-722.

25. Ali, M.M., et al., Rolling circle amplification: a versatile tool for chemical biology, materials science and medicine. Chemical Society Reviews, 2014. **43**(10): p. 3324-3341.
26. Poltronieri, P., et al., Biosensors for the detection of food pathogens. Foods, 2014. **3**(3): p. 511-526.
27. Zhou, L., et al., Aptamer-based rolling circle amplification: a platform for electrochemical detection of protein. Analytical chemistry, 2007. **79**(19): p. 7492-7500.
28. Zhang, Z., et al., A polyvalent aptamer system for targeted drug delivery. Biomaterials, 2013. **34**(37): p. 9728-9735.
29. Zhao, W., et al., Bioinspired multivalent DNA network for capture and release of cells. Proceedings of the National Academy of Sciences, 2012. **109**(48): p. 19626-19631.
30. Chen, J., et al., Detection of *E.coli* using SERS active filters with silver nanorod array. Sensors and Actuators B: Chemical, 2014. **191**: p. 485-490.
31. Martzy, R., et al., A loop-mediated isothermal amplification (LAMP) assay for the rapid detection of Enterococcus spp. in water. Water research, 2017. **122**: p. 62-69.
32. Ezenarro, J.J., et al., Rapid Detection of Legionella pneumophila in Drinking Water, Based on Filter Immunoassay and Chronoamperometric Measurement. Biosensors, 2020. **10**(9): p. 102.
33. Sun, D., et al., A microfluidic chemiluminescence biosensor based on multiple signal amplification for rapid and sensitive detection of *E.coli* O157: H7. Biosensors and Bioelectronics, 2022: p. 114390.
34. Muhsin, S.A., et al., A microfluidic biosensor for rapid simultaneous detection of waterborne pathogens. Biosensors and Bioelectronics, 2022. **203**: p. 113993.
35. Nuhiji, E., et al., Biofunctionalization of 3D nylon 6, 6 scaffolds using a two-step surface modification. ACS applied materials & interfaces, 2012. **4**(6): p. 2912-2919.
36. Bujanda, A.A., et al., Atmospheric Plasma Treatment of Nylon 6,6 for Improved Interfacial Adhesion in Thermoplastic Composites, in Advanced Composites for Aerospace, Marine, and Land Applications II, T. Sano and T.S. Srivatsan, Editors. 2016, Springer International Publishing: Cham. p. 259-271.
37. Thompson, R., et al., Low-frequency plasma activation of nylon 6. Applied Surface Science, 2021. **544**: p. 148929.
38. Hermanson, G.T., Bioconjugate techniques. 2013: Academic press.
39. Riley, M. Correlates of smallest sizes for microorganisms. in Size limits of very small microorganisms: proceedings of a workshop. 1999. National Academies Press Washington DC, USA.
40. Wang, Y., et al., Influence of size, shape, and flexibility on bacterial passage through micropore membrane filters. Environmental science & technology, 2008. **42**(17): p. 6749-6754.
41. Wang, Z., et al., Multivalent Aptamer Approach: Designs, Strategies, and Applications. Micromachines, 2022. **13**(3): p. 436.

42. Dubitsky, A., D. DeCollibus, and G.A. Ortolano, Sensitive fluorescent detection of protein on nylon membranes. Journal of Biochemical and Biophysical Methods, 2002. **51**(1): p. 47-56.
43. Kalra, P., et al., Simple methods and rational design for enhancing aptamer sensitivity and specificity. Frontiers in molecular biosciences, 2018. **5**: p. 41.
44. Bini, A., et al., Development of an optical RNA-based aptasensor for C-reactive protein. Analytical and bioanalytical chemistry, 2008. **390**(4): p. 1077-1086.
45. Jeong, S. and I. Rhee Paeng, Sensitivity and selectivity on aptamer-based assay: the determination of tetracycline residue in bovine milk. The scientific world journal, 2012. **2012**.
46. Ilgu, M., et al., An adaptable pentaloop defines a robust neomycin-B RNA aptamer with conditional ligand-bound structures. RNA, 2014. **20**(6): p. 815-824.
47. Ilgu, M., et al., Investigating the malleability of RNA aptamers. Methods, 2013. **63**(2): p. 178-187.
48. Liu, Y., et al., Highly sensitive minimal residual disease detection by biomimetic multivalent aptamer nanoclimber functionalized microfluidic chip. Small, 2020. **16**(20): p. 2000949.
49. Stokdyk, J.P., et al., Determining the 95% limit of detection for waterborne pathogen analyses from primary concentration to qPCR. Water Res, 2016. **96**: p. 105-13.

Chapter 7 Conclusions and General Discussions

7.1 Conclusions

In this thesis, four biosensors were developed using various surface modification designs based on PAMAM dendrimers, aptamers and RCA, their surface modification methods were characterized, and detection performances were examined. In general, it was shown that the surface modification strategy of using PAMAM dendrimers as aptamer-conjugation templates is very effective in promoting nonfouling properties and surface-ligand density, which results in a significantly improved S/N and target-capturing efficiency of the detection surfaces. Moreover, the developed RCAs can enhance target-capturing performances when applied on the detection surfaces (*i.e.,* cRCA) as well as significantly improve the detection signals when employed as signal amplification ligands (*i.e.,* sRCA). The key results of the applied surface modifications on the enhanced detection performances of different biosensors can be summarized as:

1) **Surface Modification of Glass-bottom 96-microwell Plates to Enhance ELISA Performances:** The G7- and G4&G7-modified glass-bottom 96-microwell plates could provide better results in terms of nonfouling, aptamer-binding capacity, and surface coverage than the G4-modified microwells, thus resulting in improved detection specificity and sensitivity. Moreover, the G7- and G4&G7 modified microwells showed improved assay performances with approximately 2 times broader linear ranges and about 4.5 times lower LODs than the standard ELISA performed using the regular microplates.
2) **Surface Modification of Poly(styrene) 96-well Plates Using Aptamers via A Dendrimer-templated Strategy to Enhance ELISA Performances:** The PS 96-well plates with G7 surface modification showed better nonfouling properties than microplates with BSA-blocked surface, thus eliminating the need to block in the bioassay to reduce background noises. Additionally, multiple copies of aptamers could be conjugated on the surface via G7 templates, further enhancing assay performance. The combined effects of enhanced nonfouling properties and aptamer

density on detection surfaces improved the linear detection range by 2.3 times and the LOD by 13 times compared with the standard ELISA.

3) **Localized Surface Plasmon Resonance Biosensor Chip Surface Modification and Signal Amplifications Toward Rapid and Sensitive Detection of COVID-19 Infections:** The (G3.5+G4) modified LSPR sensor chip showed improved surface nonfouling property, higher aptamer-binding capacity, and better detection signal than other possible surface designs (*i.e.,* gold-aptamer, G3.5-aptamer, and G4-aptamer). Moreover, the (G3.5+G4)-aptamer modified LSPR sensor chip showed an improved LOD that was 9 and 152 times lower than the LODs from the traditional gold-aptamer and gold-antibody based sensor chips, respectively. Furthermore, the developed RCA-AuNPs complex significantly amplified the detection signals of pseudo SARS-CoV-2 viral particles by approximately 10 times using the surface-modified sensor chip, resulting in a final LOD of 148 vp/mL.
4) **Developing Membranes with Dual-RCA Modification for High-throughput and Sensitive Detection of *E.coli* O157:H7 Whole Cells in Food Samples:** The G6.5-cRCA modified membranes provided significantly improved target capturing efficiencies than the G6.5-unit aptamer modified. The membranes with G6.5 modification decreased the non-specific-adsorption noises by approximately 96 times, and sRCA enhanced detection signals by 27 times. The E.coli O157:H7 detection results showed that the dual-RCA modified membranes could detect whole *E.coli* O157:H7 cells in milk and orange juice samples with excellent capturing efficiencies of 94%±8% and 96%±6%, and with high sample throughputs at 3.8 and 4.8 mL/s, respectively. The achieved LOD was 10 cells/250 mL in both milk and orange juice food samples.

7.2 General Discussion and Recommendations

The primary objective of this thesis is to develop surface modifications using PAMAM dendrimers that can enhance the non-fouling properties of various sensor surfaces, thus minimizing nonspecific binding and improving the signal-to-noise ratio. In addition,

PAMAM dendrimers are known to create improved aptamer-binding sites on the detection surfaces, enhancing detection sensitivity. This can ultimately result in more sensitive and accurate detection of the target analytes.

The thesis consists of several scientific projects (Chapters 3-6), each addressing different aspects of surface modifications using PAMAM dendrimers for biosensor applications. Chapter 3 aims to provide fundamental research on PAMAM dendrimer-modified surfaces and their application in biosensing. This chapter seeks to answer three critical scientific questions: (1) How effectively can PAMAM dendrimer-modified surfaces improve aptamer binding sites? (2) How well can these surfaces enhance non-fouling properties? (3) How can we apply these modified surfaces in biosensing applications?

To address these questions, we first investigated the optimal conditions for immobilizing PAMAM dendrimers on glass surfaces, which are the most well-studied surfaces. This was achieved using various fluorescence labeling methods, which allow for semi-quantitative characterization of the surface functional groups or immobilized molecules during the surface immobilization process. These methods are particularly useful for the glass surface, which has ultra-low autofluorescence.

Additionally, we compared the non-fouling properties, and the relative amount of aptamer-binding sites of different PAMAM dendrimer modified surfaces, including G4, G7, and G4&G7, using various methods such as WCA, protein adsorption tests, FAM, and fluorescence labeling methods. The results demonstrated that glass surfaces modified with G4&G7 exhibited better non-fouling and aptamer-binding capacity than glass surfaces modified with G4 or G7 alone. This could be due to the smaller G4 molecules filling the voids between the G7 molecules on the surface, resulting in a more densely packed surface that contributes to better non-fouling properties and more available functional groups on the surface for aptamer conjugation.

Furthermore, we explored the biosensing applications of PAMAM dendrimer-modified surfaces by combining our surface modification method with an ELISA detection platform. Glass-bottom 96-microwell plates were modified with PAMAM dendrimer-aptamers to replace the ELISA primary antibodies while leaving the signal amplification steps unchanged. The modified ELISA demonstrated improved assay performance by exhibiting broader linear ranges, higher detection sensitivities, and lower limits of detection (LODs) compared to commercial ELISA.

In Chapter 4, our goal was to broaden the practicality and cost-effectiveness of our PAMAM dendrimer surface modification by exploring potential approaches for modifying PS 96 microwell plates. Unlike glass surfaces, we recognized that the PS substrate presents unique challenges due to the absence of abundant hydroxyl functional groups on its surface, which are essential for stable surface modifications. In addition, the strong autofluorescence of PS makes it challenging to optimize and characterize surface modifications using fluorescence labeling methods, as is typically done with glass substrates.

To address these challenges, we implemented a combined wet and dry chemical surface activation method, which generated stable and uniform hydroxyl functional groups on the PS surface, thus providing a reliable reaction surface for subsequent surface modifications. To overcome the issue of autofluorescence, we replaced the fluorescence labeling method with a biotin labeling method, which enabled us to characterize and optimize surface modifications without being affected by PS autofluorescence.

We also performed several tests to confirm that the modified PS surface maintained excellent non-fouling properties and improved aptamer binding sites, which are crucial for biosensing applications. These tests included WCA, protein adsorption, fluorescence measurements, and ELISA analysis. Our findings demonstrated that the

PS surface modified with PAMAM dendrimers exhibited superior non-fouling properties and aptamer binding capacity compared to unmodified PS surfaces. Moreover, the modified assay outperformed traditional ELISA assays, indicating the potential of this modified PS surface for biosensing applications, which is a more practical and cost-effective alternative to glass substrates.

In Chapter 5, the goal was to extend the application of the PAMAM dendrimer surface modification method to more complex detection surfaces in order to expand the range of surface modification designs available to users. LSPR sensors are highly sensitive detection platforms but are often limited by nonspecific adsorption on the detection sensor chip surface, which can negatively impact their sensitivity. Surface modification with dendrimers is an effective solution to this problem. However, the surface structures of LSPR sensor chips are more complex than those of glass and PS surfaces, with different functional groups on different surface structures, such as glass surfaces with -NH_2 groups and gold nanoislands with -COOH groups. Since both structures may occur nonspecific adsorptions, it is essential and challenging to modify both areas with PAMAM dendrimers to improve the non-fouling properties of the complete surface.

To address this challenge, the detection surfaces were surface-modified with two different PAMAM dendrimers: G3.5-COOH on the glass area and G4-NH_2 on both the G3.5-COOH-modified area and the gold nanoislands. This approach differed from the glass and PS surface modification approaches, in which the surfaces were modified with identical PAMAM dendrimers (*i.e.,* G6.5-COOH) that can readily conjugate with aptamers using NHS/EDC chemistry. However, the (G3.5+G4) surface modification approach produced the complete surface with -NH_2 functional groups, which are challenging to conjugate with amino-capped aptamers. Therefore, the BS^3 linker was introduced to conjugate the aptamer with the PAMAM dendrimer templates on the surface.

In addition to the chemical modification approach, the thickness of the modified layer was another critical consideration for our surface modification design. The overall thickness of the modified layer was controlled within the range of electromagnetic field decay length of gold nanoislands to ensure maximum sensitivity. The detection sensitivity of the modified sensor chip was then characterized using the SRBD samples. The results showed that the (G3.5+G4)-modified surface significantly improved the sensor chip detection sensitivities compared to other sensor chips with possible surface modification formats.

The modified chip was then employed to detect viral particles, but the sensitivity was insufficient, as the sample concentration was very low. To further improve the detection sensitivity for viral particle detection, AuNPs-RCA complexes were used to enhance the detection signals. The challenge for the signals amplification process is that the designed RCA sequences must present both repeating aptamers and AuNPs hybridization sites while having no interactions with the surface aptamers. The results showed that the designed RCA products could specifically bind with the surface-captured targets and hybridize with AuNP probes. The low background signals also indicated that RCA products had no interactions with the surface aptamers.

Overall, the results of Chapter 4 demonstrate that the PAMAM dendrimer surface modification method can be used in detection platforms with more complex surface structures. The designed signal amplification method can improve detection signals without influencing the background signals. This work provides a potential solution to the issue of nonspecific adsorptions on LSPR sensor chips and opens up more applications for dendrimer surface modification in biosensing.

In Chapter 6, we aimed to investigate whether the dendrimer modification approach could be applied to membrane filters to achieve high-throughput bacterial detection. We found that the traditional dendrimer-aptamer approach did not work well in

detecting bacterial cells due to the larger size of the targets and the higher flow rates required in this project. Therefore, our main scientific challenge was to improve the binding avidity between the detection surface and target cells.

To address this challenge, we introduced a repeated aptamer network using cRCA on the dendrimer-modified nylon membrane. This network significantly improved the overall binding avidity of the targets, resulting in a much higher capturing efficiency compared to unit aptamer-modified surfaces. Additionally, we introduced sRCA signal amplification to the detection system to improve the detection signals of the captured targets. The combined approach of dendrimer surface modification and sRCA signal amplification significantly improved the signal-to-noise ratio, providing better detection sensitivity.

To optimize the detection system, we also studied the influence of cRCA time, membrane pore size, and food matrix on the target-capturing performances. The results showed that G6.5-cRCA (4 h) modified membranes with a pore size of 1 μm were the optimal choice for detecting *E.coli* O157:H7 in milk and orange juice samples, showing capturing efficiencies of 94%±8% and 96%±6%, and sample throughputs of 3.8 and 4.8 mL/s, respectively.

Overall, our study demonstrated the potential of using dendrimer modification and cRCA/sRCA approach in membrane filters for high-throughput bacterial detection. The findings could have important implications for food safety and public health, as they offer a more efficient and sensitive method for detecting bacterial contamination in food samples.

Recommendations for future work are made below:

1. In Chapter 3, the combination of G4&G7 immobilized surfaces showed improved surface non-fouling properties as the more densely packed surface was formed. Therefore, it is interesting to see the nonfouling behaviors and

detection performances of the detection surfaces modified with other non-fouling materials combinations, such as PEG&G9, G4&G9, and PEG&G7.

2. The current PAMAM dendrimer-modified surface showed excellent non-fouling properties against large molecules, such as proteins, aptamers, and bacteria; however, the non-fouling properties of the modified surface against small molecules have never been studied. Therefore, a systematic study should be carried out.
3. The stability of the dendrimer or dendrimer-aptamer modified substrates needs to be studied for further commercialization.
4. To further improve the detection performances of different biosensors, the dendrimer-aptamer modification approach can be incorporated into other 3D materials, such as mesoporous silica film, multi-walled carbon nanotubes, and nanofibers.
5. In Chapter 5, new dendrimer-based LSPR sensor chip preparation methods can be further explored. For example, the glass surface can be first modified with dendrimers on which to conjugate with gold nanoparticles, or the glass surface can be directly modified with dendrimers stabilized gold nanoparticles. These methods may further improve the non-fouling properties and binding site on the surface of gold nanoparticles.
6. Modifying the LSPR chip surface with the cRCA design may enable the LSPR detection system to capture large targets, such as cells and bacteria, under higher flow rates.
7. Multi-target-capturing designs can be explored to obtain multiplex detection on the same biosensor.
8. The target-responsive designs using hydrogels or mesoporous materials can be applied to affinity-based biosensors to achieve signal amplification.
9. The developed surface modification approaches integrating with other techniques, such as electrochemical biosensors, magnetic nanoparticles, and microbeads, can widen the application areas of biosensors and promote further

developments.

Even though a high number of biosensors with high detection performances for real sample analysis has been reported in the literature, these devices are still in the early stages of implementation for commercialization. The excellent and promising properties of the surface modification approaches discussed in the current thesis suggest a bright future for biosensing technology.

Scientific contributions are listed below:

Published papers and book chapters

- Hao, Xingkai, Xiuying Yang, Shan Zou, and Xudong Cao. "Surface Modification of Glass-bottom 96-microwell Plates to Enhance ELISA Performances." **Applied Surface Science** (2022): 155603.
- Hao, Xingkai, Xiuying Yang, Shan Zou, and Xudong Cao. "Surface Modification of Poly (styrene) 96-well Plates Using Aptamers via a Dendrimer-templated Strategy to Enhance ELISA Performances." **Colloids and Surfaces B: Biointerfaces** (2022): 113003.
- Hao, Xingkai, Linglin Fu, Liangliang Shao, Qi Chen, Brian Dorus, Xudong Cao, and Fang Fang. "Quantification of major milk proteins using ultra-performance liquid chromatography tandem triple quadrupole mass spectrometry and its application in milk authenticity analysis." **Food Control** 131 (2022): 108455.
- Hao, Xingkai, Poying Yeh, Yubo Qin, Yuqian Jiang, Zhenyu Qiu, Shuying Li, Tao Le, and Xudong Cao. "Aptamer surface functionalization of microfluidic devices using dendrimers as multi-handled templates and its application in sensitive detections of foodborne pathogenic bacteria." **Analytica chimica acta** 1056 (2019): 96-107.
- Li, Shuying, Xingkai Hao, Zhong Wang, Tao Le, Shan Zou, and Xudong Cao. "Lab-on-a-chip analytical devices." **In Micro-and Nanotechnology Enabled**

Applications for Portable Miniaturized Analytical Systems, pp. 355-374. Elsevier, 2022.

To be published papers

- A review of Sensitivity-enhancing Approaches in Affinity-based Biosensing: Surface Modification Materials and Strategies.
- Localized Surface Plasmon Resonance Biosensor Chip Surface Modification and Signal Amplifications Toward Rapid and Sensitive Detection of COVID-19 Infections.
- Developing Membranes with Dual-RCA Modification for High-throughput and Sensitive Detection of *E.coli* O157:H7 Whole Cells in Food Samples.

Conference presentations and posters

- Xingkai Hao and Xudong Cao."Surface Modification of Poly(styrene) 96-well Plates to Enhance ELISA Performances" October 28, 2020 at the virtual 70th Canadian Chemical Engineering Conference.
- Xingkai Hao and Xudong Cao. "Aptamer Surface Functionalization of Microfluidic Devices using Dendrimers as Multi-handled Templates and Its Application in Sensitive Detections of Foodborne Pathogenic Bacteria" poster competition 2019 at Chemical and Biological Engineering, University of Ottawa.

Appendix A

A1 Optimization of amination

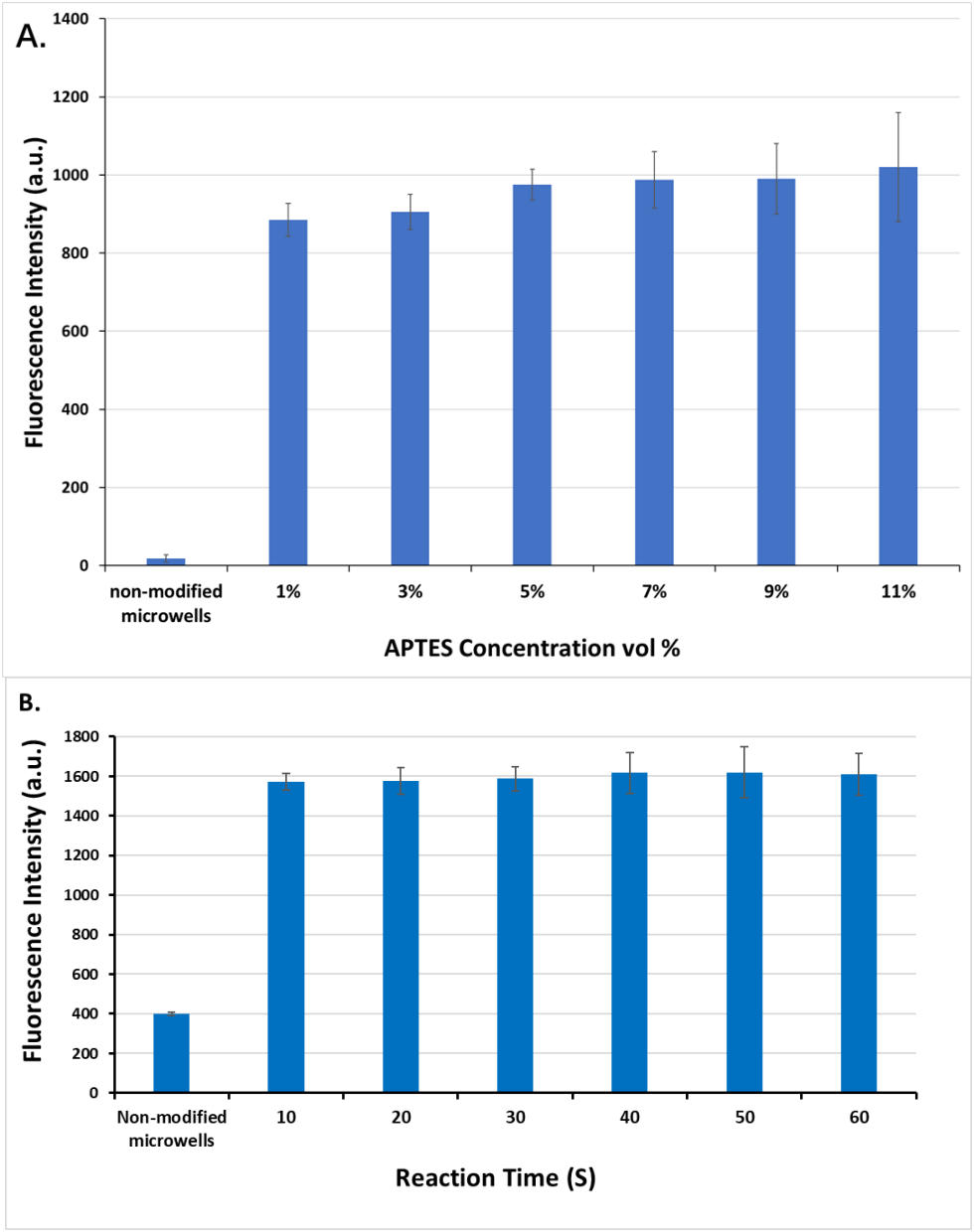

Figure A1. Optimization of APTES reaction conditions. A. optimization of APTES concentration. B. optimization of reaction time.

A2 Method：FITC-NH_2 labelling PAMAM dendrimers

To ensure the success of PAMAM immobilization, FITC-NH_2 was used to label the carboxyl functional groups of the immobilized dendrimers to evaluate the relative amount of carboxyl groups on the surfaces of microwells [3, 4]. Specifically, PAMAM modified microwells were activated by adding 100 μL reaction solution containing 5 mM NHS, 2 mM EDC, and 0.1 M MES solution (pH 6.0) at room temperature for 30 min, after which the activated microwells was washed by 300 μL PBS (0.1 M, pH=7.4) intensively. Subsequently, the resulting microwells were incubated with 20 μg/mL FITC-NH_2 in PBS (0.1 M, pH= 7.4) solutions for 2 h at room temperature and finally washed with PBS (pH 7.4) intensively to remove unreacted FITC-NH_2.

A3 Optimization of dendrimer concentration

To optimize dendrimer concentration. FITC-NH_2 was used to label the dendrimer-modified surface. G4 and G7 at various designed concentrations (i.e. 0.1 μM, 0.5μM, 1μM, 5μM, 10μM, 15μM) were studied. As shown in Figure A2. the fluorescence intensities of G7 modified microwells were maximized when 1 μM G7 was applied. The fluorescence intensities for G4 modified microwells were stabilized at the same level under any experimental concentrations. Therefore, 1 μM was selected as the optimum concentration for both G7 and G4 modifications.

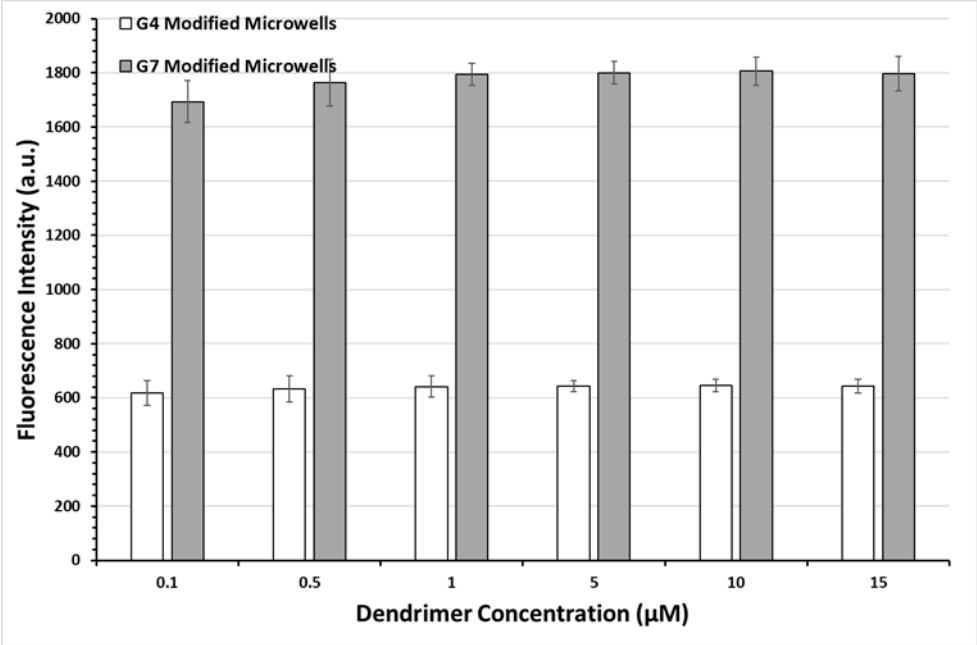

Figure A2. Optimization of G4 and G7 concentration

A4 Optimization of aptamer concentration

To optimize aptamers concentration, fluorescently labelled aptamer (cy3-aptamer) was employed. As shown in Figure A3, 5 μM cy3-aptamer treatment peaked fluorescence intensity of both G4 and G7 modified surfaces, suggesting the optimum concentration for aptamer engraftment.

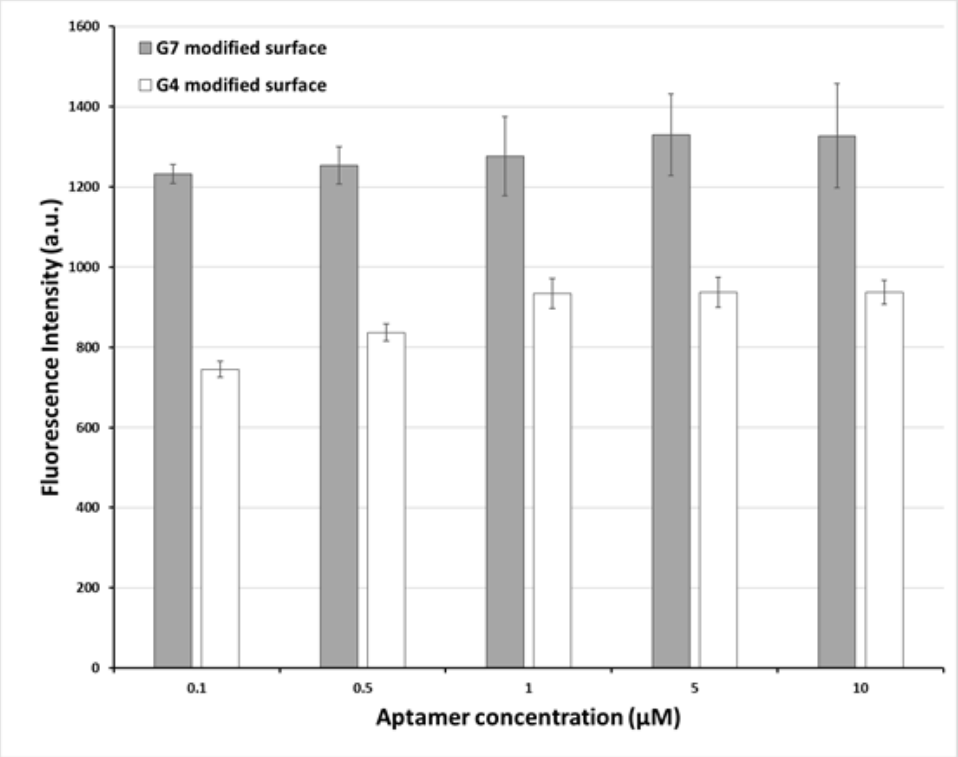

Figure A3. Optimization of aptamers concentration

A5 Dendrimer height distribution on G4, G7 and G4&G7 modified surfaces.

A Gwyddion 2.55 software was used to process the AFM data of G4, G7 and G4&G7 modified surfaces. As shown in Figure A4. the height distribution of the G4 modified surface ranged from 1.3-4.9 nm (average height= 2.8 ± 0.7 nm), that of the G7 modified surface ranged from 3.0-7.8nm (average height= 5.1 ± 0.9 nm), and that of G4&G7 modified surface ranged from 4.0 nm-13.7 nm (average height= 7.4 ± 1.8 nm).

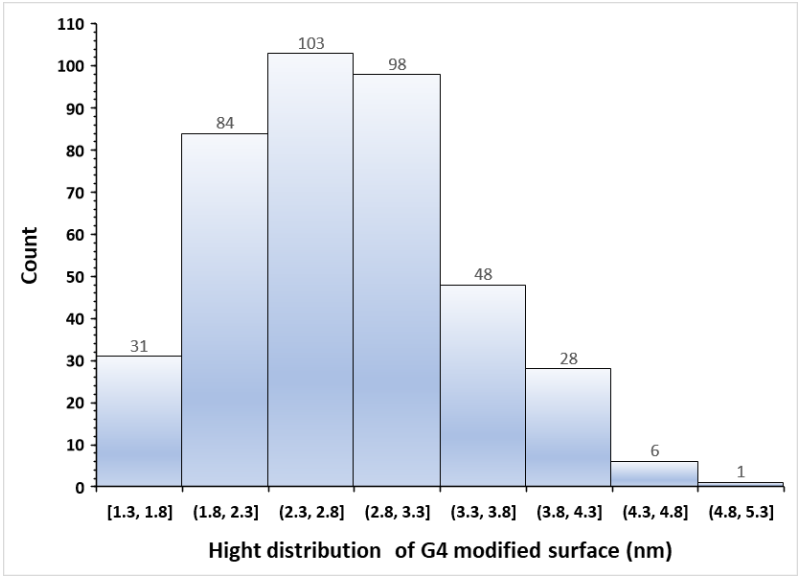

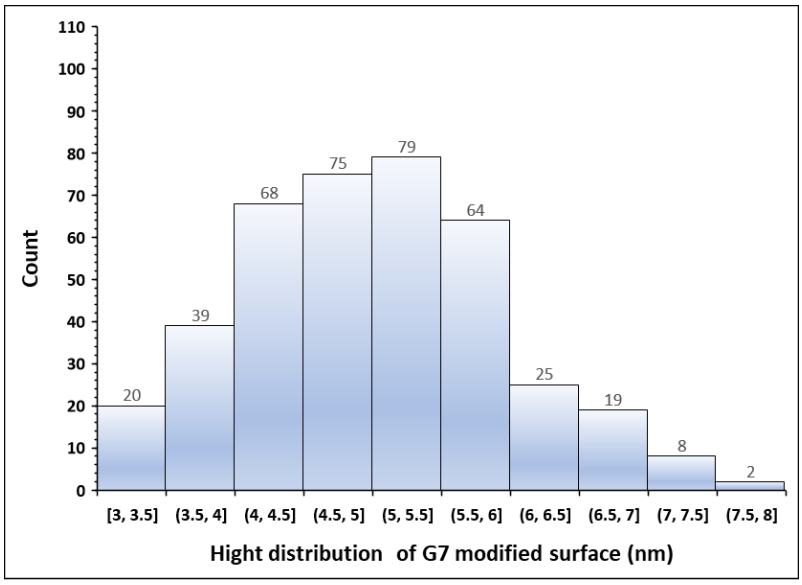

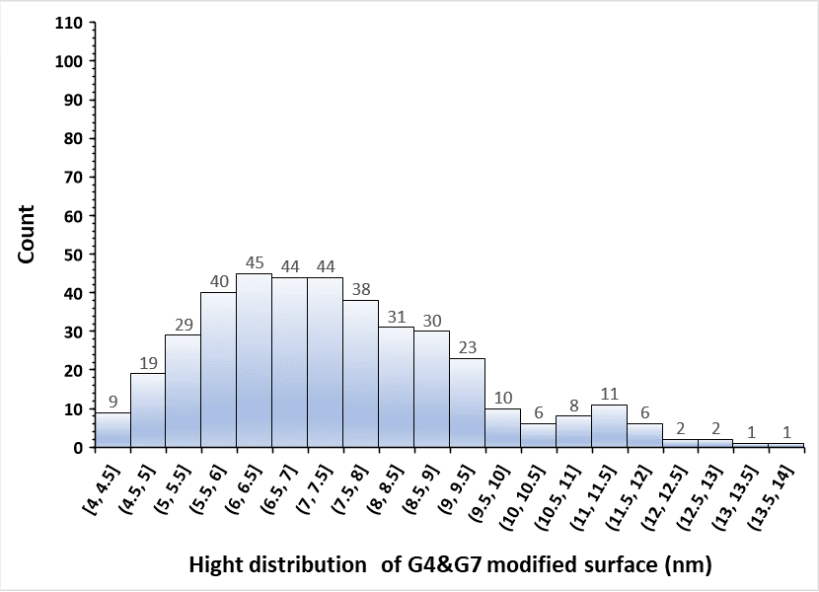

Figure A4. Height distribution of each modified surface.

A6 XPS elemental analysis of different modified surfaces

Table A1. XPS elemental analysis of different modified samples.

Modification	O 1s (%)	C 1s (%)	N 1s (%)	Si 2p (%)	C/N	Si/C
Bare Glass	57.31	12.77	0.63	29.29	20.27	2.29
APTES	41.77	24.65	4.30	29.27	5.73	1.19
G4	59.32	19.09	3.72	17.86	5.13	0.94
G7	39.06	29.50	6.22	25.22	4.74	0.85
G4&G7	42.25	28.84	6.87	22.04	4.20	0.76

References

1. Howarter, J.A. and J.P. Youngblood, Optimization of silica silanization by 3-aminopropyltriethoxysilane. Langmuir, 2006. **22**(26): p. 11142-11147.
2. Lecoq, E., et al., Plasma polymerization of APTES to elaborate nitrogen containing organosilicon thin films: influence of process parameters and discussion about the growing mechanisms. Plasma Processes and Polymers, 2013. **10**(3): p. 250-261.
3. Henry, A.C., et al., Control of electroosmotic flow in laser-ablated and chemically modified hot imprinted poly (ethylene terephthalate glycol) microchannels. Electrophoresis, 2002. **23**(5): p. 791-798.
4. Chai, H.-J., et al., Renal targeting potential of a polymeric drug carrier, poly-L-glutamic acid, in normal and diabetic rats. International journal of nanomedicine, 2017. **12**: p. 577.

Appendix B

B1 Optimization of G7 concentration for surface engraftment.

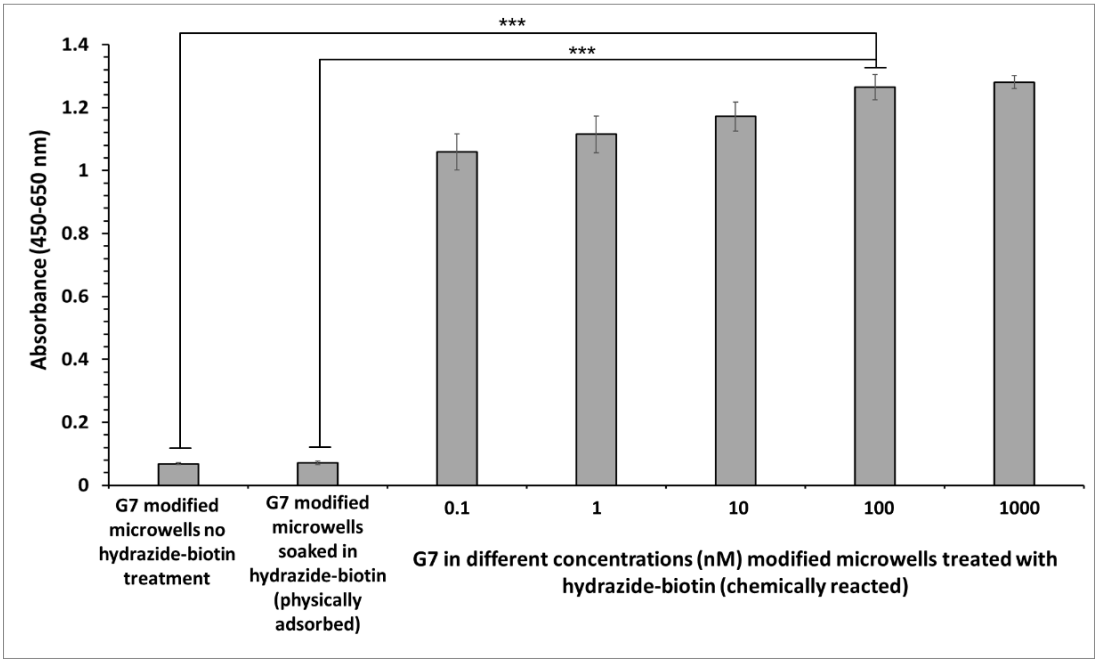

Figure B1. Optimization of G7 concentration for surface engraftment. Error bars indicate standard deviation, n=5; p values (***<0.001) were calculated by a Student's t-test, 2 tails.

B2 Optimization of aptamer concentration

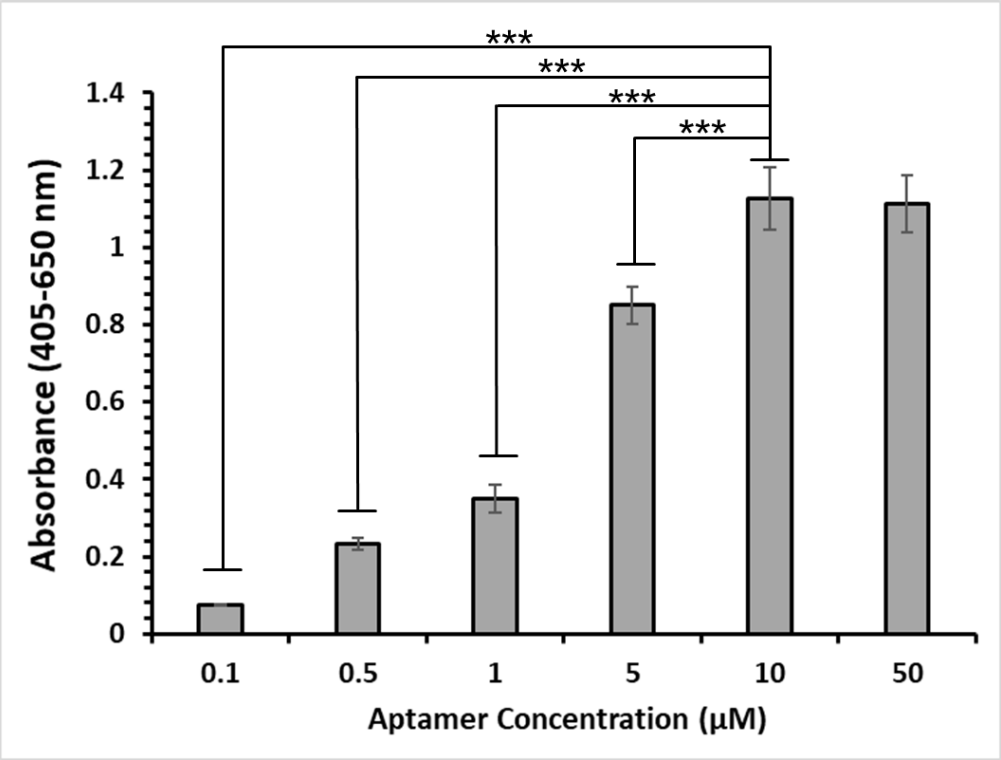

Figure B2. Optimization of aptamer concentration; error bars indicate standard deviation, n=5; P values (***<0.001) were calculated by a Student's t-test, 2 tails.

B3 X-ray photoelectron spectroscopy (XPS)

To study each step of the surface modification, surfaces of interest (*i.e.,* PS surfaces, KOH and plasma treated surfaces, APTES treated surfaces, G7-COOH modified surfaces, and G7-aptamer modified surfaces) were characterized using XPS. Specifically, XPS spectra were obtained using a Kratos Axis Ultra DLD spectrometer (Kratos Analytical Ltd, Manchester, UK) with monochromatized Al Kα X-rays. The take-off angles for all measurements were fixed at 45 °, and 284.6 eV was used as a reference position for the C-H(C) peak. Survey scan spectra and high-resolution spectra were analyzed by CasaXPS Version 2.3.19 PR1.0. (Casa Software Ltd., Teignmouth, UK).

As shown in Figure B3A, in comparison with PS surfaces, the surfaces treated with KOH and plasma showed a marked O 1s peak intensity increase, suggesting successful surface activation. Moreover, after the APTES modification, two new peaks for N 1s and Si 2p emerged, both of which can be attributed to the introduction of the APTES molecules to the surfaces. In addition, after surface modification with G7-COOH, the surface composition of N and O were increased to 9.92 % and 14.62 %, respectively, while Si dropped to 3.01 % when compared to APTES modified surfaces, suggesting the successful introduction of G7-COOH to the surfaces. Furthermore, a new P 2p peak appeared on the spectrum of the G7-aptamer modified surfaces when compared to those of other surfaces, providing support that aptamer immobilization was successful.

Moreover, the success of surface modification was further investigated using high-resolution XPS spectra, as shown in Figure B3B. Specifically, in comparison with PS surfaces, the surfaces treated with KOH and plasma showed more oxygen-related deconvoluted peaks (C 1s scan), including C-CO_2 (285.3 eV), C-O (286.1 eV), C=O (287.3 eV) and O-C=O (289.2 eV) [1-3], confirming the success of surface activation. Moreover, after the APTES treatment, the spectrum of the resulting surfaces showed new amino-related peaks at 285.8 eV (C-N, C 1s), 401.4 eV (NH_3^+, N 1s), and 399.6

eV (-NH_2, N 1s) [1, 4, 5] while all the oxygen-related C 1s peaks from KOH and plasma treated surface disappeared, indicating the success of surface amination. In addition, after G7-COOH immobilization, three new constituent peaks related to chemical structures of G7-COOH molecules emerged at 289.0 eV (O-C=O, C 1s), 288.1 eV (N-C=O, C 1s), and 400.1 eV (N-C=O, N 1s) [1, 4, 5], supporting the notion that G7-COOH surface immobilizations were successfully carried out. Furthermore, after conjugating aptamers, two new constituent peaks related to nucleic acids emerged at 289.3 eV (N-C(=O)-N, C 1s) and 398.3 eV (=NH, N 1s) [6, 7], indicating that the aptamer conjugation was successful.

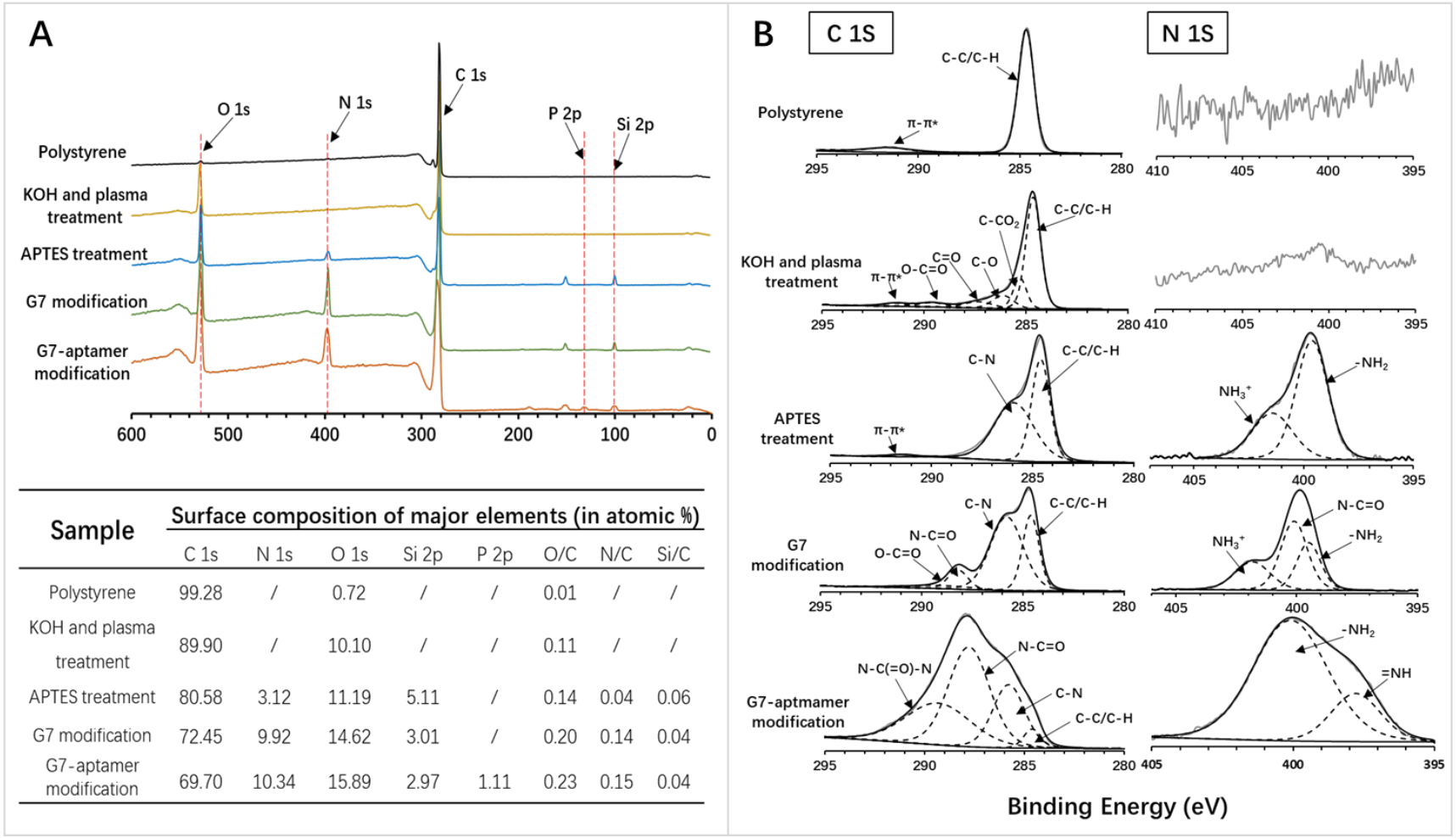

Sample	Surface composition of major elements (in atomic %)							
	C 1s	N 1s	O 1s	Si 2p	P 2p	O/C	N/C	Si/C
Polystyrene	99.28	/	0.72	/	/	0.01	/	/
KOH and plasma treatment	89.90	/	10.10	/	/	0.11	/	/
APTES treatment	80.58	3.12	11.19	5.11	/	0.14	0.04	0.06
G7 modification	72.45	9.92	14.62	3.01	/	0.20	0.14	0.04
G7-aptamer modification	69.70	10.34	15.89	2.97	1.11	0.23	0.15	0.04

Figure B3. XPS analysis of surface modification. A) Survey scan of each modified surface and the surface composition of the major elements (in atomic %). B) High-resolution XPS spectra of C 1s and N 1s of each modified surface.

B4 Surface blocking test

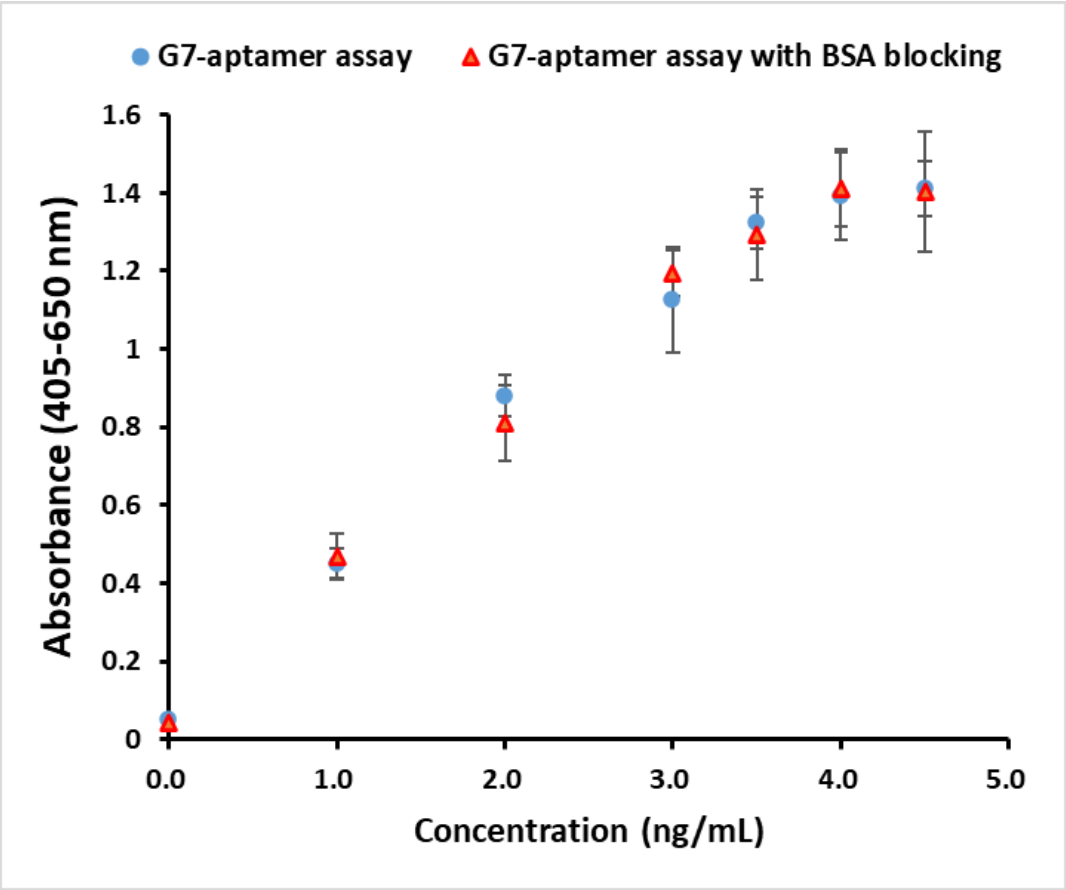

Figure B4. Comparison of G7-aptamer assay detection performances with and without BSA blocking.

B5 Materials

3-Aminopropyl-triethoxysilane, 99% (APTES), N-hydroxysuccinimide (NHS), 1-ethyl-3-(3-dimethylaminopropyl) carbodiimide hydrochloride (EDC), 2,2′-Azino-bis (3-ethylbenzothiazoline-6-sulfonic acid) (ABTS) liquid substrate solution, 2-(N-morpholino) ethanesulfonic acid (MES), and hydrazide-biotin were purchased from Thermo Fisher Scientific (Ottawa, ON). Anhydrous alcohol, Tween-20, phosphate-buffered saline (PBS) (0.01 M, pH 7.4), bovine serum albumin (BSA), Tris(hydroxymethyl) aminomethane (Tris), and NHS-biotin were purchased from Sigma-Aldrich (Oakville, ON). Poly(amidoamine) dendrimer generation 7 with carboxyl functional groups (G7-COOH) was purchased from Dendritech (Midland, MI). Human EGF, human FGF, sonic hedgehog, BMP-4, and Human PDGF-BB Standard ABTS ELISA Development Kit were purchased from PeproTech (Rocky Hill, NJ). Poly(styrene) flat bottom 96-microwell plates (not treated, product number 3370) were purchased from Corning (Kennebunk, ME). Aptamers were custom synthesized by Integrated DNA Technologies (Coralville, IA).

B6 Conjugation efficiency of the aptamer to the G7-COOH

To estimate the conjugation efficiency of the aptamer to the G7-COOH, amine capped aptamers with fluorescent tags (*i.e.,* NH_2-aptamer-cy3) were employed to conjugate with G7-COOH molecules in solution. Specifically, a reaction mixture containing 1 μM NH_2-aptamer-cy3, 1 nM G7-COOH, 5 mM NHS and 2 mM EDC in 0.1 M MES solution (pH 6.0) was reacted at room temperature for 2 h. Subsequently, the resulting mixture was filtered using an Amicon Ultra centrifugal filter (cutoff = 50 KDa) to remove the unreacted aptamers (Mw = 14.5 KDa) and to purify the resulting G7-aptamer conjugates (Mw > 100 KDa). Subsequently, the purified G7-aptamer conjugates were used to calculate the concentration of fluorescent aptamers conjugated to the G7 dendrimers against a calibration curve established using known concentrations of NH_2-aptamer-cy3. The conjugation efficiency was calculated using the equation below:

Conjugation efficiency = $\frac{\text{Concentration of the quantified aptamers}}{\text{Concentration of G7 molecules} \times 512 \text{ branches}}$.

References

1. Lock, E.H., et al., Surface composition, chemistry, and structure of polystyrene modified by electron-beam-generated plasma. Langmuir, 2010. **26**(11): p. 8857-8868.
2. North, S.H., et al., Plasma-based surface modification of polystyrene microtiter plates for covalent immobilization of biomolecules. ACS applied materials & interfaces, 2010. **2**(10): p. 2884-2891.
3. Larrieu, J., et al., Ageing of atactic and isotactic polystyrene thin films treated by oxygen DC pulsed plasma. Surface and Coatings Technology, 2005. **200**(7): p. 2310-2316.
4. Min, H., et al., Ambient-ageing processes in amine self-assembled monolayers on microarray slides as studied by ToF-SIMS with principal component analysis, XPS, and NEXAFS spectroscopy. Analytical and bioanalytical chemistry, 2012. **403**(2): p. 613-623.
5. Strle, D., et al., Chemical Selectivity and Sensitivity of a 16-Channel Electronic Nose for Trace Vapour Detection. Sensors, 2017. **17**(12): p. 2845.
6. Stypczyńska, A., T. Nixon, and N. Mason, X-ray radiation of poly-L-arginine hydrochloride and multilayered DNA-coatings. The European Physical Journal D, 2014. **68**(11): p. 333.
7. Ptasinska, S., et al., X-ray induced damage in DNA monitored by X-ray photoelectron spectroscopy. The Journal of chemical physics, 2008. **129**: p. 065102.

Appendix C

C1 Materials and Methods

C1.1 Materials

N-hydroxysuccinimide (NHS), 1-ethyl-3-(3-dimethylaminopropyl) carbodiimide hydrochloride (EDC), bis(sulfosuccinimidyl)suberate (BS^3), (tris(2-carboxyethyl)phosphine) hydrochloride salt (TCEP-HCl), phi29 DNA polymerase, 10×reaction buffer for phi29 polymerase (containing 330 mM Tris-acetate (pH 7.9), 100 mM magnesium acetate, 660 mM potassium acetate, 1% Tween 20, 10 mM dithiothreitol), T4 DNA ligase, 10×T4 ligation buffer (containing 400 mM Tris-HCl, 100 mM $MgCl_2$, 100 mM DTT, 5 mM ATP, pH 7.8), deoxynucleotide triphosphate (dNTP) solution mix were purchased from Fisher Scientific (Ottawa, ON). Phosphate-buffered saline (PBS) (0.01 M, pH 7.4), phosphate buffer (PB) (pH=8.0), bovine serum albumin (BSA), hydrogen tetrachooroaurate(III)trihydrate ($HAuCl_4$), trisodium citrate, ethanolamine-HCL solution (1 M, pH 8.5), nuclease-free water, glycine-HCL buffer (10 mM, pH 2.0), 11-Mercaptoundecanoic acid (11-MUA), gold nanoparticles (100 nm, stabilized suspension in citrate buffer), poly (allylamine hydrochloride) (PAH) (Mw 50,000) and poly(sodium 4-styrenesulfonate) (PSS) (Mw 70,000) were purchased from Sigma-Aldrich (Oakville, ON). Poly(amidoamine) (PAMAM) dendrimer generation 3.5 with carboxyl functional groups (G3.5-COOH) and generation 4 with amino functional groups (G4-NH_2) were purchased from Dendritech (Midland, MI). Pseudo-SARS-CoV-2 and negative viral particles (*i.e.*, viral particles without S protein on the surface) were purchased from MyBiosource (San Diego, CA). Recombinant SARS-CoV-2 spike protein receptor-binding domain (SRBD) and anti-SARS-CoV-2 SRBD antibodies were purchased from FANTIBODY (Chongqing, China). Recombinant MERS-CoV and SARS-CoV SRBD proteins were purchased from ABclonal Science Inc (Woburn, MA). Aptamers were custom synthesized by Integrated DNA Technologies (Coralville, IA), and aptamer sequences used for this study are listed in Table C1.

Table C1. Details of DNA sequences used in the current study.[a]

Name	Seq. #	Sequence (5’ to 3’)	Ref.
Capturing aptamer (*i.e.*, aptamer against SRBD of SARS-CoV-2)	S_1	NH_2, 12C spacer-CAG CAC CGA CCT TGT GCT TTG GGA GTG CTG GTC CAA GGG CGT TAA TGG ACA (51-nt)	[1]
RCA primer:	S_2	GGA CAT TTT TTT TTT TTT TTT CAG CA (26-nt)	this work
RCA padlock probe:	S_3	Phos-AAA AAA AAT GTC CAT TAA CGC CCT TGG ACC AGC ACT CCC AAA GCA CAA GGT CGG TGC TGA AAA AAA A-3 (67-nt)	this work
ssDNA probe:	S_4	Thio, 6C spacer-AAA AAA AAA AAA AAA A (16-nt)	this work

[a] Note: The underlined portion in the RCA padlock probe sequence S_3 is complementary to the sequence of capturing aptamer in order to produce tandem repeating aptamer (S_1) by the RCA reaction. The ssDNA probe (S_4) is complementary to the sequence of the RCA product using a circular template, a conjugation product of S_2 and S_3.

C1.2 Fabrication of Carboxyl Functionalized LSPR Sensor Chips

To fabricate carboxyl functionalized LSPR sensor chips, we employed a well-developed approach [2] by alternating depositions of PAH and PSS polymer layers on a glass surface upon which a final layer of gold nanoparticles (d=100 nm) was adsorbed. Subsequently, the resulting surface was treated with an 11-MUA solution to render carboxyl functional groups on the surface of gold nanoparticles. Eight lays of PAH/PSS each were adsorbed on the glass surface and the last layer was PAH.

C1.3 Synthesis of RCA products

To carry out the RCA reaction, a previously published RCA reaction protocol was followed with minor modifications [3, 4]. Specifically, 100 µL of 1 µM circular template was first prepared using T4 DNA ligase to ligate hybridization RCA primer (S_2, Table C1) and padlock probe (S_3, Table C1). Subsequently, the prepared circular template solution was mixed with an RCA reaction mixture, including 10 µL of phi29 DNA polymerase (10 U/ µL), 40 µL of dNTP (10 mM), 100 µL of 10×phi29 polymerase buffer, and 750 µL of nuclease-free water, to react at 37 ℃ for 1 h to obtain RCA products. The RCA reaction was stopped by heating at 65 ℃ for 10 min to inactivate the phi29 DNA polymerase.

C2 Characterization

C2.1 Characterization of Carboxyl Functionalized LSPR sensor chip

X-ray Photoelectron Spectroscopy (XPS)

Figure C1 below shows the N 1s and C 1s scan of high-resolution XPS spectra of the carboxyl functionalized LSPR sensor chip surface. For the N 1s scan, the peak at 399.7

eV, strongly indicates -NH_2 functional groups on the sensor chip surface [5, 6]. For the C 1s scan, the peak was deconvoluted into three peaks, indicating C-C (284.6 eV) [7, 8], O-C=O (288.7 eV) [7, 9] and C-N (286.2 eV) [7, 8] structures on the sensor chip surface. It should be noted that the C-N (286.2 eV) structure detected by the XPS strongly indicates a surface functionalized with amines (*i.e.,* C-NH_2). The XPS result also confirms the existence of –COOH on the sensor chip surface as evidenced by the presence of O-C=O peak at 288.7 eV.

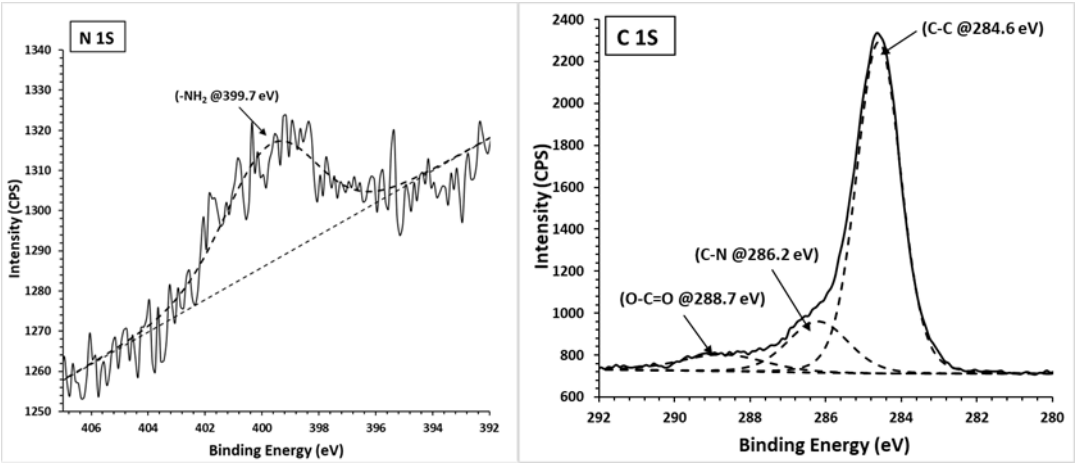

Figure C1. N 1s and C 1s scan of high-resolution XPS spectra of the sensor chip surface (take-off zero degrees). Data analysis was processed using CasaXPS software (v 2.3.19); the fitting residual standard errors (*i.e.,* residual STD) for both N 1s and C 1s scans < 0.9.

C2.2 Characterization of (G3.5+G4)-aptamer Surface Modifications

Fluorescence labeling methods

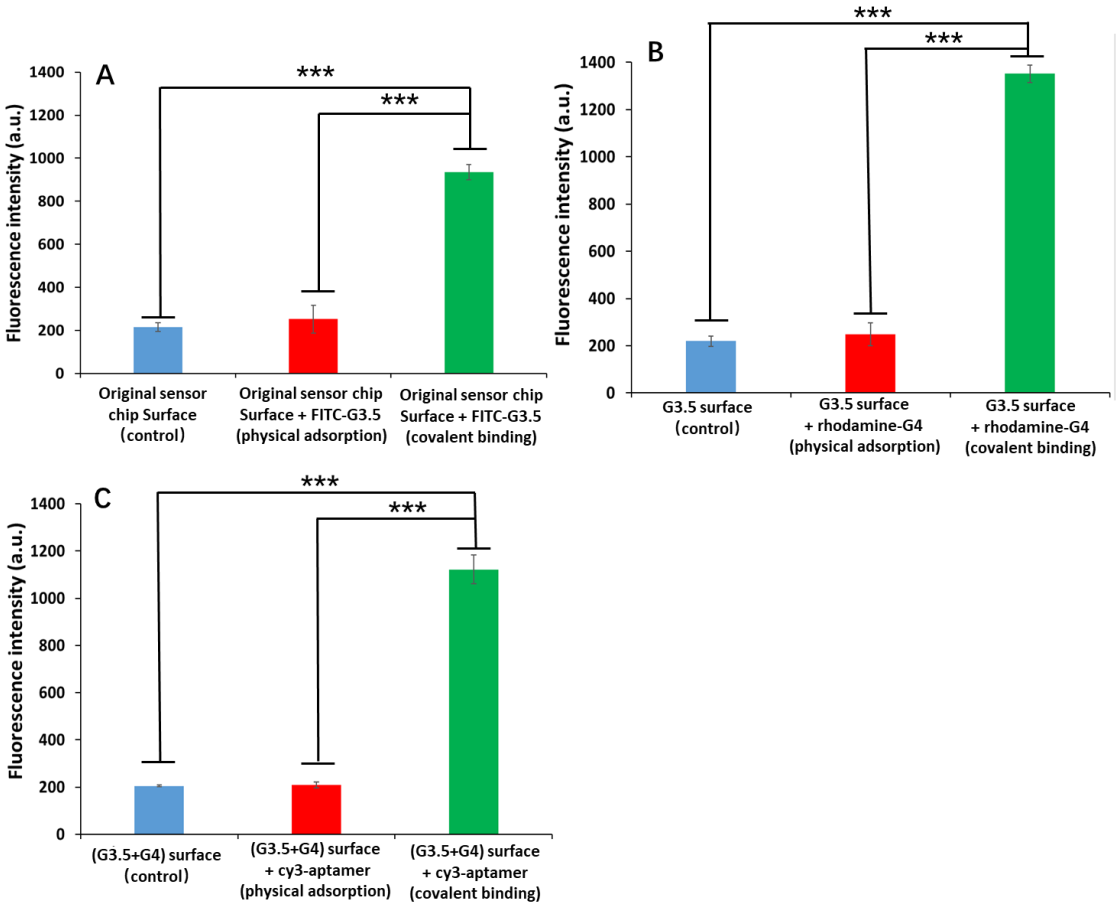

Figure C2. Changes in fluorescence intensities before and after surfaces modified with fluorescence-labeled molecules. A) Fluorescence intensities of original sensor chip surfaces modified by FITC labeled G3.5-COOH molecules (*i.e.*, FITC-G3.5) to confirm the success of G3.5 immobilization. B) Fluorescence intensities of G3.5-COOH modified surfaces modified by rhodamine-labeled G4-NH_2 molecules (*i.e.*, rhodamine-G4) to confirm the success of G4 immobilization. C) Fluorescence intensities of (G3.5+G4) modified surfaces conjugated with cy3-labeled aptamers (*i.e.*, cy3-aptamer) to confirm the success of aptamer conjugation. Error bars indicate standard deviation, n=3. The p values (***<0.001) were calculated by a Student's t-test, 2 tails.

LSPR signal changes

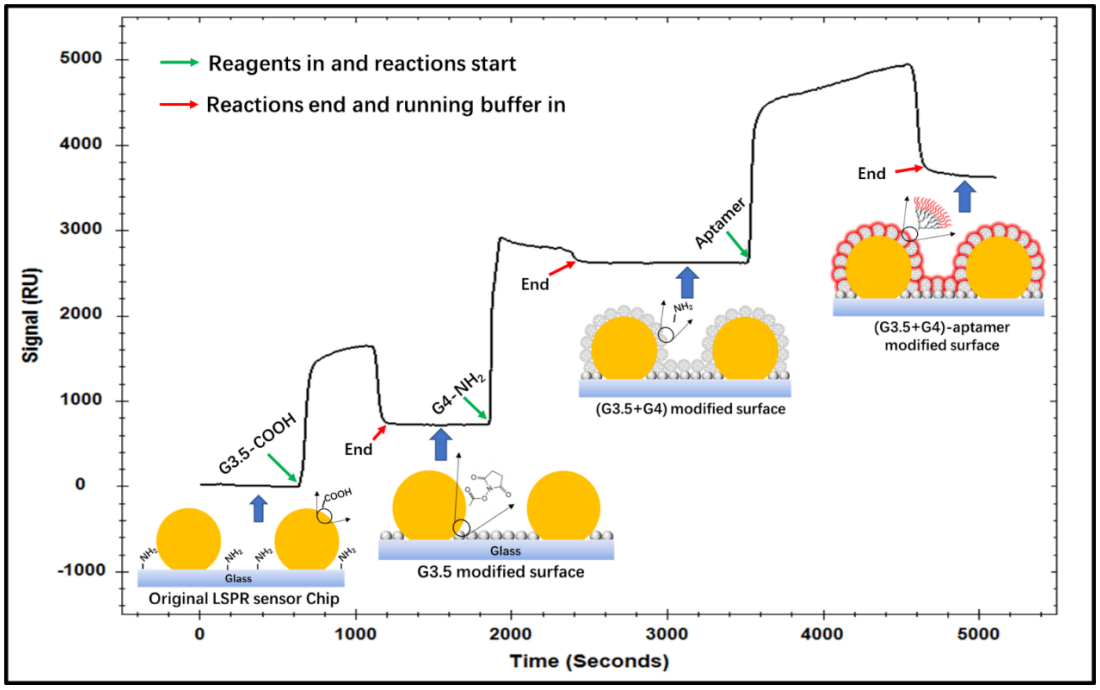

Figure C3. A sensorgraph of each step of surface modifications. Note that LSPR signals were increased after each step of surface modifications, reflecting a surface mass increase of each layer due to the successful immobilization of biomolecules (*i.e.*, G3.5, G4, and aptamers) [10], suggesting that the surface modifications of the LSPR sensor chip were successful.

C2.3 Characterization of AuNPs and ssDNA-AuNPs conjugates

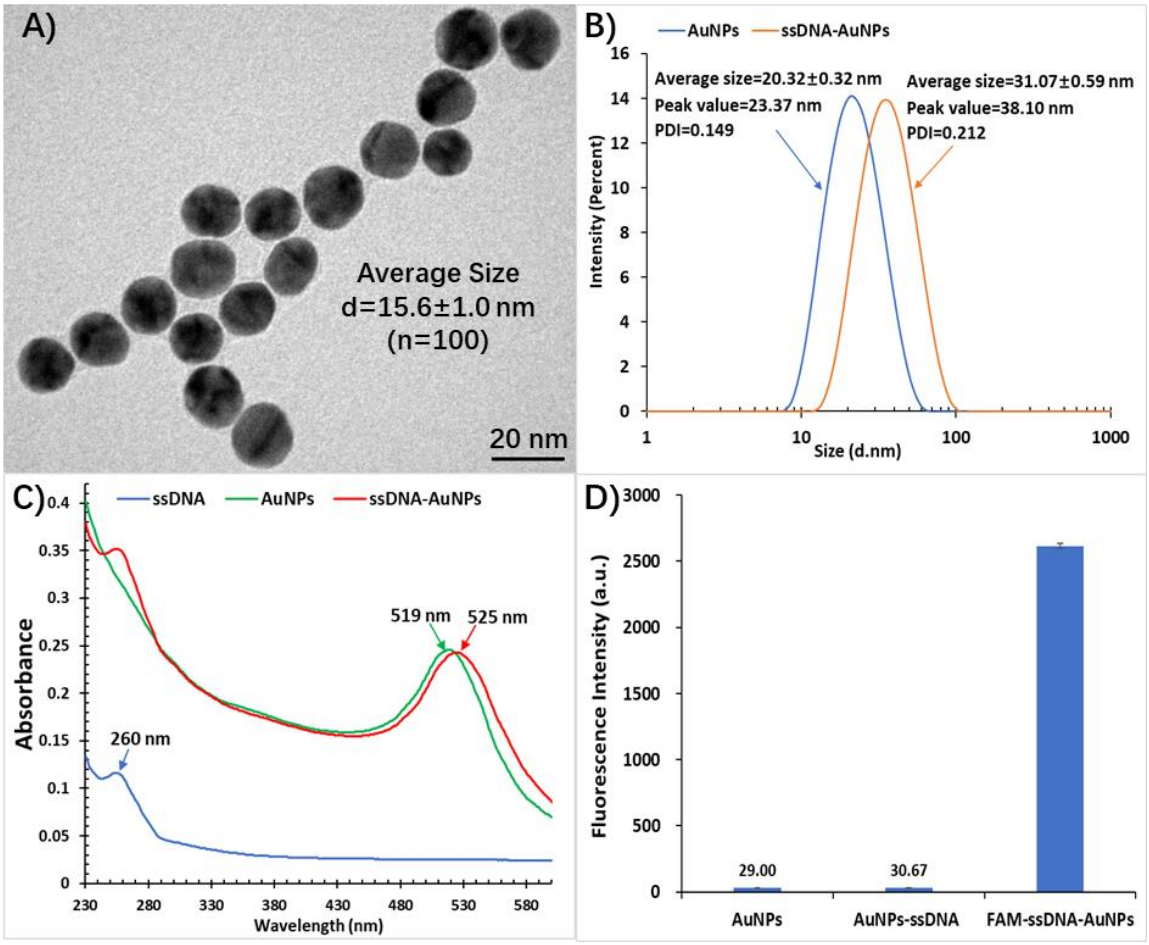

Figure C4. Characterization of AuNPs and ssDNA-AuNPs conjugates. A) A transmission electron microscopic image of AuNPs; B) particle size analysis of AuNPs and ssDNA-AuNPs conjugates using the dynamic light scattering method; C) ultraviolet-visible spectrum changes between samples of ssDNA, AuNPs, and ssDNA-AuNPs conjugates; D) fluorescence intensities changes between samples of AuNPs, ssDNA-AuNPs and ssDNA-AuNPs labeled with FAM (*i.e.*, FAM-ssDNA-AuNPs); error bars indicate standard deviation, n=3.

C2.4 Characterization of RCA products

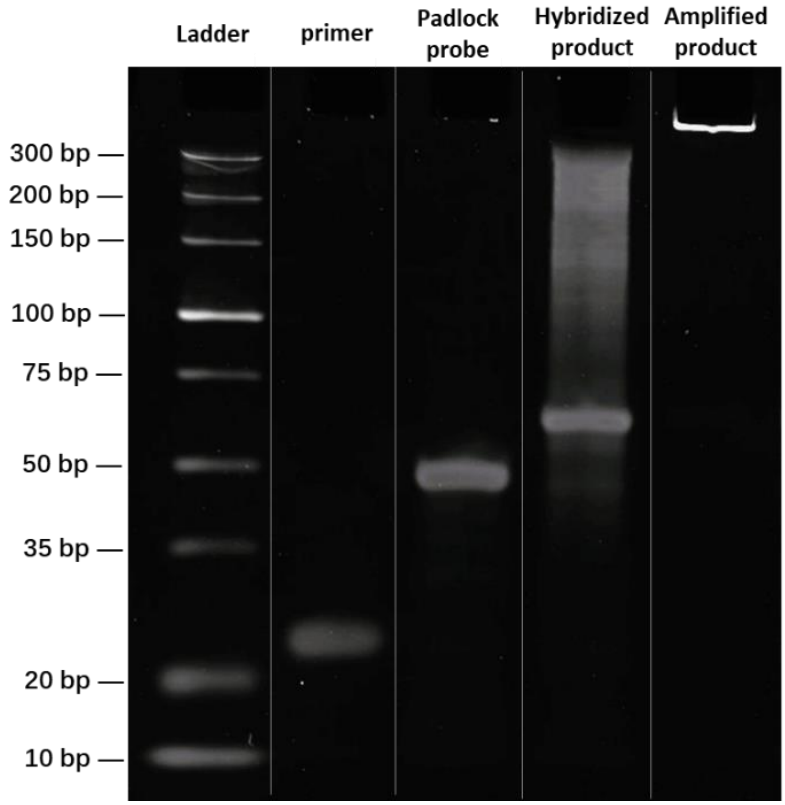

Figure C5. A gel electrophoresis image of RCA products. Note that the bands of primer and padlock probe were around 20 and 45 bp, respectively; the band of hybridized products was around 65 bp; the band of RCA products was in the well of the gel.

C3 Optimization of buffer conditions and flow rate

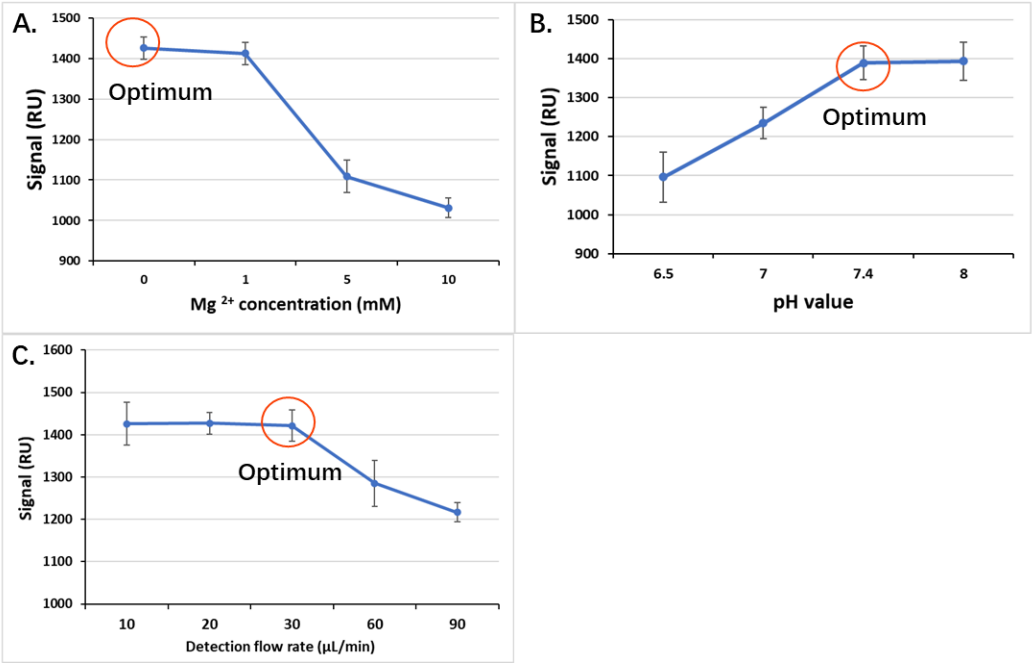

Figure C6. Optimization of buffer conditions and flow rate for (G3.5+G4)-aptamer sensor chips. A) influence of Mg^{2+} concentration on detection signals, B) influence of pH value on detection signals, and C) influence of flow rate on detection signals.

C4. Regeneration tests.

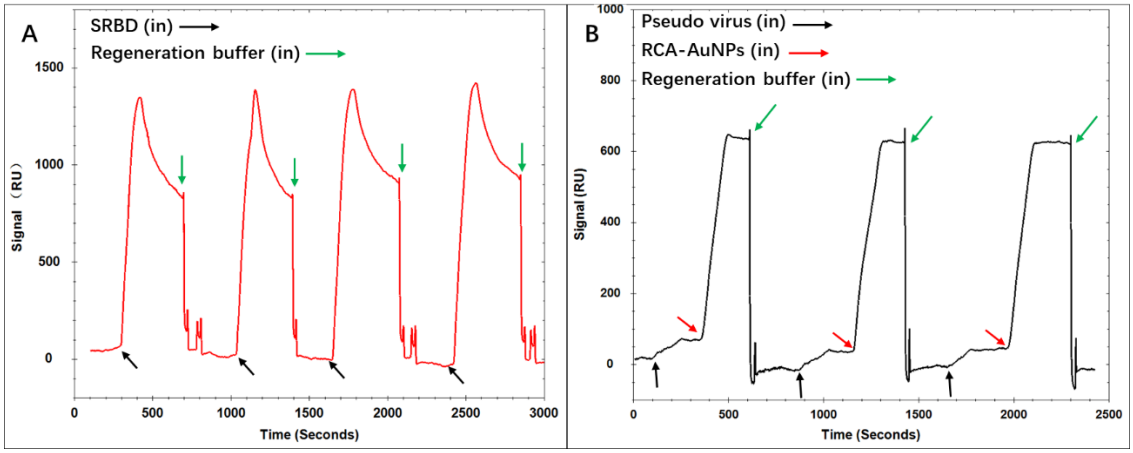

Figure C7. Regeneration test of the (G3.5+G4)-aptamer sensor chips for SRBD (A) and pseudovirus (B) detections. Note that the sensor chips can be regenerated multiple times using the regeneration buffer (*i.e.*, glycine-HCL (10 mM, pH 2.0)).

C5 Calculation Ratio of Surface Aptamer Concentration *vs.* Surface Antibody Concentration

The ratio of surface aptamer concentration *vs.* surface antibody concentration can be calculated using the following equations [11-13]

$$R = m\Delta n[1 - \exp\left(\frac{-2d}{l_d}\right)] \quad (1); \quad \Delta n = C(d_n/d_c) \quad (2)$$

where R is the sensor response to an attached layer, m is the refractive index sensitivity, d is the thickness of the attached layer, l_d is the electromagnetic field decay length, Δn is the difference in refractive index between the attached layer and the surrounding medium, C is material concentration in the attached layer, and d_n/d_c is the refractive-index increment.

In our case, we tested the surface signal $R_{antibody}$=2325 and R_{G4}=2017; the l_d value is 20 nm, and m is a constant provided by the producer; the $d_{antibody}$ =7.1 nm [14], d_{G4} =1.8 nm [15], d_n/d_c value of antibodies is 0.185 cm^3/g [16], and d_n/d_c value of G4 is 0.200 cm^3/g [17] based on the reported data. We assume that our modified surfaces are homogeneous without molecule distortion so that we can calculate the ratio of surface G4 concentration *vs.* surface antibody concentration.

Therefore, $C_{G4}/C_{antibody}$=1.24

Moreover, one G4 molecule can conjugate with 44 aptamers in solution conditions tested by conjugating fluorescence-labeled aptamers with G4 molecules. Assuming that the conjugation rate is around 30%-80% when aptamers conjugate with G4 on the LSPR surface, the estimated ratio of surface aptamer concentration *vs.* surface antibody concentration is around 16-44.

C6 LSPR Sensorgraphs of Different Modified Sensor Chips for SRBD Detection

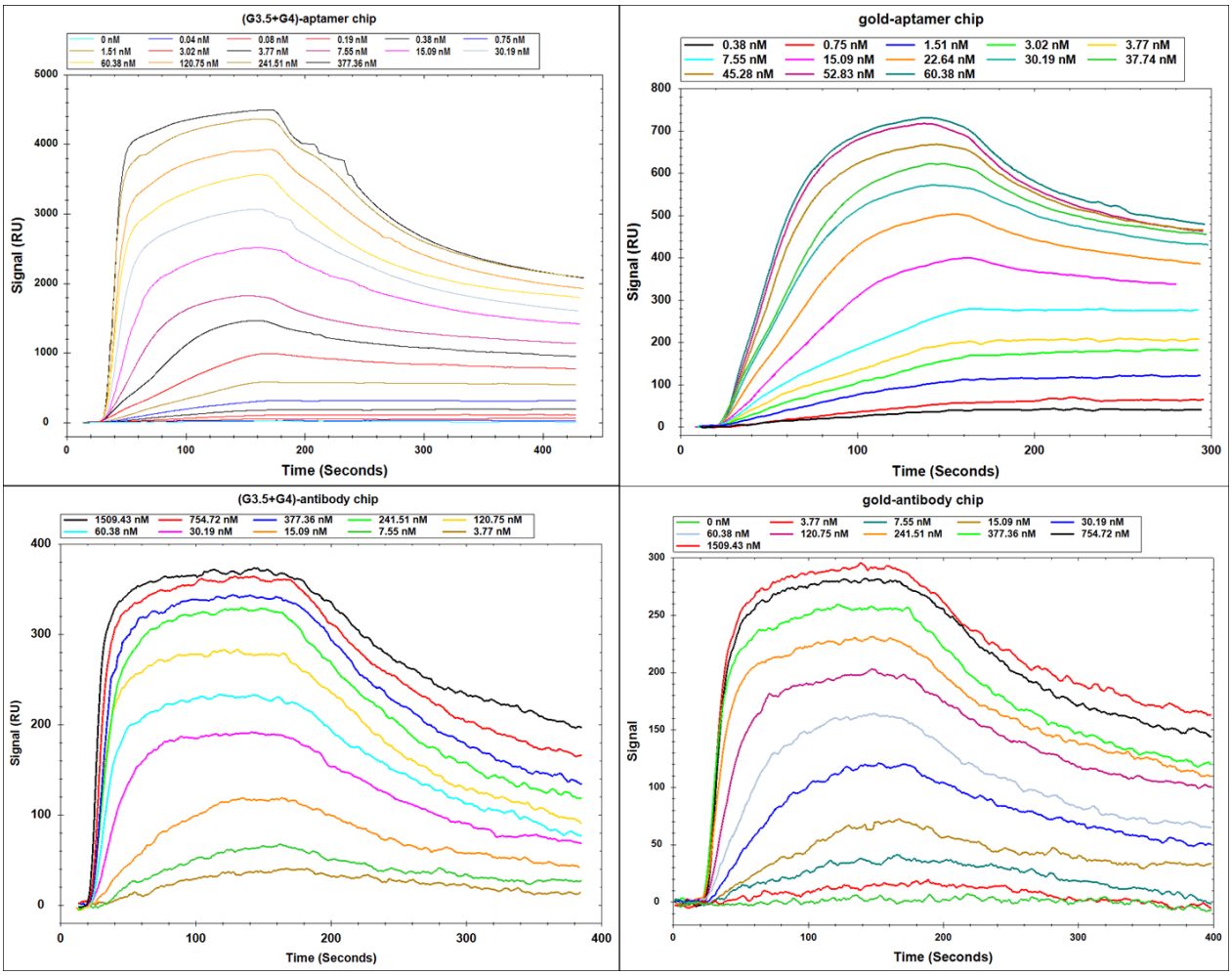

Figure C8. LSPR sensorgraphs of sensor chips with different surface modifications for SRBD detection. Response signals were collected at 165 s for creating concentration-response curves in Figure 5.3.

References

1. Song, Y., et al., Discovery of Aptamers Targeting Receptor-Binding Domain of the SARS-CoV-2 Spike Glycoprotein. 2020.
2. Lu, M., et al., Gold nanoparticle-enhanced detection of DNA hybridization by a block copolymer-templating fiber-optic localized surface plasmon resonance biosensor. Nanomaterials, 2021. **11**(3): p. 616.
3. Li, S., et al., *In situ* rolling circle amplification surface modifications to improve *E.coli* O157: H7 capturing performances for rapid and sensitive microfluidic detection applications. Analytica Chimica Acta, 2021. **1150**: p. 338229.

4. Jiang, Y., et al., Rolling circle amplification and its application in microfluidic systems for Escherichia coli O157: H7 detections. Journal of Food Safety, 2019. **39**(5): p. e12671.
5. Min, H., et al., Ambient-ageing processes in amine self-assembled monolayers on microarray slides as studied by ToF-SIMS with principal component analysis, XPS, and NEXAFS spectroscopy. Analytical and bioanalytical chemistry, 2012. **403**(2): p. 613-623.
6. Strle, D., et al., Chemical Selectivity and Sensitivity of a 16-Channel Electronic Nose for Trace Vapour Detection. Sensors, 2017. **17**(12): p. 2845.
7. Min, H., et al., Ambient-ageing processes in amine self-assembled monolayers on microarray slides as studied by ToF-SIMS with principal component analysis, XPS, and NEXAFS spectroscopy. Analytical and Bioanalytical Chemistry, 2012. **403**(2): p. 613-623.
8. Xu, Z.X., et al., Amide-linkage formed between ammonia plasma treated poly(D,L-lactide acid) scaffolds and bio-peptides: enhancement of cell adhesion and osteogenic differentiation in vitro. Biopolymers, 2011. **95**(10): p. 682-94.
9. Demirci, S., et al., Functionalization of poly-SNS-anchored carboxylic acid with Lys and PAMAM: surface modifications for biomolecule immobilization/stabilization and bio-sensing applications. Analyst, 2012. **137**(18): p. 4254-4261.
10. Schasfoort, R.B., Introduction to surface plasmon resonance. 2017.
11. Unser, S., et al., Localized surface plasmon resonance biosensing: current challenges and approaches. Sensors, 2015. **15**(7): p. 15684-15716.
12. De Feijter, J., d.J. Benjamins, and F. Veer, Ellipsometry as a tool to study the adsorption behavior of synthetic and biopolymers at the air–water interface. Biopolymers: Original Research on Biomolecules, 1978. **17**(7): p. 1759-1772.
13. Hand, D.B., The refractivity of protein solutions. Journal of Biological Chemistry, 1935. **108**(3): p. 703-707.
14. Dong, Y. and C. Shannon, Heterogeneous Immunosensing Using Antigen and Antibody Monolayers on Gold Surfaces with Electrochemical and Scanning Probe Detection. Analytical Chemistry, 2000. **72**(11): p. 2371-2376.
15. Eichman, J.D., et al., The use of PAMAM dendrimers in the efficient transfer of genetic material into cells. Pharmaceutical Science & Technology Today, 2000. **3**(7): p. 232-245.

16. Longman, E., S.E. Harding, and N. Marheineke, Identifying differences in solution conformations of two chimeric IgG3 antibodies through triple detection SEC. LC GC NORTH AMERICA, 2006. **24**(1): p. 64.
17. Yanez Arteta, M., et al., Interactions of PAMAM dendrimers with negatively charged model biomembranes. The journal of physical chemistry B, 2014. **118**(45): p. 12892-12906.

Appendix D

D1 Aptamer Sequences

Table D1. Details of aptamer sequences used in the current study.[a]

Function	Name	Seq.#	Sequences (5'-3')	Ref.
Aptamer for *E.coli* capturing	Unit aptamer	S_1	NH_2, 6C spacer/ATCG TCACA CCTGC TCTAT CAAAT GTGCA GATAT CAAGA CGATT TGTAC AAGAT GGTGT TGGCT CCCGT AT (72-nt)	[1]
RCA for *E.coli* capturing (cRCA)	cRCA primer	S_2	NH_2, 6C spacer/TTTTT TTTTT **GAAGG ACTTA GTTAC TGTCG AGCGA T** (36-nt)	[1]
	cRCA padlock probe	S_3	Phos/**AACTA AGTCC TTC***AT ACGGG AGCCA ACACC ATCTT GTACA AATCG TCTTG ATATC TGCAC ATTTG ATAGA GCAGG TGTGA CGGAT* **ATCGC TCGAC AGT** (98-nt)	[1]
	cRCA characterization probe	S_4	Cy5-TTTTC TTGTA CAAAT CGTCT (20-nt)	[1]
RCA for *E.coli* signaling (sRCA)	sRCA aptamer-primer	S_5	*ATCCG TCACA CCTGC TCTAT CAAAT GTGCA GATAT CAAGA CGATT TGTAC AAGAT GGTGT TGGCT CCCGT AT*TTT TTTT**T GTCCG TGCTA GAAGG AAACA GTTAC** (105-nt)	[2-4]
	sRCA padlock probe	S_6	Phos/**TAGCA CGGAC A**TATA TGATG GACCG CAGTA TGAGT ATCTC CTATC ACTAC TAAGT GGAAG AAAT**G TAACT GTTTC CTTC** (79-nt)	[5]
	cy5-ssDNA signaling probe	S_7	Cy5-TTTTA GTATG AGTAT CTC (18-nt)	[1]

[a] Note: The bold portions in S_2 and S_6 can respectively hybridize with those in S_3 and S_7 to form circular RCA templates. The italic portion in the cRCA padlock probe sequence S_3 is complementary to the sequence of unit aptamer in order to produce tandem repeating aptamers (S_1) by the cRCA reaction. The italic sequence in S_5 is identical to the unit aptamer sequence in order to label the captured *E.coli* O157:H7 cells. The underlined portions in S_4 can hybridize with the cRCA products (*i.e.*, the complementary sequence of S_3 underlined portion) to confirm the *in situ* synthesis of cRCA on dendrimer-nylon surfaces. The underlined portions in S_7 can hybridize with the sRCA products (*i.e.*, the complementary sequence of S_6 underlined portion) to amplify detection signals.

D2 Results of Surface Characterizations and Optimizations

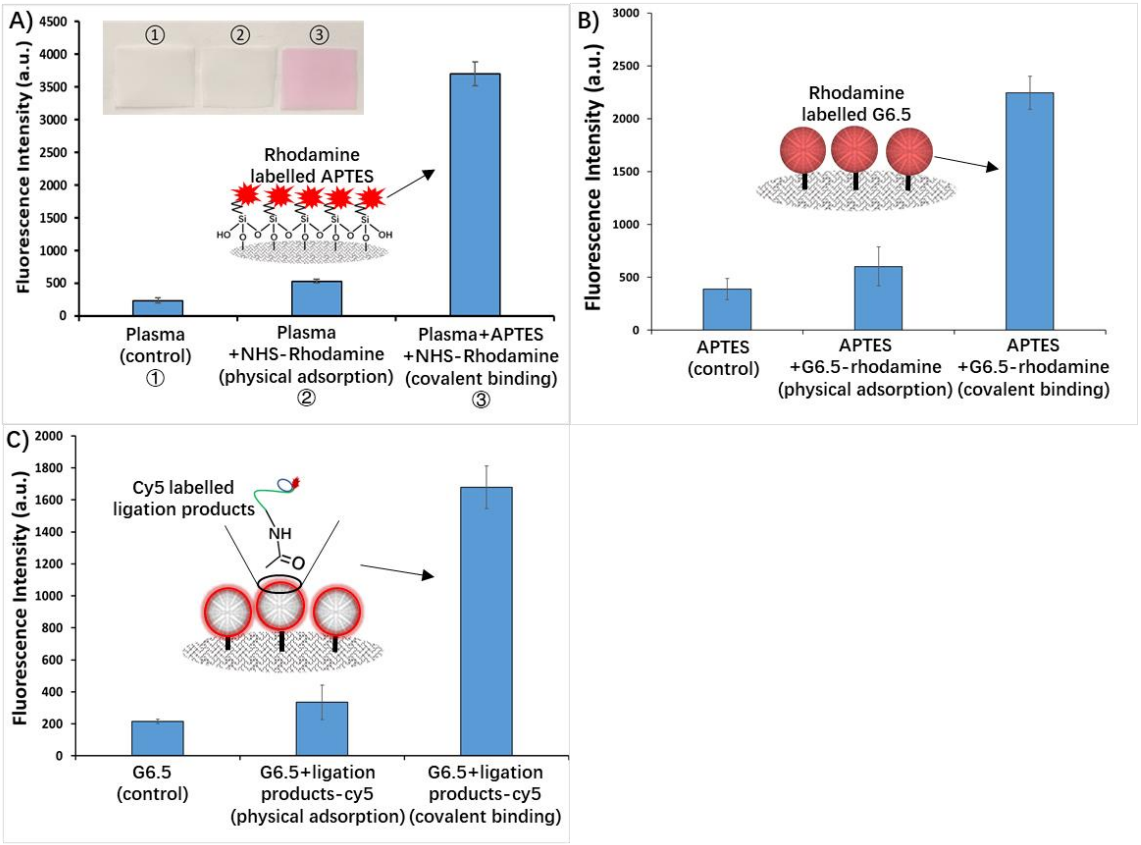

Figure D1. Surface characterization using fluorescence labeling methods to indicate the success of surface modifications. A) Fluorescence intensities of APTES-modified surfaces labeled with NHS-rhodamine to confirm the success of surface amination; inset indicates color changes of surfaces with corresponding treatments. B) Fluorescence intensities of G6.5-rhodamine modified surfaces to confirm the success of PAMAM dendrimer immobilization. and C) Fluorescence intensities of ligation products-cy5 modified surfaces to confirm the success of ligation-product conjugation. Error bars indicate standard deviations, n=3.

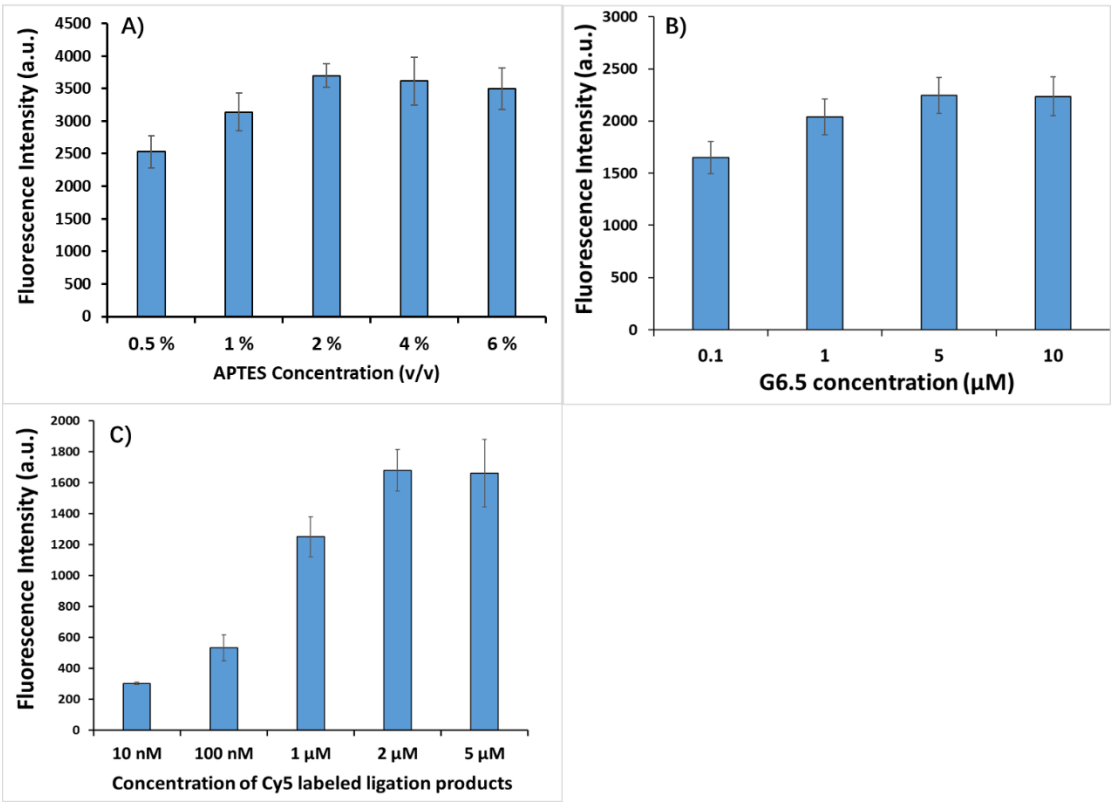

Figure D2. Optimization of parameters for surface modifications. A) APTES concentration for surface amination. B) G6.5 concentration for G6.5 surface modification. C) The concentration of ligation products for surface immobilization. Error bars indicate standard deviations, n=3. Note that the optimum concentration of APTES was 2% (v/v), G6.5 was 5 µM, and the ligation product was 2 µM.

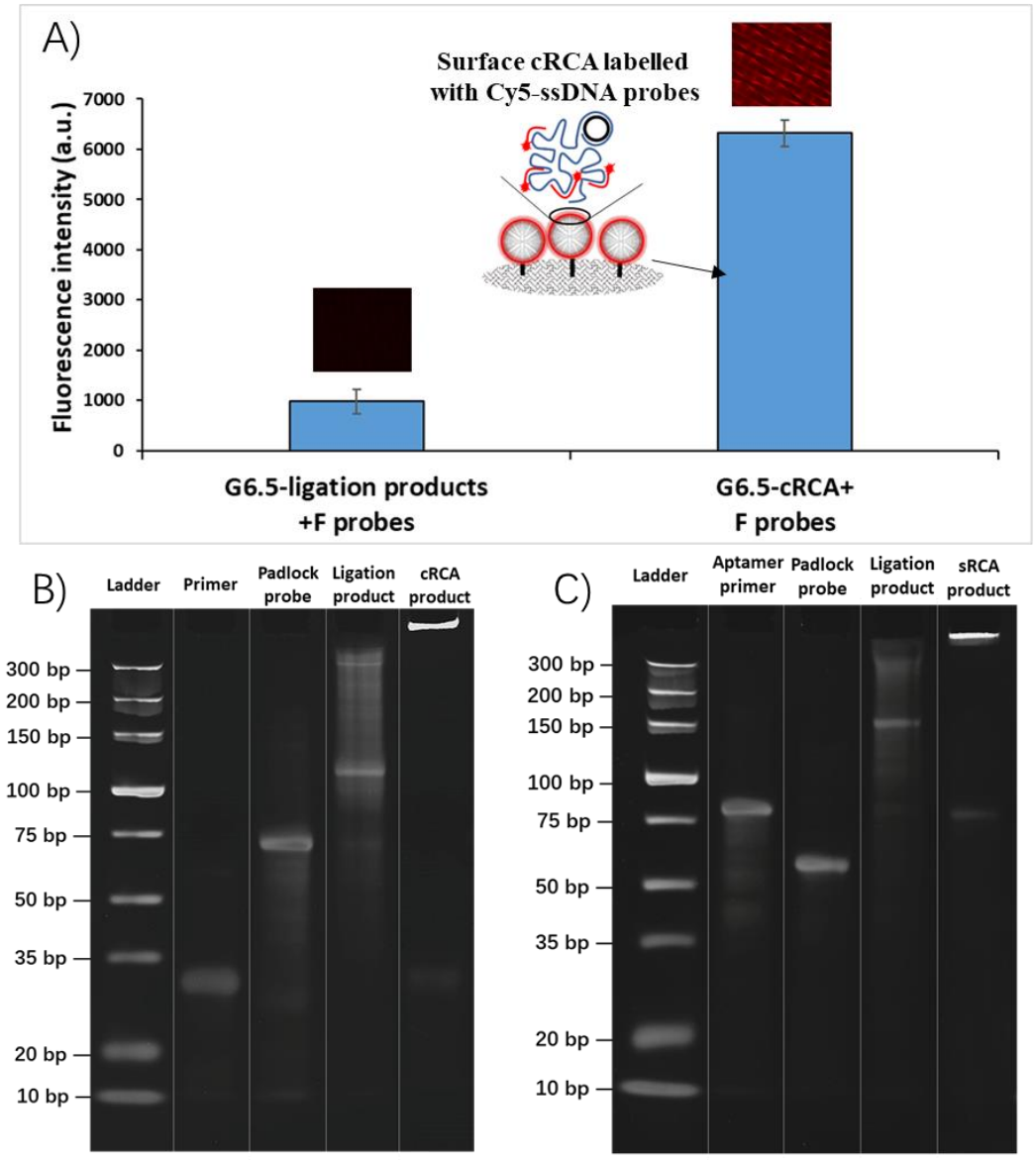

Figure D3. Characterization of RCA reactions. A) The fluorescence intensity of different modified surfaces labeled with a short fluorescently labeled complementary sequence (*i.e.*, cRCA characterization probe, S_4, Table D1) to confirm the *in situ* synthesis of cRCA on G6.5 modified surfaces, n=3; B) and C) Gel electrophoresis images of cRCA and sRCA products to confirm the success of RCA reactions. Note that bands of primers and padlock probes for both cRCA and sRCA were less than 100 bp, while their bands of ligation products presented molecular weights higher than 120 bp, suggesting the successful synthesis of ligation products. The amplified cRCA and sRCA products were trapped in the wells of the gel due to high molecule weight.

D3 Non-specific Adsorption Signals Tested in Milk and Orange Juice

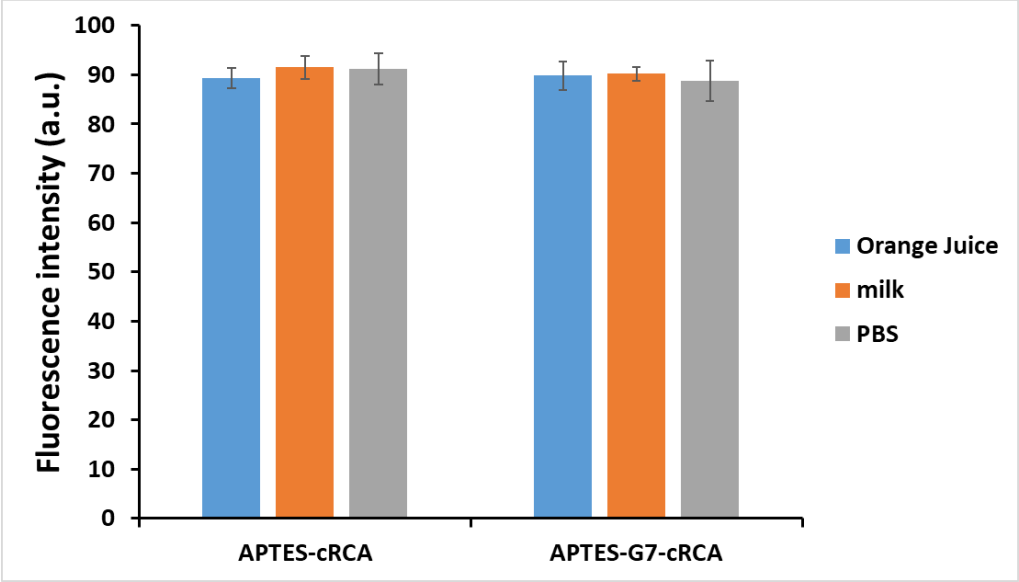

Figure D4. Background noises of membranes from non-specific adsorption of food matrices.

D4 Actual Numbers of *E.coli* O157:H7 Cells in Samples

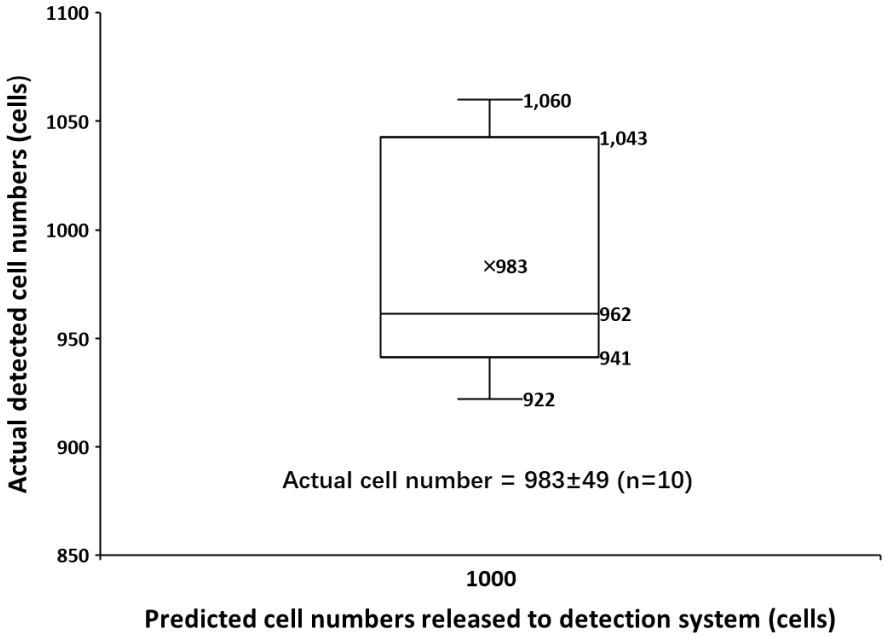

Figure D5. Actual numbers of *E.coli* O157:H7 cells in samples. The actual *E.coli* O157:H7 cells in samples were corrected using 0.45 μm membranes (4h cRCA) to test the samples by 10 times. The results showed that the actual cell numbers were close to the predicted in the experiments.

D5 Number Distributions of Captured *E.coli* O157:H7 Cells at Limit of Detection Points

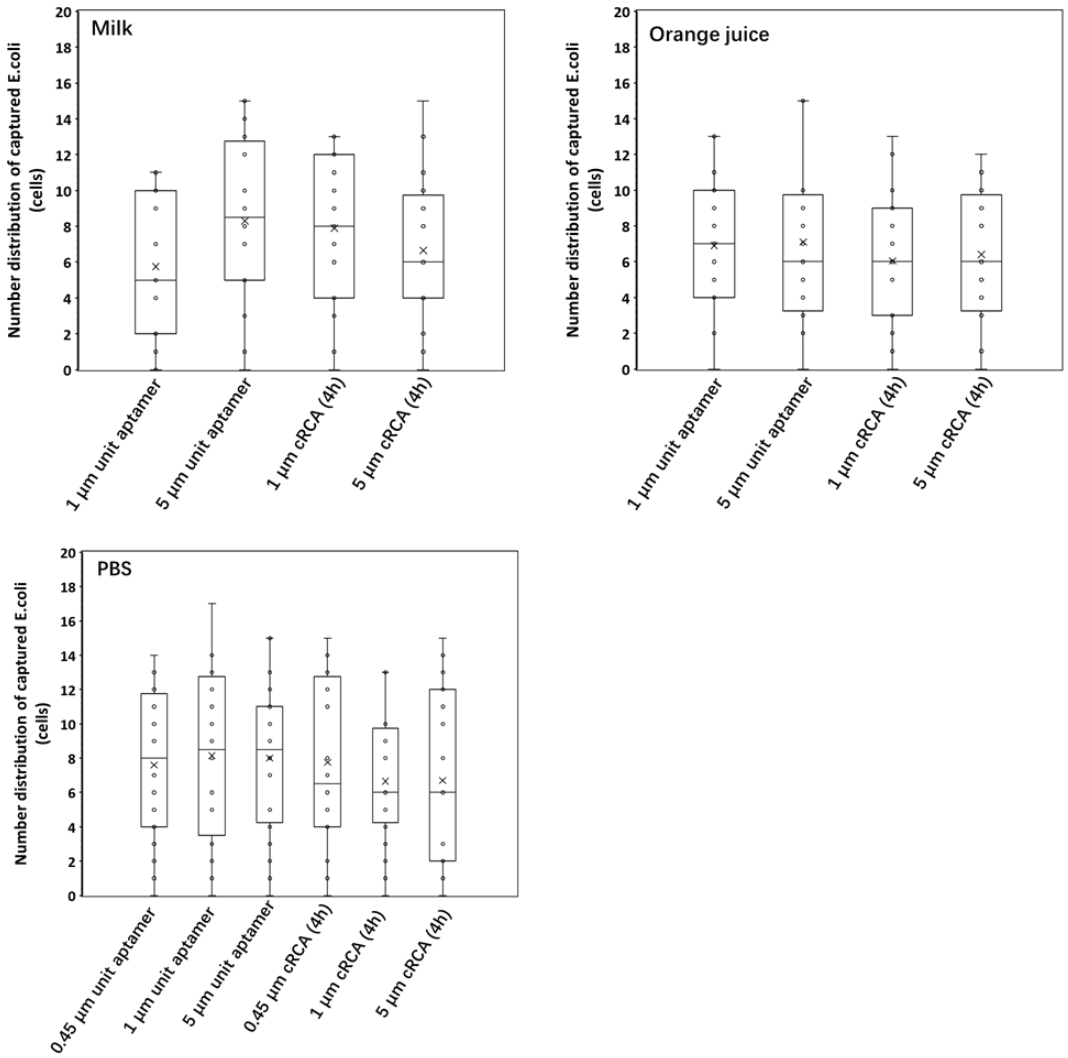

Figure D6. Number distributions of the captured *E.coli* O157:H7 cells on different membranes at the limit of detection points.

D6 Number of Ligation Products on Each G6.5 Molecules

To estimate the number of ligation products on each G6.5 molecules, cy5-labeled ligation products were employed to conjugate with G6.5 molecules in a solution condition and quantified using a calibration curve made by a known concentration of cy5-labeled ligation products. Specifically, a reaction mixture containing 1 μM ligation products (cy5 labeled), 1 nM G6.5, 5 mM NHS, and 2 mM EDC in 0.1 M MES solution (pH 6.0) was reacted at room temperature for 2 h. Subsequently, the resulting mixture was filtered using an Amicon Ultra centrifugal filter (cutoff=100 KD), so the G6.5-ligation products could be kept inside the filter while other reactants were centrifuged out. After this step, the G6.5-ligation products were collected and quantified using the calibration curve.

D7 Capturing Efficiency Tests

Table D2. Capturing efficiency of the membranes tested using PBS, milk, and orange juice samples

Surface modification method	G7-cRCA (4h)			G7-unit aptamer		
Membrane pore size (μm)	0.45	1	5	0.45	1	5
Released cell number in PBS	**Cell capturing efficiency (%) tested in PBS**					
100	94±8	96±12	72±8	92±4	69±15	29±10
1000	100±5	98±9	76±5	98±9	68±8	31±8
10000	98±7	102±5	74±5	98±6	69±11	32±5
Released cell number in milk	**Cell capturing efficiency (%) tested in milk**					
100	N/A	90±6	69±9	N/A	45±6	19±7
1000	N/A	94±8	73±7	N/A	47±7	21±6
10000	N/A	93±6	71±6	N/A	43±9	18±7
Released cell number in orange juice	**Cell capturing efficiency (%) tested in orange juice**					
100	N/A	91±7	73±8	N/A	53±6	22±6
1000	N/A	96±6	74±8	N/A	55±5	25±7
10000	N/A	94±5	74±9	N/A	52±9	24±5

N/A: blockage of membrane pores

References

1. Jiang, Y., et al., Developing a dual-RCA microfluidic platform for sensitive *E.coli* O157: H7 whole-cell detections. Analytica Chimica Acta, 2020. **1127**: p. 79-88.
2. Zhou, L., et al., Aptamer-based rolling circle amplification: a platform for electrochemical detection of protein. Analytical chemistry, 2007. **79**(19): p. 7492-7500.
3. Wu, W., et al., An aptamer-based biosensor for colorimetric detection of Escherichia coli O157: H7. PloS one, 2012. **7**(11): p. e48999.
4. Bruno, J.G. and J. Chanpong, Methods of producing competitive aptamer fret reagents and assays. 2009, Google Patents.
5. Jiang, Y., S. Zou, and X. Cao, A simple dendrimer-aptamer based microfluidic platform for *E.coli* O157: H7 detection and signal intensification by rolling circle amplification. Sensors and Actuators B: Chemical, 2017. **251**: p. 976-984.